SWITCHABLE OLEFIN ISOMERIZATION
IN IRIDIUM COMPLEXES

Andrew M. Camp

A dissertation submitted to the faculty at the University of North Carolina at
Chapel Hill in partial fulfillment of the requirements for the degree of Doctor of Philosophy in
the Department of Chemistry.

Chapel Hill
2020

Approved by:

Alexander J. M. Miller

Michel R. Gagne

Marc A. ter Horst

Frank A. Leibfarth

Cynthia K. Schauer

ABSTRACT

Andrew M. Camp: Switchable Olefin Isomerization
in Iridium Complexes
(Under the advisement of Alexander J. M. Miller)

The structure-reactivity relationships in iridium-pincer crown ether complexes is

expanded in this work. These frameworks contain a strongly donating pincer scaffold with a

flexible, weakly donating aza-crown ether moiety that can reversibly bind the metal center. The

iridium pincer-crown ether complexes can access tridentate, tetradentate, or pentadentate

coordination modes reversibly using discrete chemical steps. Careful NMR characterization of

representative complexes in each coordination mode revealed a correlation between the

difference in chemical shift between geminal diastereotopic protons of the crown and

coordination mode of the complex, allowing characterization of the binding modes of the

complexes in solution using routine and time efficient NMR experiments.

Binding studies demonstrate the modulation of affinity of the crownether for cations with

organometallic fragments. Adding transition metal centers changes 1-aza-crown ether host-guest

properties: the selectivity of the 1-aza-15-crown-5 ethers for Li^+ over Na^+ is increased; the

binding affinity for Li^+ and Na^+ salts is reduced, though increasing the ring size of the crown

ether mitigates the decrease; distinct proton-dependent reactivity is observed; and the ion

binding properties shift fundamentally to enable heteroditopic binding of ion pairs.

The observation that moving to larger crowns increases the binding affinity of pincer-crown

ether complexes towards cations motivated the synthesis of new cationic complex, [κ^5-

($^{18c6}NCOP^{iPr}$)Ir(H)]$^+$, featuring a larger 1-aza-18-crown-6 crown ether to improve salt rate

enhancement of olefin isomerization to access switchable regioselectivity. Without cation in solution, the complex is selective for the one bond isomerization product, with a strong preference for the E stereoisomer. Upon the addition of cation, the selectivity is observed to favor thermodynamic olefinic products, with complete inversion in regioselectivity observed across diverse functionalized substrates. Despite the impressive shifts in regioselectivity in the studied substrate, isomerizations with Lewis basic substituted olefins were unable to be "switched" to favor thermodynamic regioisomers.

Explorations of these substrates revealed Lewis basic olefins can form chelated species which significantly inhibit the rate of isomerization with these substrates. Using the aquated iridium complex, $[\kappa^4-(^{18c6}NCOP^{iPr})Ir(H)(OH_2)]^+$, >30% conversion to thermodynamic products were observed after 216 hours, representing an improvement to the activity seen in $[\kappa^5-(^{18c6}NCOP^{iPr})Ir(H)]^+$. Explorations with long chain olefins revealed selectivity for internal olefins in the presence of cation, while preserving preference for the one-bond isomerization product in the absence of cation. While high yielding switchable catalysis to thermodynamic products and internal olefins is elusive, this work lays the foundation for continuing efforts to increase the scope of switchable olefin isomerization to functionalized olefins.

ACKNOWLEDGEMENTS

To the other professors at UNC, thank you for your mentorship and advice over the past 5 years. Cindy, thank you for helping with DFT and laying a computational foundation that I've been able to take advantage of throughout my graduate studies. Mike and Cindy, I appreciate your leadership in 550L, and enjoyed TAing under you while I was still a naïve 1st year. Abby, Frank, and the rest of the Scia-thon team, I've really enjoyed working with you all on such a great event, and I look forward to seeing where the event goes. I also want to give a shout out to other Kenan natives – Jill, Brook, and Joe – for being a friendly face and tolerating my attempts at banter over the past 5 years.

Mom and Dad, I definitely wouldn't be here without your love and support through the past 27 and change years. Thank you for always encouraging my excitement for scholarship and science, and not taking it too hard when I decided not to go into medicine.

My friends and family, I have many a lunch, late night video game session, or evening phone call to thank for motivating me over the past 5 years. I thank you for keeping me sane and always supporting me even when I was tired or busy.

And last, but certainly not least, I'd like to thank Emily and Maddie. Having a graduate student as a husband/dad is not always the easiest, but I've appreciated your unconditional love and support. Thanks for keeping me going through long days or nights with a cup of coffee, a drawing, or a hug. Love you all so much!

TABLE OF CONTENTS

CHAPTER 5. OLEFIN ISOMERIZATION WITH CATION-SWITCHABLE
REGIOSELECTIVITY: UNDERSTANDING INHIBITION
BY LEWIS BASIC MOIETIES

LIST OF FIGURES

LIST OF SCHEMES

LIST OF TABLES

LIST OF ABBREVIATIONS AND SYMBOLS

°   degree(s)

α Greek alpha: crystallographic angle

β Greek beta: crystallographic angle

γ Greek gamma: crystallographic angle

δ Greek delta: denotes chemical shift reference scale

κ Greek kappa: denotes coordination to metal by x atoms

ν Greek mu: IR absorption band frequency

π Greek pi: denotes bond

θ Greek theta: general angle

σ Greek sigma: denotes coordination to a metal via a single atom

Δ Greek capital delta: denotes separation between values

Å   angstrom(s)

aq   aqueous

atm   atmosphere

Ar   general aromatic

br   broad (in reference to NMR shift)

BAr^F_4 tetrakis(3,5-trifluoromethylphenyl)borate

C   celsius

Cpcyclopentadiene

Cp*pentamethylcyclopentadiene

cm^{-1} wavenumber

d doublet

DBU1,8-Diazabicyclo(5.4.0)undec-7-ene

e⁻electron

equiv equivalents

Et ethyl

Et$_2$Odiethyl ether

g Gram

h(rs) hour(s)

Hz Hertz

iPrisopropyl, $-CH(CH_3)_2$

PF$_6^-$ hexafluorophosphate

IR infrared

J_{XY} magnetic coupling between atoms X and Y through a distance of x bonds

K Kelvin

K$_a$binding affinity

K$_{eq}$equilibrium constant

kcal kilocalorie

D Deuterium

L general ligand, usually 2 e- donor

M Molar

M^x general metal atom

μL microliter

μM micromolar

mg milligram

mL milliliter

mM millimolar

mmol millimole

m multiplet

m meta

Me methyl, -CH$_3$

min minute(s)

mol mole

nmnanometers

MeCNacetonitrile

NMR nuclear magnetic resonance

NHCN-heterocylclic carbenes

o ortho

OTftriflate, trifluoromethane sulfonate: CF$_3$SO$_3^-$

ppmparts per million

*p*para

Ph phenyl, -C$_6$H$_5$

ppm parts per million

PPNBis(triphenylphosphoranylidene)ammonium cation

q quartet

Rgeneral functional group

ssinglet (NMR data)

ttriplet

t$_{1/2}$half life

*t*Bu tertiary butyl, -C(CH$_3$)$_3$

THF   tetrahydrofuran

TMS   trimethylsilyl, -Si(CH$_3$)$_3$

UV   ultraviolet light

X   general halogen atom

XRD   X-ray diffraction

CHAPTER 1. PASS THE REMOTE: INCORPORATING CONTROL OF ACTIVITY IN CATALYTIC SYSTEMS

I.   The Advent of Controllable Catalysis

Catalytic Design and Reactivity

Catalysts play an essential role in driving chemical transformations that shape the world. Enzymes allow reactions that are essential for life to occur on reasonable timescales,[1] and catalysts have been harnessed to synthesize commodity chemicals,[2] fertilize the agricultural industry,[3] and synthesize natural products and pharmaceuticals.[4,5] Catalytic structure is intimately linked with the performance of a catalyst in an application, supporting the synthesis of homogenous catalytic systems to access valuable reactions and to better understand the relationships between structure and activity.[6] Synthetic modification of ligand scaffold are used to shape catalytic activity towards desired goals; however, balancing desired characteristics of durability, activity, and selectivity in catalytic systems remains a difficult challenge in catalyst design.

The typical synthetic paradigm for catalyst development is a slow evolution of catalytic structure to better improve desired selectivity or catalyst stability.[7] While such iterative design is powerful, the labor involved can be arduous and time consuming. Small synthetic changes to the ligand structure can result in large changes in catalyst selectivity or even lead to complete loss of catalytic activity.[8] Each unique catalyst is designed to have very specific reactivity: one catalyst yields one product. Once the maximum yield of a desired product is obtained, the reaction is worked-up and purified before subsequent reactions take place.

This contrasts significantly with what is observed in biological systems, where reactions are "dynamic" – reactivity is controlled by stimuli-gated reactivity, product feedback loops, and membrane compartmentalization.[9,10] Product generation is constantly changing to accommodate the needs of the system. Mapping this framework onto anthropogenic systems creates an alternate paradigm, where changes to the system can influence the outcomes of a reaction and break the 1:1 structure-reactivity relationship. Moreover, moving to such a system allows increasing responsiveness in synthetic systems, possibly allowing product distributions to be modified on-line to meet economic demands.

This intriguing possibility has motivated the incorporation of stimuli-responsive moieties into catalyst frameworks.[11] Generally, reactivity with these systems can be categorized into two-types of stimuli-controlled catalysis. In *switchable catalysis,* a catalyst is modulated between two discrete states, each with specific reactivity. This is commonly designed to change rate or product selectivity. In *tunable catalysis,* reactivity can be modulated over a spectrum states yielding fine control over reactivity. The following sections summarize major methods of stimuli controlled catalytic reactivity

Switchable Catalysis Using External Stimuli

Ideally, switchable catalysts should be selective for one reaction, and demonstrate a complete change in catalytic state upon introduction of a stimulus. In an on-off switchable system, this should maximize the difference in the rate of product formation in each catalytic state. When a difference in product selectivity is desired, maximizing the change in catalytic state upon application of a stimulus increases the selectivity for each product. This method of elaborating reactivity is an intriguing method to diversify reactivity independently of synthetic approaches. Various novel stimuli, including light, chemical additives, mechanical force, ultrasonics, and

electric and magnetic fields, have been explored to change reactivity in catalysts.[11–13] The

following paragraphs summarize the chief methods for achieving switchable catalysis.

Light is a convenient stimulus for accessing switchable catalysis, given the ability to turn

on and off light sources and target specific electronic excitations of a catalyst.[14] Branda and

coworkers demonstrate this concept using a switchable chiral Cu^I catalyst.[15] Upon UV

irradiation, an achiral structure is favored, dropping the observed enantiomeric excess to 5%.

One of the limitations in this example is that a mixture of Cu-1 and Cu-2 (3:7) is observed in

solution under UV irradiation (Scheme 1.1), hampering product selectivity. This demonstrates

the challenges in achieving high switchable selectivity. Not only must each unique catalytic state

be selective for a certain product, but the stimulus must *completely* switch the states of the catalyst

to achieve high selectivity.

Scheme 1.1. Light driven rearrangment of a ligand framework.
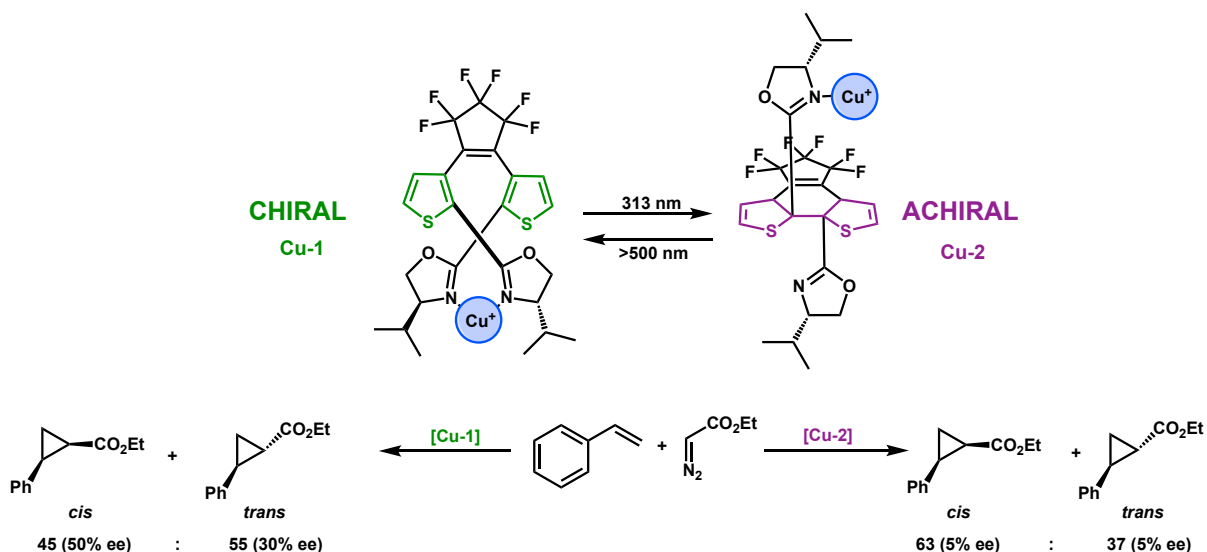
In another example, Neilson and Bielawski use light to influence ligand donation to a

rhodium metal center and modulate rates between two states. Upon photoexcitation with 313

nm light, a photocyclization is induced, reducing the donor strength of the N-heterocyclic carbene (NHC) and decreasing the rate of hydroboration 9-fold.[16] Irradiating with light >500 nm, allows the reverse reaction to occur, restoring the rate of hydroboration (Scheme 4). This photoinduced change in rate was able to be toggled *in situ*, allowing both rate regimes to be observed in a single time course.[16]

Azobenzenes are another popular photoresponsive group that is able to undergo light induced isomerization from the *E* to the *Z* isomer.[11] The photoresponsive group can be incorporated into catalytic frameworks to bring together two remote groups and generate the catalytically active species, demonstrating a reversible photoswitchable response.[17]

Changing the catalyst oxidation state offers another attractive method of switching catalytic activity. Redox-switchable catalysts have been used extensively in polymerizations to change monomer distribution in copolymers.[18–20] Redox control of catalytic reactivity has been demonstrated in other fundamental organic transformations, including rates of Michael addition and CO_2 electroreduction catalysts by switchable heterogenous catalysts.[13] Homogeneous organometallic complexes have been synthesized with redox-active ligands, that display potential-controlled polymerization, olefin reduction, imine hydrolysis, and metathesis reactions.[11] Lorkovic, Duff, and Wrighton installed a redox active cobaltocene moiety into the backbone of a Rh^I complex to switch the rate of hydrogenation.[21] Upon addition of an oxidant, the rate of cyclooctene hydrogenation drops 15 fold, which can be restored upon the addition of a reductant (Scheme 1.2).

Scheme 1.2. Redox control of hydrogenation rates.
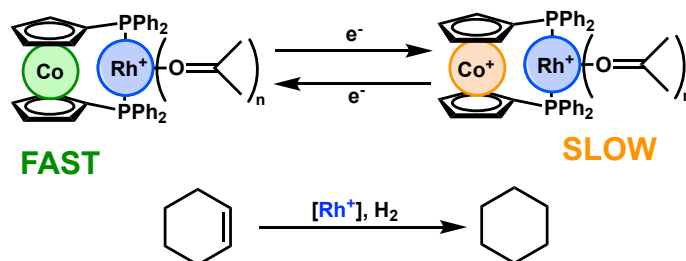
Catalytic activity can also be controlled by modification of catalytic structure with ligands, protons, or cationic additives. While opening a coordination site to increase the rate of catalysis has been used extensively,[22] the ability to *reversibly* influence catalytic activity sets catalysts switchable by chemical stimuli apart. Biological systems apply this concept extensively, modifying rate of enzymatic catalysis using downstream catalytic products and cationic binding events in allosteric regulation.[10]

Protonation of catalysts are often used to induce conformational changes in enzymes and molecular machines,[11,23] which in turn influences reactivity.[12] In organometallic examples, protonation of a ligand framework can influence electron density on the metal center, or trigger conformational shifts to change the rate of reactivity.[11] Schanz and coworkers demonstrate this concept with a proton-responsive, tertiary amine substituted NHC Hoveyda-Grubbs type catalyst.[24] Upon double protonation of the ligand, the catalyst becomes inactive to ring opening metathesis polymerization of a 7-oxanorbornene derivative, which is believed to result from decreased donation of the ammonium substituted NHC to the metal center.[24]

Chemical additives can be used as reversible stimuli to affect switchable catalysis. Mirkin and coworkers demonstrated an organometallic example of allosteric regulation with a Zn-Rh framework. Upon carbon monoxide and chloride ligands binding a Rh center, the Zn^{2+} active site is exposed, turning on phosphate hydrolysis (Scheme 1.3).[25] This conformational change was

shown to be reversible by removing the carbon monoxide and chloride with a nitrogen sparge or addition of Ag^{+}, respectively.

Scheme 1.3. Binding of a CO and Cl^{-} anion opens up the Zn^{2+} active site, turning on phosphate hydrolysis.
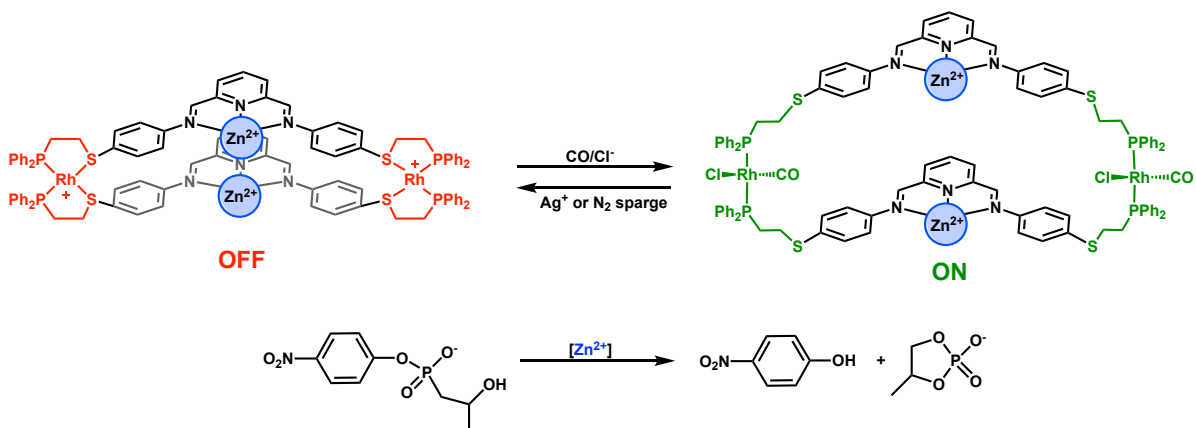
Other popular coordinating chemical additives are cationic species, which offer a variety of Lewis acidities, cation sizes, and counteranions.[12,26] Cationic additives can act to influence electron density on the metal center, control geometry of the metal center, or deprotect a coordination site from a bound ligand.[11] Dervan and coworkers recently reported a Fe[II]-ethylenediaminetetraacetic acid (EDTA) derivative for DNA cleavage.[27] Without cation, the complex is catalytically inactive, but when Ba^{2+} or Sr^{2+} binds the polyethylene glycol backbone, a conformational change is proposed to increase the affinity of the complex for DNA and turn on catalysis (Scheme 1.4).[27]

Scheme 1.4. Cation binding turns on DNA cleavage, a process that is believed to be mediated by increasing affinity of the ligand for hydrogen bond donors in the substrate.
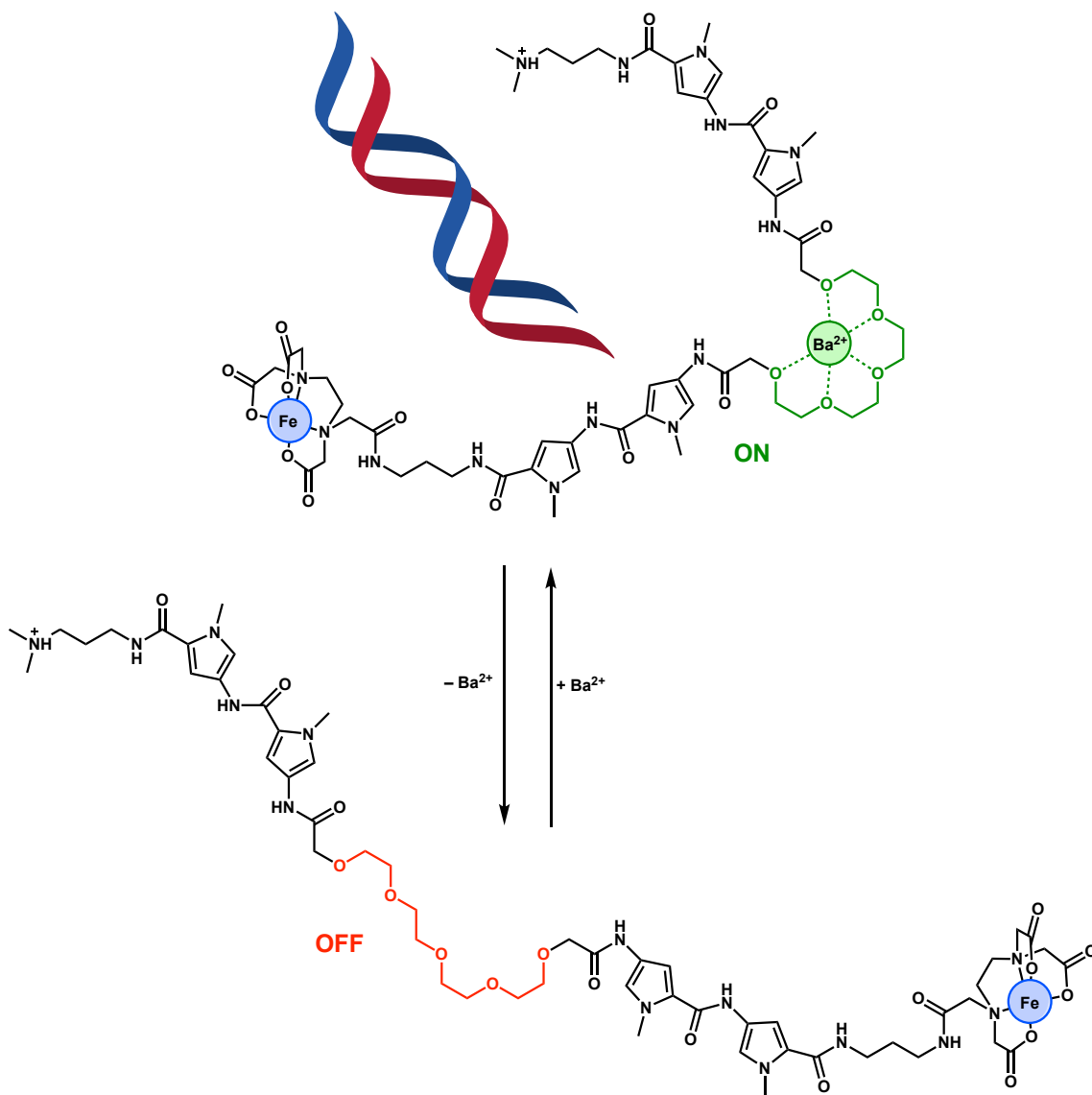
Addition of a transition metal salt to solution can compete with ligand binding around a catalytic site to turn on catalysis. Schmittel and colleagues add an Fe^{2+} salt to compete with terpyridine binding to the Cu^+ center and turning on the cycloproponation of Z-cyclooctene.[28] Fan and coworkers illustrate a similar concept with simple monocationic salts, taking advantage

of strong affinity of crown ethers for Na$^+$ to deprotect a Rh active site, turning on alkene

hydrogenation (Scheme 1.5).[29]

Scheme 1.5. Cation crown binding opens a Rh site to allow olefin binding and subsequent hydrogenation.
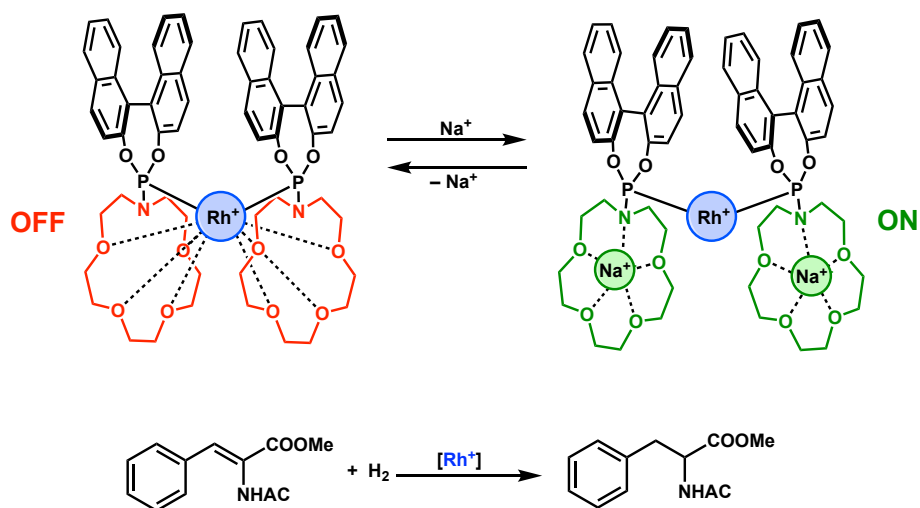
Tuning Catalytic Activity: Dynamic Control of Reaction Rates

In contrast with switchable catalysis, where two discrete catalytic states are accessed through the

application of the stimulus, tunable catalysis is able to access a continuum of rates. This allows

catalytic activity to be "dialed" towards a selected rate, allowing finer control over catalytic

activity. Many of the same stimuli that were applied to access switchable catalysis can applied to

access tunable catalysis, as long as the rate can be adjusted to access a continuum of rates. While

the studies below are not necessarily framed as "tunable catalysts", the systems studied

demonstrate access to a continuum of rates driven by an external stimulus.

Liu and Li and coworkers studied the rate of the photocatalytic decomposition of methylene

blue dye by silver nanoparticles.[30] By adjusting the power of a 443nm laser, the rate of

decomposition was able to be tuned from a 1.5-fold enhancement up to a 4-fold enhancement.[30]

In another heterogenous example, a glassy carbon electrode was coated in Pd nanoparticles for

CO_2 reduction.[31] By changing the applied potential, the distribution of the formate, hydrogen, and CO products was able to be altered.[31]

In a homogeneous example, Stratakes and Miller were able to access photoelectrocatalytic H_2 production using a cyclopentadienyl Ir bipyridine complex.[32] Upon application of light and voltage, the k_{obs} of H_2 production was found to be sensitive to the photon flux – up to an 8-fold increase – and the applied potential – up to a 40-fold increase.[32] Schanz and coworkers demonstrated tunable ring opening metathesis polymerization using their tertiary amine substituted N-heterocyclic carbene (NHC) substituted Hoveyda-Grubbs type catalyst and various amounts of tosylic acid (Scheme 1.6).[33] Upon addition of acid, up to a 12-fold decrease in the polymerization rate was observed.[33] The rate polymerization was found to be highly dependent on acid concentration.

Scheme 1.6. Protonation of basic functionalities changes the rate of polymerization.
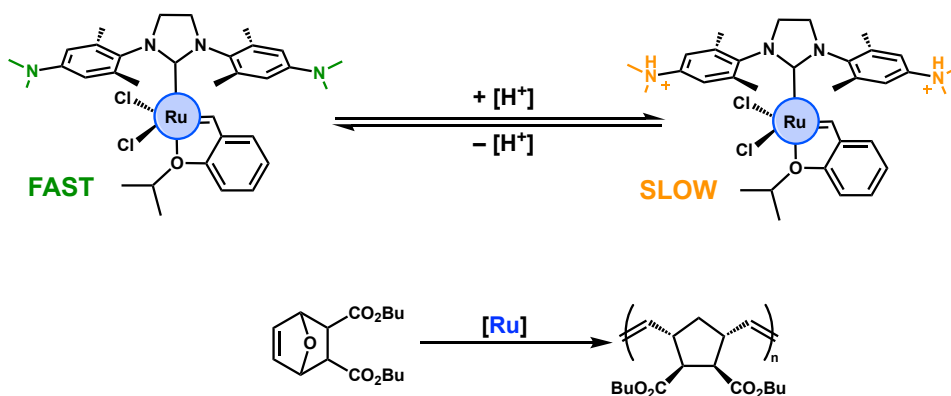
Applying switchable and tunable systems to affect both catalytic rates and selectivity remains a fascinating avenue of research area as a way to artificially apply control to a variety of fundamental reactions; applying stimulus driven control to reactions begins to mimic the extensive regulation observed in biological systems – both to match biological regulation and to

elaborate reactivity using stimuli, conditions, and catalysts beyond the purview of biological systems.

II.   Bridging Switchable and Tunable Catalysis with a Pincer Crown-Ether Framework

Controlling Catalytic Activity in Solution using Static and Dynamic Hemilability

Hemilabile ligands contain both strong donors designed to keep the ligand framework bound to the metal center and weak donors that can reversibly dissociate from the metal to allow substrate to bind.[34] Incorporating hemilabile donors into a catalytic system has yielded successful catalytic systems that optimize stability and reactivity.[35] Most of the examples of controllable catalysis modify activity using changes to the ligand scaffold without modifying the primary coordination sphere itself; additionally, elaborate supramolecular scaffolds are often used to control the control catalytic activity. If a stimulus-responsive hemilabile moiety was incorporated into the scaffold, the primary coordination sphere could be altered to control catalytic rate.[11,36,37] Modulating hemilability can be divided into three approaches. The most common approach to adjust activity in catalysts with hemilabile donors is synthetic methods, which can add stronger donors or change the sterics of the hemilabile donor to influence reactivity.[38,39] In *static hemilability,* an additive acts as a switch between a weak donor bound and weak donor dissociated state, which do not rapidly interconvert (Figure 1.1). This framework can be mapped onto switchable catalysis, since each state can have unique reactivity and rates. Another class is *dynamic hemilability,* where the weak donor bound and dissociated state of the complex are able to rapidly interconvert. Dynamic hemilability can be applied to access tunable catalysis – by adjusting the equilibria between these two states, a spectrum of rates and reactivities are accessible.

A. Static Hemilability

Strong Donors

−X
+X

Weak Donor

B. Dynamic Hemilability

Tunable
Equillibrium
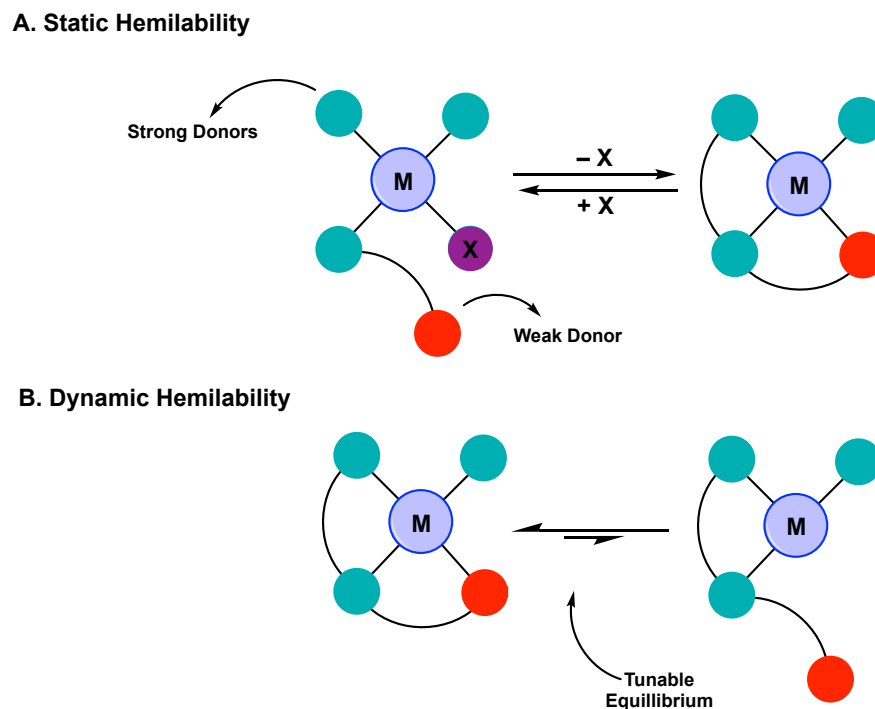
Figure 1.1. Modes of hemilabilitiy.
A. In static hemilability, two discrete states of the catalyst are toggled between two states using an external additive. **B.** In dynamic hemilability, exchange between two states is an equillibrium process, which can be tuned through external additives.

Towards the goal of tunable dynamic hemilability, a pincer-crown ether framework was developed to introduce stimuli responsive behavior to metal based catalysis. The pincer ligand contains a strong phosphine and phenyl background to anchor the ligand on the metal center, and a weak aza-crown-ether that can reversibly bind the metal center. The crown ether can then bind cations to deprotect the metal center to allow substrate to bind and turn on catalysis (Scheme 1.7). Crown-ethers are an attractive group for controlling reactivity, given the breadth of literature on well-defined binding of cationic additives.[40]

Scheme 1.7. Controlling isomerization of olefins using cation gated reactivity.
In an example of static hemilability, Cl⁻ can be extracted to open a coordination site for ligand to
bind (an equillibrium process favoring the crown bound structure, Ir-κ^5). This dynamic
hemilabile regime can be further tuned using Li⁺ to increase the rate of reactions.
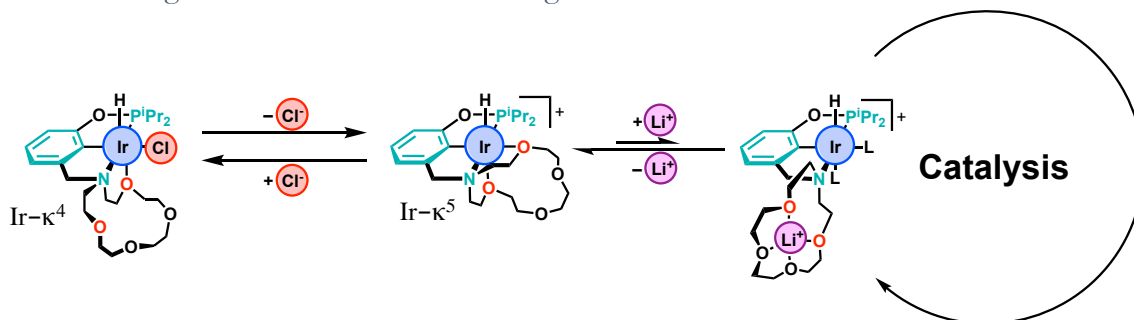
Pincer-crown ethers can assume a variety of binding modes, demonstrating its hemilabile

nature; metalation of the pincer-crown ether ligand yields a tetradentate (κ^4) iridium

hydridochloride pincer-crown ether complex, with 1 oxygen of the crown ether bound (Scheme

1.7, Ir-κ^4).[41] Abstracting the chloride yields a pentadentate (κ^5) cationic iridium pincer-crown

ether complex with two ethers bound (Scheme 1.7, Ir-κ^5).[41] The crown ether serves as a cationic

binding site, favoring a tridentate (κ^3) binding mode with both ethereal donors disassociated

from the transition metal center; added cation is proposed to regulate the equilibria between

ether-bound and free states and influence the rate of reactivity.

Controlling Catalytic Rates with Cationic Additives: Switchable and Tunable Regimes

Early studies investigating cation-controlled reactivity in iridium pincer-crown ethers

looked at deuterium scrambling into the cationic hydride complex. Without any cationic species

added, the half-life ($t_{1/2}$) for hydride signal decay under D_2 is 160 hrs. Upon the addition of 0.3

eq of NaBAr$^F_4$, the $t_{1/2}$ of hydride signal decay is reduced to 8 hrs, and upon the addition 0.4 eq

of LiBAr$^F_4$, $t_{1/2}$ was further reduced to 0.67 hrs.[41] The responsiveness to both cation identity and concentration observed in the system was the first indication of modulated dynamic hemilability, with the reaction rate tunable over two orders of magnitude depending on cation concentration and identity.

To apply cationic-modulated of catalytic activity towards productive catalysis, iridium-based isomerization of allylbenzene was explored. The chloride complex, Ir-κ^4, was found to be inactive to allylbenzene isomerization. Upon halide abstraction with 1 equiv. of NaBAr$^F_4$, the chloride anion is removed as NaCl, forming the cationic pentadentate complex, Ir-κ^5. This shows that the crown ether is under a static hemilabile regime by halide abstraction. Ir-κ^5 shows >96% conversion to β−methylstyrene over 141 hrs, This can be toggled *in situ*, by alternatively adding PPNCl and NaBAr$^F_4$, showing that *control of static hemilabilty* gives access to a *switchable catalytic regime* (Figure 1.2A).[42]
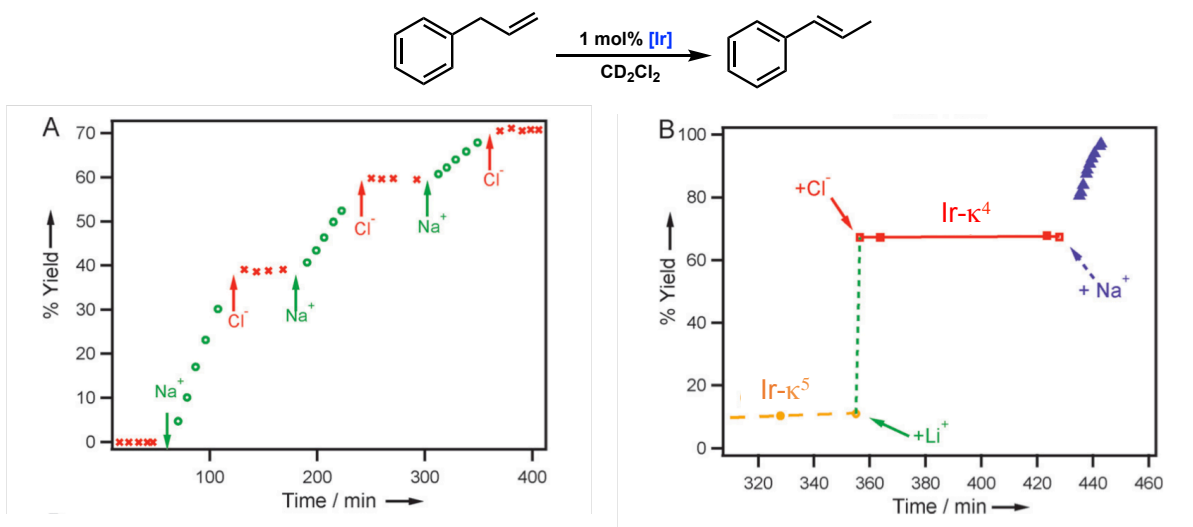
Figure 1.2. Controlling olefin isomerization using salt additives.
A. Switchable catalysis can be controlled by alternating addition of Na$^+$ salt, which opens up coordination to the metal center and increases the rate of isomerization through association with the crown ether. Addition of Cl$^-$ reverses the "switch", turning off catalysis. **B.** A four rate regime is demonstrated using various additives. Without any cation, isomerization of allylbenzene with Ir-κ^5 proceeds slowly. In the presence of Na$^+$ isomerization is fast, but is the fastest in the presence of Li$^+$ salts. Addition of Cl$^-$ turns off catalysis. Reproduced from Kita, M.

R.; Miller, A. J. M. M. An Ion-Responsive Pincer-Crown Ether Catalyst System for Rapid and Switchable Olefin Isomerization. Angew. Chemie - Int. Ed. 2017, 56 (20), 5498–5502. With permission from *Angewandte Chemie International Edition, © 2017.*

Upon addition of $LiBAr^F_4$ to Ir-κ^5, a dramatic (3 orders of magnitude) enhancement in the rate of isomerization is observed, showing the ability to control allyl benzene isomerization rates through addition of simple cationic additives. Furthermore, the Ir-κ^5 shows rates responsive to cation concentration and identity, allowing access to up three rate regimes with further modulation accessible depending on cation concentration added. By *controlling the dynamic hemilability* of the pincer-crown ether complex, *tunable catalysis* is able to be achieved (Figure 1.2B).[42] Thus, pincer-crown ether catalysts are capable of moving between a switchable and tunable catalytic regime, depending on the additives put into solution, and represent an excellent platform to generalize stimuli controllable catalysis in olefin isomerization reactions.

III.   Controlling Product Selectivity in Olefin Isomerization
Background and Challenges

Olefin isomerization is an intriguing fundamental reaction to explore the concept of controllable catalysis. Olefins are key chemical intermediates for the production of pharmaceuticals, fragrances, and natural products.[43–47] Terminal olefins are readily available synthons, which can then be isomerized to internal olefinic products.[48,49] If isomer selectivity can be controlled, isomerization represents an atom economical path to functionalized olefinic products.[50]

The availability of various isomers also acts as a challenge in catalyst design, as the thermodynamic differences between olefinic isomers are often small.[51] In the isomerization of 1-hexene to various internal isomers, the free energy difference between various internal isomers is <1 kcal/mol, demonstrating this difficulty.[52] Early isomerization efforts typically used metal salts, strong acids, or bases, at high temperatures to achieve thermodynamic isomeric

distributions, but suffered from poor selectivity and competing reactions (i.e. alkyl migrations, hydration, polymerization).[51,53–56]

Designing selectivity for a specific regio- and stereoisomer is an ongoing challenge; typically, a new catalyst is needed to alter product selectivity and reaction rates. Adding stimuli-responsive moieties to a catalytic framework for olefin isomerization offers a powerful way to control activity, further elaborating catalytic activity beyond synthetic modification. Given the efficacy of olefins as platforms to modulate regio- and stereoselectivity in subsequent derivation, controlling isomerization is an appealing way to elaborate geometries of subsequent functionalized products.[50]

Overview of Transition Metal Catalyzed Olefin Isomerization

Current efforts for olefin isomerization have focused on improving catalytic rates, functional group tolerance, and using mild conditions.[51] While many examples of allyl groups have been reported using organometallic platforms and demonstrate mild conditions needed to accomplish one bond isomerization across diverse functional groups,[54,57] an ongoing challenge for organometallic platforms is preserving activity and selectivity across substrates that have multiple possible products. Grotjahn and coworkers demonstrated an example of an alkene zipper, an impressive example of homogeneous catalysis capable of moving a double bond over 30 positions to a thermodynamic product (Scheme 1.8A).[58] In another example, Kochi and coworkers generated a cationic palladium-phenanthroline that was able to isomerize a terminal alkene over 20 position of siloxy functionalized alkenes at low catalytic loadings (Scheme 1.8B).[59] Such examples of isomerization of long chain alkenes are remarkable demonstrations of thermodynamic selectivity, accessing the thermodynamic product in reasonable time scales over a large number of bonds.

Scheme 1.8. Examples of alkene "zippers", moving double bonds over large numbers of bonds.
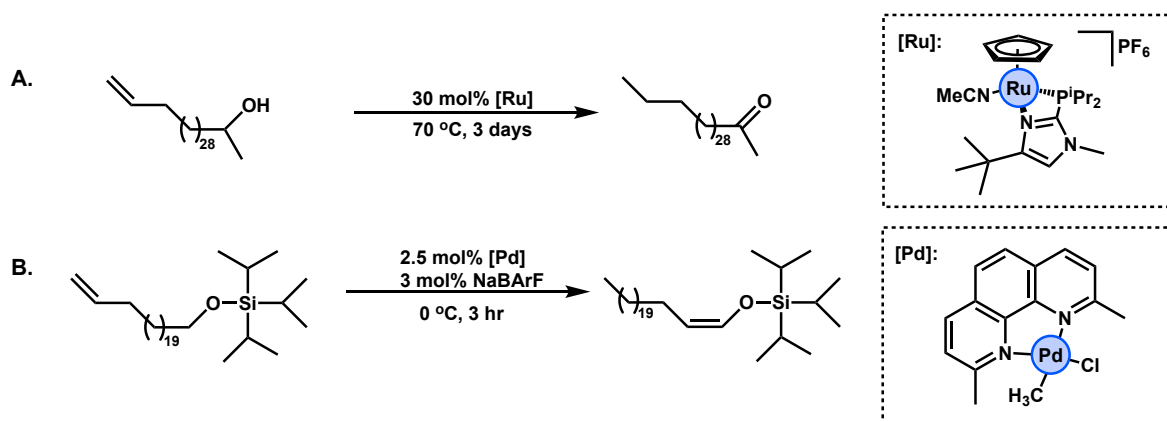
Given the small differences in energies of olefinic isomers, achieving high selectivity for kinetic products has garnered significant research interest. Huang and coworkers have shown an extremely E-selective iridium(I) pincer stabilized by agostic interactions, with E:Z ratios >20:1 (Scheme 1.9A).[60] Besides the high stereoselectivity, this system shows good substrate tolerance and selectivity for the one bond isomerization product. Shoenebeck and coworkers recently demonstrated a Ni(I) catalyst that yields high E selectivity across a wide range of substrates through a unique 1,3-hydrogen atom transfer mechanism.[46] In another example of a kinetically selective catalyst, Hilt and coworkers developed a Co(I) 1,3-bis(diphenylphosphino)propane ligand which isomerized 1-hexadecene to the Z stereoisomer (1:6 E:Z) in good yields.[61] Holland and coworkers also demonstrated a rare example of a one bond, Z selective catalysis using a sterically bulky high spin Co(II) catalyst (Scheme 1.9B).[62] While the selectivity for Z isomer is more modest and variable across substrates, accessing the thermodynamically unfavored Z isomer with reasonable selectivity is an impressive development. In a more recent report, Dobereiner and colleagues are able to access Z selectivity across a variety of functionalized olefins through *in situ* generation of Mo-H catalyst from air stable Mo(0) precatalysts.[63]

Scheme 1.9. Exempla of kinetically selective catalysts.
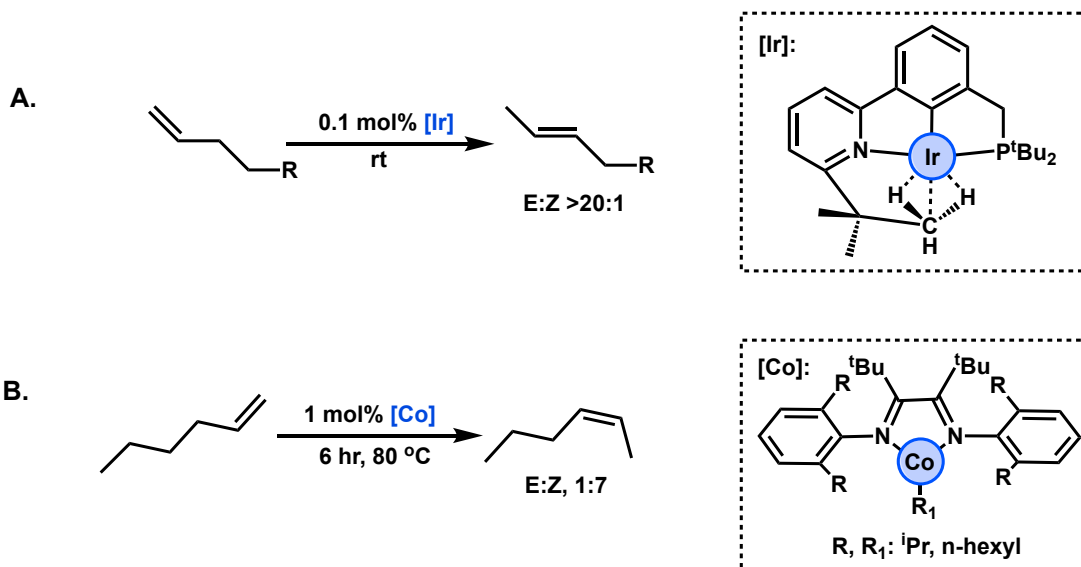
Changing Catalytic Activity in Olefin Isomerization

While remarkable achievements have been made selectively achieving one product, often very specific ligand optimization is required to access selectivity. Brookhart and Daugulis and coworkers utilized a sterically encumbered diimine-Pd sandwich catalyst to selectively perform a one bond isomerization (Scheme 1.10).[64] While professing near thermodynamic E selectivity (about 4:1 E:Z),[65] this example is notable in using synthetic modification to suppress polymerization and favor selective isomerization.

Scheme 1.10. Affecting reaction outcomes using ligand modfication.
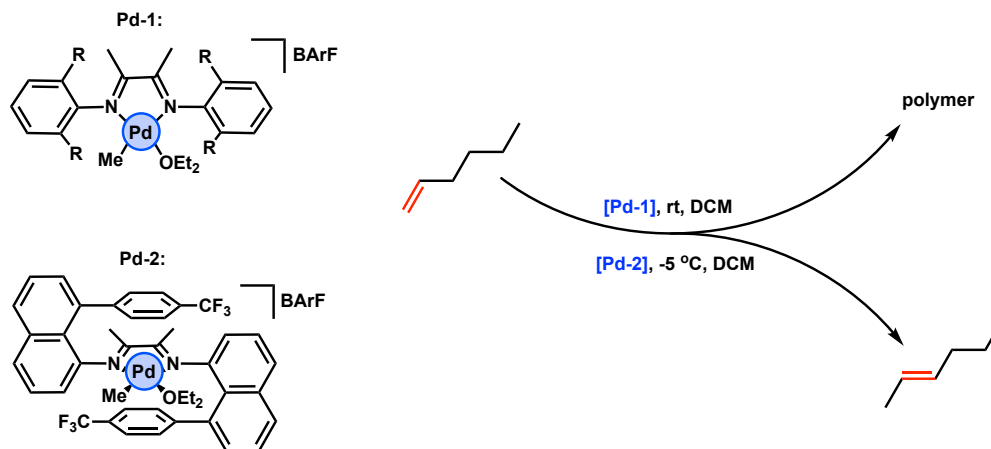
Synthesis is and will remain a powerful tool to elaborate metal-based reactivity. However, small changes to ligand scaffold can have a huge impact on selectivity. Liu and Jiao and coworkers used a cobalt amine pincer system to elegantly explore ligand modification on the isomerization activity in an olefinic precursor to (+)-Minfiensine (Table 1.1).[8] Starting with PNP isopropyl system (Co-I) no reactivity is observed. Replacing phosphine with a more labile pyridyl group (Co-II), yields a related PNN system capable of 99% conversion of the starting material and a modest 8:1 selectivity for the desired regioisomer. Increasing the steric bulk of the phosphine preserves activity (Co-III), but increases the selectivity of the desired isomer to 11:1. Interestingly, increasing the steric bulk of the pyridyl unit with a methyl group (Co-IV) completely shuts down reactivity (Table 1.1).[8] This example demonstrates difficulties in using synthetic modification to control catalytic activity and selectivity; while indeed a powerful tool to alter selectivity, minor synthetic modifications can completely alter reactivity. Creating multiple variants of a catalyst to modify reactivity creates additional burdens of characterization and synthesis of new catalytic species.

Table 1.1. Steric bulk influences catalytic outcomes of a Co-PNP system.
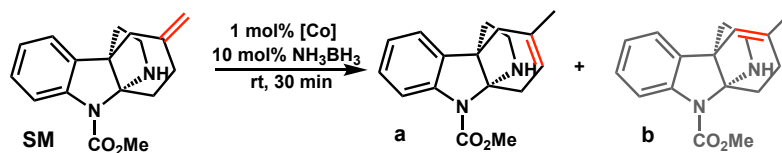
	[Co]:	Conversion SM%	a:b
I		0	–
II		99	8:1
III		99	11:1
IV		0	–

Grotjahn and coworkers are able to show a more dramatic change in catalyst selectivity using synthetic steric control. By moving to a bulkier methyl substituted cyclopentadienyl moiety (Cp*), the regioselectivity of the platform is able to be completely inverted in silyl ether substituted substrates while preserving high E selectivity; the increase in selectivity towards the one bond isomerization product is general feature of the Cp* system (Scheme 1.11).[65]

Scheme 1.11. Steric bulk dramatically influences regioselectivity in a Cp-Ru system.

A.

B.
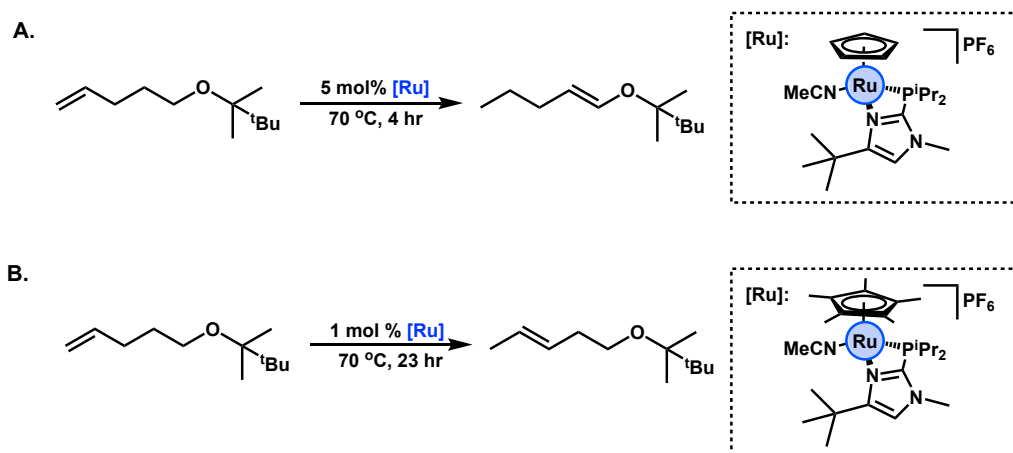
A less attested approach to controlling catalytic activity in olefin isomerization is to include stimuli-responsive moieties in the catalytic system. A dendrimer was decorated with a ferrocenyl ruthenium cymene complex to yield a redox-responsive catalytic system. Upon oxidation, an order of magnitude decrease in the rate of isomerization of 1-octen-3-ol to 3-octanone is observed, demonstrating *in situ* switchable catalysis using a redox couple.[66]

In another stimul-responsive system, light is used to access a switchable, one bond selective isomerization using cobalt and photosensitizer-based ligands. In this system, the photosensitizer/ligand is proposed to act as a photooxidant of a sacrificial reductant, which can then shuttle electrons to generate Co(I) *in situ*. Subsequent protonation yields a cobalt hydride, which can subsequently undergo alkene insertion chemistry to accomplish isomerization.[67] What sets this apart from previous examples of photoswitchable control of alkene isomerization is the access to both kinetic and thermodynamic products, depending on the choice of the photosensitizer/ligand (Scheme 1.12).

Scheme 1.12. Using ligand scaffold to control product selectivty in light driven isomerization.
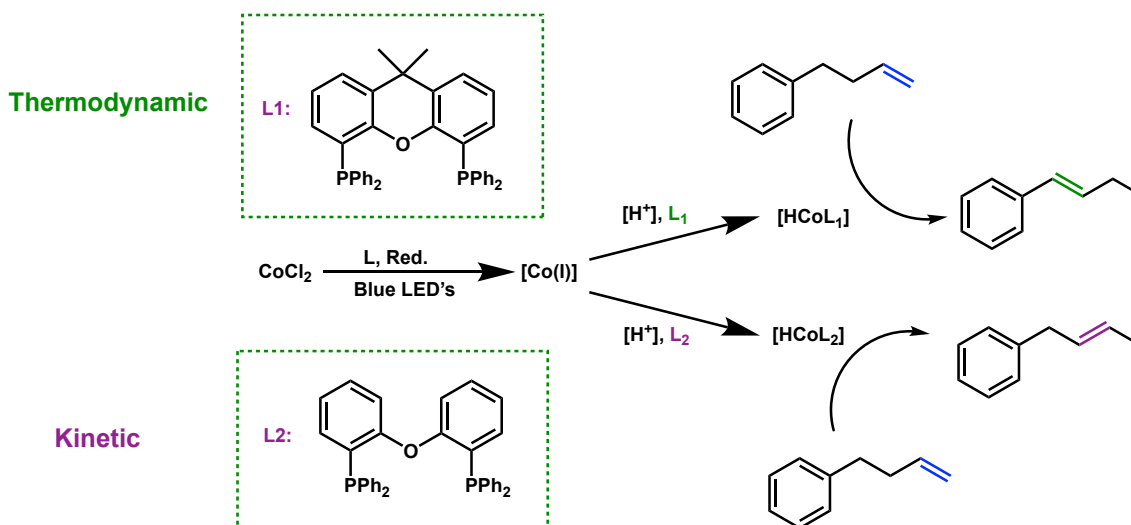
Finally, switchable catalysis provides an opportunity to change selectivity in tandem catalytic systems. Hartwig, Zhao, and coworkers demonstrate a tandem switchable photocatalytic system using iridium phenyl pyridine photosensitizers and ene-reductases. Without a photocatalyst, no reactivity is seen, but with a phototocatalyst under light, 83% yield of the R enantiomer is observed (Scheme 1.13).[68]

Scheme 1.13. Coupling photoisomerization to seletive hydrogenation.

[PC] (mol%)	Yield R (%)
None	0
5	83
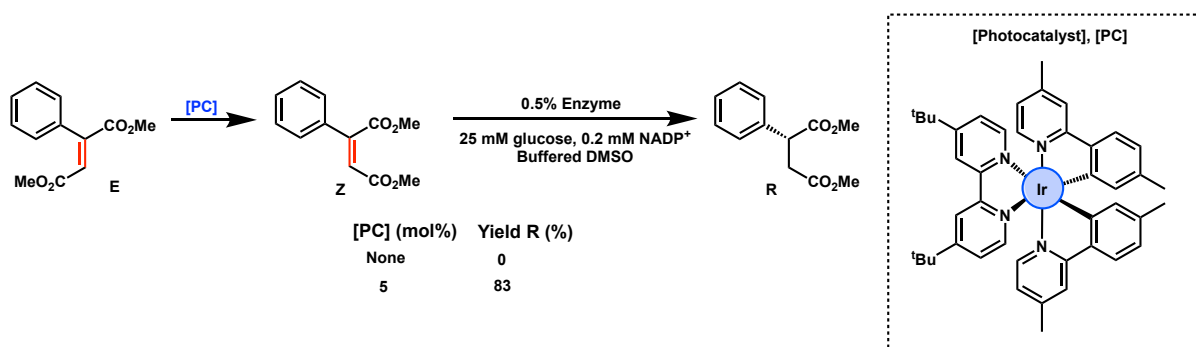
Despite the impressive control of selectivity, the general trend is that for one to access or change product selectivity, a new catalyst and ligand combination is required, followed by subsequent optimization of conditions. While indeed a powerful approach, the examples highlighted above

demonstrate not only the utility, but also the extensive characterization and screening needed to modulate activity using synthetic approaches.

Building Upon Existing Reactivity: Shedding New Light on Iridium Pincer Crown Ether Complexes

Given our ability to access cation-dependent reactivity using iridium pincer-crown ether complexes, we were interested in expanding the scope of substrates beyond aryl and alkyl olefinic species and using our ability to control reaction rates to alter selectivity. While functionalized olefins are valuable commodity chemicals, perfumes, and pharmaceuticals, [51] reactions with functionalized olefinic substrates can be challenging due to the coordination of groups on the substrate. Catalysts with hemilabile groups present unique challenges, as they include Lewis basic donors which could displace weak ethereal donors, possibly yielding a new species as the active catalyst.

This thesis examines various aspects of controlling catalysis using cation-crown interactions in iridium pincer-crown ether complexes. Understanding the spectral features of different binding modes of iridium-pincer crown ether complexes aids in the characterization of ligand coordination mode in the presence of strong donors. Binding affinity studies explored the cation-crown interaction and helped motivate synthesis of new, larger crown complexes for olefin isomerization. Using new insight gained from these studies, this work seeks to realize controllable product selectivity in functionalized olefins.

REFERENCES

(1)   Sweetlove, L. J.; Fernie, A. R. The Role of Dynamic Enzyme Assemblies and Substrate Channelling in Metabolic Regulation. *Nat. Commun.* **2018**, *9* (1) 2136-2148.

(2)   Sunley, G. J.; Watson, D. J. High Productivity Methanol Carbonylation Catalysis Using Iridium. The CativaTM Process for the Manufacture of Acetic Acid. *Catal. Today* **2000**, *58* (4), 293–307.

(3)   Smith, C.; Hill, A. K.; Torrente-Murciano, L. Current and Future Role of Haber-Bosch Ammonia in a Carbon-Free Energy Landscape. *Energy Environ. Sci.* **2020**, *13* (2), 331–344.

(4)   Shugrue, C.R.; Miller, S. J. Applications of Non-Enzymatic Catalysts to the Alteration of Natural Products. *Chem. Rev.* **2017**, *117* (18), 11894–11951.

(5)   Tsuji, J. Palladium Catalysis in Natural Product Synthesis. *Pure Appl. Chem.* **1981**, *53* (12), 2371–2378.

(6)   Copéret, C.; Chabanas, M.; Petroff Saint-Arroman, R.; Basset, J. M. Surface Organometallic Chemistry: Homogeneous and Heterogeneous Catalysis: Bridging the Gap through Surface Organometallic Chemistry. *Angew. Chemie - Int. Ed.* **2003**, *42* (2), 156–181.

(7)   Vougioukalakis, G. C.; Grubbs, R. H. Ruthenium-Based Heterocyclic Carbene-Coordinated Olefin Metathesis Catalysts †. *Chem. Rev.* **2010**, *110* (3), 1746–1787.

(8)   Liu, X.; Zhang, W.; Wang, Y.; Zhang, Z. X.; Jiao, L.; Liu, Q. Cobalt-Catalyzed Regioselective Olefin Isomerization under Kinetic Control. *J. Am. Chem. Soc.* **2018**, *140* (22), 6873–6882.

(9)   Goodey, N. M.; Benkovic, S. J. Allosteric Regulation and Catalysis Emerge via a Common Route. *Nat. Chem. Biol.* **2008**, *4* (8), 474–482.

(10)   Laskowski, R. A.; Gerick, F.; Thornton, J. M. The Structural Basis of Allosteric Regulation in Proteins. *FEBS Lett.* **2009**, *583* (11), 1692–1698.

(11)   Blanco, V.; Leigh, D. A.; Marcos, V. Artificial Switchable Catalysts. *Chem. Soc. Rev.* **2015**, *44* (15), 5341–5370.

(12)   Vlatković, M.; Collins, B. S. L.; Feringa, B. L. Dynamic Responsive Systems for Catalytic Function. *Chem. - A Eur. J.* **2016**, *22* (48), 17080–17111.

(13)   Vassalini, I.; Alessandri, I. Switchable Stimuli-Responsive Heterogeneous Catalysis. *Catalysts* **2018**, *8* (12), 569.

(14)   Ihrig, S. P.; Eisenreich, F.; Hecht, S. Photoswitchable Polymerization Catalysis: State of the Art, Challenges, and Perspectives. *Chem. Commun.* **2019**, *55* (30), 4290–4298.

(15) Sud, D.; Norsten, T. B.; Branda, N. R. Photoswitching of Stereoselectivity in Catalysis Using a Copper Dithienylethene Complex. *Angew. Chemie Int. Ed.* **2005**, *44* (13), 2019–2021.

(16) Neilson, B. M.; Bielawski, C. W. Photoswitchable Metal-Mediated Catalysis: Remotely Tuned Alkene and Alkyne Hydroborations. *Organometallics* **2013**, *32* (10), 3121–3128.

(17) Cacciapaglia, R.; Di Stefano, S.; Mandolini, L. The Bis-Barium Complex of a Butterfly Crown Ether as a Phototunable Supramolecular Catalyst. *J. Am. Chem. Soc.* **2003**, *125* (8), 2224–2227.

(18) Peterson, B. M.; Kottisch, V.; Supej, M. J.; Fors, B. P. On Demand Switching of Polymerization Mechanism and Monomer Selectivity with Orthogonal Stimuli. *ACS Cent. Sci.* **2018**, *4* (9), 1228–1234.

(19) Teator, A. J.; Lastovickova, D. N.; Bielawski, C. W. Switchable Polymerization Catalysts. *Chem. Rev.* **2016**, *116* (4), 1969–1992.

(20) Sarac, A. S. Redox Polymerization. *Prog. Polym. Sci.* **1999**, *24* (8), 1149–1204.

(21) Lorkovic, I. M.; Duff, R. R.; Wrighton, M. S. Use of the Redox-Active Ligand 1,1'phosphino) Cobaltocene To Reversibly Alter the Rate of the Rhodium(I)-Catalyzed Reduction and Isomerization of Ketones and Alkenes. *J. Am. Chem. Soc.* **1995**, *117* (12), 3617–3618.

(22) Hashmi, A. S. K. Gold-Catalyzed Organic Reactions. *Chem. Rev.* **2007**, *107* (7), 3180–3211.

(23) Gayen, A.; Leninger, M.; Traaseth, N. J. Protonation of a Glutamate Residue Modulates the Dynamics of the Drug Transporter EmrE. *Nat. Chem. Biol.* **2016**, *12* (3), 141–145.

(24) Balof, S. L.; P'Pool, S. J.; Berger, N. J.; Valente, E. J.; Shiller, A. M.; Schanz, H. J. Olefin Metathesis Catalysts Bearing a PH-Responsive NHC Ligand: A Feasible Approach to Catalyst Separation from RCM Products. *J. Chem. Soc. Dalt. Trans.* **2008**, 5791–5799.

(25) Hyo, J. Y.; Heo, J.; Mirkin, C. A. Allosteric Regulation of Phosphate Diester Transesterification Based upon a Dinuclear Zinc Catalyst Assembled via the Weak-Link Approach. *J. Am. Chem. Soc.* **2007**, *129* (46), 14182–14183.

(26) Kremer, C.; Lützen, A. Artificial Allosteric Receptors. *Chem-Eur. J.* **2013**, 6162–6196.

(27) Griffin, J. H.; Dervan, P. B. Metalloregulation in the Sequence Specific Binding of Synthetic Molecules to DNA. *J. Am. Chem. Soc.* **1987**, *109* (22), 6840–6842.

(28) De, S.; Pramanik, S.; Schmittel, M. A Monomer-Dimer Nanoswitch That Mimics the Working Principle of the SARS-CoV 3CLpro Enzyme Controls Copper-Catalysed Cyclopropanation. *Dalt. Trans.* **2014**, *43* (28), 10977–10982.

(29) Ouyang, G.-H.; He, Y.-M.; Li, Y.; Xiang, J.-F.; Fan, Q.-H. Cation-Triggered Switchable

Asymmetric Catalysis with Chiral Aza-CrownPhos. *Angew. Chemie Int. Ed.* **2015**, *54* (14), 4334–4337.

(30) Liu, X.; Yang, Y.; Shi, X.; Li, K. Fast Photocatalytic Degradation of Methylene Blue Dye Using a Low-Power Diode Laser. *J. Hazard. Mater.* **2015**, *283*, 267–275.

(31) Gao, D.; Zhou, H.; Cai, F.; Wang, D.; Hu, Y.; Jiang, B.; Cai, W. Bin; Chen, X.; Si, R.; Yang, F.; Miao, S.; Wang, J.; Wang, G.; Bao, X. Switchable CO2 Electroreduction via Engineering Active Phases of Pd Nanoparticles. *Nano Res.* **2017**, *10* (6), 2181–2191.

(32) Stratakes, B.; Miller, A. H2 Evolution at an Electrochemical "Underpotential" with an Iridium-Based Molecular Photoelectrocatalyst. *ACS Catal.* **2020**, *10*, 9006-9018.

(33) Balof, S. L.; Yu, B.; Lowe, A. B.; Ling, Y.; Zhang, Y.; Schanz, H. Eur. J. Inorg. Chem. 2009 · ©. **2009**.

(34) Miller, A. J. M. Controlling Ligand Binding for Tunable and Switchable Catalysis: Cation-Modulated Hemilability in Pincer-Crown Ether Ligands. *Dalt. Trans.* **2017**, *46* (36), 11987–12000.

(35) Riener, K.; Bitzer, M. J.; Pöthig, A.; Raba, A.; Cokoja, M.; Herrmann, W. A.; Kühn, F. E. On the Concept of Hemilability: Insights into a Donor-Functionalized Iridium(I) NHC Motif and Its Impact on Reactivity. *Inorg. Chem.* **2014**, *53* (24), 12767–12777.

(36) Yoo, C.; Dodge, H. M.; Miller, A. J. M. Cation-Controlled Catalysis with Crown Ether-Containing Transition Metal Complexes. *Chem. Commun.* **2019**, *55* (35), 5047–5059.

(37) Miller, A. J. M. Controlling Ligand Binding for Tunable and Switchable Catalysis: Cation-Modulated Hemilability in Pincer-Crown Ether Ligands. *Dalt. Trans.* **2017**, 11987–12000.

(38) Lindner, R.; Van Den Bosch, B.; Lutz, M.; Reek, J. N. H.; Van Der Vlugt, J. I. Tunable Hemilabile Ligands for Adaptive Transition Metal Complexes. *Organometallics* **2011**, *30* (3), 499–510.

(39) Hwan, J. L.; Smith, C. R.; RajanBabu, T. V. Facile Pd(II)- and Ni(II)-Catalyzed Isomerization of Terminal Alkenes into 2-Alkenes. *J. Org. Chem.* **2009**, *74* (12), 4565–4572.

(40) Gokel, G. W.; Leevy, W. M.; Weber, M. E. Crown Ethers: Sensors for Ions and Molecular Scaffolds for Materials and Biological Models. *Chem. Rev.* **2004**, *104* (5), 2723–2750.

(41) Kita, M. R.; Miller, A. J. M. Cation-Modulated Reactivity of Iridium Hydride Pincer-Crown Ether Complexes. *J. Am. Chem. Soc.* **2014**, *136* (41), 14519–14529.

(42) Kita, M. R.; Miller, A. J. M. An Ion-Responsive Pincer-Crown Ether Catalyst System for Rapid and Switchable Olefin Isomerization. *Angew. Chemie - Int. Ed.* **2017**, *56* (20), 5498–5502.

(43) Larsen, C. R.; Grotjahn, D. B. The Value and Application of Transition Metal Catalyzed Alkene Isomerization in Industry. In *Applied Homogeneous Catalysis with Organometallic Compounds*; Cornils, B., Herrmann, W. A., Beller, M., Paciello, R., Eds.; Wiley-VCH Verlag: Weinheim, Germany, 2018; pp 1365–1378.

(44) Wu, W.; Verkade, J. G. EtN=P(NMe$_2$)N=P(NMe$_2$)$_3$: An Efficient Non-Ionic Base Catalyst for the Isomerization of Allylic Compounds and Methylene-Interrupted Dienes. *Arkivoc* **2004**, *2004* (9), 88.

(45) Scarso, A.; Colladon, M.; Sgarbossa, P.; Santo, C.; Michelin, R. A.; Strukul, G. Highly Active and Selective Platinum(II)-Catalyzed Isomerization of Allylbenzenes: Efficient Access to (E)-Anethole and Other Fragrances via Unusual Agostic Intermediates. *Organometallics* **2010**, *29* (6), 1487–1497.

(46) Kapat, A.; Sperger, T.; Guven, S.; Schoenebeck, F. E-Olefins through Intramolecular Radical Relocation. *Science* **2019**, *396*, 391–396.

(47) Sharma, S. K.; Srivastava, V. K.; Jasra, R. V. Selective Double Bond Isomerization of Allyl Phenyl Ethers Catalyzed by Ruthenium Metal Complexes. *J. Mol. Catal. A Chem.* **2006**, *245* (1–2), 200–209.

(48) Mol, J. Industrial Applications of Olefin Metathesis. *J. Mol. Catal. A Chem.* **2004**, *213* (1), 39–45.

(49) Bidange, J.; Fischmeister, C.; Bruneau, C. Ethenolysis: A Green Catalytic Tool to Cleave Carbon–Carbon Double Bonds. *Chem. - A Eur. J.* **2016**, *22* (35), 12226–12244.

(50) Molloy, J. J.; Morack, T.; Gilmour, R. Positional and Geometrical Isomerisation of Alkenes: The Pinnacle of Atom Economy. *Angew. Chemie Int. Ed.* **2019**, *58* (39), 13654–13664.

(51) Paulson, E. R.; Grotjahn, D. B. Isomerization and Hydrogenation of Alkenes. *Encycl. Inorg. Bioinorg. Chem.* **2017**, 1–25.

(52) Winston, M. S.; Oblad, P. F.; Labinger, J. A.; Bercaw, J. E. Activator-Free Olefin Oligomerization and Isomerization Reactions Catalyzed by an Air- and Water-Tolerant Wacker Oxidation Intermediate. *Angew. Chemie - Int. Ed.* **2012**, *51* (39), 9822–9824.

(53) Hay, R. G.; Montgomery, C. W.; Coull, J. Catalytic Isomerization of 1-Hexene. *Ind. Eng. Chem.* **1945**, *37* (4), 335–339.

(54) Hassam, M.; Taher, A.; Arnott, G. E.; Green, I. R.; Van Otterlo, W. A. L. Isomerization of Allylbenzenes. *Chem. Rev.* **2015**, *115* (11), 5462–5569.

(55) Dunning, H. N. Review of Olefin Isomerization. *Ind. Eng. Chem.* **1953**, *45* (3), 551–564.

(56) Sparke, M. B.; Turner, L.; Wenham, A. J. M. The Isomerization of Olefins by Palladium Complexes. *J. Catal.* **1965**, *4*, 332–3340.

(57)   Krompiec, S.; Krompiec, M.; Penczek, R.; Ignasiak, H. Double Bond Migration in N-Allylic Systems Catalyzed by Transition Metal Complexes. *Coord. Chem. Rev.* **2008**, *252* (15–17), 1819–1841.

(58)   Grotjahn, D. B.; Larsen, C. R.; Gustafson, J. L.; Nair, R.; Sharma, A. Extensive Isomerization of Alkenes Using a Bifunctional Catalyst: An Alkene Zipper. *J. Am. Chem. Soc.* **2007**, *129* (31), 9592–9593.

(59)   Yamasaki, Y.; Kumagai, T.; Kanno, S.; Kakiuchi, F.; Kochi, T. Selective Long-Distance Isomerization of Terminal Alkenes via Nondissociative Chain Walking. *J. Org. Chem.* **2018**, *83* (16), 9322–9333.

(60)   Wang, Y.; Qin, C.; Jia, X.; Leng, X.; Huang, Z. An Agostic Iridium Pincer Complex as a Highly Efficient and Selective Catalyst for Monoisomerization of 1-Alkenes to Trans-2-Alkenes. *Angew. Chemie - Int. Ed.* **2017**, *56* (6), 1614–1618.

(61)   Schmidt, A.; Nödling, A. R.; Hilt, G. An Alternative Mechanism for the Cobalt-Catalyzed Isomerization of Terminal Alkenes to (Z)-2-Alkenes. *Angew. Chemie - Int. Ed.* **2015**, *54* (3), 801–804.

(62)   Chen, C.; Dugan, T. R.; Brennessel, W. W.; Weix, D. J.; Holland, P. L. Z -Selective Alkene Isomerization by High-Spin Cobalt(II) Complexes. *J. Am. Chem. Soc.* **2014**, *136* (3), 945–955.

(63)   Becica, J.; Glaze, O. D.; Wozniak, D. I.; Dobereiner, G. E. Selective Isomerization of Terminal Alkenes to (Z)-2-Alkenes Catalyzed by an Air-Stable Molybdenum(0) Complex. *Organometallics* **2018**, *37* (3), 482–490.

(64)   Kocen, A. L.; Klimovica, K.; Brookhart, M.; Daugulis, O. Alkene Isomerization by "Sandwich" Diimine-Palladium Catalysts. *Organometallics* **2017**, *36* (4), 787–790.

(65)   Larsen, C. R.; Erdogan, G.; Grotjahn, D. B. General Catalyst Control of the Monoisomerization of 1-Alkenes to Trans -2-Alkenes. *J. Am. Chem. Soc.* **2014**, *136* (4), 1226–1229.

(66)   Neumann, P.; Dib, H.; Caminade, A. M.; Hey-Hawkins, E. Redox Control of a Dendritic Ferrocenyl-Based Homogeneous Catalyst. *Angew. Chemie - Int. Ed.* **2015**, *54* (1), 311–314.

(67)   Meng, Q.; Schirmer, T. E.; Katou, K.; König, B. Controllable Isomerization of Alkenes by Dual Visible-Light-Cobalt Catalysis. *Angew. Chemie* **2019**, *131* (17), 5779–5784.

(68)   Litman, Z. C.; Wang, Y.; Zhao, H.; Hartwig, J. F. Cooperative Asymmetric Reactions Combining Photocatalysis and Enzymatic Catalysis. *Nature* **2018**, *560* (7718), 355–359.

CHAPTER 2. MAPPING THE BINDING MODES OF HEMILABILE PINCER−CROWN ETHER LIGANDS IN SOLUTION USING DIAMAGNETIC ANISOTROPIC EFFECTS ON NMR CHEMICAL SHIFT

I.   Introduction

Multiple Binding Modes of Hemilabile Ligands

Hemilabile ligands have emerged as broad and versatile tools in coordination chemistry.[1] As chelates with a weak donor that can dissociate or be displaced from the metal center, hemilabile ligands balance the stability of coordinatively saturated metal complexes with the activity provided by facile ligand substitution at the weak donor site. This balance has been particularly fruitful in the preparation of catalysts with high activity and good stability[2−4] as well as catalysts that can be recycled through control of the hemilabile ligand binding mode.[5,6]

In pursuit of catalysts that can be tuned using cationic additives, we have developed "pincer−crown ether" ligands that contain an aza-crown ether macrocycle capable of multiple hemilabile coordination modes.[7−9] As shown in Scheme 2.1, pincer−crown ether ligands can adopt a tridentate (κ^3) binding mode like that of traditional pincer ligands, or weak ether donors can bind to reach tetradentate (κ^4) or pentadentate (κ^5) binding modes.[10]

It can be challenging to characterize the different binding modes of hemilabile ligands in solution. The weak donors can bind to the metal center, dissociate to form a low-coordinate species, or be displaced by a solvent or another external donor ligand. In some cases, the binding modes interconvert rapidly ("dynamic hemilability"), while in other cases isomerization can be slow or require a chemical impetus ("static hemilability").[7,11] Crystallographic characterization

can readily identify binding modes in the solid state.[7,12] It is more difficult to probe the binding

mode of a hemilabile ligand in solution.

Scheme 2.1. Pincer—Crown Ether Ligand Binding Modes and Effect of Diamagnetic Anisotropy on Proximal Protons.
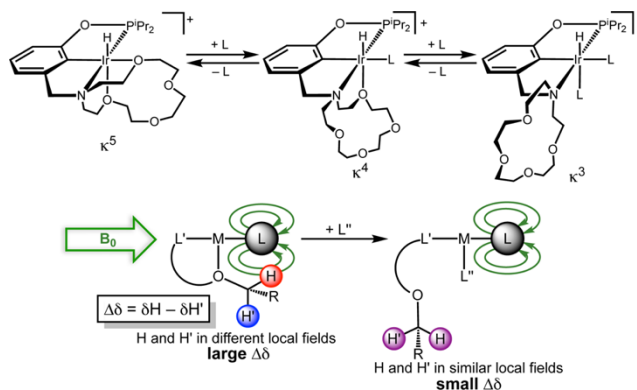
In this work, a collection of well-defined pincer—crown ether complexes has been used to

develop a new NMR protocol for identifying the coordination mode of these hemilabile ligands

in solution. The protocol connects the hemilabile ligand coordination mode to chemical shift

differences based on the presence of diamagnetic anisotropy induced by other ligands at the

metal center. Diamagnetic anisotropy influences chemical shifts through the field-induced

movement of paired electrons, which generates local secondary fields.[13] This differs from

paramagnetic anisotropy, which influences chemical shifts over hundreds of parts per million

(ppm) through field-induced movement of unpaired electrons.[14] Diamagnetic anisotropic effects

from organic arenes,[15] carbonyls,[16] and nitriles[17] have been shown to significantly influence

chemical shifts, thus providing valuable structural information on complex organic molecules

and proteins in solution.[14,18,19] While not used routinely in inorganic systems, diamagnetic

anisotropy has been productively applied to structural determination of ruthenium(II)

diastereomers,[20] characterization of metal−metal quadruple bonds,[21] and the orientation of complexes of the type (arene)M(CO)$_3$.[22,23]

In pincer−crown ether ligands, the chemical shifts of geminal protons in the crown are sensitive to the proximity of the macrocycle to other ligands bound to the metal. The difference in chemical shift between geminal protons ($\Delta\delta$) can serve as a marker of the coordination mode (Scheme 2.1). Focusing on pincer−crown ether complexes as a convenient development platform, a protocol for gaining insight into hemilabile ligand coordination mode is developed on the basis of a concise series of routine and inexpensive NMR experiments.

II.   Synthetic Access to Different Binding Modes

Synthesis and Characterization of Halide-Containing Pincer−Crown Ether Complexes

Synthetic routes to a large array of pincer−crown ether complexes with different coordination modes of the pincer−crown ether ligand are shown in Scheme 2.2. As discussed in the following paragraphs, complexes **3**, **4**, **5**, and **6-trans** have not been previously characterized. The ligand coordination modes of several complexes have been assigned on the basis of solid-state crystallographic studies. NMR spectroscopic studies suggest that the coordination mode is maintained in solution for noncoordinating solvents such as chloroform and dichloromethane, as detailed below.

The previously reported iridium hydride [κ^5-(^{15c5}NCOP^{iPr})Ir(H)][BAr$^F_4$] (**1**) adopts a pentadentate binding mode, with two crown ether oxygen atoms binding the metal center, both in the solid state and in noncoordinating, chlorinated solvents.[7] Hydride resonances in ^{1}H NMR spectra provide a convenient marker of solution-phase structure. The ligand *trans* to the hydride has a big impact on the chemical shift of the hydride resonance.[24] The hydride in **1** has a ^{1}H

NMR chemical shift (δ −30.03) in CDCl₃ that is indicative of an ether donor *trans* to the hydride.[25]

Scheme 2.2. Moving Between the Binding of Pincer-Crown Ether Ligands.
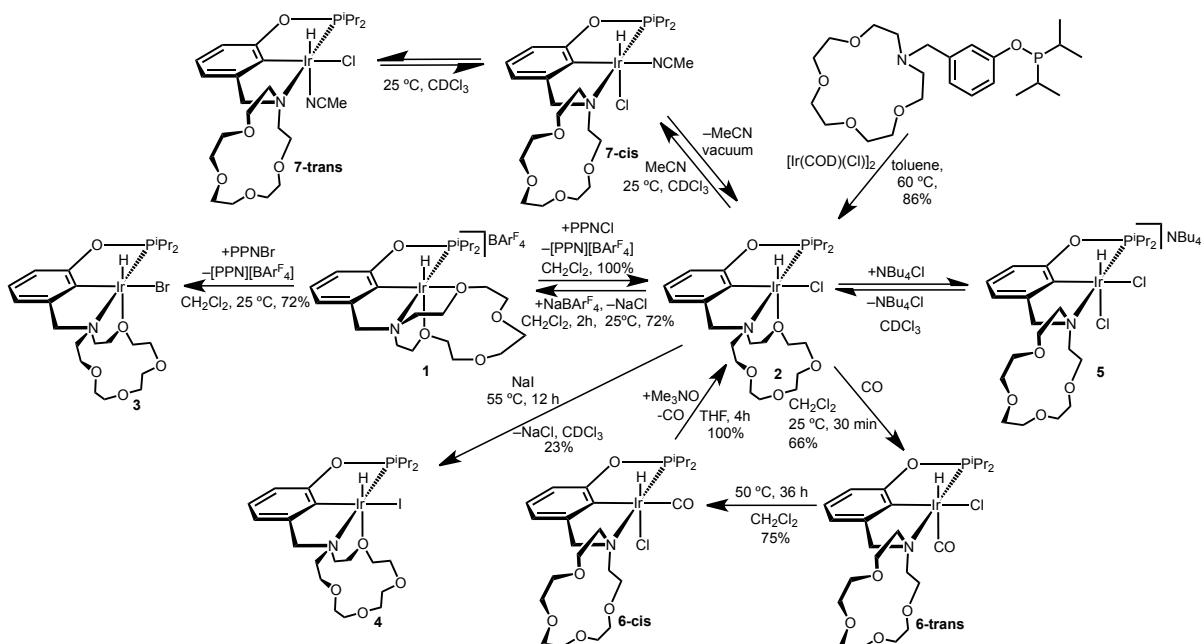
The pentadentate-bound complex **1** serves as a convenient starting place for examining changes in binding mode, as the weak ether donors can undergo ligand substitution reactions. Addition of 1 equiv of PPNCl (PPN = bis-(triphenylphosphine)iminium) to cationic hydride complex **1** in CH₂Cl₂ (Scheme 2) has been shown to yield the tetradentate-bound chloride complex κ⁴-(¹⁵ᶜ⁵NCOPⁱᴾʳ)Ir(H)(Cl) (**2**) featuring one ether bound to Ir.[26] Complex **2** can also be accessed by metalation of the pincer ligand with [Ir(COD)(Cl)]₂.[7] A crystallographic study previously established that the pincer ligand in **2** adopts a tetradentate binding mode in the solid state.[7] In CDCl₃ solution, compound **2** is characterized by a hydride resonance (δ −31.26) consistent with the weak ether donor remaining in the site *trans* to the hydride. The chloride can be abstracted from **2** with 1 equiv of NaBArᶠ₄ to reform **1** (Scheme 2.2).[7]

Tetradentate-bound complexes of other halides were also targeted. Addition of PPNBr to a solution of **1** in CH_2Cl_2 at room temperature yields a new bromide complex, κ^4–($^{15c5}NCOP^{iPr}$)Ir(H)(Br) (**3**), in 72% yield (Scheme 2.2). Successful incorporation of bromide was confirmed by high-resolution mass spectrometry (HRMS). The hydride resonance (δ −31.23) is consistent with a tetradentate pincer coordination mode with the ether donor trans to the hydride.

The analogous iodide complex was prepared in a different manner, via halide exchange in **2**. Heating a solution of **2** in $CDCl_3$ in the presence of excess NaI yields κ^4-($^{15c5}NCOP^{iPr}$)-Ir(H)(I) (**4**) (Scheme 2.2), as confirmed by HRMS studies. The hydride resonance (δ −31.20) has a chemical shift that is almost identical to that of **3**, suggesting an analogous tetradentate structure in solution.

Complexes with a meridional tridentate binding mode of the pincer ligand are accessible from the hydridochloride **2**. Sequential addition of portions of NBu_4Cl to **2** leads to a new species identified as the anionic dichloride κ^3-[($^{15c5}NCOP^{iPr}$)Ir(H)(Cl)$_2$]$^-$ (**5**) (Scheme 2.2). The growth of a new hydride peak downfield of **2** (δ −24.4) suggests that chloride has displaced the ether ligand. More than 150 equiv of NBu_4Cl was required to reach 99% conversion, precluding isolation of **5**.

Binding of CO was then investigated. When a pale-yellow solution of **2** in CH_2Cl_2 is placed under 1 atm CO at room temperature, the color immediately fades. Two products, observed in a 15:1 ratio, are assigned as *trans*-κ^3-($^{15c5}NCOP^{iPr}$)Ir(H)(Cl)(CO) (**6-trans**) and *cis*-κ^3-($^{15c5}NCOP^{iPr}$)Ir(H)(CO)(Cl) (**6-cis**) (Scheme 2.2). The major species, **6-trans**, features a hydride resonance characteristic of a carbonyl *trans* to the hydride (δ −7.02; cf. the hydride resonance of **6-cis** at δ −19.22). In the ^{13}C NMR spectrum of **6-trans**, the carbonyl carbon appears as a doublet of doublets (δ 178.88, $^2J_{HC}$ = 56.6 Hz, $^2J_{PC}$ = 3.4 Hz) with the strong carbon−proton

coupling expected in a trans-hydridocarbonyl geometry. Isomer **6-cis** shows only coupling attributed to phosphorus (δ 180.76, $^2J_{PC}$ = 4.6 Hz). Single crystals of **6-trans** suitable for an X-ray diffraction (XRD) study grew after pentane was layered over a concentrated solution of **6-trans** in toluene. The solid-state structure of **6-trans** (Figure 2.1A) features no crown ether oxygen interactions with the iridium center, confirming a tridentate binding mode of the pincer ligand.
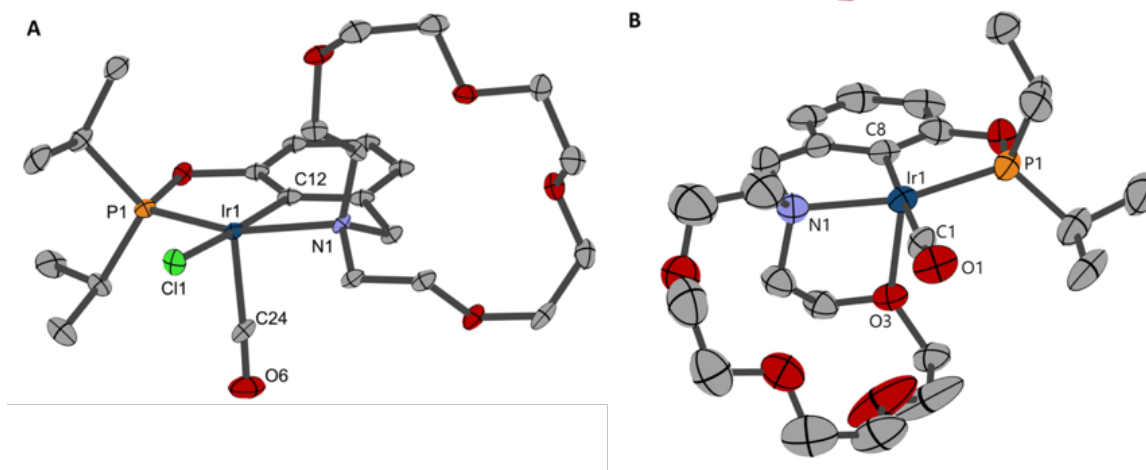
Figure 2.1. Crystal structures of new iridium pincer complexes.
Structural representations of **6-trans** (**A**) and one of the two independent cations of **8** in the asymmetric unit (**B**), with ellipsoids drawn at the 50% probability level. Hydrogen atoms and counterions have been omitted for clarity. A 14% substitutional disorder of CO and Cl ligands was observed for **6-trans**, consistent with some cocrystallized **6-cis**.
.

The coordination isomer **6-cis**, with the carbonyl *cis* to the hydride, was previously characterized (including an XRD study confirming the expected κ^3 binding mode) as the sole product of metalation of the free pincer−crown ether ligand with $Ir(CO)_2(Cl)(p\text{-toluidine})$ in refluxing toluene.[8] Hypothesizing that **6-trans** was the kinetic product of ether displacement from **2**, the 15:1 **6-trans**/**6-cis** mixture was heated at 50 °C for 36 h. Thermal redistribution of the isomers resulted in a 1:3 ratio favoring the **6-cis** isomer. Heating isolated samples of pure **6-cis** did not produce detectable levels of **6-trans**, suggesting that **6-cis** is the thermodynamic

product. This is consistent with prior reports of iridium hydridocarbonyl chloride complexes.[27–29]

The carbonyl ligands of **6-trans** and **6-cis** are stable under prolonged exposure to dynamic vacuum at room temperature. However, the carbonyl ligand of **6-cis** can be removed using trimethylamine N-oxide, a decarbonylation reagent that has been successfully applied to other systems.[30] Stirring **6-cis** and Me_3NO in THF for 48 h provides a new route to move between coordination modes, generating **2** as the only hydride containing species according to ^1H NMR spectroscopy. The expected trimethylamine byproduct was present as a singlet at δ 2.11 (Scheme 2.2).

Acetonitrile has been previously shown to bind to hydridochloride **2**, producing an equilibrium mixture comprising the starting material **2** and the two coordination isomers trans-κ^3-($^{15c5}NCOP^{iPr}$)Ir(H)(Cl)(NCCH$_3$) (**7-trans**) and cis-κ^3-($^{15c5}NCOP^{iPr}$)Ir(H)(NCCH$_3$)(Cl) (**7-cis**). Applying dynamic vacuum to the mixture at room temperature regenerates **2** (Scheme 2.2).[7]

Synthesis and Characterization of Carbonyl-Containing Pincer–Crown Ether Complexes

A larger array of carbonyl complexes could be accessed conveniently from pentadentate- bound **1**, as shown in Scheme 2.3. Placing 1 under 1 atm CO in CDCl$_3$ leads to a mixture of two products at room temperature. The minor product is assigned as the new cationic hydridocarbonyl [κ^4-($^{15c5}NCOP^{iPr}$)Ir(H)(CO)][BAr$^F_4$] (**8**), which exhibits a tetradentate binding mode with an ether donor *trans* to the hydride (δ −25.79). The major product is assigned as the new dicarbonyl complex [κ^3-($^{15c5}NCOP^{iPr}$)Ir(H)(CO)$_2$][BAr$^F_4$] (**9**) on the basis of the downfield hydride resonance at δ −9.43, which is indicative of a strong donor *trans* to the hydride.

Exposing the mixture of **8** and **9** to dynamic vacuum at room temperature yields **8** as the exclusive product. Crystals of **8** suitable for an X-ray diffraction study were grown by slow

evaporation of an Et₂O solution. Figure 2.1B shows that **8** adopts a tetradentate binding mode in the solid state, with a crown ether oxygen donor *trans* to the hydride.

Scheme 2.3. Synthetic access to a family of carbonyl containing pincer-crown complexes.
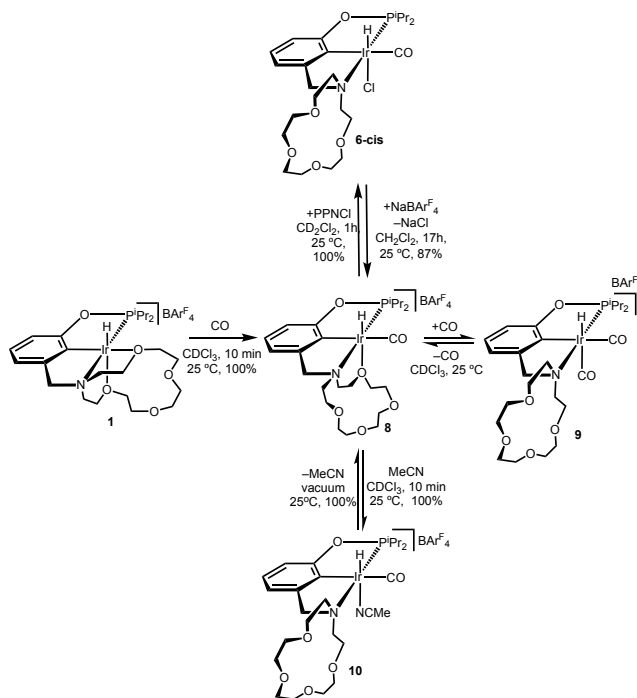
A mixed ligand system with a tridentate binding mode is accessible by addition of excess acetonitrile to **8** in CDCl₃ to yield [κ³-(¹⁵ᶜ⁵NCOPⁱᴾʳ)Ir(H)(CO)(NCCH₃)][BArᶠ₄] (**10**).[8] The hydride peak shifts to an intermediate range (δ −19.83) when acetonitrile displaces the ether donor. The acetonitrile ligand can be removed under dynamic vacuum to regenerate the tetradentate hydridocarbonyl complex **8**.

Addition of 1 equiv of PPNCl to monocarbonyl **8** in CH₂Cl₂ leads to the hydridocarbonyl chloride complex **6-cis** after 1 hr (NMR spectroscopy). This reaction offers yet another route to complex **6-cis**; the same species can also be accessed by addition of CO to hydridochloride **2** followed by thermolysis (see above) or by direct metalation of the free ligand

with a carbonyl precursor.[8] Abstracting the chloride from **6-cis** with 1 equiv of NaBAr$^F_4$ in CH$_2$Cl$_2$ generates **8** (Scheme 2.3).

Summary of Iridium Pincer−Crown Ether Substitution Reactions

Many iridium pincer−crown ether species are accessible by several different synthetic routes, and almost every reaction can be reversed by applying a vacuum or through a chemical reaction. Ligands beyond halides and carbon monoxide have also been explored and are included for the NMR studies that follow.

Table 2.1. New cationic complex of iridium pincer-crown ethers.
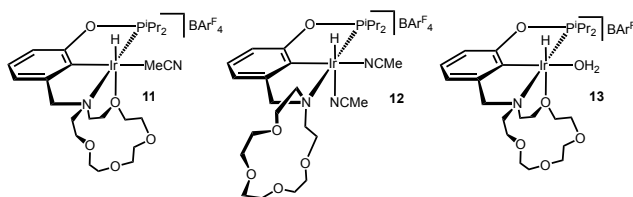
The complexes in Table 2.1 have been previously prepared by addition of a ligand to complex **1**. The tetradentate-bound acetonitrile complex [κ^4-(^{15c5}NCOP^{iPr})Ir(H)(NCCH$_3$)]-[BAr$^F_4$] (**11**) and the tridentate-bound bis(acetonitrile) complex [κ^3-(^{15c5}NCOP^{iPr})Ir(H)(NCCH$_3$)$_2$][BAr$^F_4$] (**12**) can be prepared using different amounts of acetonitrile.[7] Water can also bind to **1** to generate another tetradentate-bound species, [κ^4-(^{15c5}NCOP^{iPr})Ir(H)(H$_2$O)][BAr$^F_4$] (**13**).[7]

The wide variety of pincer−crown ether coordination modes and the range of available exogenous ligands make this system ideal for NMR studies probing hemilabile ligand binding mode

III.　　　　　NMR Methods for Identifying Pincer-crown Ether Coordination Mode

Assignment of Crown Ether Protons

In hopes of identifying a simple NMR protocol for distinguishing between different hemilabile ligand coordination modes, we first performed a full assignment on just a few selected pincer−crown ether complexes. Routine characterization always involves the acquisition of ^{1}H, ^{31}P{^{1}H}, and ^{13}C{^{1}H} NMR spectra. Full proton assignments for **1, 2, 3, 6,** and **8** were made using a combination of multidimensional experiments, including ^{1}H−^{13}C HSQC, ^{1}H−^{13}C HSQC-TOCSY, ^{1}H−^{1}H COSY, and ^{1}H−^{13}C HMBC.
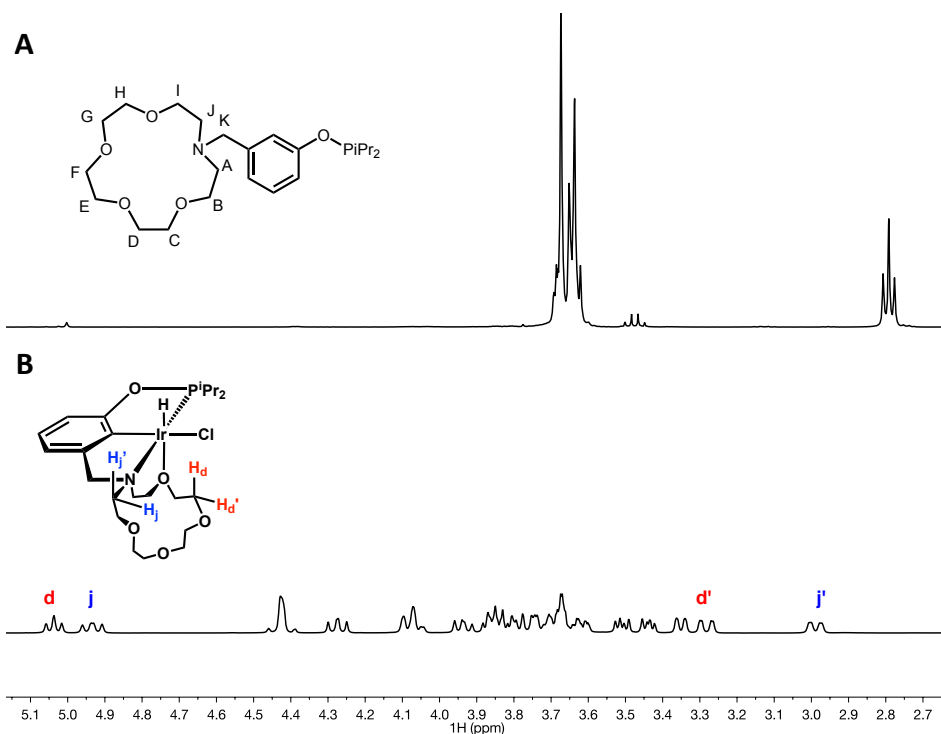
Figure 2.2. Comparison of ^{1}H NMR spectra (crown ether region) of the free ligand and **2** Atom labels are consistent across all complexes.

The ^{1}H NMR spectrum of the free ligand is shown in Figure 2.2A. The labeling scheme for all of the complexes is shown in Figure 2.2A; carbon atoms are labeled with uppercase letters, and hydrogen atoms are given lowercase letters (e.g., C_A and H_a/ $H_{a'}$). The crown ether region of the free ligand is crowded with 16 overlapping proton resonances centered at δ 3.63

and a triplet at δ 2.76 (4H integration). The upfield resonance is characteristic of a pair of equivalent methylene groups adjacent to nitrogen.[31]

The chloride complex **2** features a well-resolved ^{1}H NMR spectrum with resonances spanning a wide range (Figure 2.2B). Nuclear Overhauser effect spectroscopy (NOESY) studies confirmed that a tetradentate coordination mode is maintained in solution (Figure 2.3). Through-space coupling between the isopropyl methyl protons and crown ether protons indicates that the macrocycle adopts a conformation that places methylene protons near the metal center. Such NOE interactions have not been observed in the free ligand or in complexes that adopt a tridentate coordination mode.
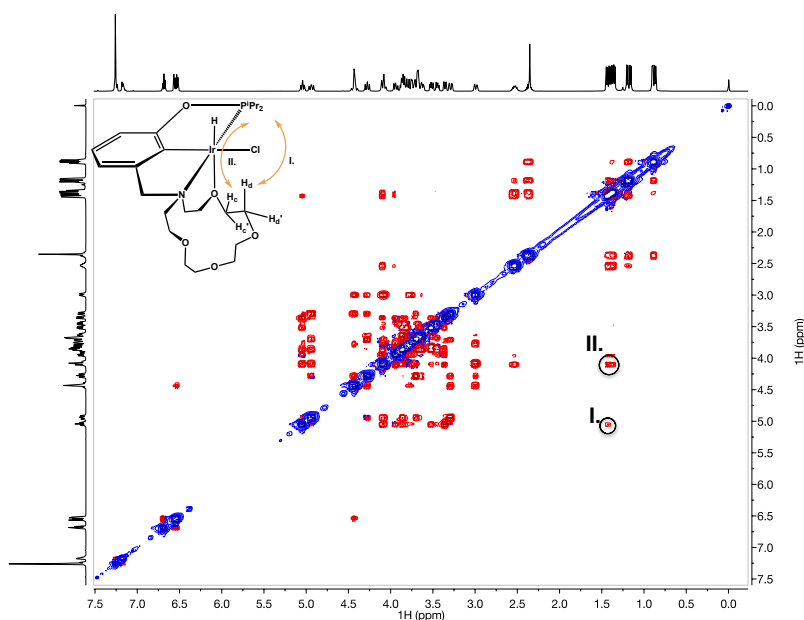
Figure 2.3. [1]H-^{1}H NOESY spectrum of **2**.
Cross-peaks between methyl protons of the isopropyl group and H_d (I) and H_c (II) support a tetradentate binding mode.

Complex **2** features two crown ether protons that are shifted dramatically downfield (H_d and H_j; Figure 2.2B). Downfield shifts have been observed in chelating ethers in Ir complexes,[32] so it would be reasonable to assign these resonances as the protons closest to the metal center. However, multinuclear, two-dimensional NMR analysis revealed that the most downfield crown

ether resonances correspond to two protons that are not adjacent to the metal center – they are

in fact *far* apart in the macrocycle.
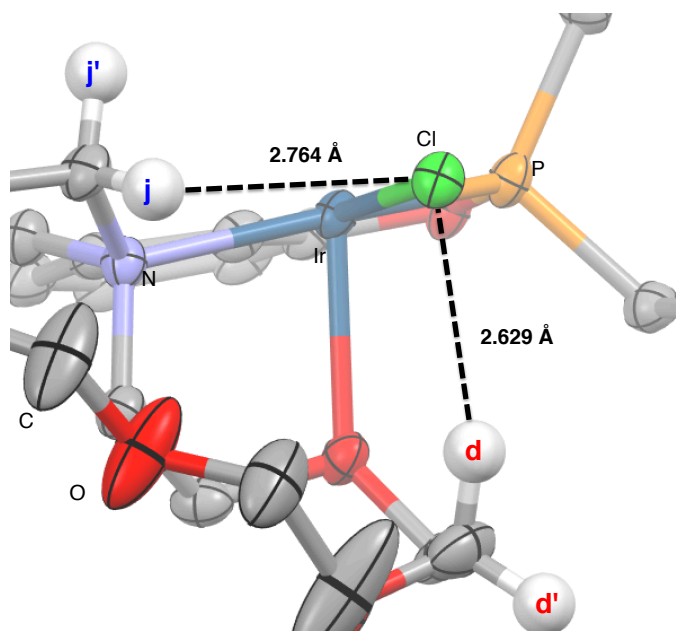
Figure 2.4. Molecular representation of **2** (from X-ray crystallographic data)[7] showing proximity of protons H_j and H_d to the chloride ligand.

Comparisons with crystallographic data show that downfield protons H_d and H_j in **2** are

in close proximity to the chloride ligand in the solid-state structure. As shown in Figure 2.4, the

$Cl-H_d$ and $Cl-H_j$ distances are 2.629 and 2.764 Å, respectively. On the other hand, the other

protons of these geminal pairs ($H_{d'}$ and $H_{j'}$) are oriented away from the group in space. The

resonances for H_d' and $H_{j'}$ are found in the typical region for ethers, leading to chemical shift

differences between the diastereotopic geminal protons ($\Delta\delta$) of 1.69 ppm ($\Delta\delta_{d/d'}$) and 1.65 ppm

($\Delta\delta_{j/j'}$). The data suggest that chloride anisotropy is responsible for the large downfield shifts for

H_d and H_j in **2** (δ 5.04 and δ 4.93, respectively, in Figure 2.2B) and the large $\Delta\delta$ values for the

geminal pairs.

If the downfield resonances of **2** are due to diamagnetic anisotropy of the chlorine lone

pairs, larger halogens should have a more dramatic effect on the chemical shifts.[33] In the

analogous bromide complex κ^4-(^{15c5}NCOP^{iPr})Ir(H)(Br) (**3**), the same protons H_d and H_j are further deshielded to δ 5.05 and δ 5.11, respectively. The differences in chemical shift between the two geminal protons increase as well ($\Delta\delta_{d/d'} = 1.72$ ppm and $\Delta\delta_{j/j'} = 1.84$ ppm). Similarly, the iodide complex κ^4-(^{15c5}NCOP^{iPr})Ir(H)(I) (**4**) features downfield crown ether resonances at δ 5.29 and δ 5.04 and even larger differences in chemical shift for the diastereotopic protons ($\Delta\delta_{d/d'} = 1.79$ ppm and $\Delta\delta_{j/j'} = 2.06$ ppm).
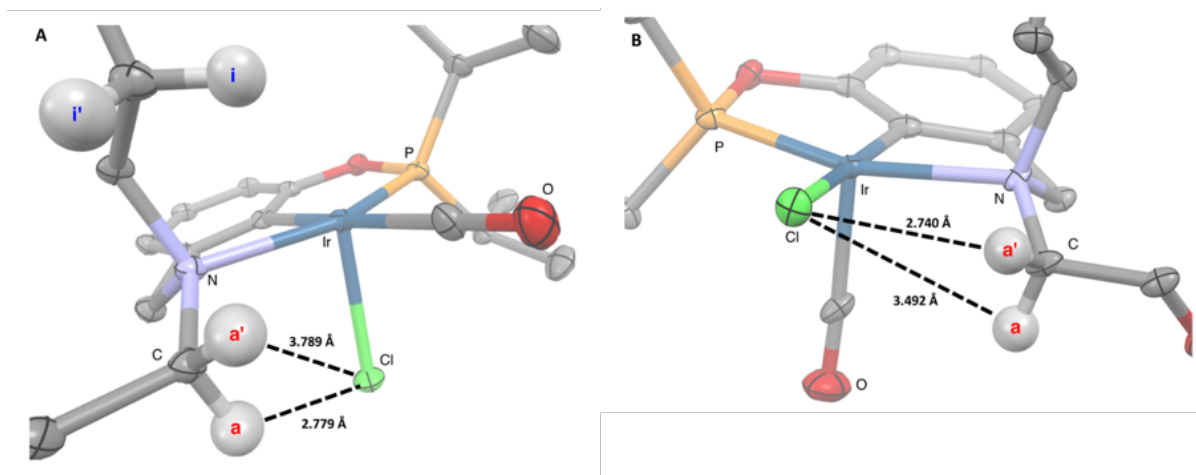
Figure 2.5. Molecular representation of **6-cis**[8] and **6-trans** (from X-ray crystallographic data). **6-trans** shows the proximity of proton H_a to the chloride ligand (**A**). Molecular representation of **6-trans** (from X-ray crystallographic data), showing that proton $H_{a'}$ is proximal to the chloride ligand (**B**).

The NMR spectra of the halide complexes suggest that anisotropic effects from the halide ligands induce the observed downfield shifts and large $\Delta\delta$ values when the ligand adopts a coordination mode that brings the macrocycle close to the transition metal center. It is worth noting that steric interactions could potentially give rise to similar shifts, although these are usually observed only in extremely rigid systems.[34−36]

Hydridocarbonyl chloride **6-cis** features a tridentate coordination mode in which the macrocycle has no ligated ethers. Only the eight ethylene linker protons proximal to the nitrogen show distinct chemical shifts in **6-cis**, while the rest of the crown ether protons are observed as

a multiplet at δ 3.6−3.7 (Figure 2.5A). The largest Δδ value is only 0.55 ppm, corresponding to a pair of protons $H_{a/a'}$ adjacent to the amine nitrogen. Proton H_a in **6-cis** (δ 4.44) is 2.779 Å from the chloride in the X-ray diffraction structure and is deshielded relative to its partner $H_{a'}$ (δ 3.89) (Figure 2.6A).[8]
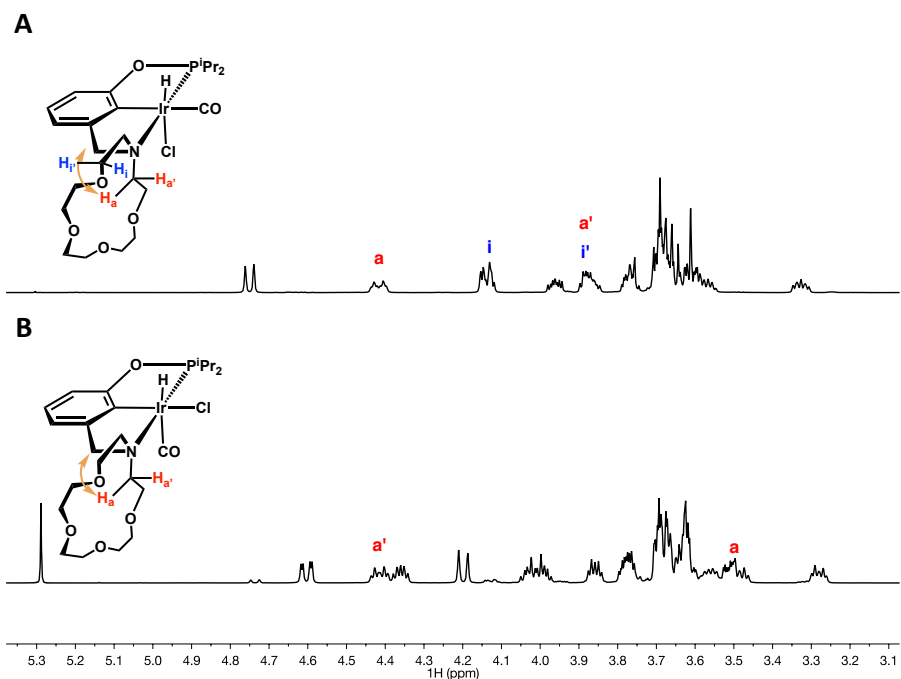
Figure 2.6. Comparison of the ^{1}H NMR spectra of complexes **6-cis** (**A**) and **6-trans** (**B**). Key protons were assigned on the basis of NOESY interactions with the benzylic linker (orange arrows).

The geometric isomer **6-trans** also shows the largest Δδ values for the methylene unit adjacent to the amine nitrogen. In **6-trans**, however, it is $H_{a'}$ that is now oriented toward the chloride (2.740 Å, Figure 2.6B), leading to a downfield shift for $H_{a'}$ (δ 4.41). H_a is oriented away from the chloride in **6-trans** and has the more upfield shift (δ 3.51; Figure 2.5B). This isomer-dependent change illustrates how proximity to the chloride ligand gives rise to anisotropy-induced changes in chemical shift.

Tridentate-bound complexes experience less chloride induced anisotropy overall: anisotropic shifting is limited to the methylene units closest to the amine (and closest to the metal center). This suggests that $\Delta\delta$ values are markers of hemilabile ligand coordination modes.

To determine whether $\Delta\delta$ could be applied in halide-free cases, pentadentate-bound cation **1** and tetradentate-bound carbonyl cation **8** were fully assigned. As shown in Figure 2.7A, the largest chemical shift difference between geminal protons in 1 is observed for $H_{j/j'}$ (δ 4.20 and δ 3.37, $\Delta\delta$ = 0.83 ppm), followed by $H_{d/d'}$ ($\Delta\delta$ = 0.55 ppm). The significant $\Delta\delta$ values may originate from oxygen diamagnetic anisotropy from the ethers in the crown,[37,38] from steric congestion,[35] or from constraint of the methylene groups.[39]

One large $\Delta\delta$ of 1.27 ppm is seen in **8**, consistent with the rigid conformation of the tetradentate coordination mode bringing crown protons close to the ligand (Figure 2.7B). The other diastereotopic protons show low-to-moderate $\Delta\delta$, ranging from 0.01 to 0.57 ppm. In general, the $\Delta\delta$ values are lower for halide-free systems, indicating weaker anisotropic effects from the bound carbonyl ligand.[22] However, the tridentate bis(carbonyl) **9** still has smaller chemical shift differences than the tetradentate and pentadentate analogues. Most of the geminal pairs have $\Delta\delta$ less than 0.1 ppm; the largest $\Delta\delta$ value of 0.37 ppm is assigned to the protons nearest to nitrogen. Taken together, these examples show that $\Delta\delta$ values are sensitive to the pincer−crown ether ligand binding mode.
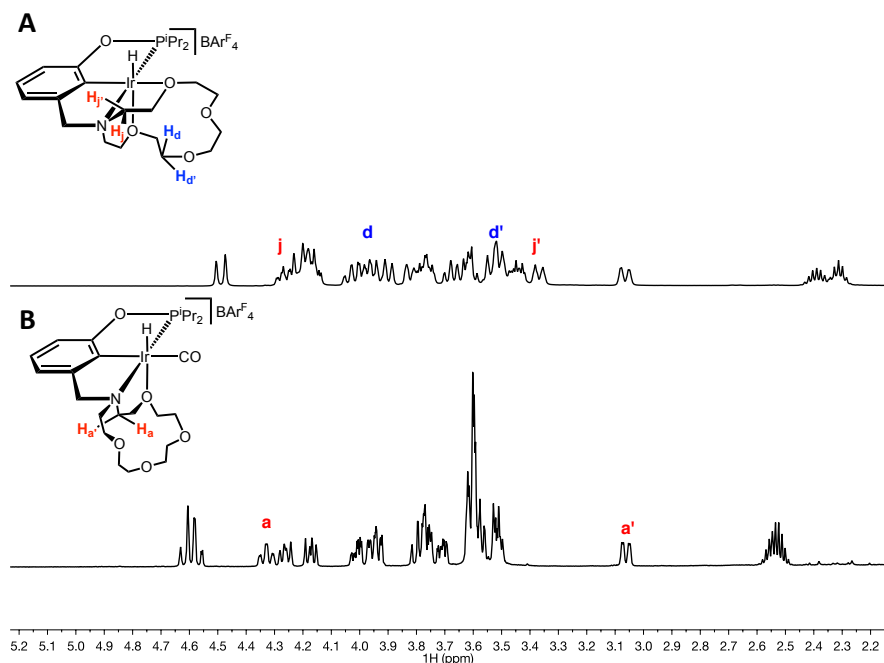
Figure 2.7. ^{1}H NMR spectra (crown ether region) of **1** (**A**) and **8** (**B**).

Average Differences in Chemical Shift (Δδ_avg) of Geminal Protons as a Marker of Pincer−Crown Ether Coordination Mode

The full family of complexes was evaluated by ^{1}H NMR spectroscopy along with [1]H−^{13}C HSQC and [1]H−^{1}H COSY experiments. The HSQC experiment identifies which protons are attached to the same carbon, allowing facile measurement of Δδ values for each geminal pair in the crown ether macrocycle, while the ^{1}H NMR and COSY data assist with calculation of Δδ values in cases where HSQC cross-peaks are not resolved. The values of Δδ for the individual geminal pairs in the macrocycle were averaged to give $\Delta\delta_{avg}$. Each value of Δδ has some uncertainty stemming from the ability to resolve the protons in the NMR experiments. In general, the 2D experiments provide resolution of about 0.01 ppm, but when many protons have similar chemical shifts (more common in the tridentate binding mode), there is more uncertainty in each Δδ value and thus in the composite value of $\Delta\delta_{avg}$. Explanations of uncertainty can be found in the Experimental section.

43

The power of this method lies in its ability to provide a useful metric of the coordination mode (the value of $\Delta\delta_{avg}$) without requiring full structural assignment of all protons in the system; only a ^{1}H NMR spectrum and ^{1}H$-$^{13}C HSQC and ^{1}H$-$^{1}H COSY experiments are needed. For example, samples of complex **9** contain small amounts of **8** (see above); this prevents full assignment of each proton in **9**, but $\Delta\delta$ values can still be readily extracted. The value of $\Delta\delta_{avg}$ is sensitive to large $\Delta\delta$ values, but because $\Delta\delta_{avg}$ weights each crown proton equally, macrocycles with little variation in the chemical shift of diastereotopic pairs will shift the average toward smaller values.
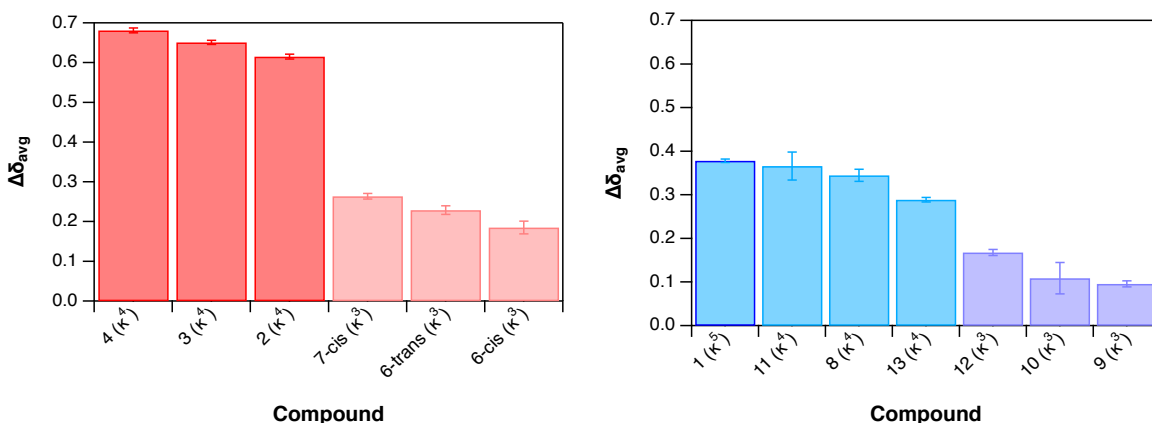
Figure 2.8. Bar graphs showing the average difference in chemical shift ($\Delta\delta_{avg}$). $\Delta\delta_{avg}$ of geminal protons in the macrocycles of halide-containing (**A**) and halide-free (**B**) pincer crown ether complexes. Tetradentate- and pentadentate-bound complexes are shown in dark red (A) or blue (B), while tridentate-bound complexes are shown in light pink (A) or purple (B).

The $\Delta\delta_{avg}$ values for 13 complexes are collected in Figure 2.8. A significant difference in $\Delta\delta_{avg}$ is apparent when comparing complexes assigned to tridentate and tetradentate binding modes. In halogen-free examples, tetradentate and pentadentate species have $\Delta\delta_{avg}$ values around 0.34, more than double that of tridentate species ($\Delta\delta_{avg} \approx 0.12$). This effect is amplified in chloride-containing species, resulting in an approximately 4-fold difference in $\Delta\delta_{avg}$ between coordination modes. This protocol readily distinguishes between hemilabile ligand binding modes of pincer$-$crown ethers using a relatively concise number of NMR experiments.

IV.   Conclusions

Facile synthetic access to a structurally diverse series of iridium pincer−crown ether complexes has enabled the development of an NMR protocol that reports the presence of iridium−oxygen interactions of these hemilabile ligands in solution. Assignment of each crown ether proton of a few complexes and comparison to solid-state structures revealed that diamagnetic anisotropy dramatically influences the chemical shift in the tetradentate and pentadentate coordination modes, which bring the macrocycle close to the metal center through ether donation to iridium. A parameter based on the difference in chemical shift between diastereotopic methylene protons, $\Delta\delta_{avg}$, was found to be sensitive to the pincer−crown ether ligand binding mode. Tetradentate and pentadentate binding modes that feature ether(s) binding iridium have more than 2-fold larger $\Delta\delta_{avg}$ values compared with tridentate examples that lack Ir−O bonds.

The pincer−crown ether complexes feature hemilabile oxygen donor ligands, as is common in other hemilabile ligands,[2,3,40−42] and the metal coordination sphere is completed by commonly encountered ligands such as halides, carbon monoxide, and acetonitrile. Many hemilabile ligands feature methylene linkers that would be suitable for obtaining $\Delta\delta$ values when the protons are diastereotopic.[32,43−46] Thus, it is possible that future studies might find diamagnetic anisotropy to be a helpful probe of the coordination chemistry of hemilabile ligands beyond pincer−crown ether systems. Every system will be different, of course, but the present example shows that the meaning of $\Delta\delta$ in a particular system can be made clear through full assignments of a few key complexes, followed by rapid collection of $^{1}H-^{13}C$ HSQC data for a wider range of complexes.

V.   Experimental Details

General Considerations

Air- and moisture-free reactions were performed using a vacuum line, Schlenk techniques, or in a glovebox under nitrogen. Under standard glovebox operating conditions, pentane, diethyl ether, benzene, toluene, and tetrahydrofuran were used without purging, such that traces of these solvents were present in the atmosphere and in solvent bottles. NMR samples were prepared in Teflon-sealed NMR tubes under a nitrogen atmosphere in the glovebox. A purge was performed prior to sample preparation to minimize solvent impurities in NMR spectra. NMR solvents were purchased from Cambridge Isotope Laboratories. Benzene-d6 (C_6D_6), chloroform-d with tetramethylsilane (0.03%) ($CDCl_3$ w/TMS), and dichloromethane-d2 (CD_2Cl_2) were freeze−pump−thawed three times for degassing and dried by passage through a small plug of activated alumina.

^{1}H, ^{31}P{^{1}H}, and 2D homo- and heteronuclear NMR experiments were performed on 400, 500, and 600 MHz spectrometers at 298 K. ^{1}H and 2D homonuclear (^{1}H−^{1}H) NMR spectra were referenced to residual NMR solvent peaks as appropriate, ^{31}P NMR spectra are reported relative to an 85% H_3PO_4 external standard (0 ppm), and 2D heteronuclear (^{13}C−^{1}H) spectra are referenced relative to TMS (0 ppm). κ^5-[(^{15c5}NCOP^{iPr})Ir(H)][BAr$^F_4$] (**1**),[7] κ^4-(^{15c5}NCOP^{iPr})Ir(H)(Cl)(**2**),[7] *cis*-κ^3-(^{15c5}NCOP^{iPr})Ir(H)(CO)(Cl) (**6-cis**),[8] *cis*-κ^3-(^{15c5}NCOP^{iPr})Ir(H)(NCCH$_3$)(Cl) (**7-cis**),[7] *trans*-κ^3-(^{15c5}NCOP^{iPr})Ir(H)(Cl)(NCCH$_3$) (**7-trans**),[7] [κ^4-(^{15c5}NCOP^{iPr})Ir(H)(NCCH$_3$)][BAr$^F_4$] (**11**),[7] [κ^3-(^{15c5}NCOP^{iPr})Ir(H)(NCCH$_3$)$_2$][BAr$^F_4$] (**12**),[7] [κ^4-(^{15c5}NCOP^{iPr})Ir(H)(H$_2$O)][BAr$^F_4$] (**13**),[7] (^{15c5}NCOP^{iPr})(H),[7] PPNBr,[47] PPNI,[47] and NaBAr$^F_4$[48] were prepared according to literature procedures. All of the other reagents were commercially available and used without modification.

HRMS measurements (resolution 100 000, mass error ≤1 ppm) were performed with a Q Exactive Orbitrap mass spectrometer (ThermoFisher, Bremen, Germany). Samples were introduced via syringe pump into an atmospheric pressure photoionization source at a flow rate of 10 µL/min. Xcalibur (ThermoFisher, Breman, Germany) was used to analyze the data. Molecular formula assignments were determined with Molecular Formula Calculator (version 1.2.3).

Single-crystal X-ray diffraction data were collected on a Bruker APEX-II CCD diffractometer at 100 K with Cu Kα radiation (λ = 1.54175 Å). Structures were solved and refined using the Bruker SHELXTL[49,50] software package within Apex[3,51] and/or OLEX.[2.52]

Δδ Methodology

Individual Δ**δ** values are calculated from ^{1}H-^{13}C HSQC spectra by assessing the difference between chemical shifts of diastereotopic protons. For a Δδ value, only a ^{1}H and ^{1}H-^{13}C HSQC spectra are required, with a ^{1}H-^{1}H COSY aiding identification of germinal protons when ^{13}C chemical shifts are very close. Longer experiments were used for absolute assignment. From the ten Δδ in the crown, a $\Delta\delta_{avg}$ can be calculated. Additionally, a standard deviation (S_n) marks the spread of Δδ values in a complex. Complexes with strong anisotropic effects will have larger standard deviations. Error is dependent on the resolution in the NMR spectra. Overlapping ^{1}H-^{13}C HSQC cross peaks will reduce the accuracy of Δδ values calculated, resulting in larger error in the $\Delta\delta_{avg}$. Resolved ^{1}H-^{13}C HSQC cross peaks are assigned an error of 0.1 ppm. Through propagation of error for the $\Delta\delta_{avg}$, error bars for each Δδ value can be calculated.

*Synthesis of κ⁴-(^{15c5}NCOP^{iPr})Ir(H)(Br) (**3**)*

In a 20 mL scintillation vial, 26.4 mg of **1** (39.5 μmol) and 23 mg of PPNBr (40.07 μmol) were dissolved in CH_2Cl_2 (5 mL), and the mixture was stirred for 2 h in a glovebox. The solvent was removed under vacuum, and the byproduct, [PPN][BAr$^F_4$], was removed with an ether wash (2 × 2 mL) to yield 14.3 mg (72% yield) of a yellow solid. The product was 92% pure according to multinuclear NMR spectroscopy (with 8% complex 2 present that carried over during the synthesis), so elemental analysis is not reported; this was sufficient purity for the present NMR studies.

^{1}H NMR (500 MHz, CDCl3): δ −31.23 (d, J = 25.9 Hz, 1H), Ir−H), 0.88 (dd, J = 15.6, 7.6 Hz, 3H, $CH(CH_3)_2$), 1.21 (m, 3H, $CH(CH_3)_2$), 1.37 (dd, J = 13.9, 6.9 Hz, 3H, $CH(CH_3)_2$), 1.45 (dd, J = 16.3, 7.2 Hz, 3H, $CH(CH_3)_2$), 2.36 (m, 1H, $CH(CH_3)_2$), 2.55 (m, 1H, $CH(CH_3)_2$), 3.01 (dd, J = 15.0, 2.5 Hz, 1H, crown-CH_2), 3.25 (dd, J = 15.7, 1.8 Hz, 1H, crown-CH_2), 3.33 (d, J = 11.4 Hz, 1H, crown-CH_2, 3.42−3.55 (m, 2H, crown-CH_2), 3.57−3.97 (m, 8H, crown-CH_2), 4.08−4.13 (m, 2H, crown-CH_2), 4.42 (m, 2H, ArCH$_2$N, 5.04 (t, J = 10.9 Hz, 1H, crown-CH_2), 5.10 (dd, J = 11.7, 11.5 Hz, 1H, crown- CH_2), 6.54 (d, J = 8.2 Hz, 1H, Ar−H), 6.57 (d, J = 8.2 Hz, 1H, Ar− H), 6.71 (t, J = 7.5 Hz, 1H, Ar−H). ^{13}C{^{1}H} NMR (151 MHz, CDCl$_3$): δ 16.59 (d, J = 2.9 Hz). 17.41 (d, J = 3.0 Hz, $CH(CH_3)_2$)), 17.56 (s, $CH(CH_3)_2$) 17.95 (d, J = 6.6 Hz, $CH(CH_3)_2$)), 29.68 (d, J = 38.5 Hz, $CH(CH_3)_2$), 31.39 (d, J = 32.9 Hz, $CH(CH_3)_2$)), 63.51 (d, J = 2.7 Hz, crown-CH_2), 65.00 (d, J = 2.1 Hz, crown-CH_2), 67.54 (d, J = 2.5 Hz, crown-CH_2), 68.61 (s, crown-CH_2), 69.25 (s, crown-CH_2), 70.43 (s, crown-CH_2), 70.59 (s, crown-CH_2), 72.40 (d, J = 2.0 Hz, ArCH$_2$N), 72.95 (s, crown-CH_2), 73.22 (s, crown-CH_2), 76.19 (s, crown-CH_2), 107.32 (d, J = 11.5 Hz), 113.21 (s, CAr), 122.70 (s, CAr), 134.76 (s, CAr), 148.15 (d, J = 3.2 Hz, CAr), 162.81 (d, J = 3.4 Hz, CAr). ^{31}P{1H} NMR (243 MHz, CDCl$_3$): δ 144.88. HRMS: (**3**$^+$−H, m/z 713.12744, calcd 713.127423).
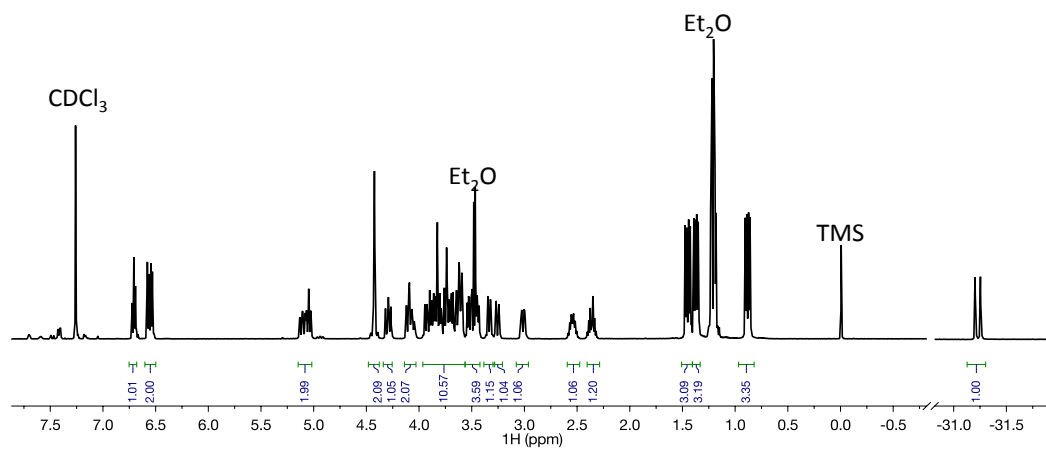
Figure 2.9. ^{1}H NMR spectrum of κ^4-(^{15c5}NCOP^{iPr})Ir(H)(Br) (**3**) in CDCl$_3$.
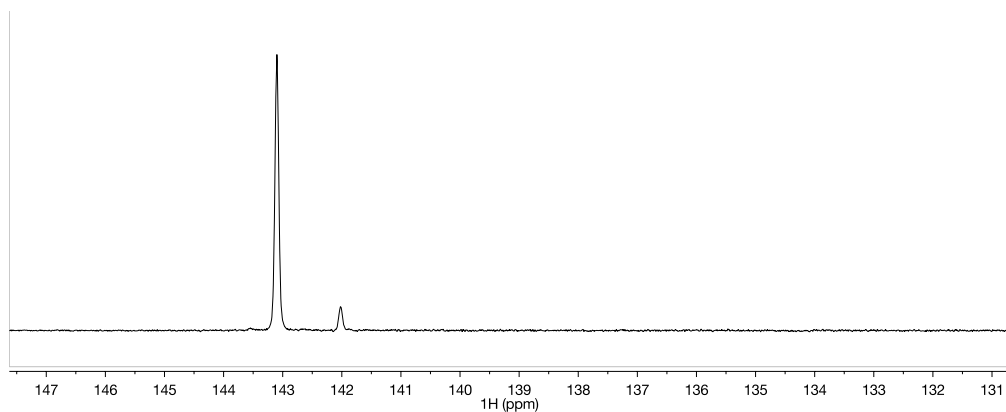
Figure 2.10. ^{31}P{^{1}H} NMR spectrum of κ^4-(^{15c5}NCOP^{iPr})Ir(H)(Br) (**3**) in CDCl$_3$.
Trace of compound 2 is present.
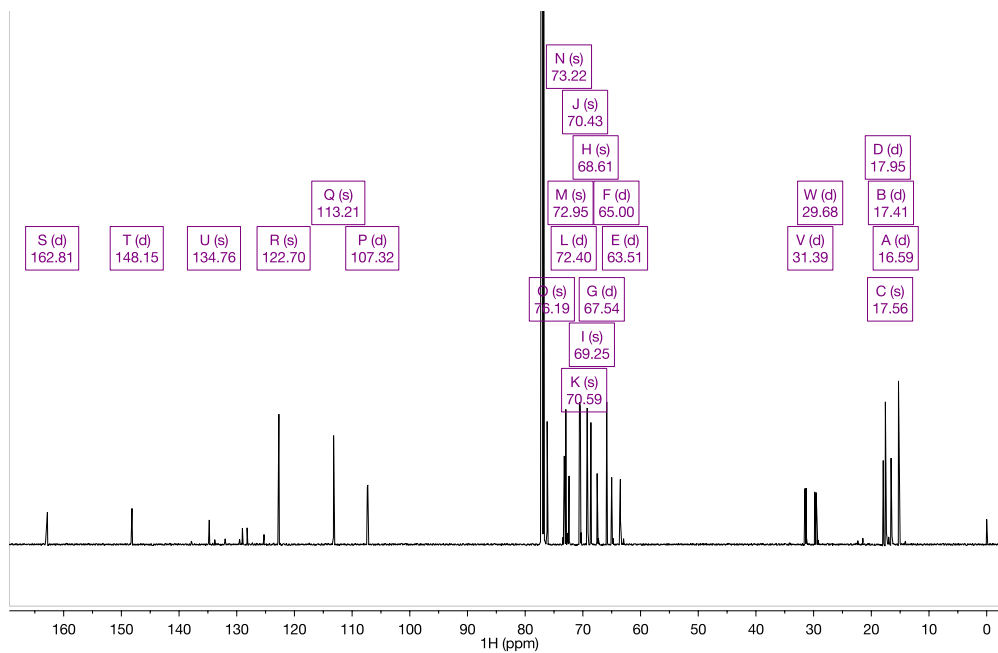
Figure 2.11. $^{13}C\{^1H\}$ NMR spectrum of κ^4-(^{15c5}NCOP^{iPr})Ir(H)(Br) (**3**) in CDCl$_3$.
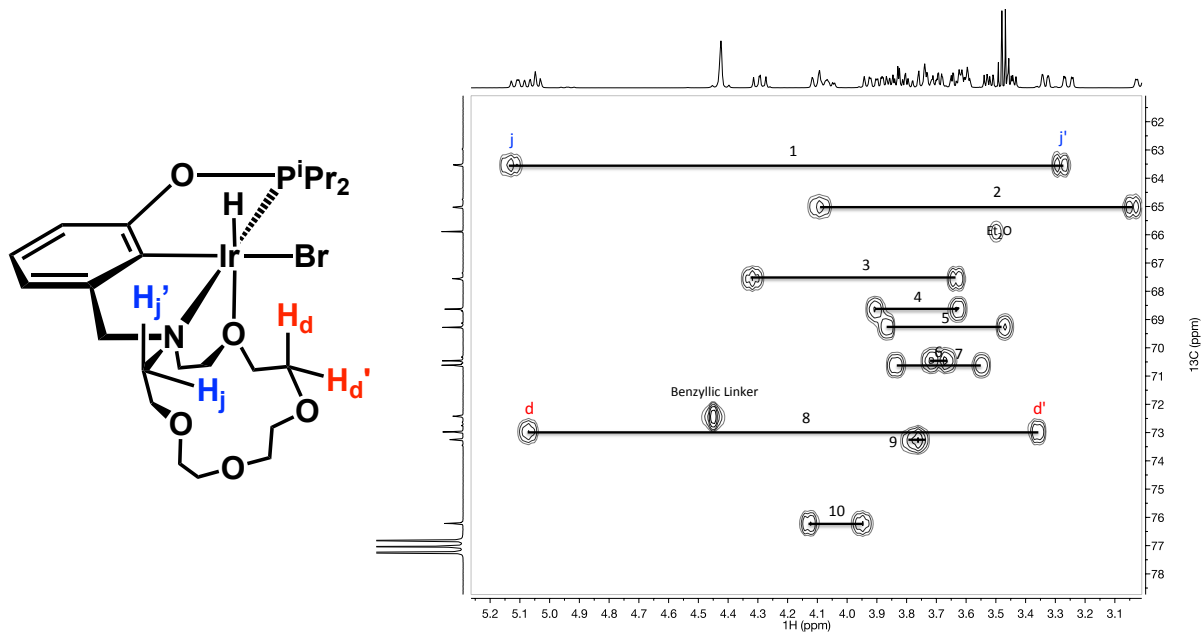
Figure 2.12. ^1H-^{13}C HSQC NMR spectrum of κ^4-(^{15c5}NCOP^{iPr})Ir(H)(Br) (**3**) in CDCl$_3$.

Synthesis of κ⁴-(¹⁵ᶜ⁵NCOPⁱᴾʳ)Ir(H)(I) (4)

In air, an NMR tube was charged with **2** (11.7 mg, 11.7 μmol), NaI (22.8 mg, 152 μmol), and CDCl$_3$. The mixture was heated overnight at 55 °C. Excess salt was filtered off, and the solvent was removed by rotary evaporation, yielding a yellow film (3.1 mg, 23% yield).

^{1}H NMR (500 MHz, CDCl$_3$): δ −31.17 (d, J = 24.4 Hz, 1H, Ir−H), 0.90 (dd, J = 15.5, 6.9 Hz, 3H, CH(CH$_3$)$_2$), 1.25 (m, 3H, CH(CH$_3$)$_2$), 1.38 (dd, J = 14.2, 7.0 Hz, 3H, CH(CH$_3$)$_2$), 1.47 (dd, J = 16.2, 7.3 Hz, 3H, CH(CH$_3$)$_2$), 2.36 (m, 1H, CH(CH$_3$)$_2$), 2.58 (m, 1H, CH(CH$_3$)$_2$), 3.04 (d, J = 12.3 Hz, 1H, crown-CH$_2$), 3.25 (m, 2H, crown-CH$_2$), 3.45 (m, 1H, crown- CH$_2$), 3.54 (m, 2H, crown-CH$_2$), 3.62 (m, 2H, crown-CH$_2$), 3.72 (m, 3H, crown-CH$_2$), 3.86 (m, 4H, crown-CH$_2$), 4.04 (m, 1H, crown- CH$_2$), 4.14 (m, 1H, crown-CH$_2$), 4.29 (dd, J = 14.7, 12.8 Hz, 1H, crown-CH$_2$), 4.42 (m, 2H, ArCH$_2$N), 5.05 (t, J = 10.3 Hz, 1H, crown- CH$_2$), 5.31 (dd, J = 15.4, 12.1 Hz, 1H, crown-CH$_2$), 6.56 (d, J = 7.4 Hz, 1H, Ar−H), 6.60 (d, J = 7.8 Hz, 1H, Ar−H), 6.75 (t, J = 7.7 Hz, 1H, Ar−H). ^{13}C{^{1}H} NMR (126 MHz, CDCl$_3$): δ 17.10 (s, C(CH$_3$)$_2$), 17.64 (s, C(CH$_3$)$_2$), 18.22 (s, C(CH$_3$)$_2$), 19.21 (d, J = 5.4 Hz, C(CH$_3$)$_2$), 30.36 (d, J = 38.8 Hz, C(CH$_3$)$_2$), 31.25 (d, J = 33.6 Hz, C(CH$_3$)$_2$), 65.41 (d, J = 8.2 Hz, crown-CH$_2$), 68.11 (s, crown-CH$_2$), 68.65 (s, crown-CH$_2$), 69.37 (s, crown-CH$_2$), 70.54 (s, crown-CH$_2$), 70.63 (s, crown-CH$_2$), 72.11 (s, ArCH$_2$N), 72.99 (overlapping s, crown-CH$_2$), 76.42 (s, crown-CH$_2$), 107.49 (d, J = 11.7 Hz, CAr), 113.39 (s, CAr), 122.89 (s, CAr), 137.21 (s, CAr), 148.63 (s, CAr), 162.43 (s, CAr). ^{31}P{^{1}H} NMR (202 MHz, CDCl$_3$): δ 145.63. HRMS: (**4**$^+$− H, m/z 759.11467, calcd 759.11561). Anal. Calcd for C$_{40}$H$_{40}$IIrNO$_5$P: C, 36.32; H, 5.30; N, 1.84. Found: C, 35.14; H, 4.82; N, 1.75. Although the product was pure by NMR analysis and the expected mass was confirmed by HRMS, the analysis results suggest that a minor impurity (perhaps residual NaI) was present. No impact on the NMR analysis was expected.
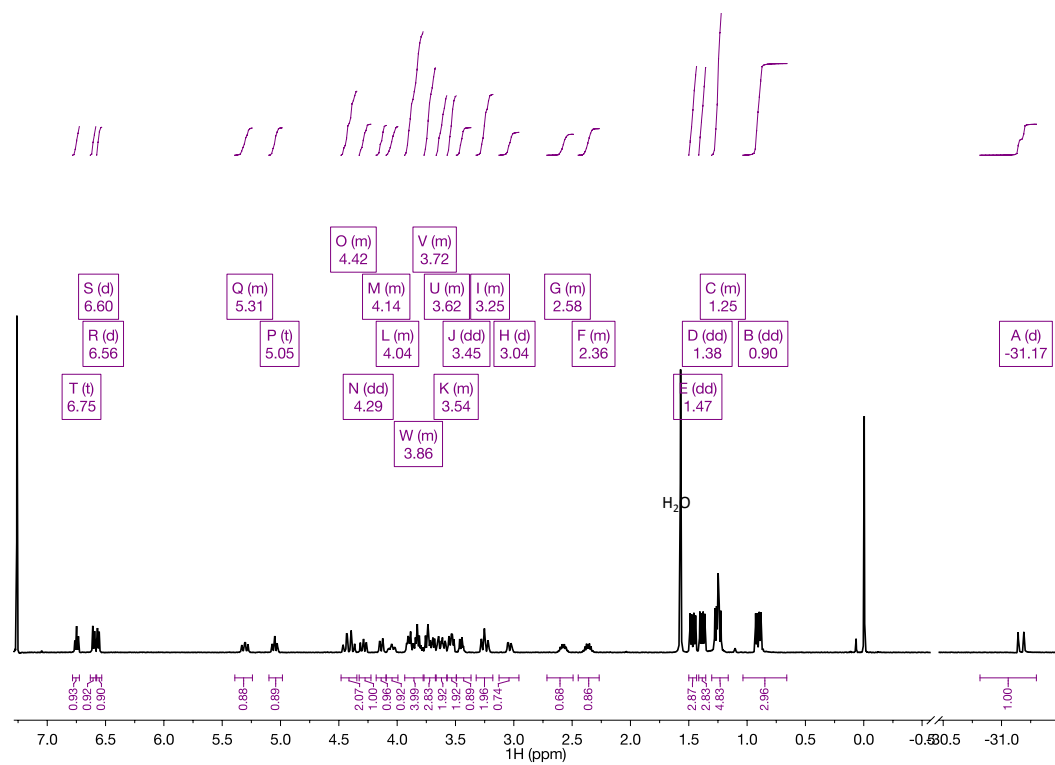
Figure 2.13. ^{1}H NMR spectrum of κ^4-(^{15c5}NCOP^{iPr})Ir(H)(I) (**4**) in CDCl$_3$.
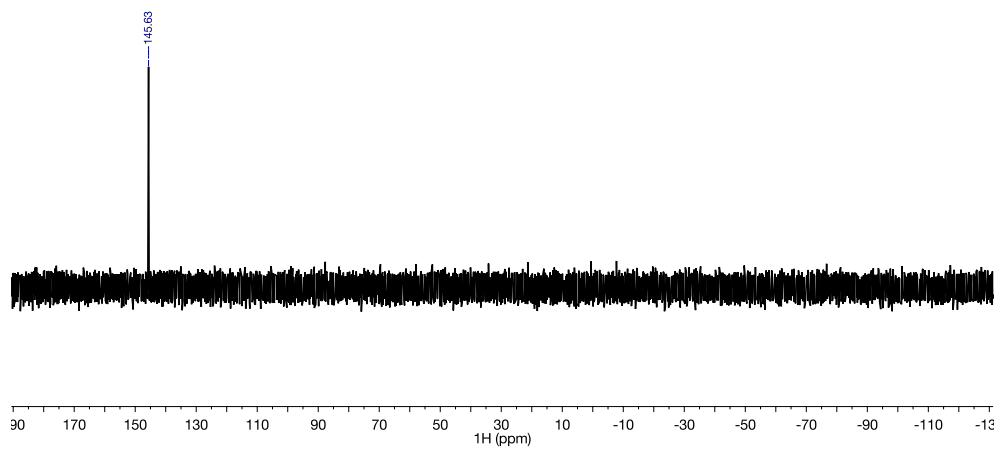
Figure 2.14. ^{31}P{^{1}H} NMR spectrum of κ^4-(^{15c5}NCOP^{iPr})Ir(H)(I) (**4**) in CDCl$_3$.

Figure 2.15. $^{13}C\{^1H\}$ NMR Spectrum of κ^4-(^{15c5}NCOP^{iPr})Ir(H)(I) (**4**) in CDCl$_3$.

Figure 2.16. ^{1}H-^{13}C HSQC NMR spectrum (crown region) of κ^4-(^{15c5}NCOP^{iPr})Ir(H)(I) (**4**) in CDCl$_3$ w/ TMS.

Equilibrium Formation of κ³-[(¹⁵ᶜ⁵NCOPⁱᴾʳ)Ir(H)(Cl)₂]⁻ (5)

In air, complex **2** (21.60 mg, 23.3 µmol) was dissolved in CDCl₃. To this solution a stock solution of NBu₄Cl (89.7 mg, 322.8 µmol dissolved in 4 mL of CDCl₃) was added portionwise to the solution of **2**. An additional 20 equiv of NBu₄Cl (179.4 mg, 645.6 µmol) was added, with 44% conversion observed. Addition of over 150 equiv of NBu₄Cl drove the reaction forward to 99% conversion. Separation of **5** from excess chloride proved to be difficult; this species was not isolated.
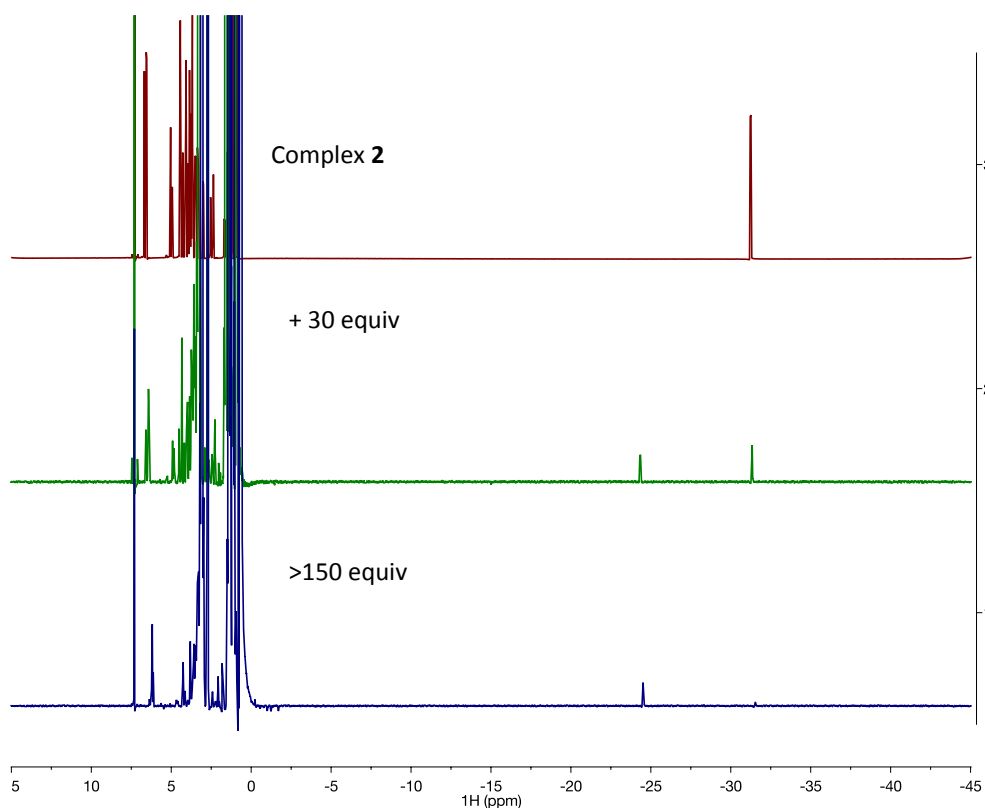
Figure 2.17. ¹H NMR spectrum after addition of [NBu₄][Cl] to **2** in CDCl₃ w/TMS. Greater than 150 equiv of [NBu₄][Cl] are needed to generate the new hydride species at –24.29 ppm, assigned as [NBu₄][κ³-(¹⁵ᶜ⁵NCOPⁱᴾʳ)Ir(H)(Cl)₂] (**5**).

Synthesis of trans-κ³-(¹⁵ᶜ⁵NCOPⁱᴾʳ)Ir(H)(Cl)(CO) (6-trans)

In a Teflon-sealed 50 mL reaction vessel, **2** (34.9 mg, 52.2 µmol) was dissolved in CH₂Cl₂ (10 mL). The solution was freeze−pump−thaw degassed, and 1 atm CO was admitted to

the reaction vessel at room temperature. Upon addition of CO, the yellow color faded, affording a clear, colorless solution. The solvent was removed by vacuum, yielding a white solid (23.8 mg, 66% yield). Single crystals suitable for X-ray diffraction were grown by layering pentanes over a concentrated solution of **6-trans** in toluene.

^{1}H NMR (600 MHz, CDCl$_3$): δ −7.02 (d, 23.8 Hz, 1H, Ir-H), 1.16−1.34 (m, 12H, CH(CH$_3$)$_2$), 2.45 (m, 1H, CH(CH$_3$)$_2$), 2.57 (m, 1H, CH(CH$_3$)$_2$), 3.28 (dt, J = 12.8, 5.90 Hz, 1H, crown-CH$_2$), 3.51 (m, 3H, crown-CH$_2$), 3.66 (m, 10H, crown- CH$_2$), 3.78 (m, 2H, crown-CH$_2$), 3.86 (dt, J = 10.8, 5.25 Hz, 1H, crown-CH$_2$), 4.01 (m, 2H, crown-CH$_2$), 4.20 (d, J = 13.1 Hz, 1H, ArCH$_2$N), 4.36 (m, 1H, crown-CH$_2$), 4.42 (dt, J = 14.4, 6.2 Hz, 1H, crown-CH$_2$), 4.60 (dd, J = 14.0, 3.4 Hz, 1H, ArCH$_2$N), 6.64 (d, J = 7.8 Hz, 1H, Ar−H), 6.73 (d, J = 7.8 Hz, 1H, Ar−H), 6.83 (t, J = 7.8 Hz, 1H, Ar−H). ^{13}C{^{1}H} NMR (151 MHz, CDCl$_3$): δ 16.42 (s, CH(CH$_3$)$_2$), 16.57 (s, CH(CH$_3$)$_2$), 17.35 (d, J = 3.4 Hz, CH(CH$_3$)$_2$), 17.63 (s, CH(CH$_3$)$_2$), 30.96 (d, J = 42.4 Hz, CH(CH$_3$)$_2$), 33.30 (d, J = 33.6 Hz, CH(CH$_3$)$_2$), 33.30 (s, crown-CH$_2$), 53.44 (s, crown-CH$_2$), 61.36 (d, J = 2.3 Hz, crown-CH$_2$), 62.86 (s, crown-CH$_2$), 66.56 (d, J = 2.1 Hz, crown-CH$_2$), 69.87 (s, crown-CH$_2$), 70.18 (s, crown-CH$_2$), 70.26 (s, crown-CH$_2$), 70.35 (s, crown-CH$_2$), 70.64 (s, crown-CH$_2$), 71.18 (s, crown-CH$_2$), 75.44 (d, J = 2.4 Hz, ArCH$_2$N), 108.58 (d, J = 11 Hz, CAr), 117.01 (s, CAr), 124.15 (s, CAr), 129.28 (d, J = 3.3 Hz, CAr), 143.42 (d, J = 2.4 Hz, CAr), 160.88 (CAr), 178.90 (dd, J = 56.6, 3.4 Hz, Ir−CO; note that the 1H decoupler did not reach this downfield signal). ^{31}P{^{1}H} NMR (243 MHz, CDCl$_3$): δ 150.17. IR (toluene): ν(CO) 2017 cm^{-1}. Anal. Calcd for C$_{24}$H$_{40}$ClIrNO$_6$P: C, 41.34; H, 5.78; N, 2.01. Found: C, 41.08; H, 5.49; N, 1.91.
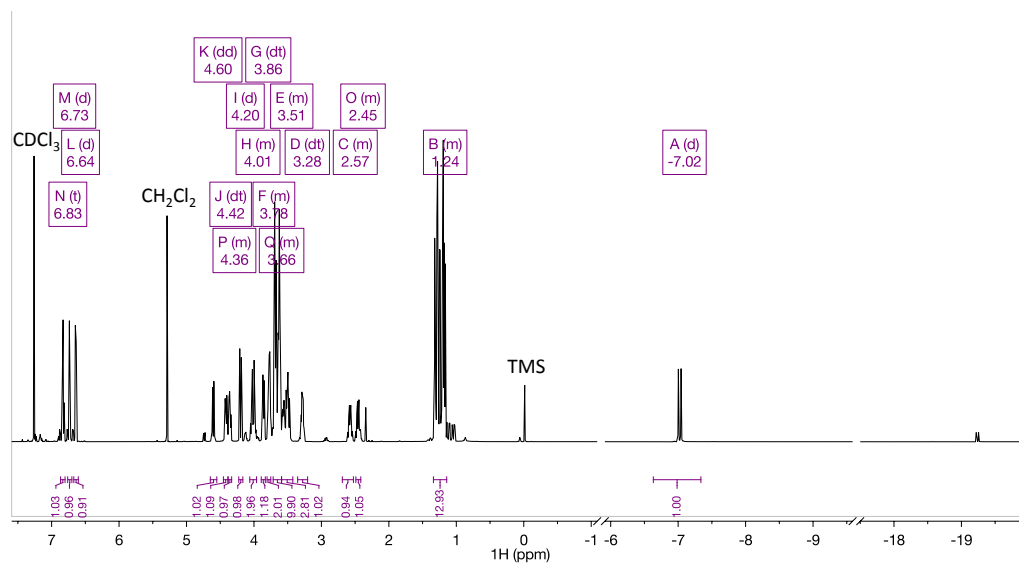
Figure 2.18. ¹H NMR spectrum of *trans*-κ³-(¹⁵ᶜ⁵NCOP^{iPr})Ir(H)(Cl)(CO) (**6-trans**) in CDCl₃. Trace amounts of *cis*-κ³-(¹⁵ᶜ⁵NCOP^{iPr})Ir(H)(CO)(Cl) (**6-cis**) are present.
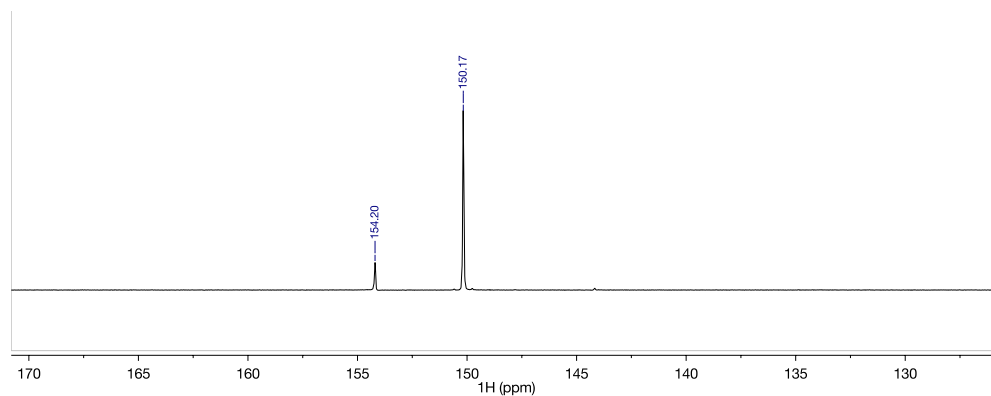
Figure 2.19. ³¹P{¹H} NMR spectrum of *trans*-κ³-(¹⁵ᶜ⁵NCOP^{iPr})Ir(H)(Cl)(CO) (**6-trans**) in CDCl₃. Trace amounts of *cis*-κ³-(¹⁵ᶜ⁵NCOP^{iPr})Ir(H)(CO)(Cl) (**6-cis**) are present.
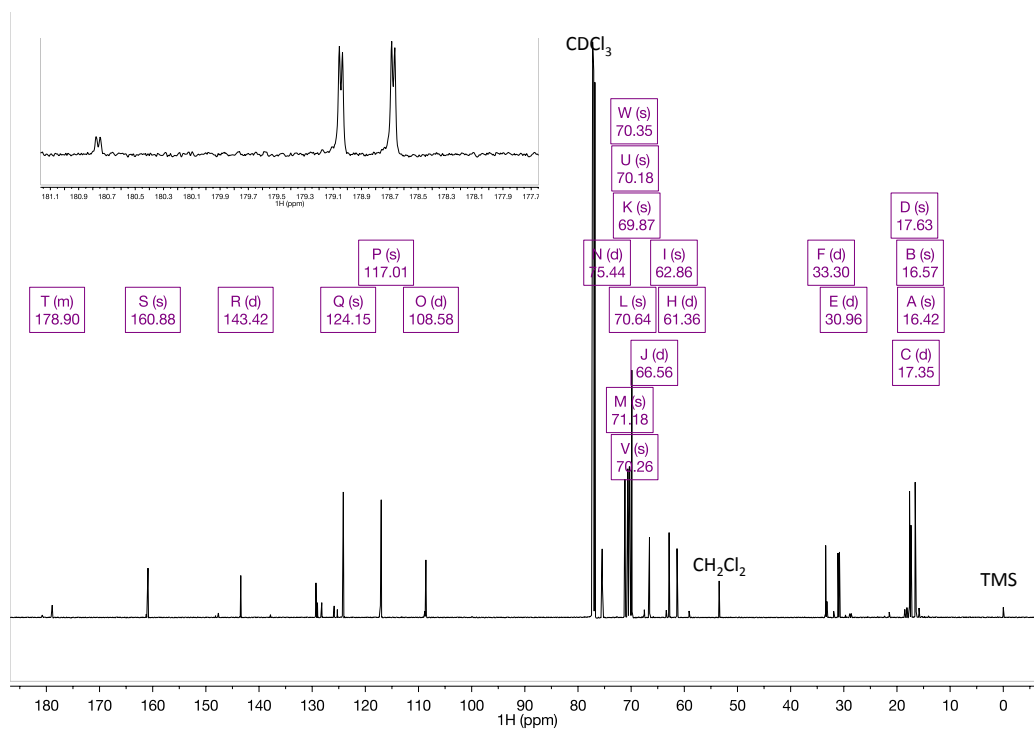
Figure 2.20. $^{13}C\{^1H\}$ NMR spectrum of trans-κ^3-(^{15c5}NCOP^{iPr})Ir(H)(Cl)(CO) (**6-trans**) in CDCl$_3$. Trace amounts of *cis*- κ^3-(^{15c5}NCOP^{iPr})Ir(H)(CO)(Cl) (**6-cis**) are present. Inset: Carbonyl region of the ^{13}C NMR spectrum of *trans*-κ^3-(^{15c5}NCOP^{iPr})Ir(H)(Cl)(CO) (**6-trans**).
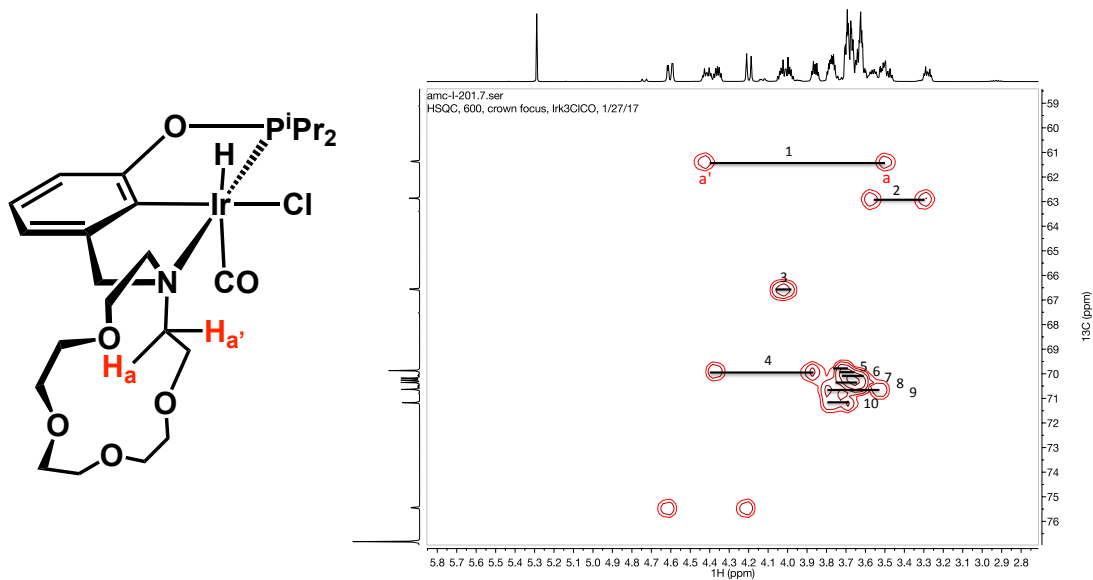
Figure 2.21. ^1H-^{13}C HSQC NMR spectrum (crown focus) of *trans*-κ^3-(^{15c5}NCOP^{iPr})Ir(H)(Ir)(Cl)(CO) (**6-trans)** in CDCl$_3$.

*Synthesis of [κ⁴-(¹⁵ᶜ⁵NCOP^iPr)Ir(H)(CO)][BArᶠ₄] (**8**)*

A 20 mL scintillation vial was charged with (¹⁵ᶜ⁵NCOP^ipr)Ir(H)(CO)(Cl) (0.0522 g, 0.0749 mmol), NaBArᶠ₄ (0.0732 g, 0.0826 mmol), and CH_2Cl_2 (8 mL). The resulting yellow slurry was stirred for 17 h. The mixture was filtered, and the light-golden-yellow filtrate was concentrated to ~1 mL under vacuum. Pentane (5 mL) was added, and the solvent was removed under vacuum, affording **8** as an off-white solid (0.0997 g, 87% yield). Single crystals suitable for X-ray diffraction were grown by slow evaporation of an Et_2O solution of **8** into $(Me_3Si)_2O$. ¹H NMR (600 MHz, CD_2Cl_2): δ −25.67 (d, J = 21.4 Hz, 1H, Ir−H), 0.92 (dd, J = 16.8, 7.0 Hz, 3H, $CH(CH_3)_2$), 1.05 (dd, J = 20.9, 6.9 Hz, 3H, $CH(CH_3)_2$), 1.38 (dd, J = 18.9, 7.5 Hz, 3H, $CH(CH_3)_2$), 1.44 (dd, J = 14.8, 6.8 Hz, 3H, $CH(CH_3)_2$), 2.55 (overlapping m, 2H, $CH(CH_3)_2$), 3.06 (m, 1H, crown-CH_2), 3.58 (m, 9H, crown-CH_2), 3.78 (m, 4H, crown-CH_2), 3.93 (m, 1H, crown-CH_2), 4.01 (m, 2H, crown-CH_2), 4.18 (m, 1H, crown-CH_2), 4.28 (m, 2H, crown-CH_2), 4.58 (dd, J = 15.6, 2.9 Hz, 1H, ArCHHN), 4.63 (d, J = 15.7 Hz, 1H, ArCHHN), 6.80 (d, J = 7.7 Hz, 1H, Ar−H), 6.82 (d, J = 8.3 Hz, 1H, Ar−H), 7.07 (t, J = 7.8 Hz, 1H, Ar−H), 7.56 (s, 4H, p−B−Ar−H), 7.72 (s, 8H, o− B−Ar−H). ¹³C{¹H} NMR (151 MHz, CD_2Cl_2): δ 16.12 (d, J = 4.7 Hz, $CH(CH_3)_2$), 17.37 (d, J = 2.3 Hz, $CH(CH_3)_2$), 17.86 (d, J = 4.0 Hz, $CH(CH_3)_2$), 18.20 (d, J = 6.3 Hz, $CH(CH_3)_2$), 29.69 (d, J = 38.9 Hz, $CH(CH_3)_2$), 31.93 (d, J = 36.0 Hz, $CH(CH_3)_2$), 66.13 (d, J = 1.4 Hz, crown-CH_2), 67.50 (s, crown-CH_2), 69.08 (s, crown-CH_2), 69.42 (d, J = 2.0 Hz, crown-CH_2), 70.52 (d, J = 2.4 Hz, crown-CH_2), 70.66 (s, crown-CH_2), 70.83 (s, crown-CH_2), 71.75 (s, crown-CH_2), 73.12 (s, crown-CH_2), 75.69 (d, J = 1.4 Hz, ArCH₂N), 78.56 (s, crown-CH_2), 110.16 (d, J = 12.3 Hz, CAr), 115.57 (s, CAr), 117.87 (p, J = 4.1 Hz, p- CH, BArF), 124.99 (q, J = 272.4 Hz, CF3, BArF), 129.05 (s, CAr), 129.26 (qdd, J = 31.2, 5.8, 2.9 Hz, C−CF3, BArF), 135.19 (s, o-CH, BArF), 145.87 (d, J = 5.0 Hz, CAr), 152.27 (d, J = 3.3 Hz, CAr), 162.14 (dd, J = 99.7, 49.9 Hz, B−C, BArF), 162.80 (d, J = 1.4 Hz, CAr), 183.35 (s, Ir−CO). ³¹P{¹H}

NMR (243 MHz, CD$_2$Cl$_2$): δ 152.77. IR (solid): ν(CO) 2041 cm−1. Anal. Calcd for

C$_{56}$H$_{52}$BF$_{24}$IrNO$_6$P: C, 44.11; H, 3.44; N, 0.92. Found: C, 44.38; H, 3.28; N, 0.95.
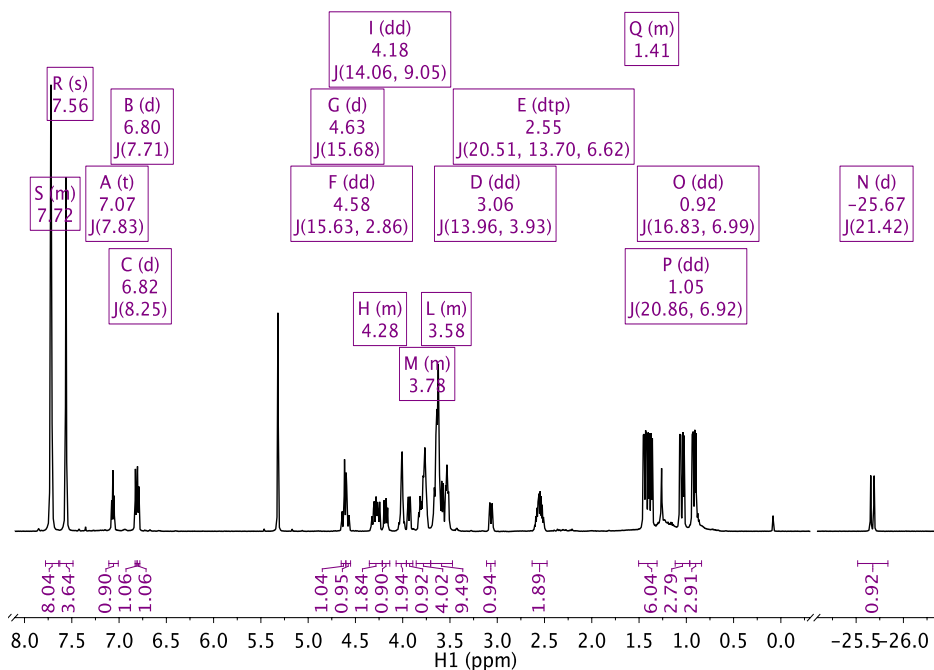
Figure 2.22. ^{1}H NMR spectrum of κ^4-[(^{15c5}NCOP^{iPr})Ir(H)(CO)][BAr$^F_4$] (**8**) in CD$_2$Cl$_2$.
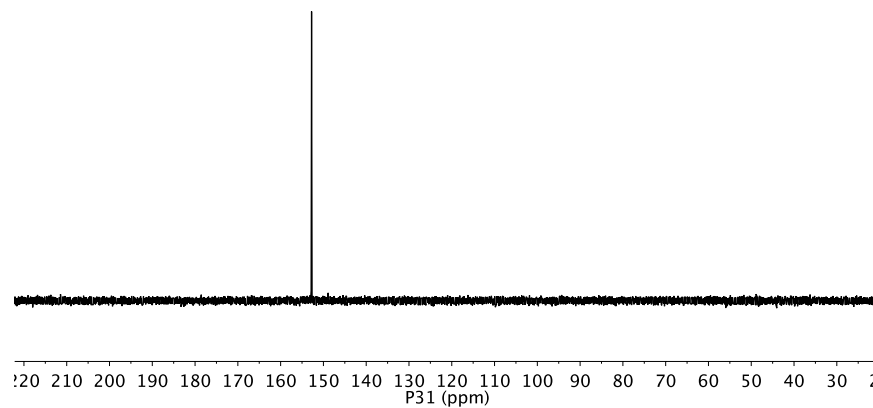
Figure 2.23. ^{31}P{^{1}H} NMR spectrum of κ^4-[(^{15c5}NCOP^{iPr})Ir(H)(CO)][BAr$^F_4$] (**8**) in CD$_2$Cl$_2$.
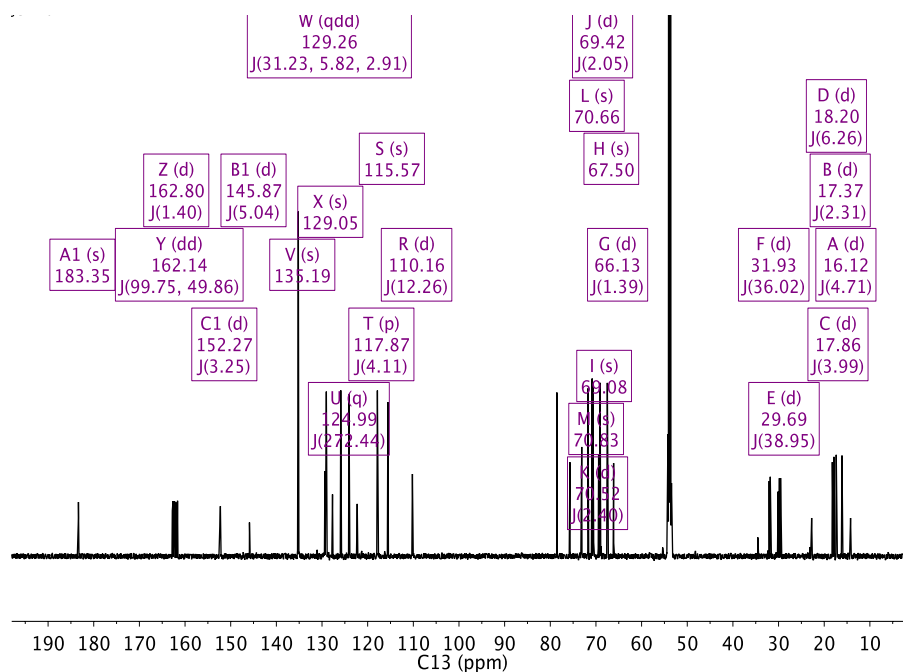
Figure 2.24. $^{13}C\{^1H\}$ NMR spectrum of κ^4-[$(^{15c5}NCOP^{iPr})Ir(H)(CO)$][$BAr^F_4$] (**8**) in CD_2Cl_2.
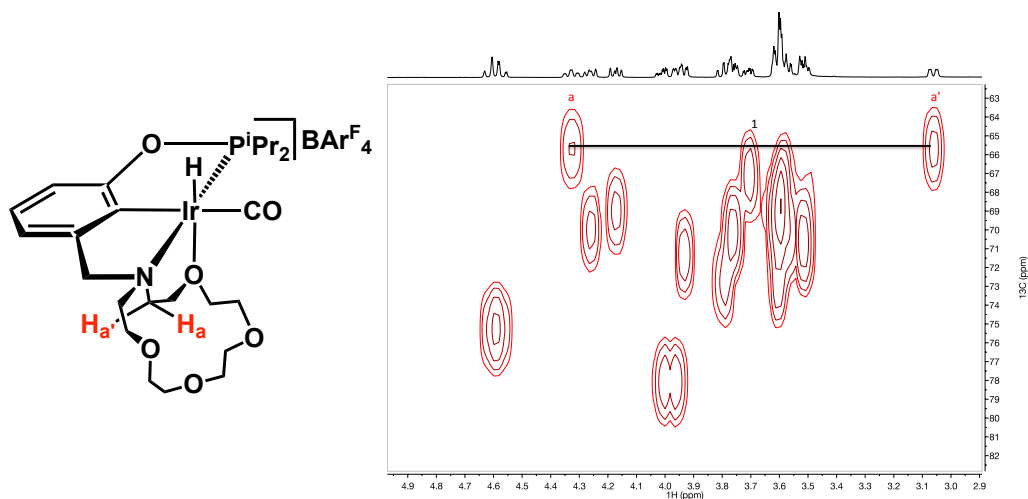
Figure 2.25. ^1H-^{13}C HSQC NMR spectrum (crown region) of [κ^4-$(^{15c5}NCOP^{iPr})Ir(H)(CO)$][$BAr^F_4$] (**8**) in $CDCl_3$.

*Synthesis of [κ^3-$(^{15c5}NCOP^{iPr})Ir(H)(CO)_2$][$BAr^F_4$] (**9**)*

A sample of 1 was dissolved in $CDCl_3$ and transferred to a Teflon-sealed NMR tube. The tube was freeze−pump−thaw degassed three times, and 1 atm CO was added at room temperature. After 30 min, an equilibrium mixture of **8** and **9** was apparent by NMR

60

spectroscopy. Backfilling again with CO saw further conversion to 87%. Complex **9** is stable only under a CO atmosphere, so this product was not isolated.

^{1}H NMR (600 MHz, CDCl$_3$): δ −9.42 (d, J = 20.8 Hz, 1H, Ir−H), 1.07− 1.14 (m, 6H, CH(CH$_3$)$_2$), 1.15−1.26 (m, 6H, CH(CH$_3$)$_2$), 2.52 (m, 2H, CH(CH$_3$)$_2$, 3.56−3.82 (m, 14H, crown-CH$_2$), 3.83−3.92 (m, 2H, crown-CH$_2$), 4.03 (m, 1H, crown-CH$_2$), 4.21 (m, 1H, crown-CH$_2$), 4.46 (d, J = 14.7 Hz, 1H, ArCH$_2$N), 4.59 (dd, J = 14.7, 3.43 Hz, 1H, ArCH$_2$N), 6.85 (d, J = 8.2 Hz, 1H, Ar−H) 6.99 (d, J = 7.0 Hz, 1H, Ar−H), 7.08 (m, 1H, Ar−H). ^{13}C{^{1}H} NMR (151 MHz, CDCl$_3$): δ 16.45 (s, 3H, CH(CH$_3$)$_2$), 16.61 (s, 3H, CH(CH$_3$)$_2$), 17.29 (d, J = 2.6 Hz, 3H, CH(CH$_3$)$_2$), 17.43 (d, J = 3.4 Hz, 3H, CH(CH$_3$)$_2$), 30.64 (d, J = 42.1 Hz, 1H, CH(CH$_3$)$_2$), 33.88 (d, J = 34.8 Hz, 1H, CH(CH$_3$)$_2$), 67.14 (s, crown-CH$_2$), 67.55 (s, crown-CH$_2$), 67.71 (s, crown-CH$_2$), 69.76 (s, crown-CH$_2$), 69.89 (s, crown-CH$_2$), 70.07 (s, crown-CH$_2$), 70.27 (s, crown-CH$_2$), 70.48 (s, crown-CH$_2$), 70.48 (s, crown-CH$_2$), 70.55 (s, crown-CH$_2$), 70.95 (s, ArCH$_2$N), 111.02 (d, J = 12.3 Hz, CAr), 117.44 (p, J = 11.7 Hz, p-CH, BArF), 119.3 (s, CAr), 124.52 (q, J = 272.5 Hz, BArF), 128.7 (s, CAr), 128.76 (qdd, J = 31.5, 5.9, 2.9 Hz, C−CF3, BArF), 129.87 (d, J = 4.0 Hz, CAr), 134.76 (s, o-CH, BArF), 145.37 (d, J = 2.0 Hz, CAr), 161.13 (s, CAr), 161.54 (dd, J = 100.7, 48.67 Hz, ipso-C, BArF), 168.51 (d, J = 2.9 Hz, trans-CO), 169.81 (s, cis-CO). ^{31}P{^{1}H} NMR (243 MHz, C$_5$D$_5$Cl): δ 152.8. IR (CH$_2$Cl$_2$): ν(CO) 2099, 2062 cm^{-1}.
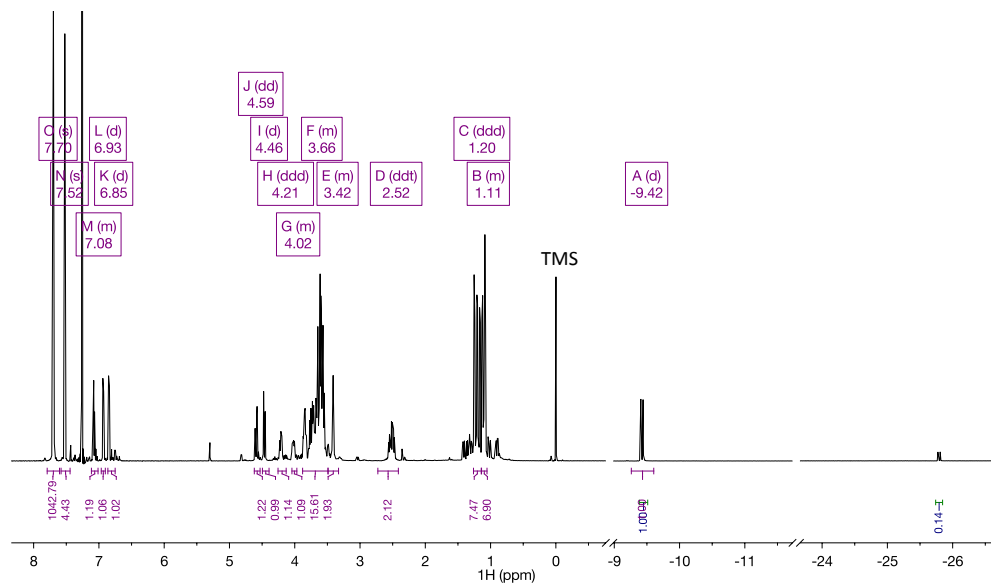
Figure 2.26. ^{1}H NMR spectrum of $[\kappa^3\text{-}(^{15c5}\text{NCOP}^{i\text{Pr}})\text{Ir}(\text{H})(\text{CO})_2][\text{BAr}^{\text{F}}_4]$ (**9**) in CDCl$_3$.
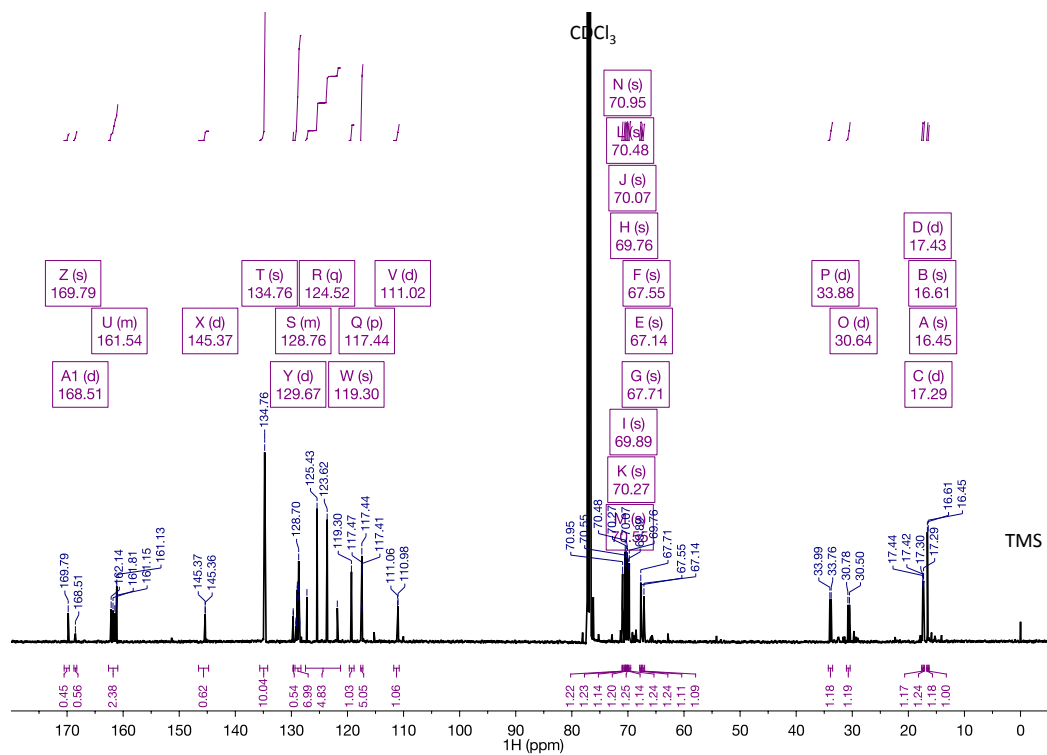
Figure 2.27. ^{13}C{^{1}H} NMR spectrum of $[\kappa^3\text{-}(^{15c5}\text{NCOP}^{i\text{Pr}})\text{Ir}(\text{H})(\text{CO})_2][\text{BAr}^{\text{F}}_4]$ (**9**) in CDCl$_3$.
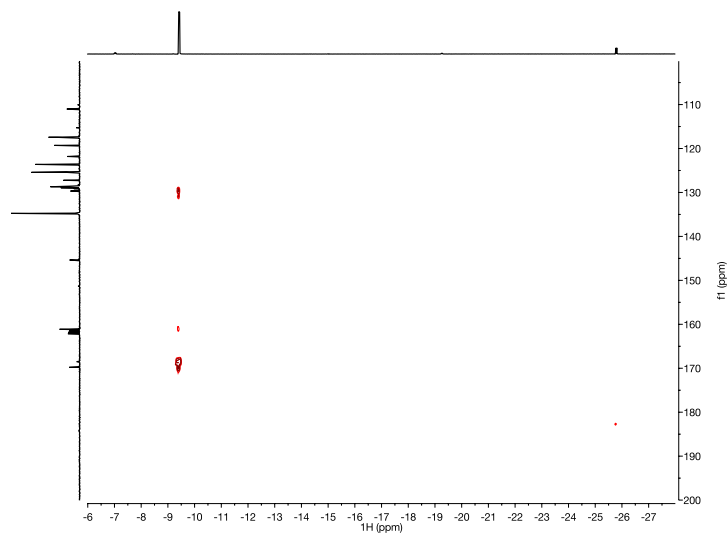
Figure 2.28. ^{1}H-^{13}C HMBC NMR spectrum of the hydride region of κ^3-[(^{15c5}NCOP^{iPr})Ir(H)(CO)$_2$][BAr$^F_4$] (**9**) in CDCl$_3$.
Two cross-peaks corresponding to bound carbonyls are observed at 168.51 and 169.81 ppm.
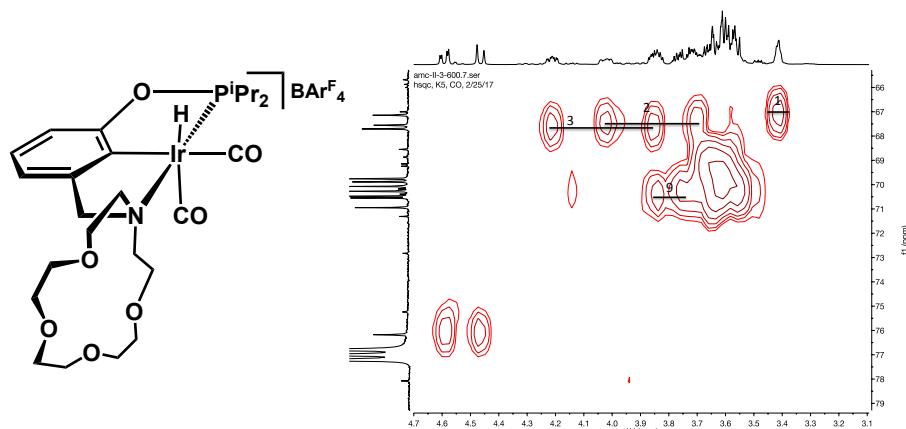
Figure 2.29. ^{1}H-^{13}C HSQC NMR spectrum (crown region) of [κ^3-(^{15c5}NCOP^{iPr})Ir(H)(CO)$_2$][BAr$^F_4$], (**9**) in CDCl$_3$.

Decarbonylation of 6-cis

A 20 mL scintillation vial charged with compound 6-cis (9.6 mg, 6.3 μmol), trimethylamine N-oxide (5 mg, 66.6 μmol), and THF was allowed to stir overnight. The solvent was removed under vacuum, and the crude reaction mixture was taken up in C$_6$D$_6$ for NMR analysis.

REFERENCES

(1)   Jeffrey, J. C.; Rauchfuss, T. B. Metal Complexes of Hemilabile Ligands. Reactivity and Structure of Dichlorobis(o- (diphenylphosphino)anisole)ruthenium(II). *Inorg. Chem.* **1979**, 18, 2658−2666.

(2)   Bader, A.; Lindner, E. Coordination Chemistry and Catalysis with Hemilabile Oxygen-Phosphorus Ligands. *Coord. Chem. Rev.* **1991**, 108, 27−110.

(3)   Kwong, F.; Chan, A. Recent Developments on Hemilabile P,O- Type Ligands in Cross-Coupling Reactions. *Synlett.* **2008**, 1440−1448.

(4)   Mark, S.; Wadepohl, H.; Enders, M. Molecular Weight Control in Organochromium Olefin Polymerization Catalysis by Hemilabile Ligand-Metal Interactions. *Beilstein J. Org. Chem.* **2016**, 12, 1372− 1379.

(5)   Kingsbury, J. S.; Harrity, J. P. A.; Bonitatebus, P. J.; Hoveyda, A. H. A Recyclable Ru-Based Metathesis Catalyst. *J. Am. Chem. Soc.* **1999**, 121, 791−799.

(6)   Matsugi, M.; Curran, D. P. Synthesis, Reaction, and Recycle of Light Fluorous Grubbs-Hoveyda Catalysts for Alkene Metathesis. *J. Org. Chem.* **2005,** 70, 1636−1642.

(7)   Kita, M. R.; Miller, A. J. M. Cation-Modulated Reactivity of Iridium Hydride Pincer-Crown Ether Complexes. *J. Am. Chem. Soc.* **2014**, 136, 14519−14529.

(8)   Grajeda, J.; Kita, M. R.; Gregor, L. C.; White, P. S.; Miller, A. J. M. Diverse Cation-Promoted Reactivity of Iridium Carbonyl Pincer- Crown Ether Complexes. *Organometallics* **2016**, 35, 306−316.

(9)   Gregor, L. C.; Grajeda, J.; Kita, M. R.; White, P. S.; Vetter, A. J.; Miller, A. J. M. Modulating the Elementary Steps of Methanol Carbonylation by Bridging the Primary and Secondary Coordination Spheres. *Organometallics* **2016**, 35, 3074−3086.

(10)   Miller, A. J. M. Cation-Modulated Hemilability in Pincer-Crown Ether Ligands: A Strategy for Tunable and Switchable Catalysis. *Dalton Trans.* **2017**, 46, 11987-12000.

(11)   Slone, C. S.; Weinberger, D. A.; Mirkin, C. A. The Transition Metal Coordination Chemistry of Hemilabile Ligands. Prog. *Inorg. Chem.* **1999**, 48, 233−350.

(12)   Machan, C. W.; Lifschitz, A. M.; Stern, C. L.; Sarjeant, A. A.; Mirkin, C. A. Crystallographic Snapshots of the Bond-Breaking Isomerization Reactions Involving Nickel(II) Complexes with Hemilabile Ligands. *Angew. Chem., Int. Ed.* **2012**, 51, 1469−1472.

(13)   Baranac-Stojanović, M. New Insight into the Anisotropic Effects in Solution-State NMR Spectroscopy. *RSC Adv.* **2014,** 4, 308−321.

(14)   Otting, G. Protein NMR Using Paramagnetic Ions. *Annu. Rev. Biophys.* **2010**, 39, 387−405.

(15) Pascal, R. A.; Grossman, R. B.; Van Engen, D. Synthesis of in- [34,10][7]metacyclophane: Projection of an Aliphatic Hydrogen toward the Center of an Aromatic Ring. *J. Am. Chem. Soc.* **1987**, 109, 6878−6880.

(16) Karabatsos, G. J.; Sonnichsen, G. C.; Hsi, N.; Fenoglio, D. J. Structure by Nuclear Magnetic Resonance. XIV. Anisotropic Effects of the Carbonyl Group. *J. Am. Chem. Soc.* **1967**, 89, 5067−5068.

(17) Cross, A. D.; Harrison, I. T. Spectra and Stereochemistry. VII. Long-Range Shielding by Nitrile Groups. *J. Am. Chem. Soc.* **1963**, 85, 3223−3228.

(18) Prestegard, J. H. New Techniques in Structural NMR Anisotropic Interactions. *Nat. Struct. Biol.* **1998**, 5, 517−522.

(19) Liu, Y.; Saurí, J.; Mevers, E.; Peczuh, M. W.; Hiemstra, H.; Clardy, J.; Martin, G. E.; Williamson, R. T. Unequivocal Determination of Complex Molecular Structures Using Anisotropic NMR Measurements. *Science* **2017**, 356, eaam5349.

(20) Hua, X.; von Zelewsky, A. Enantiomerically Pure Chiral RuII(L- L)2 Building Blocks for Coordination Compounds. *Inorg. Chem.* **1995**, 34, 5791−5797.

(21) Cotton, F. A.; Kitagawa, S. Preparation, Spectroscopic Properties, and Characterization of anti- and syn-α- Mo₂Cl₄[(C₆H₅)₂PCH₂CH₂P(p-CH₃C₆H₄)₂] in Solution and in the Solid State. *Inorg. Chem.* **1987**, 26, 3463−3468.

(22) McGlinchey, M. J. 2000 Alcan Award Lecture Adventures in Organometallic NMR: Steric Restraints, Slowed Rotations, and Skeletal Rearrangements. *Can. J. Chem.* **2001**, 79, 1295−1309.

(23) Mitchell, R. H.; Brkic, Z.; Berg, D. J.; Barclay, T. M. Effective Aromaticity of Tricarbonylchromiumbenzene, about 25% Enhanced over that of Benzene: Structural Evidence from a Complexed Benzannulene. *J. Am. Chem. Soc.* **2002**, 124, 11983−11988.

(24) Appleton, T. G.; Clark, H. C.; Manzer, L. E. The Trans- Influence: Its Measurement and Significance. *Coord. Chem. Rev.* **1973**, 10, 335−422.

(25) Babbini, D. C.; Iluc, V. M. Iridium PCsp3P-Type Complexes with a Hemilabile Anisole Tether. *Organometallics* **2015**, 34, 3141−3151.

(26) Kita, M. R.; Miller, A. J. M. An Ion-Responsive Pincer−Crown Ether Catalyst System for Rapid and Switchable Olefin Isomerization. *Angew. Chem., Int. Ed.* **2017**, 56, 5498−5502.

(27) Rybtchinski, B.; Ben-David, Y.; Milstein, D. Unexpected Isomerization of a Cis - into a Trans - Dihydride Complex. A Neutral Late Transition Metal Complex as a Hydride Donor. *Organometallics* **1997**, 16, 3786−3793.

(28)   Goldberg, J. M.; Wong, G. W.; Brastow, K. E.; Kaminsky, W.; Goldberg, K. I.; Heinekey, D. M. The Importance of Steric Factors in Iridium Pincer Complexes. *Organometallics* **2015**, 34, 753−762.

(29)   Adams, J. J.; Arulsamy, N.; Roddick, D. M. Acceptor PCP Pincer Iridium(I) Chemistry: Stabilization of Nonmeridional PCP Coordination Geometries. *Organometallics* **2011**, 30, 697−711.

(30)   Luh, T.-Y. Trimethylamine N-Oxide-A Versatile Reagent For Organometallic Chemistry. *Coord. Chem. Rev.* **1984**, 60, 255−276.

(31)   Semenov, V. A.; Samultsev, D. O.; Krivdin, L. B. Theoretical and Experimental Study of ^{15}N NMR Protonation Shifts. *Magn. Reson. Chem.* **2015**, 53, 433−441.

(32)   Iglesias,M.;Peŕez-Nicolaś,M.;Miguel,P.J.S.;Polo,V.; Fernańdez-Alvarez,F.J.;Peŕez-Torrente, J.J.; Oro,L.A. A Synthon for a 14-Electron Ir(III) Species: Catalyst for Highly Selective β-(Z) Hydrosilylation of Terminal Alkynes. *Chem. Commun.* **2012**, 48, 9480−9482.

(33)   Iguchi, K.; Kaneta, S.; Mori, K.; Yamada, Y.; Honda, A.; Mori, Y. Bromovulone I and Iodovulone I, Unprecedented Brominated and Iodinated Marine Prostanoids with Anittumour Activity Isolated from the Japanese Stolonifer Clavularis viridis Quoy and Galmard. *J. Chem. Soc., Chem. Commun.* **1986**, 981−982.

(34)   Kleinpeter, E.; Koch, A.; Seidl, P. R. Visualization and Quantification of the Anisotropic Effect of C–C Double Bonds on 1H NMR Spectra of Highly Congested Hydrocarbons-Indirect Estimates of Steric Strain. *J. Phys. Chem. A* **2008**, 112, 4989−4995.

(35)   Winstein, S.; Carter, P.; Anet, F. A. L.; Bourn, A. J. R. The Effects of Steric Compression on Chemical Shifts in Half-Cage and Related Molecules. *J. Am. Chem. Soc.* **1965**, 87, 5247−5249.

(36)   Kleinpeter, E.; Klod, S. Separation of Anisotropic and Steric Substituent Effects - Nuclear Chemical Shielding Analysis of H-4 and C-4 in Phenanthrene and 11-Ethynylphenanthrene. *J. Am. Chem. Soc.* **2004**, 126, 2231−2236.

(37)   Afonin, A. V. Effect of Aromatic Ring Anisotropy on the 1H NMR Shielding Constants and Conformational Equilibrium of Sterically Strained Aryl Vinyl Ethers. *Russ. J. Org. Chem.* **2011**, 47, 496−499.

(38)   Tori, K.; Aono, K.; Kitahonoki, K.; Takano, Y.; Muneyuki, R.; Tanida, H.; Tsuji, T. NMR Studies of Bridged Ring Systems. X. Long- Range Anisotropic Shielding Effects of an Epoxide and an Azridine Ring. *Tetrahedron Lett.* **1966**, 7, 2921−2926.

(39)   Kleinpeter, E.; Stoss, S.; Gabler, M.; Schroth, W. The Stereochemistry of Crown Ethers. *Magn. Reson. Chem.* **1989**, 27, 676−683.

(40)   Vougioukalakis, G. C.; Grubbs, H. Ruthenium-Based Hetero- cyclic Carbene-Coordinated Olefin Metathesis Catalysts. *Chem. Rev.* **2010**, 110, 1756−1787.

(41) Weng, Z.; Teo, S.; Hor, T. S. A. Metal Unsaturation and Ligand Hemilability in Suzuki Coupling. Acc. Chem. Res. 2007, 40, 676−684.

(42) Ryken, S. A.; Schafer, L. L. N,O-Chelating Four-Membered Metallacyclic Titanium(IV) Complexes for Atom-Economic Catalytic Reactions. *Acc. Chem. Res.* **2015**, 48, 2576−2586.

(43) Bei, X.; Uno, T.; Norris, J.; Turner, H. W.; Weinberg, W. H.; Guram, A. S.; Petersen, J. L. Phenyl Backbone-Derived P, O- and P, N- Ligands for Palladium/Ligand-Catalyzed Aminations of Aryl Bromides, Iodides, and Chlorides. Syntheses and Structures of (P, O)n- Palladium(II)Aryl(Br) Complexes. *Organometallics* **1999**, 18, 1840− 1853.

(44) Lindner, E.; Scheytt, C.; Wegner, P. Neuartige Basische Liganden Fur Die Homogenkatalytische Methanolcarbonylierung. *J. Organomet. Chem.* **1986**, 308, 311−323.

(45) Jung, S.; Brandt, C. D.; Werner, H. A Cationic Allenylideneruthenium(II) Complex with Two Bulky Hemilabile Phosphine Ligands. *New J. Chem.* **2001**, 25, 1101−1103.

(46) Liu, Y.; Kean, Z. S.; d'Aquino, A. I.; Manraj, Y. D.; Mendez- arroyo, J.; Mirkin, C. A. Palladium(II) Weak-Link Approach Complexes Bearing Hemilabile N-Heterocyclic Carbene−Thioether Ligands. *Inorg. Chem.* **2017,** 56, 5902−5910.

(47) Martinsen, A.; Songstad, J.; Larsson, R.; Pouchard, M.; Hagenmuller, P.; Andresen, A. F. Preparation and Properties of Some Bis(triphenylphosphine)iminium Salts, [(PhP)N]X. *Acta Chem. Scand.* **1977**, 31a, 645−650.

(48) Yakelis, N. A.; Bergman, R. G. Safe Preparation and Purification of Sodium Tetrakis[(3,5-trifluoromethyl)phenyl]borate (NaBArF24): Reliable and Sensitive Analysis of Water in Solutions of Fluorinated Tetraarylborates. *Organometallics* **2005**, 24, 3579−3581.

(49) Sheldrick, G. M. Crystal Structure Refinement with SHELXL. *Acta Crystallogr., Sect. C: Struct. Chem.* **2015**, 71, 3−8.

(50) Sheldrick, G. M. A Short History of SHELX. *Acta Crystallogr., Sect. A: Found. Crystallogr.* **2008**, 64, 112−122.

(51) Saint; SADABS; Apex3; Bruker AXS: Madison, WI, 2012.

(52) Dolomanov, O. V.; Bourhis, L. J.; Gildea, R. J.; Howard, J. A. K.; Puschmann, H. OLEX2: A Complete Structure Solution, Refinement and Analysis Program. *J. Appl. Crystallogr.* **2009**, 42, 339−341.

CHAPTER 3. ORGANOMETALLIC ELABORATION AS A STRATEGY FOR TUNING THE SUPRAMOLECULAR CHARACTERISTICS OF AZA-CROWN ETHERS

I.   Introduction

Host-Guest Interactions in Crown Ethers

Crown ethers are quintessential cation-binding macrocycles in supramolecular chemistry. The discovery of crown ethers helped spark a wave of research into synthetically tunable constructs for molecular recognition.[1−3] The fundamental knowledge of host−guest properties has enabled applications in a variety of fields including sensing,[4] separations,[5,6] and molecular machines.[7−11]

Hundreds of macrocyclic structures have been prepared using synthetic organic methods to tailor ion recognition properties.[12,13] New crown ethers are typically prepared via macrocyclization reactions that can be tedious, unselective, and low-yielding.[14,15] Post-macrocyclization synthetic modification, as in the installation of pendent donors ("lariat" ethers), offers an attractive alternative for systematic tuning.[16,17] We hypothesized that organometallic elaboration – installing an organotransition metal fragment on the periphery of a crown ether – would represent a robust, versatile, and reversible means of tuning host−guest properties.

Organometallic complexes offer several attractive features for tunable binding. First, strong transition metal−carbon bonds in the organometallic binding pocket could enforce guest molecule binding in the crown ether. Second, organometallic synthetic transformations could be used to change the structure of the metalla-crown ether and tune the host−guest properties. Of

particular interest was the ability of the proximal transition-metal center to support ion pair (ditopic) binding.[18−20] The ability of transition metals to control supramolecular traits is apparent in the coordination chemistry underpinning advances in on/off switching in artificial allosteric regulation of supramolecular constructs.[21−28] While many "metalla-crown ethers" (defined here as the broad class of crown ethers that incorporate a distinct transition-metal binding pocket) have been examined in the context of sensing and catalysis,[29−31] we are not aware of any systematic study of how changes at the transition-metal center influence the host−guest properties of the macrocycle.

 Our interest in the cation-modulated catalysis of "pincer-crown ether" ligands that incorporate an aza-crown ether macrocycle into a phenylphosphinite pincer framework led us to consider this platform for organometallic tuning of crown ether host−guest properties (Figure 3.1).[32] For applications in organometallic catalysis, we considered the cation−macrocycle interactions as tuning the reactivity of the transition-metal center.[33−38] However, the intramolecular communication can also be considered from the other perspective: changes to the transition-metal center should tune the host−guest properties of the crown ether.
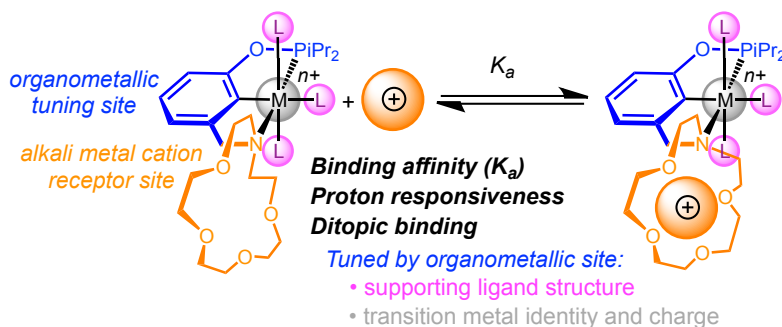
Figure 3.1. Overview of organometallic elaboration approach to tuning cation binding properties of an aza-crown ether

 In a prior study of nickel pincer-crown ether complexes which focused on drawing comparisons to catalytic inter-mediates, alkali metal cation binding affinity studies revealed some striking differences between organic crown ethers and the pincer-crown ether complexes.[38]

Because the amine donor of the aza-crown ether is bound to nickel, there are fewer donors available to bind alkali-metal cations, leading to a decrease in the binding affinity of the 1:1 cation:pincer-crown ether adducts. This change is accompanied by an increase in the selectivity for Li^+ over Na^+, however.

Herein, we show that straightforward synthetic modifications at the transition-metal center of pincer-crown ether complexes can tune the cation binding affinity, modulate Li^+/Na^+ selectivity, and enable ion pair recognition. This strategy is noteworthy for both for establishing dramatic changes in the supramolecular characteristics and providing a mechanism of subtle tuning of binding affinities.

II.   Results and Discussion

Tuning Supramolecular Properties through Installation of Organometallic Iridium on 1-Aza-15-crown-5-Ether

Initial studies tracked changes in the binding affinity and Li^+/Na^+ selectivity through the process of metalating an organic aza-crown ether. To enable comparisons with organic macrocycles, measurements were made in acetonitrile solution. The macrocycle 1-aza-15-crown-5 ether was selected as a starting point based on possible selectivity for Li^+ when the nitrogen donor is bound to a transition metal. We chose to focus on iridium complexes because of the ability of these species to readily access multiple oxidation states, coordination numbers, and charges through facile synthetic transformations.

Starting from 1-aza-15-crown-5 ether (**a15c5**),[39] reductive amination provides m-(aza-15-crown-5)methylphenol (**1,** Figure 3.5).[36,38] The pincer-crown ether ligand precursor **1** binds Li^+ and Na^+ cations tightly in a 1:1 fashion in CD_3CN at 25 ± 1 °C, as evidenced by the linear response of ^1H NMR spectroscopic titrations up until 1 equiv of the cation relative to the macrocycle. A competitive binding technique (experimental details in the Experimental Section)

70

provided association constants (K_a) for **1** with both LiOTf ($K_a(Li^+) = 130000 \pm 4000$ M^{-1}) and

NaBAr$^F_4$ ($K_a(Na^+) = 79000 \pm 4000$ M^{-1}, BAr$^F_4$ = 3,5-bis(trifluoromethyl)phenyl).[40] These values

are reasonable in comparison to those for other substituted N-benzylaza-15-crown-5 ethers,

which exhibit strong substituent effects in CH$_3$CN.[41] Phosphination of **1** provides the known

pincer-crown ether ligand (^{15c5}NCOP^{iPr})H (**2**),[33] which maintains $K_a(Li^+)$ and $Ka(Na^+)$ values

identical with those of **1** in CD$_3$CN at 25 $\pm$ 1 °C. Scheme 3.1 summarizes the synthetic steps and

binding affinity values. The salts LiOTf and NaBAr$^F_4$ were chosen to ensure solubility under

these conditions; comparisons of LiOTf and LiBAr$^F_4$ here and in a prior study show that

solvation by acetonitrile is sufficient to minimize counteranion effects.[38]

Scheme 3.1. Organometallic elaboration of 1-aza-15-crown-5 ether.
Synthetic modification changes binding affinity (K_a) and Li$^+$/Na$^+$ selectivity ($K_a(Li^+)/K_a(Na^+)$) in
CD$_3$CN. Reaction conditions: (i) 3-hydroxybenzaldehyde, NaHB(OAc)$_3$, THF; iPr$_2$PCl, NEt$_3$,
THF; (iii) Ir(CO)$_2$(Cl)(p-toluidine); (iv) KO^{t}Bu.
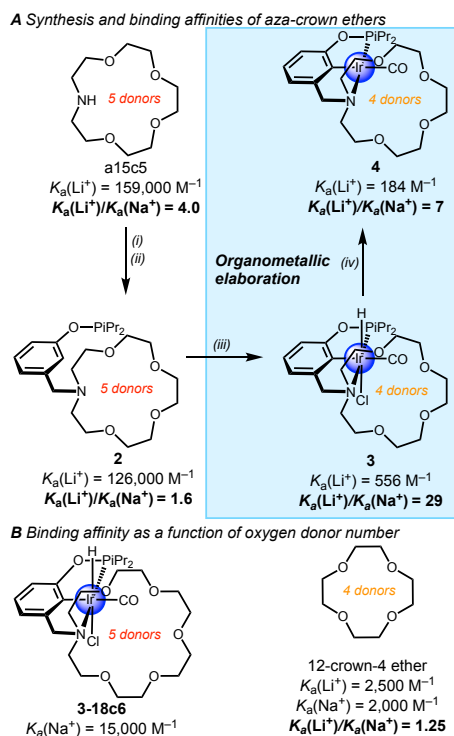
Metalation of **2** with Ir(CO)$_2$(Cl)(p-toluidine) provides the known d^6 Ir(III) complex (κ^3–

15c5NCOPiPr)Ir(H)(CO)(Cl) (**3**, Scheme 3.1).[42,43] Binding affinity curves were generated by

titration of Li^+ and Na+ salts into each host complex and measurement of changes in chemical shift. The binding isotherm curves were nicely fit by the expression for a 1:1 model at various concentrations and combined to yield an average binding affinity (see Experimental Details).[44] Titrations of **3** with LiOTf and $NaBAr^F_4$ provided binding affinities: $K_a(Li^+) = 560 \pm 44$ M^{-1} and $K_a(Na^+) = 19 \pm 2$ M^{-1}. An analogous titration of **3** with $LiBAr^F_4$, $K_a(Li^+) = 500 \pm 13$ M^{-1}, confirmed that counter-anion effects are minimal in acetonitrile.

The iridium metalla-crown ether complex **3** features exquisite selectivity for Li^+ over Na^+ ($K_a(Li^+)/K_a(Na^+)$ =29), as observed for nickel pincer-crown ether complexes.[38] Consistent with the independent measurements, complex **3** binds Li^+ preferentially in CD_3CN solutions containing an equimolar amount of $LiBAr^F_4$ and $NaBAr^F_4$ (Figure 3.2). The smaller K_a values for complex **3** relative to the organic crown ethers are the expected result of the nitrogen donor no longer participating in cation binding. Smaller K_a values are also observed on going from **a15c5** ($K_a(Li^+) = 160000$ M^{-1}; $K_a(Na^+)$ =40000 M^{-1} in CH_3CN) to the smaller, amine-free 12-crown-4 ether ($K_a(Li^+) = 2500$ M^{-1}; $K_a(Na^+) = 2000$ M^{-1}).[45,46] The binding affinity of the aza-15-crown-5-based pincer-crown ether complexes is in the same range of those of other four-oxygen macrocycles.
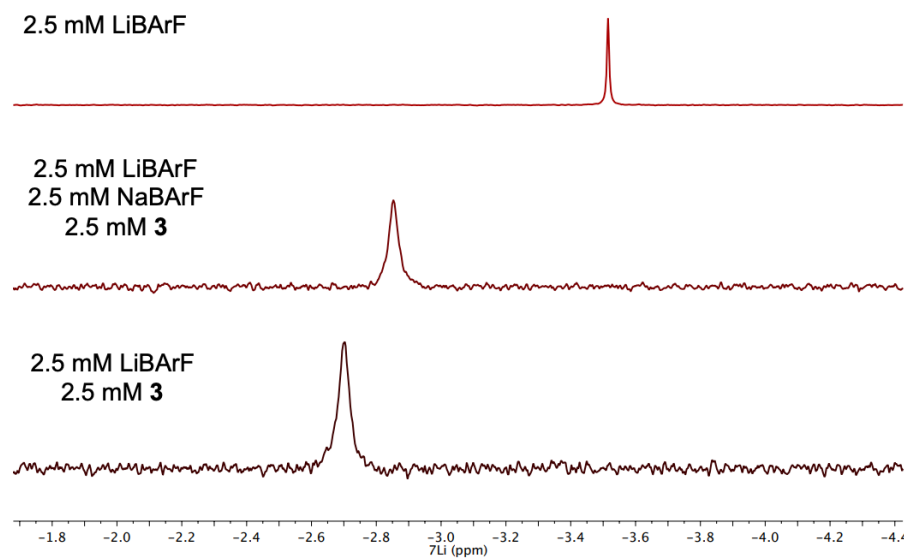
Figure 3.2. Li and Na$^+$ competitive binding in **3**.
Comparing the ^{7}Li chemical shift of Li$^+$, Na$^+$, and **3** (middle) with free LiBAr$^F_4$ (top) and Li$^+$ and **3** alone (bottom), shows that coordinated Li$^+$ is favored even in the presence of Na$^+$.

Higher affinities in the metalla-crown ethers can be accessed by starting with a larger macrocycle. A previously synthesized analogue containing an aza-18-crown-6 ether group, **3-18c6**,[36] has $K_a(Na^+) = 15000 \pm 4000$ M^{-1}, binding that cation much more tightly than **3**. Comparison of **3-18c6** and **a15c5**, which feature the same number of donor atoms in the crown ether, reveals only a 10-fold difference in K_a (Scheme 3.1).

Treating 15-crown-5-based complex **3** with KOtBu provides another neutral iridium species, (κ^3–^{15c5}NCOP^{iPr})Ir(CO) (**4**).[43] Alkali-metal salt titrations revealed a reduction in Li$^+$ binding affinity ($K_a(Li^+) = 180 \pm 6$ M^{-1}) without a significant change in Na$^+$ affinity ($K_a(Na^+) = 27 \pm 1$ M^{-1}). The cation binding properties of **3** and **4** foreshadow a broader ability to tune macrocyclic properties via the organometallic center. Complex **3** is an octahedral six-coordinate complex with a +3 formal Ir oxidation state, while complex **4** is a square planar four-coordinate complex with a +1 formal oxidation state. These structural and electronic differences are accompanied by a 3-fold change in both K_a and the relative binding affinity $K_a(Li^+)/K_a(Na^+)$.

To better understand how routine synthetic modifications of the transition-metal center can tune the cation binding properties of the crown ether, $K_a(Li^+)$ was determined for a series of pincer-crown ether complexes in which the identity of the transition metal, nature and orientation of ancillary ligands, and overall charge were systematically varied.

Tuning Lithium Ion Binding Affinity by Changing the Identity of the Transition Metal

The identity of the transition-metal ion was varied to compare binding affinity across an isoelectronic series of d^8 square-planar organo-metallic fragments. Figure 3.3A depicts the synthesis of new chloride complexes of nickel (κ^3-^{15c5}NCOP^{iPr})Ni(Cl) (**5-Cl**) (analogous to the known bromide),[35,38] palladium (κ^3-^{15c5}NCOP^{iPr})Pd(Cl) (**6**), and platinum (κ^3-^{15c5}NCOP^{iPr})-Pt(Cl) (**7**). Multinuclear NMR spectroscopy and single-crystal X-ray diffraction (XRD) analysis confirm a tridentate binding mode for complexes **5-Cl**, **6**, and **7** (Figure 3.3B) that leaves all four ether oxygen atoms free for binding cations.
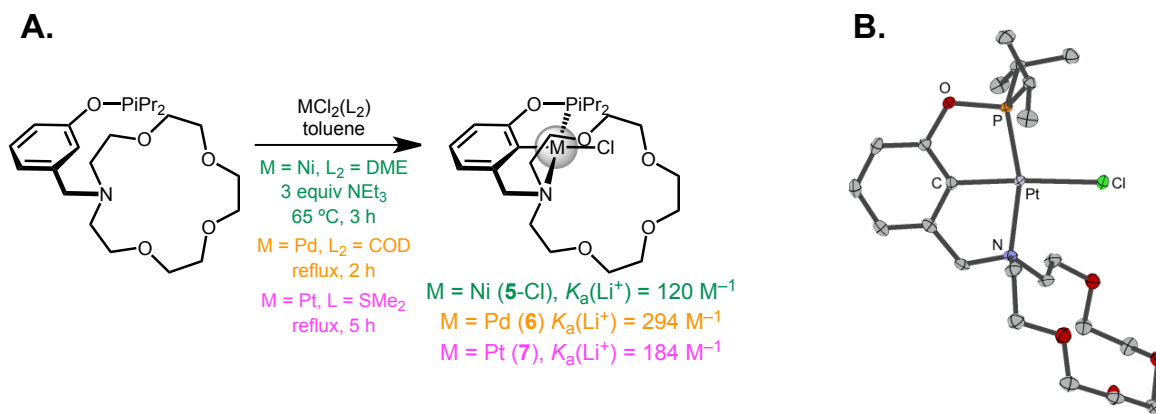
Figure 3.3. (**A**) Synthesis of group 10 pincer-crown ether complexes. (**B**) Structural representation of **7** from X-ray diffraction data.

The binding affinity of each group 10 organometallic complex with LiOTf was established by ^{1}H NMR titration in CD$_3$CN. The Ni complex **5-Cl** ($K_a = 110 \pm 13$ M^{-1}) has the

weakest Li^+ interaction of the series, while the Pd complex **6** (K_a = 290 ± 16 M−1) has the

strongest interaction, about a 3-fold enhancement. The Pt complex **7** (K_a = 190 ± 6 M^{-1}) and Ir

complex **4** (180 ± 6 M^{-1}) exhibit intermediate Li^+ binding. The complexes with lower LiOTf

binding affinity feature the most electronegative metals, consistent with the organometallic

fragment withdrawing more electron density from the amine nitrogen and ether oxygen

atoms.[38,41,47,48]

Tuning Lithium Ion Binding Affinity through Transition-Metal Ligand Substitution: Halide, Geometry, and Charge Effects

The various metalla-crown ethers were further elaborated using routine organometallic synthesis,

with the expectation that structural changes in the primary coordination sphere might influence

cation−macrocycle interactions. One of the simplest structural changes involves altering the

stereochemistry of the transition-metal complex (Figure 3.4A). The complex trans-(κ^3-

$^{15c5}NCOP^{iPr}$)Ir(H)(Cl)(CO) (**3-trans**), an isomer of **3** in which the carbonyl group is *trans* to the

hydride, was prepared by addition of CO to (κ^4-$^{15c5}NCOP^{ipr}$)Ir(H)(Cl).[33,49] Complex **3-trans**

($K_a(Li^+)$ = 790 ± 120 M^{-1}) has a slightly higher binding affinity for LiOTf in comparison to **3**

($K_a(Li^+)$ = 560 ± 44 M^{-1}). The increased affinity is attributed to favorable interactions between a

chloride lone pair and the crown-intercalated lithium ion, with the halide *cis* to the *hydride* better

positioned to help the macrocycle bind cations (Figure 3.4C).
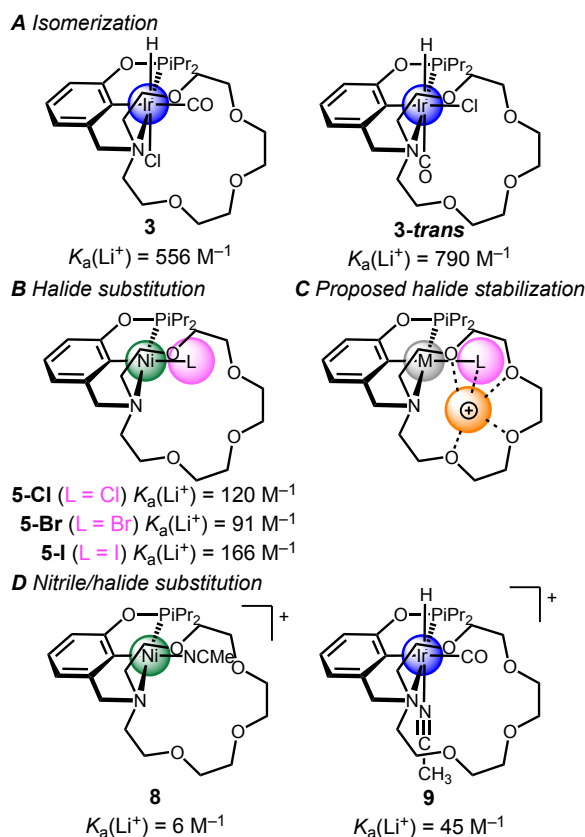
Figure 3.4. Tuning LiOTf binding affinity ($K_a(Li+)$) by isomerization.
(A) and halide substitution (B), along with the proposed role of halide bridges (C). Change in $K_a(Li^+)$ upon halide substitution by nitrile (D).

Ligand substitution is a fundamental inorganic reaction that offers another way to tune crown ether binding affinity remotely. As shown in Figure 3.4B, varying the halide in pincer-crown ether nickel complexes leads to a nearly 2-fold change in LiOTf binding affinity. The iodide complex (κ^3-^{15c5}NCOP^{iPr})NiI (**5-I**), prepared by addition of excess NaI to an acetone solution of **5-Br**,[50] binds LiOTf more tightly in comparison to the other halide complexes: $K_a(Li^+) = 170 \pm 70$ M^{-1}. The observed differences in binding affinity are hypothesized to derive from variations in the electron richness of nickel, as well as cooperative effects from halide lone pair donation to Li$^+$ (Figure 3.4C). The importance of interactions between cations and halide ligands is further underscored by the observation of a Ni−Na−Br bridge in the solid-state structure of (κ^3-^{15c5}NCOP^{iPr})Ni(Br)@NaBAr$^F_4$.[38]

Substitutions exchanging neutral and cationic ligands were also explored. Bromide substitution by the neutral donor acetonitrile forms the cationic complex [(κ^3-^{15c5}NCOP^{iPr})Ni(NCCH$_3$)][PF$_6$] (**8**).[35,38] Titration of **8** with LiPF$_6$ gave K$_a$ = 6 ± 4 M^{-1} – a 20-fold decrease in binding affinity. Similarly, iridium complex **3** undergoes facile halide substitution by acetonitrile to produce cationic [(κ^3-^{15c5}NCOP^{iPr})Ir(H)(CO)(NCCH$_3$)][BAr$^F_4$] (**9**). Titration of **9** with LiBArF4·3Et$_2$O gave K$_a$ = 45 ± 12 M^{-1} (Figure 3.4D). Changing the charge on the transition metal complex leads to a roughly 10-fold change in affinity in both Ni and Ir complexes. This decrease in binding affinity is attributed to unfavorable electrostatic interactions between the cationic alkali metal and the cationic nickel center, as well as the loss of any stabilizing interactions with halide lone pairs.

Proton-Responsive Behavior of Pincer–Crown Ether Complexes

One of the defining features of aza-crown ethers is proton responsive binding affinity.[51,52] Organic aza-crown ethers generally forfeit essentially all cation binding affinity upon protonation. Accordingly, the protonated form of **1**, [H(m-(aza-15-crown-5)methylphenol][BAr^{F}4] (**1-H$^+$**), exhibits a 4 orders of magnitude decrease in binding affinity toward Li$^+$(K$_a$(Li$^+$) = 6 ± 1 M^{-1}, Figure 3.5A). Some of the iridium pincer-crown ether complexes described above can be interconverted via proton transfer reactions, as shown in Figure 3.5B. For example, protonation of Ir(I) complex **4** (Ka(Li$^+$) = 180 M^{-1}) using an acid paired with a non-coordinating anion gives complex **9** (K$_a$(Li$^+$) = 45 ± 12 M^{-1}).[43] This 4-fold decrease in affinity stands in stark contrast to the 20000-fold decrease in affinity for the organic macrocycle.

The Ir(I) complex **4** is related to the Ir(III) complex **3** (K$_a$(Li$^+$) = 560 M^{-1}) by 1 equiv of HCl. Yet HCl addition results in a 3-fold increase in binding affinity (Figure 3.5B). The

organometallic pendant thus features distinct proton-responsive behavior relative to the free aza-crown ether: instead of a complete shutdown in the presence of acids seen in **a15c5**, the pincer-crown ether complexes maintain cation affinity upon protonation, with HCl addition even enhancing cation binding.
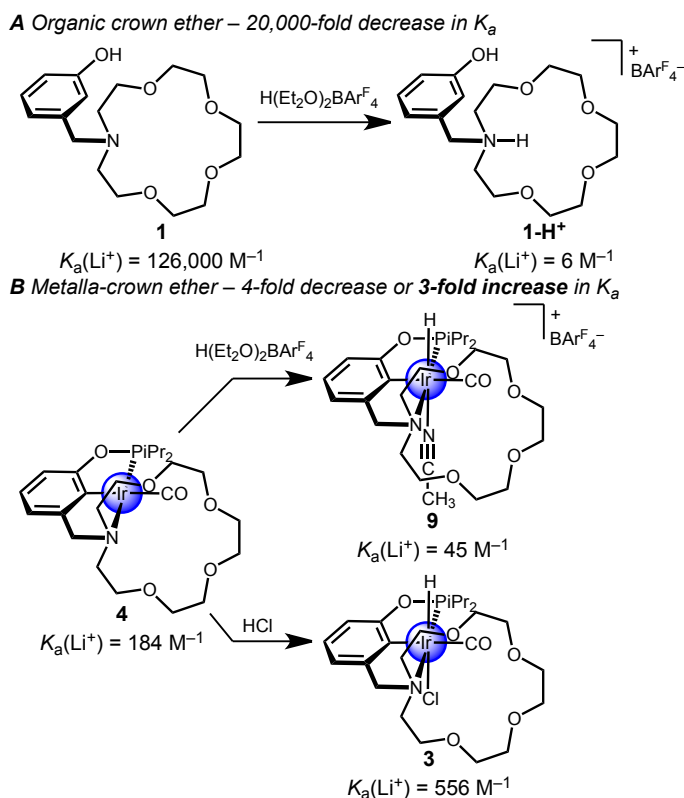
Figure 3.5. Proton-responsive behavior of pincer-crown ether complexes compared with organic crown ethers.

Turning on Ion Pair Recognition by Facile Synthetic Modification at the Iridium Center

The various iridium halide complexes examined above suggest that pincer-crown ether complexes should be capable of ion pair recognition (i.e., ditopic binding). Organic aza-crown ethers are generally only suitable for cation binding. Ditopic binding by transition-metal-based metalla-crown ethers is relatively rare.[53,54] In pincer-crown ethers, however, an appropriately configured transition-metal center could be harnessed to access ion pair recognition.[55,56]

To engage anion binding capabilities, a cationic iridium complex was targeted. The bis(acetonitrile) complex salt [(κ³-¹⁵ᶜ⁵NCOP^iPr)Ir(H)(NCCH₃)₂][BAr^F₄] (**10**) was prepared by dissolution of the known complex [(κ⁵-¹⁵ᶜ⁵NCOP^iPr)Ir(H)][BAr^F₄][33] in acetonitrile. LiI was selected for ion pair binding studies on the basis of the favorable solubility of this salt (Table 3.1).

Table 3.1. Salt solubility screening.
Salts screened at an approximately 50 mM concentration. Heat map of observed solubility is reported: insoluble (red), partially soluble (orange), soluble (green), not tested (white).

	Cl⁻	Br⁻	I⁻	OTf⁻	OAc⁻	BF₄⁻	PF₆⁻	BPh₄⁻	B(C₆F₅)₄⁻	BAr^F₄
Li⁺	red	white	green	green	red	green	green	orange	green	green
Na⁺	red	red	green	green	red	green	red	white	green	green
K⁺	white	white	green	green	red	white	green	white	green	white
Bu₄N⁺	green	green	green	green	green	white	green	white	white	white
PPN⁺	green	green	green	orange	white	white	orange	white	white	white

Addition of 0.5 equiv of LiI to **10** results in partial conversion to two new species. Further addition of 20 equiv of LiI led to 97% conversion. The crown ether resonances of the products shifted with increasing LiI concentration, as expected for a Li⁺ binding process. The products are assigned as isomeric iodide complexes, given that the same species form upon dissolution of the iodide complex (κ⁴-¹⁵ᶜ⁵NCOP^iPr)Ir(H)(I)[49] (**11**) in CH₃CN. 2D NMR analysis, Δδ analysis,[49] and ¹⁵NCCH₃ labeling experiments (Assignment details in the Experimental Section) enabled assignment as the geometric isomers *cis*-(κ³-¹⁵ᶜ⁵NCOP^iPr)Ir(H)(NCCH₃)(I) (**12-cis**) and *trans*-(κ³-¹⁵ᶜ⁵NCOP^iPr)Ir(H)(I)(NCCH₃) (**12-trans**), where *cis* and *trans* refer to the relationship between the hydride and nitrile.

To quantitatively assess cooperativity,[57,58] the thermochemical cycle of Figure 3.6 was examined by independently establishing binding affinities for Li⁺ and I⁻. The Li⁺ binding

affinity of **10**, $K_a(Li^+) = 160 \pm 1\ M^{-1}$, was determined by fitting a binding isotherm from an NMR titration using the salt LiBAr$^F_4$, which features a noncoordinating anion. The iodide binding affinity was then examined with PPNI as a salt featuring a bulky cation that would not interact with the crown ether. Slow exchange among **10**, **12-cis**, and **12-trans** enabled the iodide binding affinity of **10** to be determined by NMR integration, with $K_a(I) = 370 \pm 32\ M^{-1}$ for **12-cis** and $K_a(I) = 200 \pm 12\ M^{-1}$ for **12-trans**.
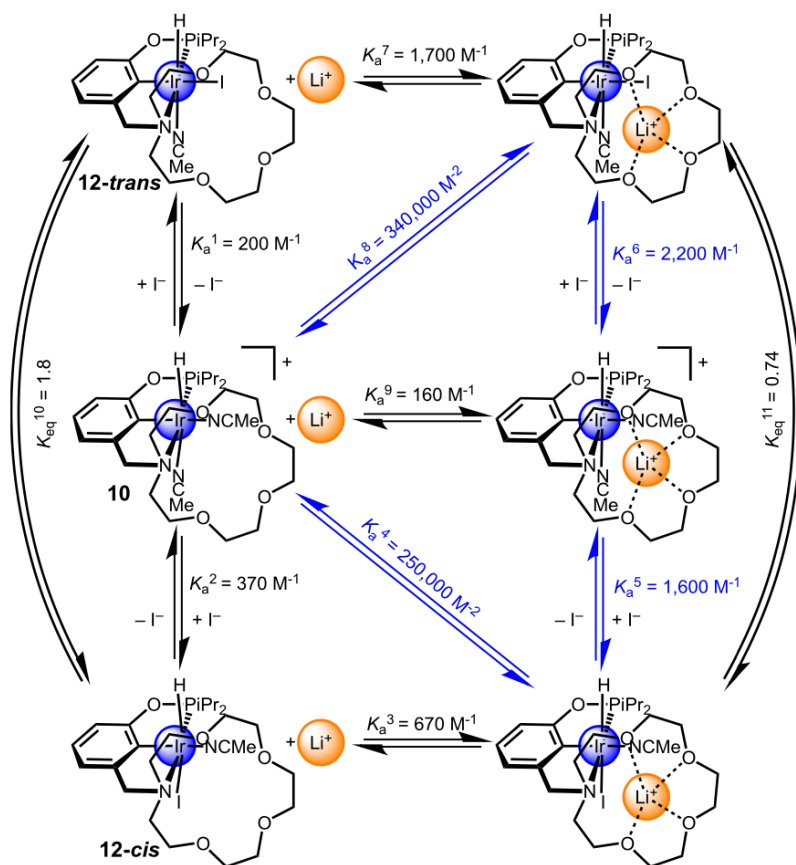
Figure 3.6. Ditopic binding map showing experimentally determined (black) and mathematically calculated (blue) binding affinities for LiBAr$^F_4$, PPNI, and LiI in CD$_3$CN.

The enhancement of Li$^+$ binding at the crown ether site engendered by iodide binding at the iridium center was probed by titration of **12-cis**/**12-trans** with LiBAr$^F_4$ under conditions of excess iodide, with $K_a(Li^+) = 670 \pm 12\ M^{-1}$ for **12-cis** and $K_a(Li^+) = 1700 \pm 65\ M^{-1}$ for **12-trans**.

The Li$^+$ binding affinity of **12-cis** is 4 times that of **10**. An even larger, 10-fold enhancement in Li$^+$ binding affinity is observed when **12-trans** and **10** are compared. The higher Li$^+$ affinity of **12-trans** is attributed to improved iodide donation to the encapsulated Li$^+$ ion, which leads to a striking change in the isomeric distribution: LiI addition favors formation of **12-trans**, while PPNI addition favors formation of **12-cis**. (Note that the K$_a$(Li$^+$) values obtained with LiBAr$^F_4$ are similar to those of other Ir(III) complexes obtained using LiOTf). Although LiCl is not sufficiently soluble for a full analysis, at least 10-fold enhancement in Li$^+$ binding is observed upon chloride binding to the analogous Ir carbonyl complex **9** (see above). These studies confirm that aza-crown ethers can be readily modified to enable ion pair recognition.

III.   Conclusions

Installing an organometallic pendant on 1-aza-15-crown-5 ether leads to four dramatic changes in host−guest properties. (1) The selectivity for Li$^+$ over Na$^+$ increases by as much as 29- fold. (2) The binding affinity for Li$^+$ and Na$^+$ salts is reduced substantially, although this decrease can be mitigated by increasing the donor number of the metalla-crown ether. (3) Distinct proton-dependent reactivity is observed, with protonation of Ir pincer-crown ether complex **4** leading to an increase in binding affinity. (4) The ion binding properties shift fundamentally to enable heteroditopic binding of ion pairs.

These properties can be further tuned through organometallic synthesis. The choice of transition-metal ion has a significant effect on the binding affinity, for example. In addition, ligand substitution on a particular transition-metal complex leads to substantial shifts in the crown ether Li$^+$ binding affinity. The electronic structure of the transition metal can favor or disfavor ditopic binding as well, with neutral square-planar transition-metal complexes expected to have low halide affinity relative to cationic transition-metal complexes with d^6 configuration.

No competition for the binding sites is observed in this system, thanks to the strong phenyl-phosphinite donor set.

This new strategy for post-macrocyclization modification takes advantage of the synthetic versatility and structural diversity of organometallic complexes to give both transformational changes and fine-tuned adjustments in the host−guest properties of crown ethers.

IV.   Experimental Details

General Considerations

Standard vacuum line and glovebox techniques were utilized to maintain a N_2 atmosphere during manipulation of all compounds, unless otherwise noted. Organic solvents were dried and degassed with argon using a Pure Process Technology solvent system and stored over 3 Å molecular sieves. Under standard glovebox operating conditions, pentane, diethyl ether, benzene, toluene, and tetrahydrofuran were used without purging, so traces of those solvents were present in the atmosphere and in the solvent bottles. ^{1}H, ^{31}P, and ^{13}C NMR spectra were recorded on 400, 500, 600, or 850 MHz spectrometers. NMR characterization data are reported at 25 °C, unless specified otherwise. All NMR solvents were purchased from Cambridge Isotopes Laboratories. Acetonitrile-d_3 (CD$_3$CN), benzene-d_6 (C$_6$D$_6$), and methylene chloride-d_2 (CD$_2$Cl$_2$) were freeze−pump−thaw-degassed three times, dried by passage through a small column of activated alumina, and stored over 3 Å molecular sieves. ^{1}H and ^{13}C chemical shifts are reported in parts per million relative to residual protio solvent resonances. All ^{31}P resonances are reported relative to 85% H$_3$PO$_4$ external standard (δ 0).

All ^{15}N experiments were referenced using absolute refencing relative to MeNO$_2$. The following compounds were synthesized according to literature procedures: *m*-(aza-15-crown-5)methylphenol (by reductive amination),[33,36] (^{15c5}NCOP^{iPr})H,[33] NaBAr$^F_4$,[59] LiBAr$^F_4$,[33] Pd(COD)Cl$_2$,[60] Pt(SMe$_2$)$_2$Cl$_2$,[61] (κ^3-^{15c5}NCOP^{iPr})Ni(Br),[35,38] [(κ^4-^{15c5}NCOP^{iPr})Ni][BAr$^F_4$],[38] (κ^3-^{15c5}NCOP^{iPr})Ir(CO),[43] (κ^3-^{15c5}NCOP^{iPr})Ir(H)(CO)(Cl),[43] and [(κ^3-^{15c5}NCOP^{iPr})Ir(H)(CO)(NCCH$_3$)][BAr$^F_4$].[43] Experimental details for **5-Cl, 5-I, 6,** and **7** are reported in the original text. LiOTf was dried under reduced pressure at 100 °C for 24 h prior to storage in

a N_2 glovebox. All other reagents were commercially available and used without further purification. Elemental analyses were performed by Robertson Microlit Laboratories (Ledgewood, NJ).

Competitive Binding Methodology

The calibrated competitive method for determining binding constants by NMR spectroscopy reported by Heath et al.[10] was used to determine binding affinities of **1** and **2** via competition with 15-crown-5 and 18-crown-6 (**1** only). Calibration curves were constructed for 15-crown-5 and LiOTf and $NaBAr^F_4$ in CD_3CN. A calibration curve was constructed with 18-crown-6 and $NaBAr^F_4$ in CD_3CN (18-crown-6 does not exhibit a linear response to $[Li^+]$ due to a lower binding affinity). The reference value (K_{ref}) used for Li^+ complexation by 15-crown-5 was $\log K_{ref} = 4.96$. The K_{ref} used for Na^+ complexation by 15-crown-5 was $\log K_{ref} = 5.1$. The K_{ref} used for Na^+ complexation by 18-crown-6 was $\log K_{ref} = 4.6$.

Triplicate samples of each reference/macrocycle/salt combination were prepared and analyzed as follows. A 60 mM stock solution of a reference molecule (15-crown-5 or 18-crown-6), a 60 mM stock solution of a (pre)ligand (**1, 2, 3-18c6**), and a 24 mM stock solution of salt (LiOTf or $NaBAr^F_4$) were prepared in CD_3CN. 100 μL aliquots of the reference and (pre)ligand stock solutions and 250 μL aliquots of the salt solution were combined in a 4 mL glass vial. The samples were diluted to 600 μL with CD_3CN, transferred to NMR tubes, and analyzed by ^1H NMR spectroscopy at 25 ± 1 °C. The resulting concentrations of all three species in each sample were 10 mM. The chemical shift of the organic crown ether was determined for each sample and compared to the calibration curve to obtain a binding affinity value. The standard deviation of the measured chemical shift values (~0.0002 ppm) was within the resolution limit of the spectrometer (0.006 ppm), so all binding affinity values measured in this way have an estimated uncertainty of ±4,000 M^{-1} based on the spectrometer resolution. Spectra of **3-18c6** and Na^+ are

provided as representative experiments; experiments with **1** and **2** are elaborated in the parent text.
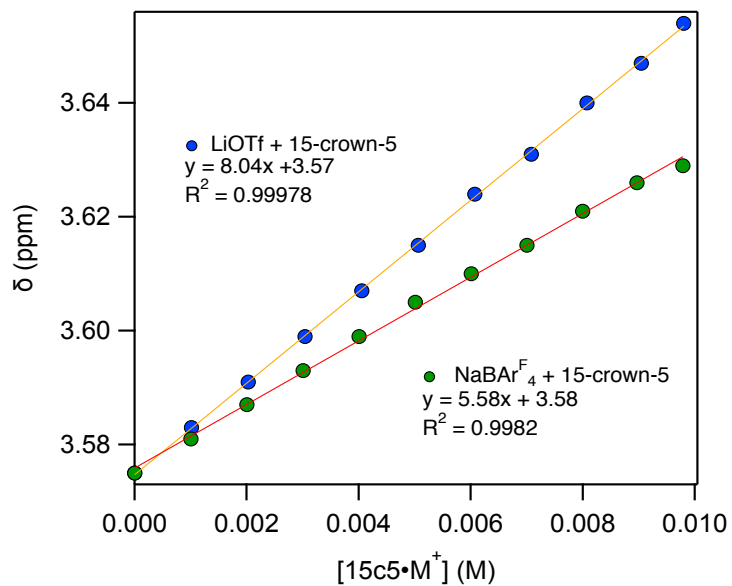
Figure 3.7. Calibration curves for binding of LiOTf and NaBAr$^F_4$ by 15-crown-5 in CD$_3$CN.
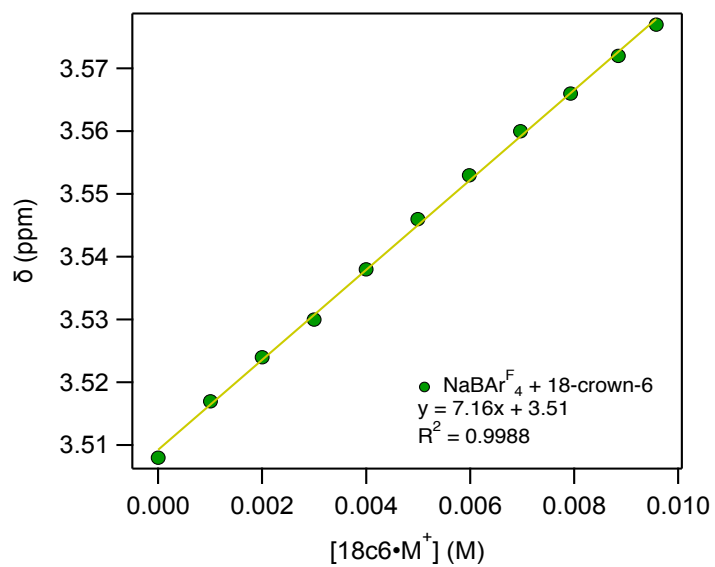
Figure 3.8. Calibration curves for binding of NaBAr$^F_4$ by 18-crown-6 in CD$_3$CN.
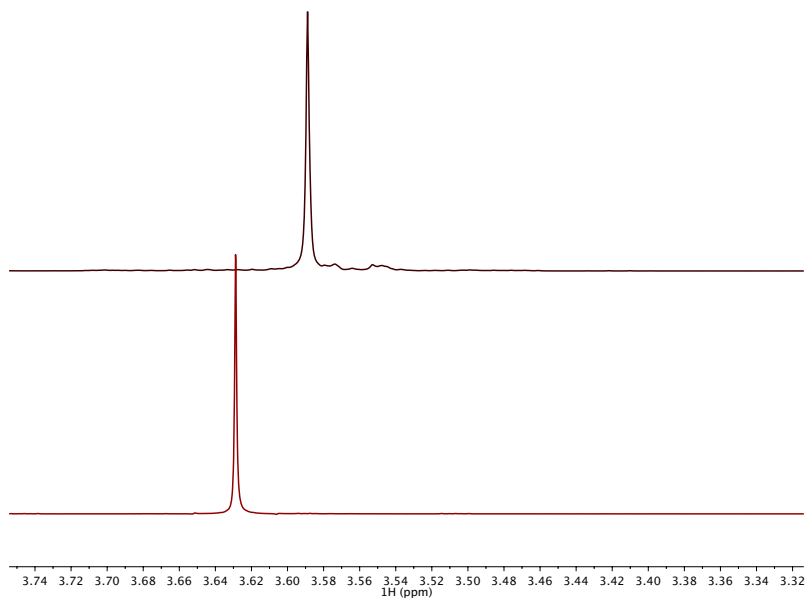
Figure 3.9. Competitive binding of 15-crown-5 ether with 3-18c6.
^{1}H NMR spectra (600 MHz) of 15-crown-5 ether. 1 equivalent NaBAr[F]$_4$, and **3-18c6** (top); 15-crown-5 ether and 1 equivalent NaBAr[F]$_4$ (bottom). Average of 3 tubes yields a K_a of 15000 ± 500 M^{-1}.
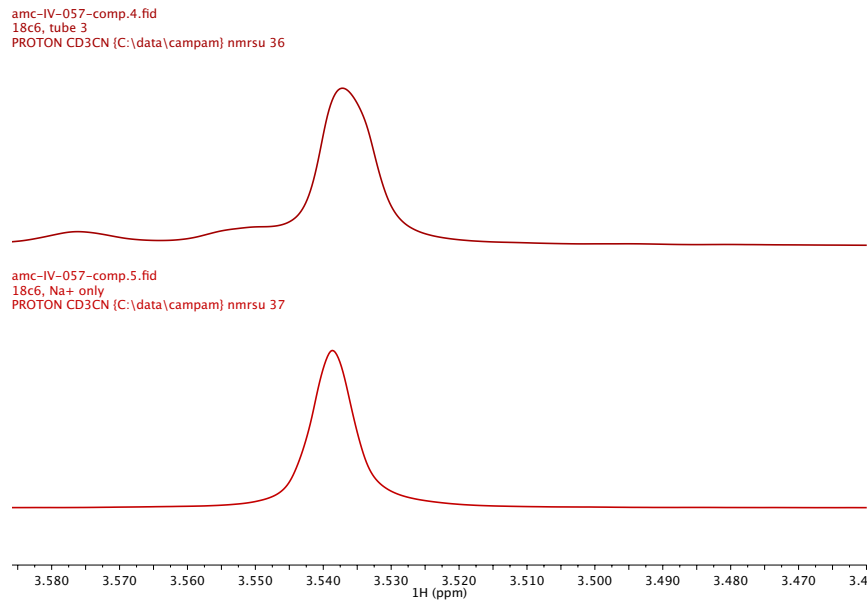
Figure 3.10. Competitive binding of 18-crown-6 ether with 3-18c6.
^{1}H NMR spectra (600 MHz) of 18-crown-6 ether, 1 equivalent NaBAr[F]$_4$, **3-18c6** (top); 18-crown-6 ether and 1 equivalent NaBAr[F]$_4$ (bottom). Average of 2 tubes yields a K_a of 15000 ± 500 M^{-1}.

General Procedure for Titration

The following general procedure is for titrations with a final analyte concentration of approximately 2.5 mM. Masses of solid reagents were obtained using balance with precision to 0.0001 g. A 12.3 mM stock solution of a macrocycle and a 48.4 mM stock solution of an alkali metal salt were prepared in CH_3CN. 125 µL aliquots (1.53×10^{-3} mmol) of the analyte solution were added to ten glass vials. Aliquots of the alkali metal stock solution corresponding to 0−60 equiv (up to 96.7×10^{-3} mmol) of alkali metal salt to analyte were then added to the vials containing the analyte. The protio solvent was completely evaporated under vacuum. The samples were then dissolved in 500 µL of CD_3CN, transferred to NMR tubes, and analyzed by ^1H NMR spectroscopy at 25 ± 1 °C. The final concentration of analyte in solution was 2.55 mM. The final concentration of alkali metal in the samples ranged from 0.00 to 161 mM.

The change in proton chemical shift vs. host/guest ratio was fit to the well-known 1:1 binding equilibrium model by least-squares analysis using the BindFit online software package.[44,62] All reported binding affinity values are derived from at least two titrations performed at different concentrations of the guest using the general procedure. The reported uncertainty is based on the standard deviation of K_a values obtained from fitting the binding isotherm data at the three different concentrations, which leads us to report K_a values to two significant figures. Representative titrations are reported here, with the remaining titration details in supplement of the parent text.
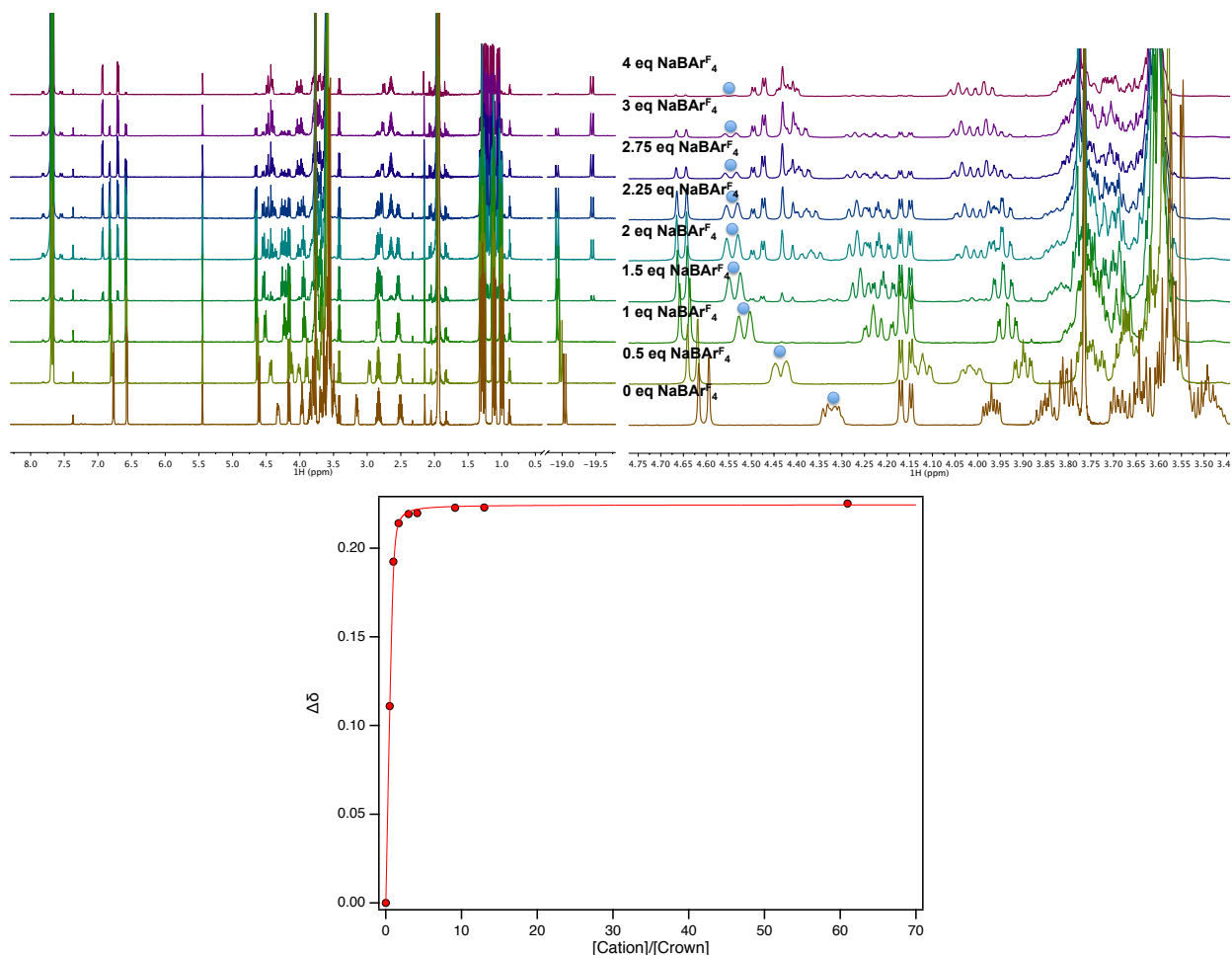
Figure 3.11. Titration of **3-18c6** with NaBAr$^F_4$.

(**Top**) ^{1}H NMR spectra of κ^3-(^{18c6}NCOP^{iPr})(H)Ir(CO)(Cl) (**3-18c6**) in CD$_3$CN in the presence of increasing concentrations of NaBAr$^F_4$, with blue circles marking peaks used to measure the change in chemical shift ($\Delta\delta$). At concentrations of NaBAr$^F_4$ greater than 1 equiv, halide abstraction is observed, leading to a new set of hydride peaks at -19.5. Concentrations of **3-18c6** were determined by integrating both iridium species to determine the mole fraction of **3-18c6** and multiplying by initial concentration. As the binding affinity of the new halide abstracted species was unknown, the amount of free Na$^+$ in solution was approximated by assuming complete binding of Na$^+$ and no binding of cation, with both approximations yielding a K$_a$ of 15,200 M^{-1} within error. (**Bottom**) Plot of $\Delta\delta$ as a function of Na$^+$/**3-18c6** concentration ratio (markers) and least squares fit for 1:1 binding. Initial concentration at 2.5 mM, but decreases due to halide abstraction with Na$^+$ addition. While a K$_a$ of 15,200 was able to be extracted by global fitting, this value is on the edge of what can accurately measured using this titration method. Competition experiments yielded the same value within error.
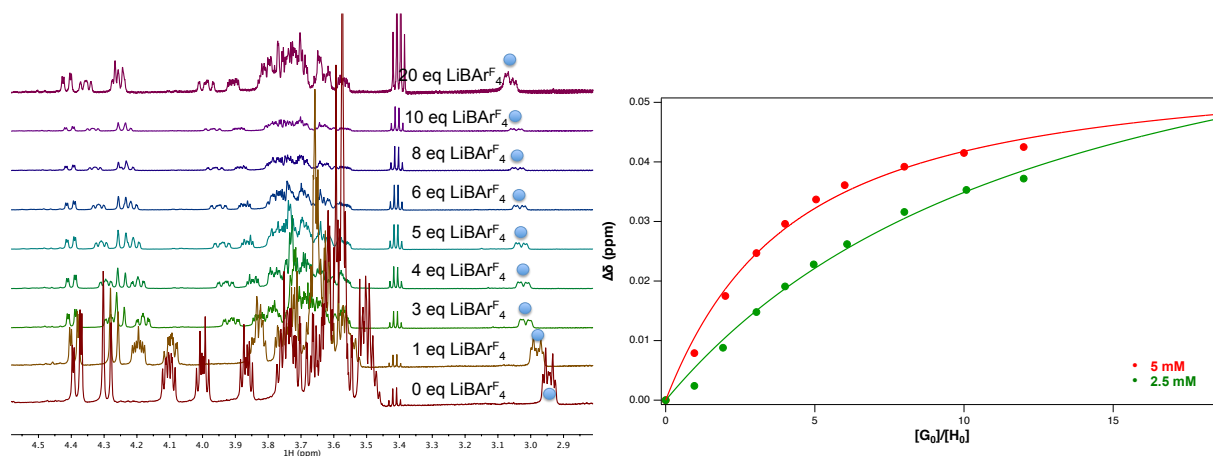
Figure 3.12. Binding isotherms for the titration of $[(\kappa^3\text{-}^{15c5}\text{NCOP}^{iPr})\text{Ir(H)(CO)(NCCH}_3)][\text{BAr}^F_4]$ (**9**) with LiBAr$^F_4$.

Binding isotherms for the titration $[(\kappa^3\text{-}^{15c5}\text{NCOP}^{iPr})\text{Ir(H)(CO)(NCCH}_3)][\text{BAr}^F_4]$ (**9**) with LiBAr$^F_4$. (**Left**) ^{1}H-NMR spectra of $[(\kappa^3\text{-}^{15c5}\text{NCOP}^{iPr})\text{Ir(H)(CO)(NCCH}_3)][\text{BAr}^F_4]$ (**9**) in CD$_3$CN in the presence of increasing concentrations of LiBAr$^F_4$, with blue circles marking peaks used to measure the change in chemical shift ($\Delta\delta$). (Right) Plots of $\Delta\delta$ as a function of the Li$^+$/**9** concentration ratio (markers) and least squares fit for 1:1 binding used to obtain K_a(Li$^+$): 57 M^{-1} (5.0 mM **9**) and 33 M^{-1} (2.5 mM **9**), average K_a(Li$^+$) = 50 ± 20 M^{-1}.

Ditopic Binding of LiI: Equilibrium Constants of Species in Slow Exchange

Mixtures of the iridium complexes **10**, **12-cis**, and **12-trans** in acetonitrile feature distinct resonances for each complex by ^{1}H NMR spectroscopy, indicating slow chemical exchange relative to the timescale of the NMR acquisition. This situation enables calculation of equilibrium constants for the interconversion of any two of these species directly by integration.

A 2.6 mM solution of iridium complex was prepared in CD$_3$CN. To this solution, 4.3 μL mesitylene was added as an internal standard. A separate stock solution containing 9 mM solution of PPNX (X = halide) in CH$_3$CN was prepared, and aliquots containing 0.52, 1.04, 2.08, and 4.16 equivalents of PPNX relative to iridium were distributed to four glass vials. Each vial was evaporated to dryness under vacuum, at which point 0.5 mL of the iridium stock solution was added to each vial. After the solids were dissolved, the solution was transferred to NMR tubes for analysis by ^{1}H NMR spectroscopy at 25 ± 1 °C.

Concentrations of each iridium species were determined by integration of the distinct resonances for each complex relative to the mesitylene internal standard. Iodide binding affinities or isomerization equilibria were calculated at each concentration of salt additive using the equilibrium

expressions in equations 1 and 2 (Figure 3.15). The equilibrium constant for interconversion between the two iodide complex isomers was calculated according to equation 3 (Figure 3.15). The reported iodide binding affinity and isomerization equilibrium values are the average of four values, with uncertainty given as the standard deviation.
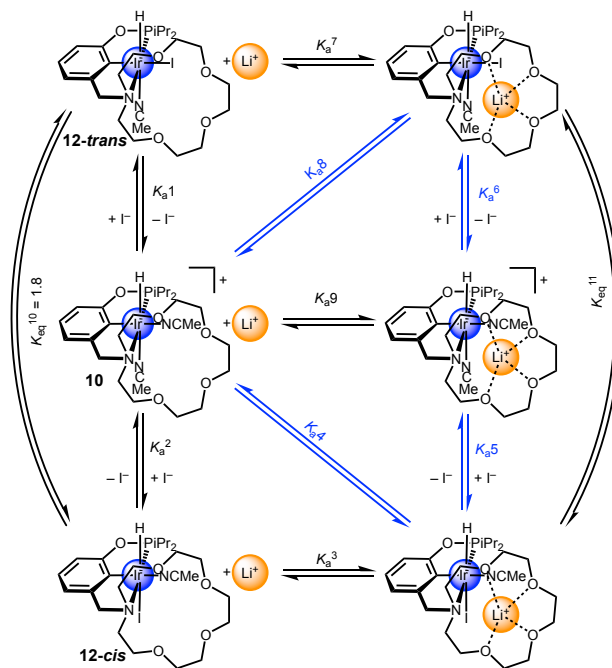
Figure 3.13. Square scheme of all I^- and Li^+ binding equilibria.
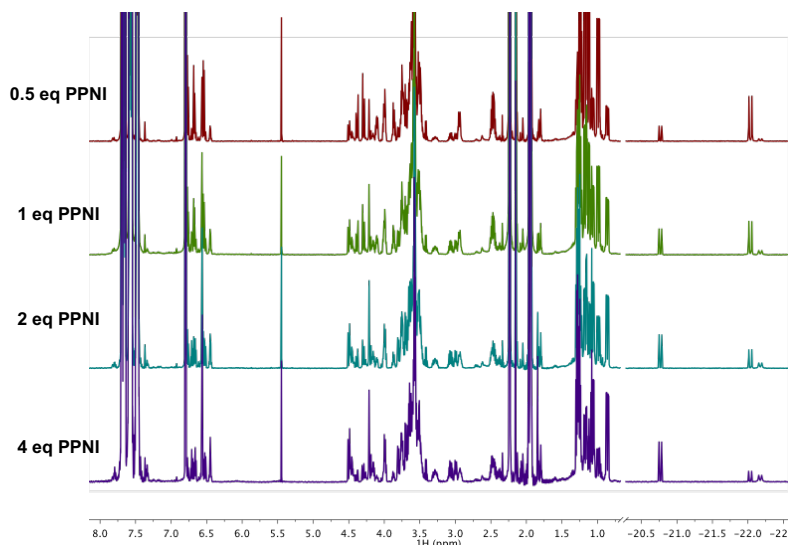
Figure 3.14. ^{1}H NMR spectra of $[\kappa^3\text{-}(^{15c5}NCOP^{iPr})Ir(H)(NCMe)_2][BAr^F_4]$ in CD_3CN with increasing amounts of PPNI.
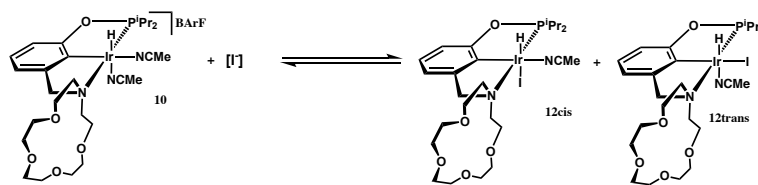
$$[I] = [MI]_o - ([12cis] + [12trans]) \ (1)$$

$$K_a^2 = \frac{[12cis]}{[10][I]} \ (2)$$

$$K_a^1 = \frac{[12trans]}{[10][I]} \ (3)$$

$$K_{eq}^{10} = \frac{[12cis]}{[12trans]} (4)$$

Equiv PPNI	K_a^2 (M^{-1})	K_a^1 (M^{-1})	K_{eq}^{10} (M^{-1})	Sum of K_a for I^- (M^{-1})
0.52	401	212	1.89	612
1.04	391	211	1.85	603
2.08	364	202	1.8	567
4.16	318	183	1.74	501
Average	369	202	1.82	571
Stdev	37	13	0.06	50

Figure 3.15. Binding affinity for iodide binding and cation free **12-cis/trans** isomerization equilibrium.

Ditopic Binding of LiI: Determining Ion-Pair Binding Affinity

The ion pair binding affinity can be obtained from the thermochemical cycle drawn below. The most useful comparison is how the Li^+ binding affinity, $K_a(Li^+)$, changes when I^- is bound to the host. The Li^+ binding affinity of **10**, in the absence of any iodide, was determined using standard titration method as described above. The situation is somewhat more complicated in the presence of free iodide ion, because Li^+ can bind to any of the three iridium complexes shown in Figure 3.15. Two assumptions are taken in order to simplify the treatment. First, it is assumed that complex **10** can be ignored. This is a reasonable assumption because the concentration of complex **10** is negligible under conditions of excess iodide (**10** constitutes <5% of Ir-containing species at 10 equiv PPNI, <2% of Ir-containing species at 20 equiv PPNI). Second, it is assumed that the total Li^+ concentration is available for binding by each of the individual complexes **12-cis** and **12-trans**. While the same pool of Li^+ supplies the two isomeric hosts, this assumption is reasonable because the Li^+ is present in relatively large excess during the titrations. Binding affinity values were then obtained by fitting the change in chemical shift of protons in **12-cis** and **12-trans** as a function of the Li^+/macrocycle ratio, as described above. At high concentrations of Li^+, where the binding isotherms have leveled off indicating high conversion to the Li^+ adducts of **12-cis** and **12-trans**, the relative ratio of these species was used to calculate K_{eq}[11].

Table 3.2. Changes in K_{eq}^{obs}, the observed ratio of **12-cis** vs **12-trans.**

At low Li^+ concentrations, values are closer to K_{eq}^{10}. At higher Li^+, the ratio approaches a new value, K_{eq}^{11}. Averaging the high Li^+ K^{obs} values (>5 equiv LiBArF4), yields an average K_{eq}^{11} of 0.74 ± 0.04.

	K_{eq}	
Equiv LiBArF$_4$	10 equiv PPNI	20 equiv PPNI
0	1.76	1.86
1	1.28	1.21
2	0.76	1.04
3	0.82	0.79
4	0.78	0.84
5	0.81	0.83
6	0.77	0.76
8	0.79	0.76
10	0.71	0.76
20	0.64	0.77
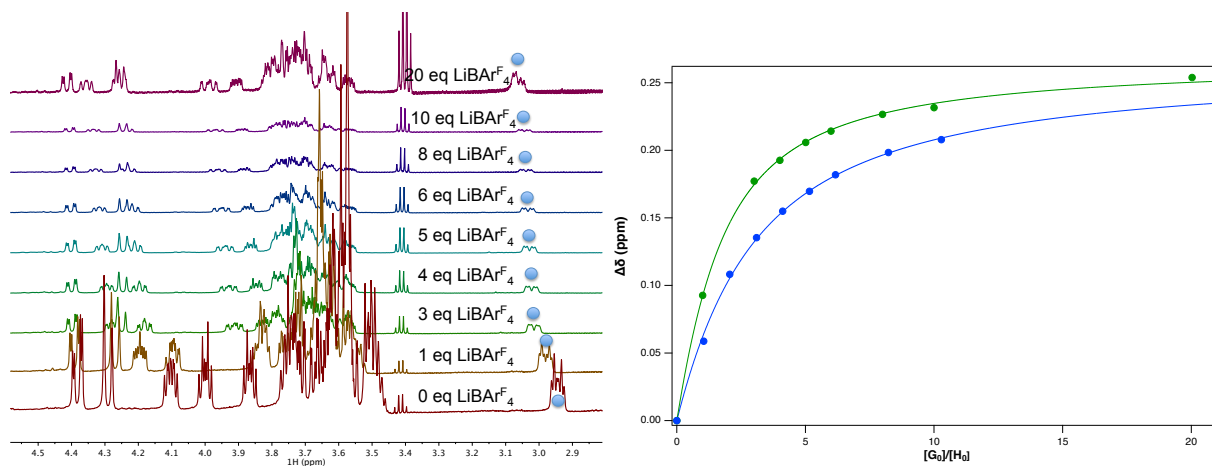
Figure 3.16. Binding isotherms for the titration of $[(\kappa^3-^{15c5}NCOP^{iPr})Ir(H)(NCCH_3)_2][BAr^F_4]$ (**10**) with LiBAr$^F_4$.

Binding isotherms for the titration $[(\kappa^3-^{15c5}NCOP^{iPr})Ir(H)(NCCH_3)_2][BAr^F_4]$ (**10**) with LiBAr$^F_4$. (**Left**) ^{1}H-NMR spectra of 5mmol $[(\kappa^3-^{15c5}NCOP^{iPr})Ir(H)NCCH_3)_2][BAr^F_4]$ (**10**) in CD$_3$CN in the presence of increasing concentrations of LiBAr$^F_4$, with blue circles marking peaks used to measure the change in chemical shift ($\Delta\delta$). (**Right**) Plots of $\Delta\delta$ as a function of the $Li^+/$**10** concentration ratio (markers) and least squares fit for 1:1 binding used to obtain $K_a(Li^+)$: 160 M^{-1} (5.0 mM **10**) and 159 M^{-1} (2.5 mM **10**), average $K_a(Li^+) = 159 \pm$ **1** M^{-1}.
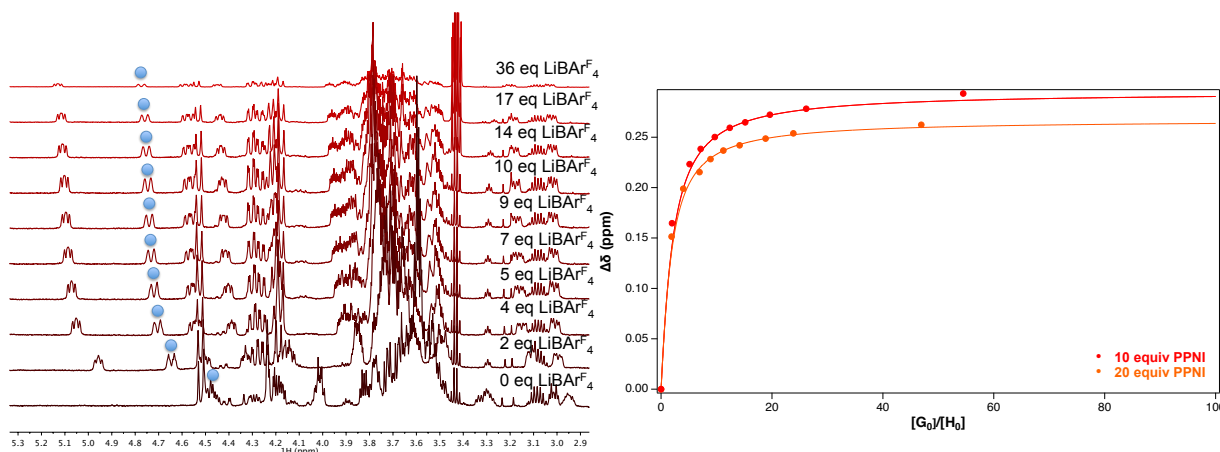
Figure 3.17. Binding isotherms for the titration of (κ^3-^{15c5}NCOP^{iPr})Ir(H)(NCCH$_3$)(I) (**12-cis**) with LiBAr$^F_4$.

Binding isotherms for the titration (κ^3-^{15c5}NCOP^{iPr})Ir(H)(NCCH$_3$)(I) (**12cis**) with LiBAr$^F_4$. (**Left**) ^{1}H-NMR spectra of (κ^3-^{15c5}NCOP^{iPr})Ir(H)(NCCH$_3$)(I) (**12cis**) in CD$_3$CN in the presence of increasing concentrations of LiBAr$^F_4$, with blue circles marking peaks used to measure the change in chemical shift ($\Delta\delta$). Iodide complex was generated in situ by adding excess 10 and 20 eq PPNI, and the concentration of the host calculated as a mol fraction of the initial 2.5 mM Ir added. (**Right**) Plots of $\Delta\delta$ as a function of the Li$^+$/**12-cis** concentration ratio (markers) and least squares fit for 1:1 binding used to obtain K$_a$(Li$^+$): 680 M^{-1} (20 eq PPNI, orange) and 657 M^{-1} (10 eq PPNI), average K$_a$(Li$^+$) = 670 ± 16 M^{-1}.
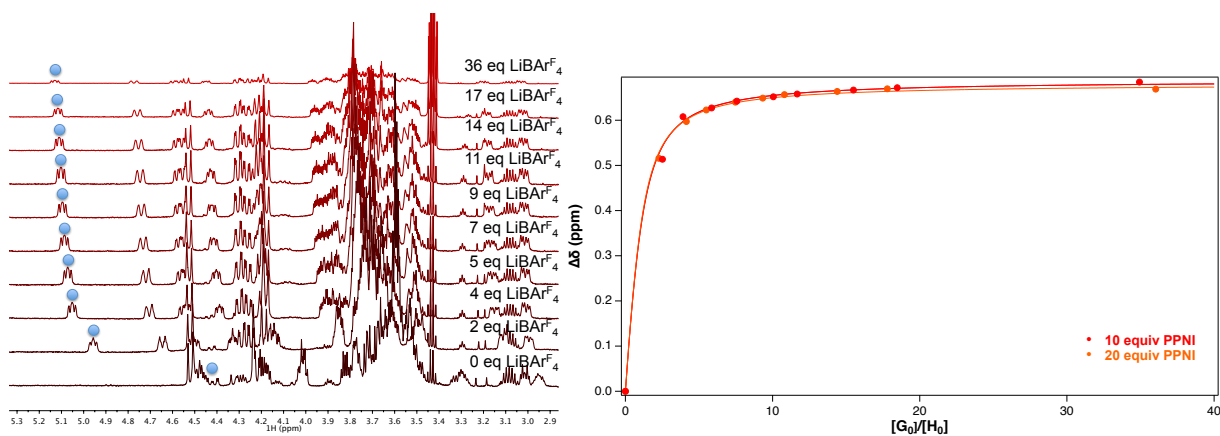
Figure 3.18. Binding isotherms for the titration of (κ^3-^{15c5}NCOP^{iPr})Ir(H)(I)(NCCH$_3$) (**12-trans**) with LiBAr$^F_4$.

Binding isotherms for the titration (κ^3-^{15c5}NCOP^{iPr})Ir(H)(I)(NCCH$_3$) (**12-trans**) with LiBAr$^F_4$. (**Left**) ^{1}H-NMR spectra of (κ^3-^{15c5}NCOP^{iPr})Ir(H)(I) (NCCH$_3$) (**12-trans**) in CD$_3$CN in the presence of increasing concentrations of LiBAr$^F_4$, with blue circles marking peaks used to measure the change in chemical shift ($\Delta\delta$). Iodide complex was generated in situ by adding excess 10 and 20 eq PPNI, and the concentration of the host calculated as a mol fraction of the initial 2.5 mM Ir added. (**Right**) Plots of $\Delta\delta$ as a function of the Li$^+$/**12-trans** concentration ratio (markers) and least squares fit for 1:1 binding used to obtain K$_a$(Li$^+$): 1780 M^{-1} (20 eq PPNI, orange) and 1650 M^{-1} (10 eq PPNI, red), average K$_a$(Li$^+$) = 1720 ± 90 M^{-1}.

Table 3.3. Equations for Calculating K_a in the LiI Square Scheme.

$$K_a^4 = \frac{[12cis]_{Li}}{[10][Li][I]} \ (8)$$

Substituting equations 2,5 into 8 yields:
$$K_a^4 = K_a^2 * K_a^3$$

Substituting equations 3,6 into 9 yields:
$$K_a^8 = K_a^1 * K_a^7$$

$$K_a^3 = \frac{[12cis]_{Li}}{[12cis][Li]} \ (5)$$

$$K_a^8 = \frac{[12cis]_{Li}}{[10][Li][I]} \ (9)$$

$$K_a^5 = \frac{[12cis]_{Li}}{[10]_{Li}[I]} \ (10)$$

$$K_a^7 = \frac{[12trans]_{Li}}{[12trans][Li]} \ (6)$$

$$K_a^9 = \frac{[10]_{Li}}{[10][Li]} \ (7)$$

$$K_a^6 = \frac{[12trans]_{Li}}{[10]_{Li}[I]} \ (11)$$

Substituting Equations 8,7 into 10:
$$K_a^5 = K_a^4/K_a^9$$

Substituting Equations 9,7 into 11:
$$K_a^6 = K_a^8/K_a^9$$

Plugging in calculated values of 4, 5, and 6 into 12 yields:
$$1.8 * 670 = K_{eq}^{11} * 1,720$$
$$K_{eq}^{11} = 0.70; \text{ within error of experimental value.}$$

$$K_{eq}^{10} * K_a^3 = K_{eq}^{11} * K_a^7 \ (12)$$

*Synthesis and Titration of [H(m-(aza-15-crown-5)methylphenol)][BArF4] (**1-H⁺**)*

In a glovebox, a vial was charged with 10.3 mg (0.0317 mmol) *m*-(Aza-15-crown-5)methylphenol and dissolved in ether (1 mL). Another vial was charged with $HBAr^F_4 \bullet 2Et_2O$ (34.2 mg, 0.0338 mmol) and dissolved in ether (1 mL). The two vials were allowed to cool in the freezer (-35 °C) for approximately twenty minutes. The $HBAr^F_4 \bullet 2Et_2O$ solution was then added dropwise to the solution of *m*-(aza-15-crown-5)methylphenol while stirring, and the reaction was allowed to warm up to room temperature. After approximately a half hour, the product was dried *in vacuo*, and washed with pentane to afford a white solid (35.7 mg, 94% yield).

^{1}H NMR (600 MHz, CD_2Cl_2): 7.72 (8H, t, J = 2.17 Hz, BArF), 7.56 (4H, s, BArF), 7.39 (1H, broad s, *H*N), 7.33 (1H, t, J = 7.89 Hz, Ar-*H*), 7.15 (1H, t, J = 1.68, Ar-*H*), 7.07 (1H, s, Ar-O*H*), 7.00 (1H, dd, J = 8.33, 2.06 Hz Ar-*H*), 6.87 (1H, dd, J = 7.54, 0.74 Hz, Ar-*H*), 4.30 (2H, d, J = 5.37 Hz, Ar-*CH₂*), 3.86-3.76 (4H, m, crown-*H*), 3.76-3.67 (8H, m, crown-*H*), 3.53-3.48 (4H, m, crown-*H*), 3.46-3.40 (2H, m, N-CH₂-C*H₂*), 3.36-3.29 (2H, m, N-C*H₂*-CH₂). ^{13}C{^{1}H} NMR (150.903 MHz, CD_2Cl_2): 161.81 (q, $^1J_{BC}$ = 49.9 Hz), 157.48, 134.73, 131.01, 128.77 (q, $^2J_{FC}$ = 31.7), 124.54 (q, $^1J_{FC}$ = 278.0 Hz), 121.37, 118.67, 117.43, 115.54, 69.88, 68.40, 62.64, 58.48, 55.16. HRMS: m/z calcd for $C_{17}H_{29}O_5N$ (M⁺) 326.1967, found m/z 326.19678.
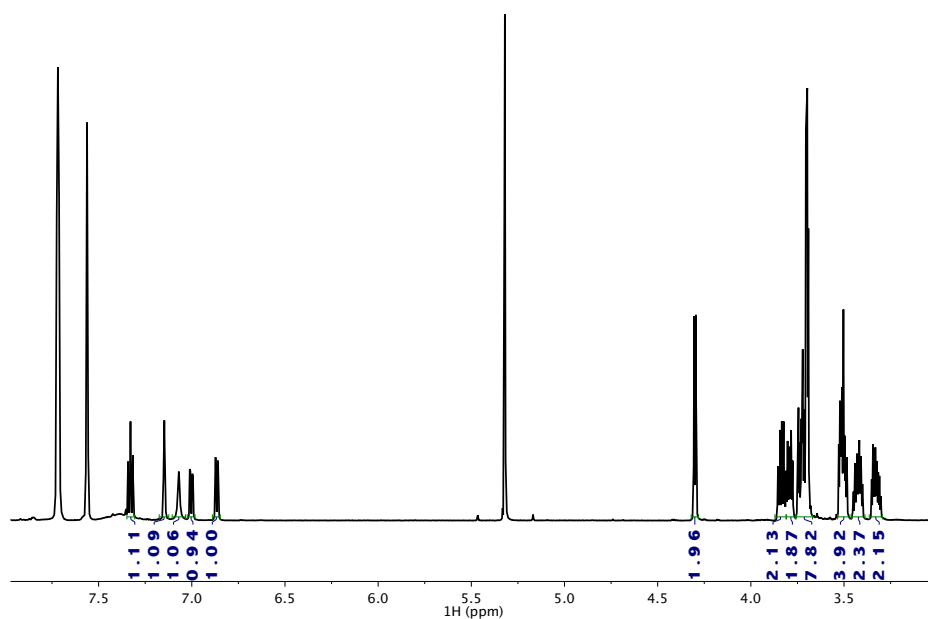
Figure 3.19. ^{1}H NMR spectrum (600 MHz) of [H(m-(aza-15-crown-5)methylphenol)][BAr$^F_4$] (**1-H$^+$**) in CD$_2$Cl$_2$.
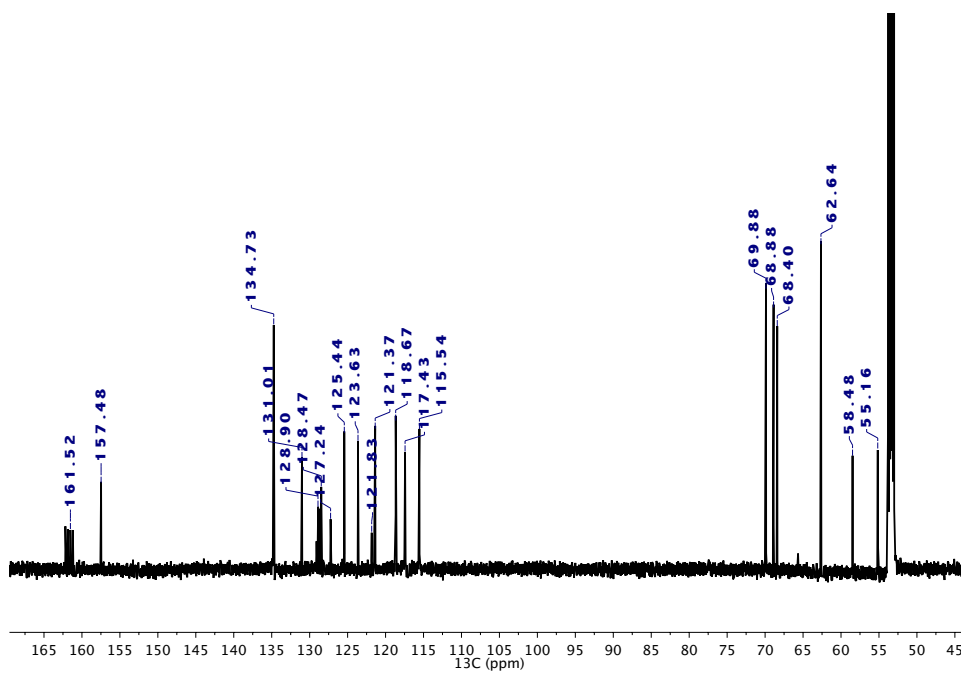
Figure 3.20. ^{13}C{^{1}H} NMR spectrum (151 MHz) of [H(m-(aza-15-crown-5)methylphenol)][BAr$^F_4$] (**1-H$^+$**) in CD$_2$Cl$_2$.
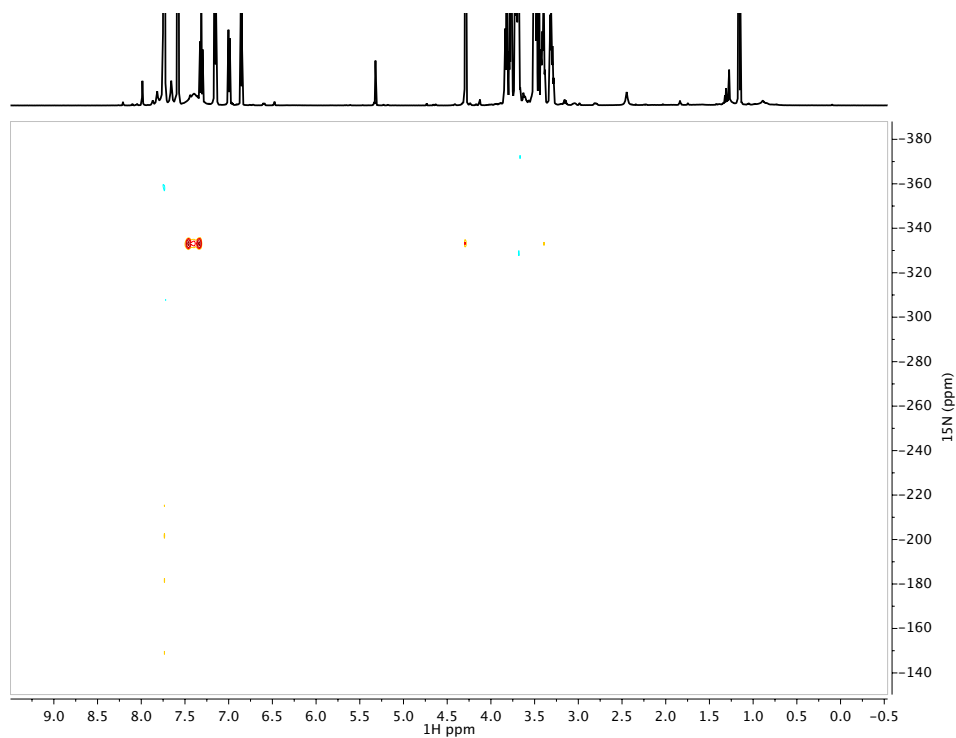
Figure 3.21. ^{15}N-^{1}H HMBC NMR (600 MHz, C) of [H(m-(aza-15-crown-5)methylphenol)][BAr$^F_4$] (**1-H$^+$)** in CD$_2$Cl$_2$.
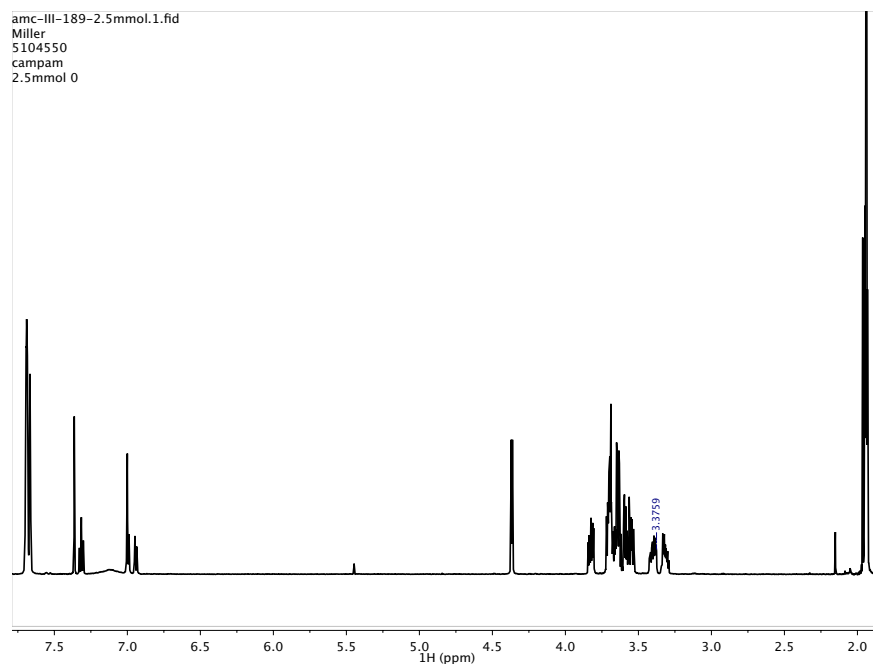
Figure 3.22. ^{1}H NMR spectrum (600 MHz) of [H(m-(aza-15-crown-5)methylphenol)][BAr$^F_4$] (**1-H$^+$)** in CD$_3$CN.
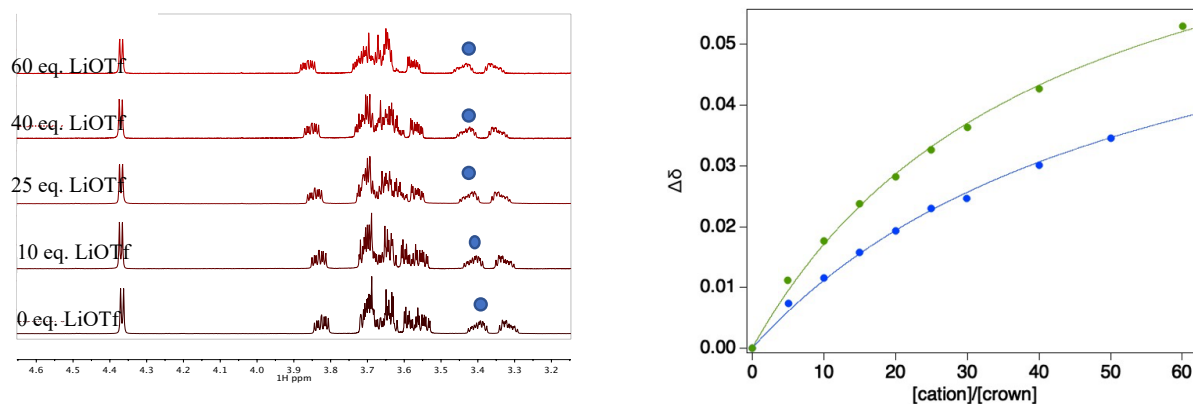
Figure 3.23. Binding isotherms for the titration of [H(m-(Aza-15-crown-5)methylphenol)][BAr$^F_4$] (**1-H$^+$**) with LiOTf.

Binding isotherms for the titration of [H(m-(Aza-15-crown-5)methylphenol)][BAr$^F_4$] (**1-H$^+$**) with LiOTf. (**Left**) ^{1}H-NMR spectra of [H(m-(Aza-15-crown-5)methylphenol)][BAr$^F_4$] (**1-H$^+$**) in CD$_3$CN in the presence of increasing concentrations of LiOTf, with blue circles marking peaks used to measure the change in chemical shift ($\Delta\delta$). ($\Delta\delta$) Plots of $\Delta\delta$ as a function of the Li$^+$/**1-H$^+$** concentration ratio (markers) and least squares fit for 1:1 binding used to obtain K$_a$(Li$^+$): 5.0 M^{-1} (5 mM **1-H$^+$**) and 7.0 M^{-1} (2.5 mM **1-H$^+$**), average K$_a$(Li$^+$) = 6.0 ± 1.4 M^{-1}.

*Speciation of (κ^{4}-^{15c5}NCOP^{iPr})Ir(H)(I) (**11**) in CD$_3$CN*
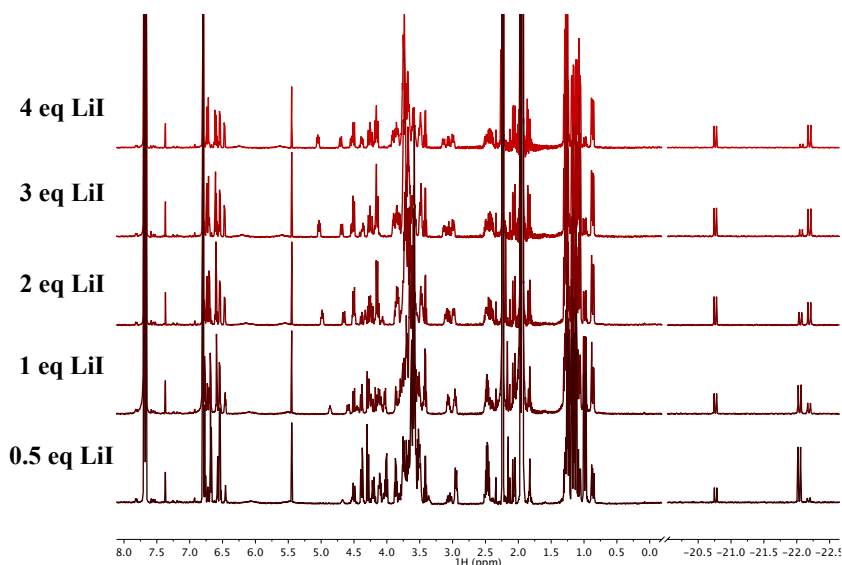
Figure 3.24. ^{1}H spectra (600 MHz, CD$_3$CN) of a titration of LiI into a solution containing 5mM **10.**

At low equivalents of LiI, the spectrum resembles cation free I$^-$ titrations, with **12-cis** being the favored iodine containing product. At high concentrations of LiI, speciation is flipped, with **12-trans** becoming the favored isomer.
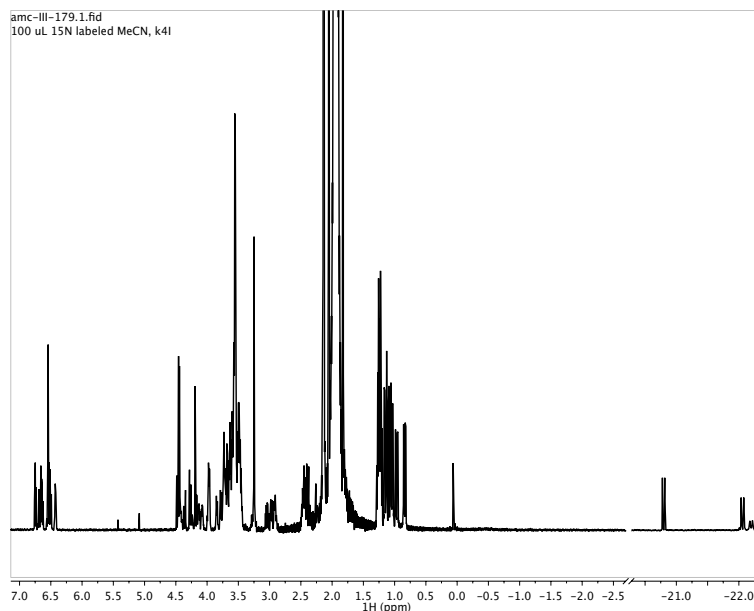
Figure 3.25, ^{1}H NMR spectrum after dissolution of (κ^4-^{15c5}NCOP^{iPr})Ir(H)(I) in CD$_3$CN spiked with 10% CH$_3$C^{15}N.

The hydride resonance at –20.8 ppm is consistent with an iodine trans to the hydride and ^{1}H-^{13}C HSQC analysis is consistent with a κ^3 species ($\Delta\delta_{avg}$ = 0.25 ppm).[49]
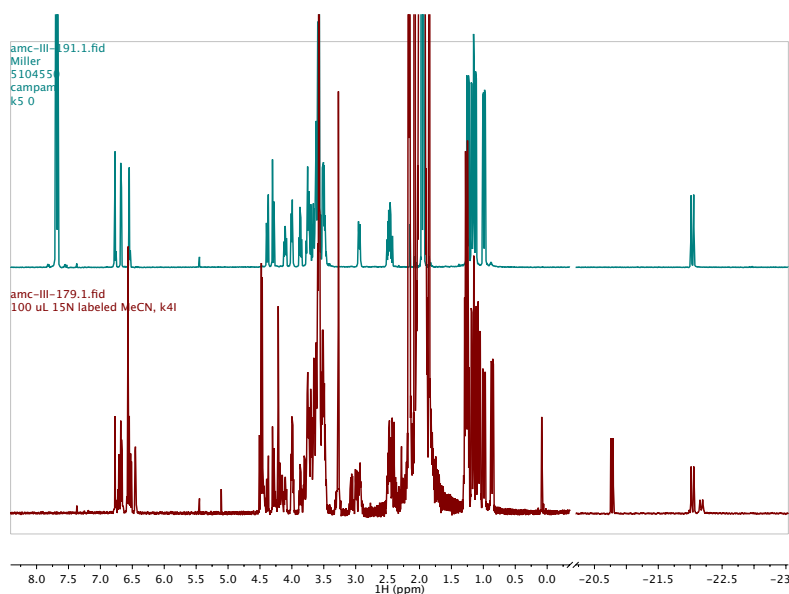
Figure 3.26. Assignment of the speciation of (κ^4-^{15c5}NCOP^{iPr})Ir(H)(I) (**11**).

^{1}H NMR spectra of [κ^3-^{15c5}NCOP^{iPr})Ir(H)(NCMe)$_2$][BAr$^F_4$] (**top**) and the mixture formed upon dissolution of (κ^4-^{15c5}NCOP^{iPr})Ir(H)(I) in CD$_3$CN (**bottom**). The species with a hydride resonance at –22.0 ppm is assigned as [$\varkappa^3$-(^{15c5}NCOP^{iPr})Ir(H)(NCMe)$_2$][I] based on the closely matched spectral features in the two spectra.

97
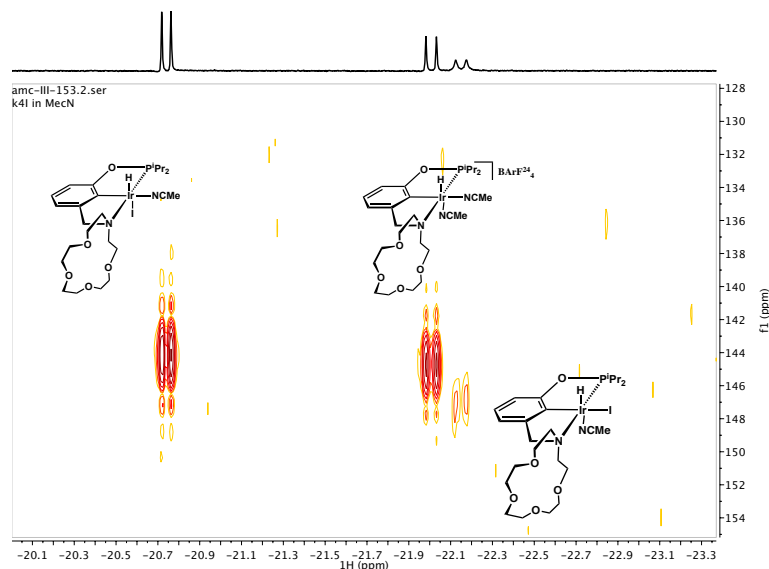
Figure 3.27. ^{1}H-^{31}P HMBC spectrum after dissolution of (κ^4-^{15c5}NCOP^{iPr})Ir(H)(I) (**11**) in CD$_3$CN. The ^{31}P chemical shifts are as follows: **12-cis,** δ 143.2; **10,** δ 143.8; **12-trans**, δ 146.1.
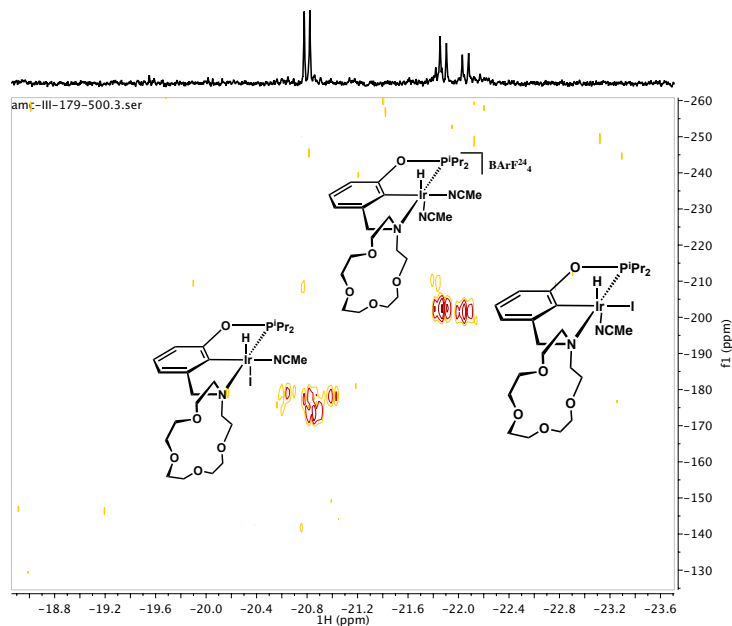
Figure 3.28. ^{1}H-^{15}N HMBC spectrum after dissolution of (κ^4-^{15c5}NCOP^{iPr})Ir(H)(I) (**11**) in CD$_3$CN spiked with 10% CH$_3$C^{15}N.

Cross-peaks are observed for each hydride at –30 °C, demonstrating that acetonitrile is bound in each species. While **10** shows evidence of a triplet in the proton spectrum (resulting from ^{31}P and ^{15}N coupling), the **12-cis** and **12-trans** do not. In the case of the **12-cis**, the coupling constants for a cis bound ^{15}N are expected to be small (<2 Hz) so observable coupling is not expected. **12-trans** should present itself as a triplet at room temperature, but this is not observed, presumably due to dynamic exchange with bulk acetonitrile.

REFERENCES

(1)   Cram, D. J. The Design of Molecular Hosts, Guests, and Their Complexes (Nobel Lecture). *Angew. Chem., Int. Ed. Engl.* **1988**, 27, 1009−1020.

(2)   Pedersen, C. J. The Discovery of Crown Ethers. *Angew. Chem., Int. Ed. Engl.* **1988**, 27, 1021−1027.

(3)   Lehn, J.-M. Supramolecular Chemistry: Scope and Perspectives Molecules, Supermolecules, and Molecular Devices(Nobel Lecture). *Angew. Chem., Int. Ed. Engl.* **1988**, 27, 89−112.

(4)   Gokel, G. W.; Leevy, W. M.; Weber, M. E. Crown Ethers: Sensors for Ions and Molecular Scaffolds for Materials and Biological Models. *Chem. Rev.* **2004**, 104, 2723−2750.

(5)   Zolotov, I. A. Macrocyclic Compounds in Analytical Chemistry; Wiley: New York, NY, 1997.

(6)   Industrial and Environmental Applications. Separation and Purification. In Applications of Supramolecular Chemistry; Lüning, U., Ed.; CRC Press: Boca Raton, FL, 2012; pp 159−172.

(7)   Leigh, D. A. Genesis of the Nanomachines: The 2016 Nobel Prize in Chemistry. *Angew. Chem., Int. Ed.* **2016**, 55, 14506−14508.

(8)   Feringa, B. L. The Art of Building Small: From Molecular Switches to Motors (Nobel Lecture). *Angew. Chem., Int. Ed.* **2017**, 56, 11060−11078.

(9)   Sauvage, J.-P. From Chemical Topology to Molecular Machines (Nobel Lecture). *Angew. Chem., Int. Ed.* **2017**, 56, 11080−11093.

(10)   Stoddart, J. F. Mechanically Interlocked Molecules (MIMs)- Molecular Shuttles, Switches, and Machines (Nobel Lecture). *Angew. Chem., Int. Ed.* **2017**, 56, 11094−11125.

(11)   Erbas-Cakmak, S.; Leigh, D. A.; McTernan, C. T.; Nussbaumer, A. L. Artificial Molecular Machines. *Chem. Rev.* **2015**, 115, 10081− 10206.

(12)   Izatt, R. M.; Pawlak, K.; Bradshaw, J. S.; Bruening, R. L. Thermodynamic and Kinetic Data for Macrocycle Interactions with Cations and Anions. *Chem. Rev.* **1991**, 91, 1721−2085.

(13)   Izatt, R. M.; Pawlak, K.; Bradshaw, J. S.; Bruening, R. L. Thermodynamic and Kinetic Data for Macrocycle Interaction with Cations, Anions, and Neutral Molecules. *Chem. Rev.* **1995**, 95, 2529− 2586.

(14) Bradshaw, J. S. Twenty-Five Years of "Crowning" Around: Synthesis of Crown Ethers at Brigham Young University. *J. Inclusion Phenom. Mol. Recognit. Chem.* **1997**, 29, 221−246.

(15) Krakowiak, K. E.; Bradshaw, J. S.; Zamecka-Krakowiak, D. J. Synthesis of Aza-Crown Ethers. *Chem. Rev.* **1989**, 89, 929−972.

(16) Elwahy, A. H. M.; Abbas, A. A. Synthesis of N -Pivot Lariat Ethers. *J. Heterocycl. Chem.* **2008**, 45, 1−65.

(17) Abbas, A. A.; Elwahy, A. H. M. Synthesis of C -Pivot Lariat Ethers. *J. Heterocycl. Chem.* **2009,** 46, 1035−1079.

(18) Tagne Kuate, A. C.; Iovkova, L.; Hiller, W.; Schurmann, M.; Jurkschat, K. Organotin-Substituted [13]-Crown-4 Ethers: Ditopic Receptors for Lithium and Cesium Halides. *Organometallics* **2010**, 29, 5456−5471.

(19) Arens, V.; Dietz, C.; Schollmeyer, D.; Jurkschat, K. Intra- molecularly Coordinated Bis(Crown Ether)-Substituted Organotin Halides as Ditopic Salt Receptors. *Organometallics* **2013**, 32, 2775− 2786.

(20) Wendji, A. S.; Lutter, M.; Dietz, C.; Jouikov, V.; Jurkschat, K. Novel Tin-Containing Crown Ether Substituted Ferrocenophanes as Redox-Active Hosts for the Ditopic Complexation of Lithium Chloride. *Organometallics* **2013**, 32, 5720−5730.

(21) Kremer, C.; Lützen, A. Artificial Allosteric Receptors. *Chem. - Eur. J.* **2013,** 19, 6162−6196.

(22) Wiester, M. J.; Ulmann, P. A.; Mirkin, C. A. Enzyme Mimics Based upon Supramolecular Coordination Chemistry. *Angew. Chem., Int. Ed.* **2011**, 50, 114−137.

(23) Lifschitz, A. M.; Rosen, M. S.; McGuirk, C. M.; Mirkin, C. A. Allosteric Supramolecular Coordination Constructs. *J. Am. Chem. Soc.* **2015**, 137, 7252−7261.

(24) Zhang, M.; Yan, X.; Huang, F.; Niu, Z.; Gibson, H. W. Stimuli- Responsive Host-Guest Systems Based on the Recognition of Cryptands by Organic Guests. *Acc. Chem. Res.* **2014**, 47, 1995−2005.

(25) Rebek, J.; Trend, J. E.; Wattley, R. V.; Chakravorti, S. Allosteric Effects in Organic Chemistry. Site-Specific Binding. *J. Am. Chem. Soc.* **1979**, 101, 4333−4337.

(26) Rebek, J.; Marshall, L. Allosteric Effects: An On-Off Switch. *J. Am. Chem. Soc.* **1983**, 105, 6668−6670.

(27) Rebek, J.; Costello, T.; Marshall, L.; Wattley, R.; Gadwood, R. C.; Onan, K. Allosteric Effects in Organic Chemistry: Binding Cooperativity in a Model for Subunit Interactions. *J. Am. Chem. Soc.* **1985**, 107, 7481−7487.

(28)   d'Aquino, A. I.; Cheng, H. F.; Barroso-Flores, J.; Kean, Z. S.; Mendez-Arroyo, J.; McGuirk, C. M.; Mirkin, C. A. An Allosterically Regulated, Four-State Macrocycle. *Inorg. Chem.* **2018**, 57, 3568−3578.

(29)   van Veggel, F. C. J. M.; Verboom, W.; Reinhoudt, D. N. Metallomacrocycles: Supramolecular Chemistry with Hard and Soft Metal Cations in Action. *Chem. Rev.* **1994**, 94, 279−299.

(30)   Gray, G. M. Metallacrown Ethers: Unique Organometallic Ligands. *Comments Inorg. Chem.* **1995**, 17, 95−114.

(31)   Yoo, C.; Dodge, H. M.; Miller, A. J. M. Cation-Controlled Catalysis with Crown Ether-Containing Transition Metal Complexes. *Chem. Commun.* **2019**, 55, 5047.

(32)   Miller, A. J. M. Controlling Ligand Binding for Tunable and Switchable Catalysis: Cation-Modulated Hemilability in Pincer- Crown Ether Ligands. *Dalton Trans* **2017**, 46, 11987−12000.

(33)   Kita, M. R.; Miller, A. J. M. Cation-Modulated Reactivity of Iridium Hydride Pincer-Crown Ether Complexes. *J. Am. Chem. Soc.* **2014**, 136, 14519−14529.

(34)   Kita, M. R.; Miller, A. J. M. An Ion-Responsive Pincer-Crown Ether Catalyst System for Rapid and Switchable Olefin Isomerization. *Angew. Chem., Int. Ed.* **2017**, 56, 5498−5502.

(35)   Smith, J. B.; Miller, A. J. M. Connecting Neutral and Cationic Pathways in Nickel-Catalyzed Insertion of Benzaldehyde into a C-H Bond of Acetonitrile. *Organometallics* **2015**, 34, 4669−4677.

(36)   Gregor, L. C.; Grajeda, J.; Kita, M. R.; White, P. S.; Vetter, A. J.; Miller, A. J. M. Modulating the Elementary Steps of Methanol Carbonylation by Bridging the Primary and Secondary Coordination Spheres. *Organometallics* **2016**, 35, 3074−3086.

(37)   Gregor, L. C.; Grajeda, J.; White, P. S.; Vetter, A. J.; Miller, A. J. M. Salt-Promoted Catalytic Methanol Carbonylation Using Iridium Pincer-Crown Ether Complexes. *Catal. Sci. Technol.* **2018**, 8, 3133− 3143.

(38)   Smith, J. B.; Kerr, S. H.; White, P. S.; Miller, A. J. M. Thermodynamic Studies of Cation-Macrocycle Interactions in Nickel Pincer-Crown Ether Complexes Enable Switchable Ligation. *Organometallics* **2017**, 36, 3094−3103.

(39)   Hojo, M.; Hisatsune, I.; Tsurui, H.; Minami, S. Interaction between Monoaza-, Diaza-, or Polyazacrown Ethers and Alkali Metal Ions in Acetonitrile by Polarography. *Anal. Sci.* **2000**, 16, 1277−1284.

(40)   Heath, R. E.; Dykes, G. M.; Fish, H.; Smith, D. K. Rapid Screening of Binding Constants by Calibrated Competitive ^{1}H NMR Spectroscopy. *Chem. - Eur. J.* **2003**, 9, 850−855.

(41)   Gustowski, D. A.; Gatto, V. J.; Mallen, J.; Echegoyen, L.; Gokel, G. W. Direct Correlation of Cation Binding Strengths to Hammett Parameters in Substituted N-Benzylaza-15-Crown-5 Lariat Ether and N,N'-Dibenzyl-4,13-Diaza-18-Crown-6 BiBLE Derivatives. *J. Org. Chem.* **1987**, 52, 5172−5176.

(42)   Roberto, D.; Cariati, E.; Psaro, R.; Ugo, R. Formation of [Ir(CO)$_2$Cl]$_x$ (x = 2, n) Species by Mild Carbonylation of [Ir(Cyclooctene)$_2$Cl]$_2$ Supported on Silica or in Solution: A New Convenient Material for the Synthesis of Iridium(I) Carbonyl Complexes. *Organometallics* **1994,** 13, 4227−4231.

(43)   Grajeda, J.; Kita, M. R.; Gregor, L. C.; White, P. S.; Miller, A. J. M. Diverse Cation-Promoted Reactivity of Iridium Carbonyl Pincer- Crown Ether Complexes. *Organometallics* **2016,** 35, 306−316.

(44)   Thordarson, P. Determining Association Constants from Titration Experiments in Supramolecular Chemistry. *Chem. Soc. Rev.* **2011**, 40, 1305−1323.

(45)   Arnaud-Neu, F.; Delgado, R.; Chaves, S. Critical Evaluation of Stability Constants and Thermodynamic Functions of Metal Complexes of Crown Ethers (IUPAC Technical Report). *Pure Appl. Chem.* **2003**, 75, 71−102.

(46)   Danil de Namor, A. F.; Ng, J. C. Y.; Llosa Tanco, M. A.; Salomon, M. Thermodynamics of Lithium-Crown Ether (12-Crown-4 and 1-Benzyl-1-Aza-12-Crown-4) Interactions in Acetonitrile and Propylene Carbonate. The Anion Effect on the Coordination Process. *J. Phys. Chem.* **1996**, 100, 14485−14491.

(47)   Allred, A. L.; Rochow, E. G. A Scale of Electronegativity Based on Electrostatic Force. *J. Inorg. Nucl. Chem.* **1958**, 5, 264−268.

(48)   Little, E. J.; Jones, M. M. A Complete Table of Electronegativities. *J. Chem. Educ.* **1960**, 37, 231.

(49)   Camp, A. M.; Kita, M. R.; Grajeda, J.; White, P. S.; Dickie, D. A.; Miller, A. J. M. Mapping the Binding Modes of Hemilabile Pincer- Crown Ether Ligands in Solution Using Diamagnetic Anisotropic Effects on NMR Chemical Shift. *Inorg. Chem.* **2017**, 56, 11141− 11150.

(50)   Pace, R. D.; Regmi, Y. The Finkelstein Reaction: Quantitative Reaction Kinetics of an SN2 Reaction Using Nonaqueous Conductivity. *J. Chem. Educ.* **2006**, 83, 1344−1348.

(51)   Shinkai, S. Functionalization of Crown Ethers and Calixarenes: New Applications as Ligands, Carriers, and Host Molecules. In Bioorganic Chemistry Frontiers; Springer: Berlin, 1990; pp 161−195.

(52)   Matsushima, K.; Kobayashi, H.; Nakatsuji, Y.; Okahara, M. Proton Driven Active Transport of Alkali Metal Cations by Using Alkyl Monoaza Crown Ether Derivatives. *Chem. Lett.* **1983**, 12, 701− 704.

(53)   Kim, S. K.; Sessler, J. L. Ion Pair Receptors. *Chem. Soc. Rev.* **2010**, 39, 3784−3809.

(54)   Smith, D. C., Jr.; Lake, C. H.; Gray, G. M. Synthesis and Characterization of [Pd$_2$X$_2$(µ-X)$_2${Ph$_2$P(CH$_2$CH$_2$O)$_n$CH$_2$CH$_2$PPh$_2$- P,P'}]$_m$ (n = 3, 5, X = Cl, I) Dimetallacrown Ethers and the Related Dinuclear [Pd$_2$Cl$_2$(µ-Cl)$_2${Ph$_2$P(CH$_2$)$_{12}$PPh$_2$-P,P'}]$_m$ and [Pd$_2$X$_2$(µ- X$_2$){Ph$_2$P(CH$_2$CH$_2$O)$_2$CH$_2$CH$_3$-P)$_2$}] (X = Cl, I) Complexes. *Dalton Trans* **2003**, 2008, 2950−2955.

(55)   Macrocyclic Chemistry; Gloe, K., Ed., Springer-Verlag: Berlin/ Heidelberg, 2005.

(56)   Kirkovits, G. J.; Shriver, J. A.; Gale, P. A.; Sessler, J. L. Synthetic Ditopic Receptors. *J. Inclusion Phenom. Mol. Recognit. Chem.* **2001**, 41, 69−75.

(57)   Thordarson, P.; Coumans, R. G. E.; Elemans, J. A. A. W.; Thomassen, P. J.; Visser, J.; Rowan, A. E.; Nolte, R. J. M. Allosterically Driven Multicomponent Assembly. *Angew. Chem., Int. Ed.* **2004**, 43, 4755−4759.

(58)   Deutman, A. B. C.; Monnereau, C.; Moalin, M.; Coumans, R. G. E.; Veling, N.; Coenen, M.; Smits, J. M. M.; de Gelder, R.; Elemans, J. A. A. W.; Ercolani, G.; et al. Squaring Cooperative Binding Circles. Proc. *Natl. Acad. Sci. U. S. A.* **2009**, 106, 10471−10476.

(59)   Yakelis, N. A.; Bergman, R. G. Safe Preparation and Purification of Sodium Tetrakis[(3,5-Trifluoromethyl)Phenyl]Borate (NaBArF24): Reliable and Sensitive Analysis of Water in Solutions of Fluorinated Tetraarylborates. *Organometallics* **2005**, *24*, 3579–3581.

(60)   Drew, D.; Doyle, J. R.; Shaver, A. G. Cyclic Diolefin Complexes of Platinum and Palladium. In *Inorganic Syntheses, Volume 13*; Cotton, F. A., Ed.; McGraw-Hill, 1972; pp 47–55.

(61)   Hill, G. S.; Irwin, M. J.; Levy, C. J.; Rendina, L. M.; Puddephatt, R. J.; Andersen, R. A.; Mclean, L. Platinum(II) Complexes of Dimethyl Sulfide. In *Inorganic Syntheses, Volume 32*; Darensbourg, M., Ed.; Wiley: Hoboken, NJ, 2007; Vol. 32, pp 149–153.

(62)   BindFit, http://supramolecular.org.

CHAPTER 4. OLEFIN ISOMERIZATION WITH CATION-SWITCHABLE REGIOSELECTIVITY: REGULATING ACCESS TO SELECTED DOUBLE BOND POSITIONS FROM A SINGLE CATALYST

Camp, A.M., with contributions from: Kita, M. K., Dodge, H. M., Blackburn, P. T., Chen, C. H., Miller, A. J. M.

I.   Introduction

Targeting Selective Olefin Isomerization

Olefins are essential intermediates and products in the fragrance, commodity chemicals, and pharmaceutical industries.[1–3] Industrial methods using the Shell Higher Olefin Process (SHOP) or Fisher-Tropsch chemistry readily generate hydrocarbon α-olefins,[4] and ethenolysis provides access to a wide variety of substituted α-olefins.[5] Once an unsaturated linkage is present, olefin isomerization offers a convenient, atom-economical method for relocating the double bond to a different position.[6–9] Preparing specific alkene stereo- and regioisomers remains a major challenge, however. Classical isomerization methods require strong acids or simple metal salts and high temperatures, giving a thermodynamic distribution.[10,11] These methods can work well for alkenes that feature one double bond position that is much more stable than others, such as allylbenzene isomerization to β-methylstyrene.[3] When multiple possible products of double bond positional isomerization are energetically similar, however, isomerization often results in a poorly selective distribution of alkenes. Current catalytic systems usually have custom-tailored supporting ligands to select specific isomers, particularly selective isomerization from 1- to 2-position with *E* or *Z* stereochemistry.[12–19]

If olefin isomerization could be controlled to achieve the selective generation of various individual isomers with diverse structures and physical properties, attractive applications based

on rapid diversification upon subsequent elaboration would become possible.[20] The current

paradigm for controlling selectivity is that for each different product, a new metal/ligand

combination is needed (Figure 4.1A).[21–23] We set out to explore an alternative approach, in which

a single metal/ligand combination selectively produces multiple products using switchable

catalysis (Figure 4.1B).
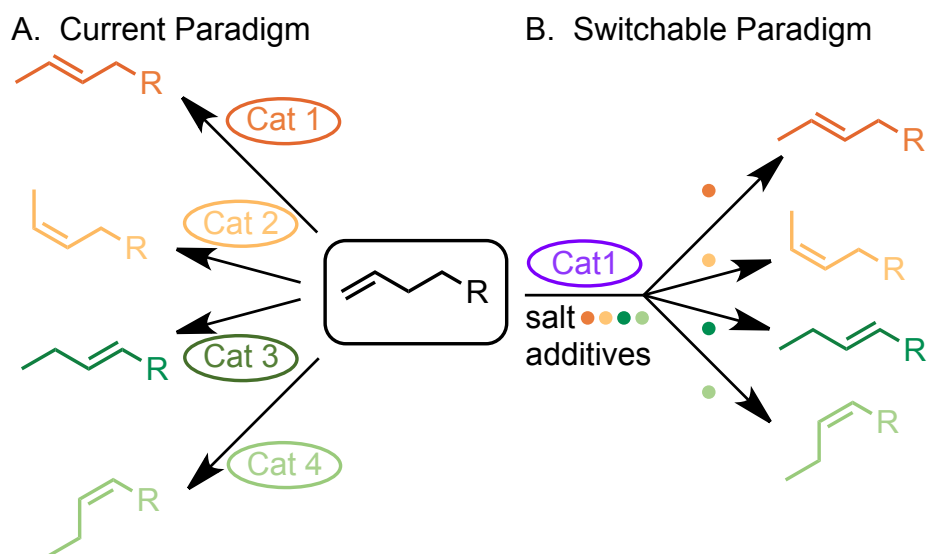
Figure 4.1. Using isomerization to control product selectivity.
A. Using synthesis to generate new catalysts with distinct selectivity. **B.** Using additives to tune the reactivity of a single catalyst towards particular selectivity.

We hypothesized that a catalyst with kinetic selectivity in one state could be toggled to a

different state that exhibits thermodynamic selectivity, thereby controllably generating either of

two desired olefinic products using a single catalyst. Such a platform could be used to create

unique catalytic outcomes with external additives, without laborious synthetic modifications.[20]

Catalytic olefin isomerization with *stimulus-driven switchable regioselectivity* remains unknown, to the

best of our knowledge.

Herein, we introduce new cationic pincer-crown ether iridium hydride complexes featuring

hemilabile 1-aza-18-crown-6 receptors and demonstrate cation-programmable regioselectivity

from a single pincer-crown ether catalyst. The degree of hemilability is directly related to the rate and stereoselectivity of olefin isomerization, and the inclusion of a crown ether in the catalyst structure enables cationic stimuli to tune this key parameter.[24,25] Switchable and tunable allylbenzene isomerization was previously reported with a 1-aza-15-crown-5-based catalyst.[26] Compared to prior studies of catalysts with 1-aza-15-crown-5 receptors, the new 18-crown-6-based pincer-crown ether catalysts are more active, exhibit larger degree of cation enhancement (including the use of more readily available Na$^+$ salts), and are more tolerant of water and other Lewis bases. These features enabled the development of a single catalyst platform with *cation-switchable selectivity* for specific isomers.

II.   Results

Synthesis of New Catalysts Featuring 1-Aza-18-crown-6 Ether

The binding pocket of 1-aza-15-crown-5 ether based pincers is selective for Li$^+$, as the nitrogen donor is coordinated to the iridium ion and is analogous to the binding pocket of 12-crown-4 ethers.[25,27] Given that 1-aza-18-crown-6 ether phenyl phosphonite pincer complexes showed very high binding affinity for alkali metal cations,[25] we hypothesized that a new catalyst with a larger macrocycle would result in larger reactivity differences between the two catalyst states (Figure 4.2). In targeting cation-switchable selectivity, we therefore started by preparing a new cationic iridium hydride complex containing the 1-aza-18-crown-6 ether macrocycle.
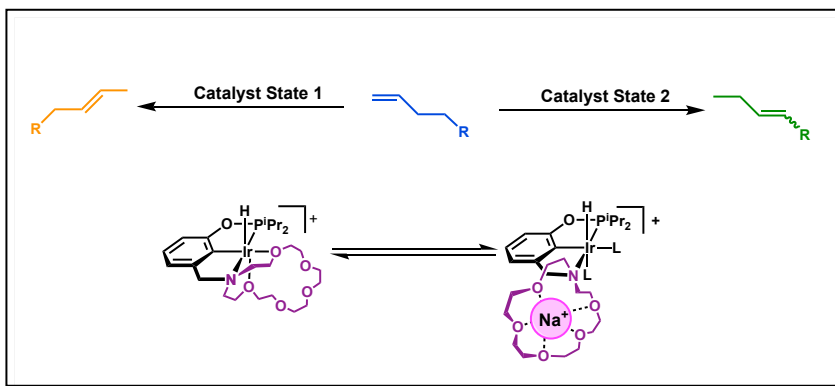
Figure 4.2. Controlling catalyst state with cation-crown interactions.
Choosing a crown-ether that has a higher binding affinity should yield a strong "switch"
between catalyst states.

The 1-aza-18-crown-6-ether-based pincer-crown ether iridium chloride complex, κ^4-(^{18c6}NCOP^{iPr})Ir(H)(Cl) (**1-18c6a**) was synthesized as previously reported.[28] Chloride ligands block olefin binding, however, so a new halide-free complex was targeted as a catalyst candidate. Addition of NaBAr$^F_4$ to **1-18c6a** in CH$_2$Cl$_2$ resulted in a color change from yellow to red. The isolated product featured a hydride ^{1}H resonance at –33 ppm (ca. 1 ppm downfield relative to **1-18c6a**) and a ^{31}P resonance at –132 ppm (ca. 11 ppm upfield relative to **1-18c6a**). X-ray quality crystals obtained by layering CH$_2$Cl$_2$/pentanes revealed the new species to be a Na$^+$ adduct of **1-18c6a**, [κ^4-(^{18c6}NCOP^{iPr})Ir(H)(Cl)@Na)][BAr$^F_4$] **(1-18c6a@Na),** isolated in 89% yield (Figure 4.3). Instead of the removing the chloride ligand as a NaCl precipitate, the Na$^+$ ion was intercalated by the crown ether, with an additional interaction between a chloride bridging the Ir and Na$^+$ ions. A similar interaction was previously observed with the Na$^+$ adduct of a nickel

pincer-crown ether complex,[29] and proposed to play a key role during on/off switchable catalysis by 15-crown-5-based Ir complex.[26]
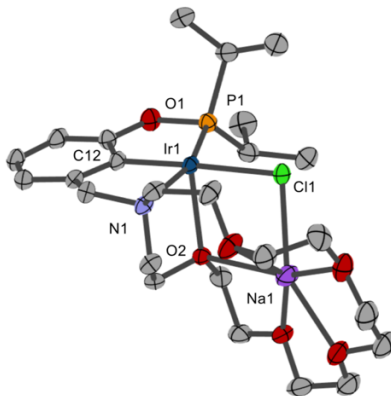
Figure 4.3. Na$^+$ adduct of 1-18c6 (1-18c6@Na).
BAr$^F_4$ cation omitted for clarity. Ellipsoids shown at the 50% probability level.

Removal of chloride was eventually accomplished by stirring **1-18c6a@Na** in 1:1 CH$_2$Cl$_2$:H$_2$O mixtures. The Na$^+$ and Cl$^-$ ions migrate to the aqueous phase and the iridium center aquates to yield [κ^5-(^{18c6}NCOP^{iPr})Ir(H)(OH$_2$)][BAr$^F_4$] (**3-18c6a**) in 94% yield. Diagnostic ^{1}H NMR signatures of **3-18c6a** include a downfield doublet at –32.5 ppm for the hydride and a broad singlet at 5.56 ppm that integrates to 2 protons for the bound water.

Scheme 4.1. Synthesis of 18-crown-6 based iridium pincer complexes.
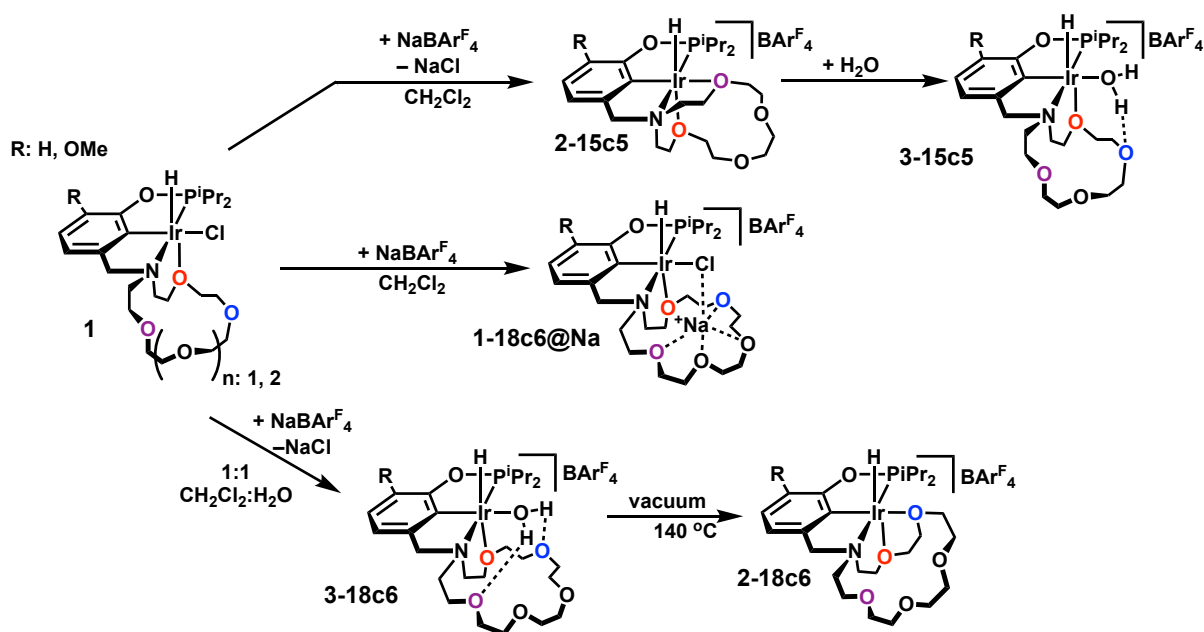
Heating solid samples of complexes **3-18c6a** at 145 °C under vacuum overnight generated the desired complexes [κ^5-(^{18c6}NCOP^{iPr})Ir(H)][BAr$^F_4$] at a 98% yield (**2-18c6a**, Scheme 4.1). The cationic hydride complex has a characteristic doublet (–29.5 ppm) for the hydride ligand. A broad peak at 139.1 ppm was observed by ^{31}P NMR spectroscopy, and extensive broadening is seen in the crown region, which is attributed to crown ether oxygen hemilability involving bound and free oxygen atoms exchanging on the timescale of the NMR acquisition. Dynamic behavior was seen as low as –80 °C, preventing structural analysis of the conformers in exchange. This conformational exchange is not observed at room temperature for the analogous complex containing the smaller aza-15-crown-5 macrocycle.[24]

In the course of this study, it was found that adding a methoxy group to the phenyl backbone *ortho* to the phosphinite blocks C–H activation pathways that lead to catalyst deactivation.[30–32] Structural comparisons of catalysts with and without "blocking" methoxy groups was therefore sought. The hydrido chloride complex with the methoxy group in the backbone, κ^4-($^{Meo-}$ ^{18c6}NCOP^{iPr})Ir(H)(Cl) (**1-18c6b**), was synthesized as previously reported (Scheme 4.2).[28] The new

cationic hydrido aquo complex was accessed using the same biphasic halide abstraction procedure that was successful for the parent complex, providing [κ^5-($^{MeO-}$ ^{18c6}NCOP^{iPr})Ir(H)(OH$_2$)][BAr$^F_4$] (**3-18c6b**) according to Scheme 4.2 in a 63% yield, post-crystallization. The methoxy-containing aquo complex has almost identical spectroscopic patterns to **3-18c6a**, other than the resonances of the methoxy group. Heating solid samples of complexes **3-18c6b** at 145 °C for 24 hours yielded the blocked cationic hydride complex [κ^5-($^{Meo-}$ ^{18c6}NCOP^{iPr})Ir(H)][BAr$^F_4$] in a 98% yield, with a characteristic hydride (–29.5 ppm) and a broad peak at 140.7 ppm was observed by ^{31}P NMR. Like **2-18c6a**, dynamic behavior of **2-18c6b** was seen as low as –80 °C, indicating rapid exchange of ether ligands.

Scheme 4.2. Synthesis of methoxy substituted iridium pincer-crown ethers.
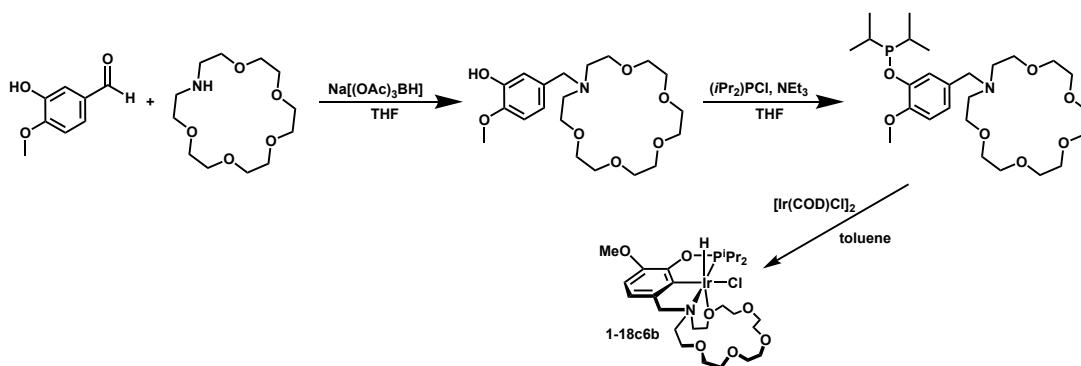
Structural and Thermodynamic Comparisons of Pincer-Crown Ether Complexes

The growth of single crystals of both **2-18c6a** and **2-18c6b** enabled comparative X-ray diffraction (XRD) studies. The solid-state structure of **2-18c6a** features two crown ether oxygen atoms donating to the Ir center (Figure 4.4). The oxygen closest to the amine (O1) and its nearest neighbor (O2) bind the iridium center. Surprisingly, complex **2-18c6b** is a different linkage isomer in the solid state. While two crown ether oxygen atoms still donate to Ir, it is the

two oxygen atoms proximal to the amine (O1 and O5) that donate, rather than two consecutive ethers.
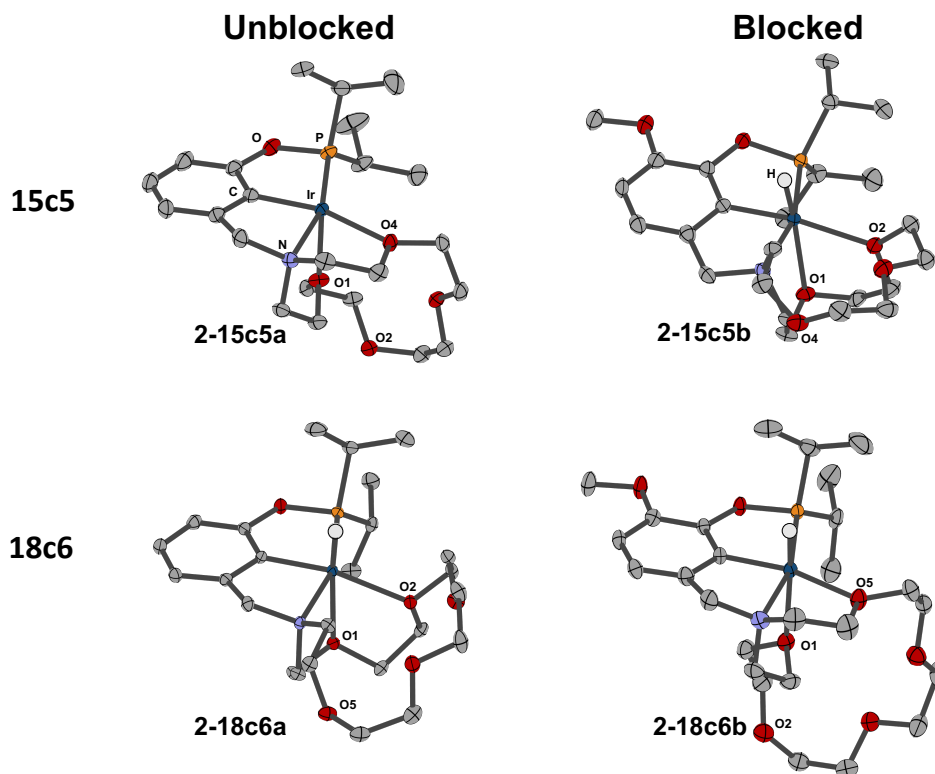
Figure 4.4. Crystal structures of **2** orthologues.
Two conformation modes are observed, either oxygens 1 and 2 bind to the iridium center (**2-15c5b, 2-18c6a**), or oxygens 1 and 4 **(2-15c5a, 2-18c6b)**. 15c5 structures were previously published and provided for comparison.[24,30] The hydride was located in the difference map and allowed to freely refine (except for the previously reported **2-15c5a**); BAr^F_4 and solvent molecules are not shown for clarity. Thermal ellipsoids are represented at the 50% probability level.

The Ir-O bond lengths are similar in both conformers (Ir-O1 = 2.274 Å, Ir-O2 = 2.269 Å for **2-18c6a** and Ir-O1 = 2.297 Å, Ir-O5 = 2.254 Å for **2-18c6b**), indicating the larger crown size can access similarly stable chelates in both linkage isomers.

The relative energies of the different linkage isomers were examined computationally. The optimized structures obtained from Density Functional Theory (DFT) using

B3LYP/LANL2DZ[33,34] with 1,2-dichloroethane (DCE) solvent modeled as a polarizable continuum (see Experimental section for computational details) are very similar to the crystallographically determined structures. The two conformers of **2-18c6b** were computed to differ in energy by only 0.5 kcal/mol. A 5-coordinate complex with one ether dissociated, a likely intermediate in a dissociative substitution mechanism to interconvert the conformers, is endergonic by only 6 kcal/mol (Figure 4.5). The DFT studies indicate that both conformers should be present in solution and that interconversion through a low-energy intermediate may be facile, consistent with the dynamic behavior observed by NMR spectroscopy (*vide supra*).
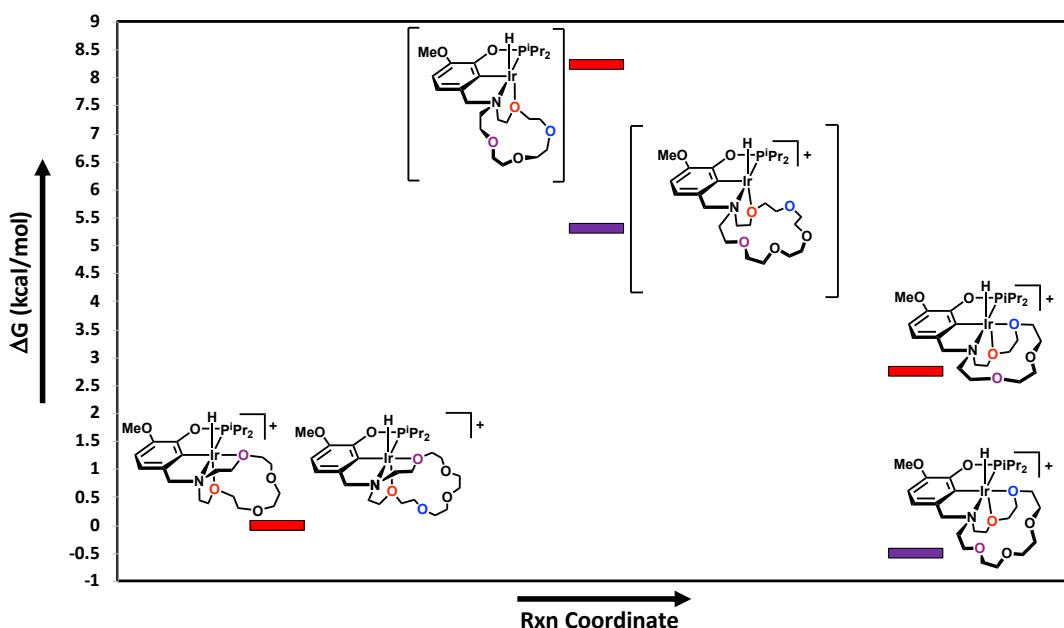
Figure 4.5. Thermodynamic landscape of crown ether linkage isomers.
15-crown-5 based complexes are show in red, while the 18-crown-6 based structures are shown in purple.

Comparisons of **3-18c6a** and **3-18c6b** with variants containing the smaller 15-crown-5 ether macrocycle are possible thanks to previous crystallographic studies.[30] Figure 5 shows the "unblocked" complex, $[\kappa^5-(^{15c5}NCOP^{iPr})Ir(H)][BAr^F_4]$ (**2-15c5a**), with two amine-adjacent oxygen atoms that donate (O1 and O4), while in the "blocked" complex $[\kappa^5-(^{MeO-}$

[15c5]NCOP[iPr])Ir(H)][BAr[F]$_4$] (**2-15c5b**) two adjacent ethers (O1 and O2) bind to Ir. Installing a methoxy group thus leads to a change in the observed solid-state conformer in both 15-crown-5- and 18-crown-6-containing complexes, but with opposite binding modes featured in the two cases. Despite structural characterization revealing both linkage isomers of 15-crown-5 complexes, NMR and DFT studies support that one linkage isomer is the major species solution at room temperature. In the absence of crystal packing effects, the linkage isomer with the two amine-adjacent ether oxygen donors is thermodynamically favored by –2.5 kcal/mol according to DFT (Figure 4.5); furthermore, the 5-coordinate intermediate is higher in energy for the aza-15-crown-5-based complexes than for the 1-aza-18-crown-6-based complexes. NMR spectra are consistent with this picture, with sharp resonances observed **2-15c5a** and **2-15c5b** indicating a single linkage isomer dominates under standard conditions.[24]

Structural comparisons of aqua complexes are also instructive. The large macrocycle-containing complexes **3-18c6a** and **3-18c6b** were examined by XRD after the growth of single crystals from Et$_2$O solutions layered with pentane (Figure 4.6). The solid-state structures of the aqua adducts are essentially identical, contrasting the case of **2-18c6a/b**. In both complexes, one crown ether oxygen (O1) binds to the Ir center in the primary coordination sphere while the bound water engages in hydrogen bonding with two other crown ether oxygen atoms (O2 and O5). The

hydrogen bonding network in the secondary coordination sphere draws the crown ether

macrocycle around the metal center.
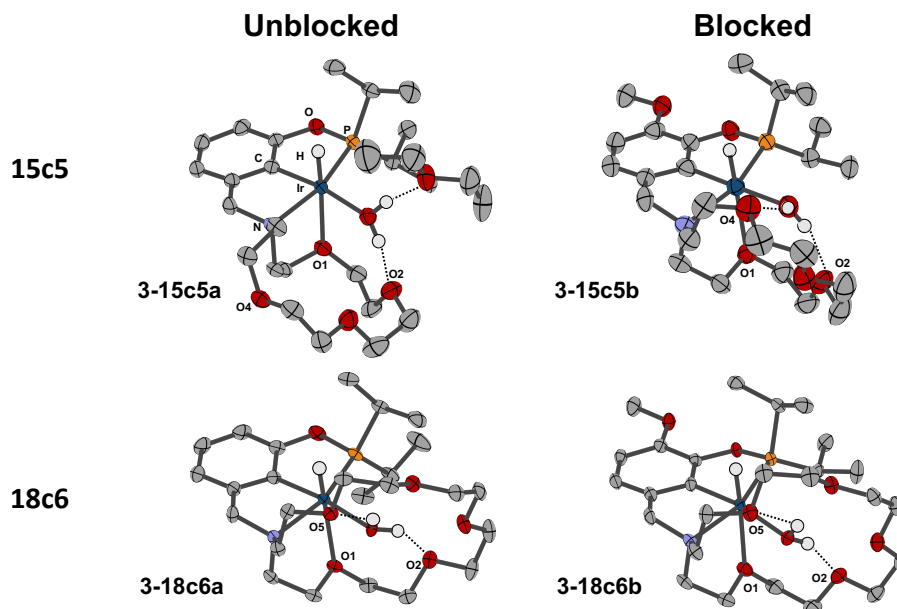
Figure 4.6. Comparison of aquated iridium complexes.
Hydride and water hydrogens were found in the difference map and allowed to freely refine. BArF4 counteranion and non-bonding solvent molecules ignored for clarity. Crown size determines the hydrogen bonding environment of the aquo complexes. In the 18c6 structures, the aquo molecule is encapsulated by the crown. In the 15c5 analogue, either one or two hydrogen bonding contacts are observed with the crown. Aqua protons were located in the difference map and allowed to freely refine. Thermal ellipsoids shown at the 50% probability level.

The aqua complexes with smaller macrocycles had not been structurally characterized, so

the 15-crown-5 analogues $[\kappa^4\text{-}(^{15c5}NCOP^{iPr})Ir(H)(H_2O)][BAr^F_4]$ (**3-15c5a**)[26] and $[\kappa^4\text{-}(^{MeO\text{-}}$

$^{15c5}NCOP^{iPr})Ir(H)(H_2O)][BAr^F_4]$ (**3-15c5b**) were synthesized by dissolving **2-15c5a** or **2-15c5b** in

wet solvent. Colorless single crystals of **3-15c5a/b**, grown from wet Et$_2$O layered with pentanes,

were analyzed by XRD (Figure 6). The solid-state structure of **3-15c5a** retains a single Ir-bound

ether (O1), but features a distinct hydrogen bonding environment. The bound water engages in

just one hydrogen bonding interaction with the crown ether (O2), with a cocrystallized ether

molecule supporting an additional intermolecular hydrogen bond. Conversely, the methoxy-

containing aqua complex **3-15c5b** has only intramolecular hydrogen bonds, as seen in the larger

crown variants. The flexibility of the larger 18-crown-6 macrocycle enables the ring to fully

encapsulate the water ligand, whereas the 15-crown-5 macrocycle only interacts with the water

ligand from one side. This structural difference, as well as the structural differences that suggest

Et_2O solvent hydrogen bonding, is energetically similar to crown ether hydrogen bonding,

foreshadow possible differences in reactivity of these Ir aqua complexes as a function of

macrocycle size.

Influence of Macrocycle Size on Cation-gated Isomerization

To assess the performance of the new 18-crown-6-based catalysts with the original 15-

crown-5-based catalysts, isomerization with 4-phenyl-1-butene (**4a**) was examined in a

comparative study. Reactions were initiated by injecting substrate and monitored at room

temperature by NMR spectroscopy. The conversion of **4a** to **4b** was fit as a first order decay,

consistent with previous results in the presence of Et_2O.[26] In each case, *E*-4-phenyl-2-butene

(**4b**) was obtained as the major product. The half-life ($t_{1/2}$) derived from pseudo-first-order rate

constants for isomerization of **4a** to **4b** for each catalyst are compared in Figure 4.7.

Catalyst, [Ir]	Salt, MBArF	$t_{1/2}$ (hr(min))
2-15c5b	–	69
	Li$^+$	0.58
	Na$^+$	22
3-15c5b	–	339
	Li$^+$	2
	Na$^+$	48

Catalyst, [Ir]	Salt, MBArF	$t_{1/2}$ (hr(min))
2-18c6b	–	190
	Li$^+$	0.53
	Na$^+$	0.041 (2.5)
3-18c6b	–	2300
	Li$^+$	1.2
	Na$^+$	0.13 (7.8)

Figure 4.7. Comparative isomerization of 4-phenyl-1-butene iridium pincer crown-ether complexes.
Conversion of **4a** was tracked as a function of time. On the time scales monitored, **4b** was the only product observed.

The reactivity of **2-15c5b** agreed nicely with our prior study of allylbenzene isomerization, featuring a 120-fold rate enhancement in the presence of Li^+ but only a 3-fold rate enhancement in the presence of Na^+.[26] Gratifyingly, **2-18c6b** demonstrated an excellent reactivity profile. In the absence of cation, **2-18c6b** showed slow isomerization kinetics ($t_{1/2}$ = 190 hr), but upon the addition of Na^+, the rate of isomerization saw a 4,600-fold enhancement ($t_{1/2}$ = 0.041 hr). The relative rate difference between the two states is 40-fold greater for **2-18c6b**/Na^+ than for **2-15c5b**/Li^+. The new catalyst **2-18c6b** even outperforms **2-15c5b** in the presence of Li^+, providing a 360-fold rate enhancement relative to the salt-free condition (c.f. 120-fold difference for **2-15c5b**±Li^+).
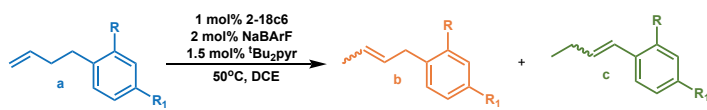
The aqua bound structures were subsequently tested for isomerization activity. **3-15c5** was unable to be generated exclusively; addition of 2 equiv of H_2O to **2-15c5b** resulted in a mixture of **2-15c5b** and **3-15c5b** (1:4) in solution. Higher loadings of water were avoided to prevent inhibition of Li^+ by free water. The rates of isomerization were 2- to 5-fold slower in the presence of water relative to water-free conditions (Figure 4.7). While discriminating rate influences of a changing equilibria of **2-15c5b** and **3-15c5b** and Li^+ inhibition by added water is difficult, the inhibitory effect of water on catalytic activity is clear (Figure 4.7). Aqua complex **3-18c6b** is easily isolated, even without requiring excess water, and remains intact throughout catalysis, contrasting with the shifting equilibrium between **2-15c5b** and **3-15c5b**. In the absence of salts, **3-18c6b** is drastically inhibited relative to **2-18c6b**, $t_{1/2}$ = 2300 hrs. Yet, surprisingly, aqua catalyst **3-18c6b** is almost as fast as water-free catalyst **2-18c6b** in the presence of salts. A massive 18,000-fold enhancement in the rate of isomerization by **3-18c6b** is observed upon addition of Na^+ salts. In the presence of Li^+ salts, **3-18c6b** is an order of magnitude faster than **2-15c5/3-15c5** mixtures under analogous conditions (Figure 4.7).

Comparing the reactivity profiles of the studied catalysts, **2-18c6b** emerged as the most promising candidate to access switchable selectivity. Given the larger discrepancy in rate between the salt-free vs Na$^+$ condition, faster catalysis of the water bound analogue, **3-18c6b,** increased tolerance to ethereal Lewis bases and commercial availability of NaBAr$^F_4$, **2-18c6b** was selected to access switchable regioselectivity.

Cation-Switchable Regioselectivity in the Isomerization of 4-Phenyl-1-Butene Derivatives

The promising new catalyst **2-18c6b** was examined as a platform for the cation-switchable isomerization of olefins to specific regioisomers. A variety of 4-aryl-1-butenes was examined initially. Reactions were heated at 50 °C, with or without salts, in a multi-well shaker until a stable distribution of isomers was observed, with reaction aliquots typically collected (and quenched with excess chloride to deactivate the catalyst)[26] at 24, 48, 120, and 216 hours.

Table 4.1. Isomerization of functionalized arenes.

Substrate	R,R'	Salt Added?	Time	b (E:Z)	c (E:Z)	b	:	c
4	H, H	–	48	94% (14 : 1)	<1%	>90	:	1
		Na$^+$	24	7% (4 : 1)	93% (50 : 1)	1	:	10
5	H, OMe	–	48	92% (14 : 1)	<1%	>90	:	1
		Na$^+$	24	6% (5 : 1)	94% (>90 : 1)	1	:	20
6	OMe, H	–	48	95% (14 : 1)	2%	60	:	1
		Na$^+$	24	10% (4 : 1)	89% (50 : 1)	1	:	8.9
7	H, F	–	216	93% (15 : 1)	1%	90	:	1
		Na$^+$	24	4% (4 : 1)	96% (50 : 1)	1	:	20
8	H, Br	–	216	95% (10 : 1)	1%	90	:	1
		Na$^+$	24	7% (4 : 1)	93% (70 : 1)	1	:	9
9	H, Cl	–	216	88% (14 : 1)	2%	40	:	1
		Na$^+$	24	4% (4 : 1)	96% (60 : 1)	1	:	20
10	Cl, H	–	120	91% (15 : 1)	<1%	>90	:	1
		Na$^+$	48	20% (4 : 1)	79% (30 : 1)	1	:	4
11	H, CF$_3$	–	216	84% (12 : 1)	<1%	>80	:	1
		Na$^+$	24	7% (3 : 1)	84% (40 : 1)	1	:	12
12	H, COOEt	–	216	92% (7.1 : 1)	1%	60	:	1
		Na$^+$	216	40% (3.4 : 1)	58% (5.1 : 1)	1	:	1.5

Table 4.1 demonstrates cation-switchable regioselectivity in olefin isomerization, with a single catalyst generating either the 2-isomer (denoted **b**) or 3-isomer (denoted **c**) based on whether or not Na$^+$ is included in the reaction. The degree of control over regioselectivity *and* stereoselectivity is striking: regioisomer **b** is formed in 84 to 95% yield and 7:1 to 15:1 *E:Z* selectivity (in the absence of salts), and regioisomer **c** is formed 79 to 96% yield and 36:1 to >90:1 *E:Z* selectivity (in the presence of NaBAr$^F_4$, excepting substrate **12** which is discussed below). The salt-containing mixtures generally generate isomer **c** faster (48 h or less) than the salt-free solutions produce isomer **b** (48-216 h). Electron donating functional groups show faster conversion, in line with prior evidence that substrate binding is the rate limiting step for catalysis.[26]

The cation-free conditions demonstrate a remarkable conservation of regioselectivity even after long periods of heating. An exemplum is seen in the isomerization of substrate **6a**. A 95% yield of **6b** is seen at 48 hours and is highly selective for the **6b** (**6b:6c** = 60:1). Heating the reaction solution for 216 hours still dramatically favors the kinetic regioisomer, yielding 88% **6b** (**6b:6c** = 10:1). While regioselectivity is maintained over long time scales, the 14:1 *E:Z* stereoselectivity at 48 hrs is observed to decay to 7:1 at 216 hrs. In contrast, upon the addition of 2 equiv. of NaBAr$^F_4$, a yield of 89% **6c** is obtained (**6b:6c** = 1:9), demonstrating the expected thermodynamic distribution. The kinetic preference of **2-18c6b** affords selectivity for the **6b** isomer across long timescales, and is observed across the studied substituted arenes.

The exception to the trends noted above is the ester functionalized arene (R1: COOEt, **12a**). This substrate proceeded noticeably slower, even compared to the other electron deficient arenes. To test for possible catalyst inhibition by the ester functional group, a 1:1 mixture of ethyl acetate and **4a** was isomerized at 50°C in the presence of cation. After 120 hours, only 6% of *E*-**4c** isomer was observed, with the dominant product being the **b** regiosiomer (93%). While

conversion is faster with **4a** alone (93% **c** at 24 hrs), the system tolerates added ethyl acetate

enough to produce **4b** in high yields. The electron withdrawing effects of the ester group and

modest inhibition by the phenyl ester likely explains the slow isomerization of **12a** in the

presence of cation. The differences in regioselectivity will be discussed below.

While in principle one could imagine simply running the salt-promoted reaction for short

times to obtain the **b** isomer, and for long times to obtain the **c** isomer, this is not possible in

practice. The *E:Z* ratio of **4b** was tracked as a function of time at room temperature (Figure 4.8).

Without salt additives, the **b** isomer is formed with exceptional *E* selectivity. During catalysis

under the salt-free condition, the *E*-**4b** is drastically favored (*E:Z* = 23:1). In the presence of

Na$^+$, the *E*-**4b** isomer is only moderately favored (*E:Z* = 5:1 at early times, later decaying further

toward the expected thermodynamic ratio of 4:1). Thus, the two catalyst states have distinct

stereoselectivity, and high selectivity for both *E*-**b** and *E*-**c** is only possible when using

switchable catalysis.
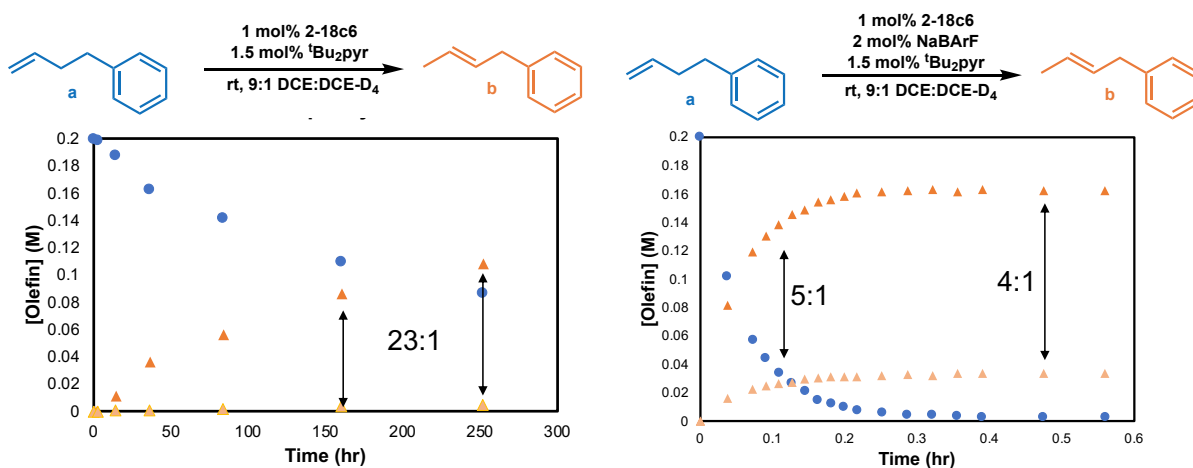
Figure 4.8. Comparing stereoselectivity during isomerization.
The isomerization **4a** to **4b** with **2-18c6b** alone (left) and in the presence of NaBAr$^F_4$ (right). The ratio of **E-4b** (orange) to **Z-4b** (yellow) are marked.

Cation-Switchable Isomerization of Functionalized 1-Butenes

Various 1-butene derivatives containing functional groups were examined to assess the generality of isomerization with cation-switchable regioselectivity (Table 4.2). A purely aliphatic substrate, 4-methyl-1-pentene (**13a**), was chosen as a representative alkyl-substituted alkene lacking any resonance stabilization from a phenyl ring. Good yields of the two regioisomers were obtained using the switchable catalyst **2-18c6b** (Table 4.2). Without salts, singly isomerized product **13b** was obtained in 94% yield (13:1 *E*:*Z*); in the presence of NaBAr$^F_4$, the doubly isomerized product **13c** was obtained in 75% yield (Table 4.2; a small amount of disubstituted terminal alkene **13d** was also observed, in accord with reported distributions with Pd catalysts.[11]

Table 4.2. Switchable regioselectivity in other classes of substrate

	Salt?	Time (hr)	Isomer Distribution (*E*:*Z*)				Regioselectivity (b:c)
13			a	b	c	d	
	–	120	5%	94% (13:1)	<1%	<1%	>100 : 1
	Na$^+$	48	<1%	12% (7:1)	75%	13%	1 : 7.5
14			a	b	c		
	–	120	10%	89% (18:1)	1% (1:1)		90 : 1
	Na$^+$	24	1%	4% (2:1)	96% (1:2)		1 : 30
15			a	b	c		
	–	24	12%	76% (16:1)	12% (8 :1)		6.4 : 1
	Na$^+$	24	<1%	35% (3.4:1)	64% (16:1)		1 : 1.8

Silyl ethers are popular protecting groups in organic chemistry and the isomerization of silyl ether functionalized olefins allows access to the synthetically valuable enol silyl ethers at mild

conditions.[35,36] The triisopropylsilyl-ether-protected olefin (**14a**) was readily isomerized to either regioisomer with excellent control using **2-18c6b** (Table 4.2). This substrate is noteworthy as regioisomer **14c** was produced as predominantly the *Z* stereoisomer (*E:Z* = 1:2). Previous isomerization studies demonstrate that a higher preference for the *Z* isomer is often expected for silyl enol ethers, including the triisopropyl variant.[8,36]

Boronic esters are valuable synthetic intermediates, such as in the construction of C–C bonds via the Suzuki-Miyaura reaction.[37] The boronic ester-functionalized butene **15a** underwent isomerization with **2-18c6** to give 76% yield of **15b**. Isomer **15c** was also present, leading to 6.4:1 selectivity at 24 hours. In the presence of Na^+, **2-18c6** catalyzes the isomerization of **15a** to **15c** in 64% yield with excellent stereoselectivity (16:1 *E:Z*, Table 4.2). Of the substrates studied, only isomerization with **15a** exhibited less stable regioselectivity. At 24 hours, 86% **15b** is observed (6b:6c = 6.4:1) while at 48 hrs the yield of **6b** decreases to 73% (**6b:6c** = 2.9:1).

Some olefins could not be controllably isomerized. Olefins with Lewis basic sites typically reacted too slowly for synthetic practice, with 5-hexen-2-one, 5-pentenoate, and 5-hexen-1-ol all undergoing slow isomerization to **b** (and no further) even in the presence of cations (**c** <5% at 216 hrs). 4-methoxy-1-butene showed only poor conversion to the **c** isomer at 216 hrs (15% **c**). Other olefins isomerized rapidly, but to unselective mixtures of regioisomers. The acetal-protected ketone substrate 2-(but-3-en-1-yl)-2-methyl-1,3-dioxolane (**16a**)[12] isomerized rapidly to **16b** in the presence of Na^+, but no further isomerization to **16c** was observed (Table 4.3). Less than 10% yield of **17c** and **18c** were obtained during Na^+-activated isomerization of but-3-en-1-yltrimethylsilane nor 3-butenyl acetate could be brought to the **c** regioisomers in the presence of salt (Table 4.3). The origin of the lack of switchable regioselectivity is examined in the Discussion section below. Nonetheless, these substrates showed excellent *E* selectivity for isomerization to the **b** isomer.[38,39] Substrates **16b**, **17b**, and **18b**

have *E:Z* ratios **>**7:1 upon isomerization with **2-18c6b** (Table 4.3); upon addition of Na$^+$, the

E:Z ratio decays to around 3:1 near the calculated thermodynamic values.

Table 4.3. Isomerization of substrates without kinetic and thermodynamic discrimination

1 mol% 2-18c6
2 mol% NaBAr$^F_4$
1.5 mol% ^{t}Bu$_2$pyr
50 °C, DCE

a → b + c

	Salt?	Time (hr)	Isomer Distribution % (E:Z)			Regioselectivity (b:c)
16			a	b	c	
	–	120	3%	96% (8:1)	1%	70 : 1
	Na$^+$	24	1%	97% (3:1)	2%	60 : 1
17			a	b	c	
	–	48	2%	98% (7.4:1)	<1%	>100 : 1
	Na$^+$	24	1%	89% (1.5:1)	8% (10:1)	10 : 1
18			a	b	c	
	–	216	16%	84% (15:1)	<1%	>100 : 1
	Na$^+$	120	19%	76% (4.0:1)	5% (1:1)	10 : 1

The sesquisterpene β-caryophyllene (**19-I**) was examined as an example of an alkene of higher

structural complexity (Table 4.4). Caryophyllene is used in the pharmaceutical and fragrance

industry and has shown anti-cancer activity,[40] motivating our investigations of cation-controlled

selectivity of isomerization. Initial isomerization attempts at 50 °C without salt and at 1 mol%

catalyst saw no conversion of **19-I**. To engage isomerization in salt-free conditions, heating to 80

°C and 5 mol% of **2-18c6b** was required, leading to the double bonds in caryophyllene

redistributing as shown in Table 4. Without salts, 64% of the products represent *E/Z* or

positional isomerization of the trisubstituted alkene. When the reaction was performed at 50 °C

in the presence of NaBAr$^F_4$, however, 69% of the products represent positional isomerization of the exocyclic gem-disubstitued alkene. Additionally, **2-18c6b** is selective for only olefinic isomerization, a stark contrast from reported acid catalyzed isomerizations, which cause significant structural rearrangements and hydration of the double bonds.[41–43]

Table 4.4. Isomerization of b-Caryophyllene

			19-II	19-III	19-IV	19-V
80 ºC 5 mol% Ir 1.5 mol% ^{t}Bu$_2$pyr	216 hrs	9.6	30%	34%	17%	10%
50 ºC 1 mol% Ir 2mol% NaBArF 1.5 mol% ^{t}Bu$_2$pyr	120 hrs	12	13%	17%	23%	46%

Computational Studies of Relative Energetics of Olefin Isomers

DFT computations were carried out to examine the relative stability of regioisomers of the 1-butene derivatives examined in the catalytic studies. Two methods were compared, each with DCE solvent modeled as a polarizable continuum (further details are provided in the Experimental section). MP2[44–47]/aug-cc-pVDZ[48], which has been used to predict isomer distributions of long-chain functionalized olefins,[49] was compared with B3LYP/ 6-311++G(d,p),[33,34] with the assessment based on literature values proposed to represent the thermodynamic distribution of isomers of butenyl ester,[50] butenyl boronic esters,[51] 4-methyl-1-pentene,[11] and substituted butenyl arenes.[52] For the substrates studied here, B3LYP/6-311++G(d,p)[33,34] reflects the experimentally observed thermodynamic distributions. Figure 4.9 summarizes the computational results.
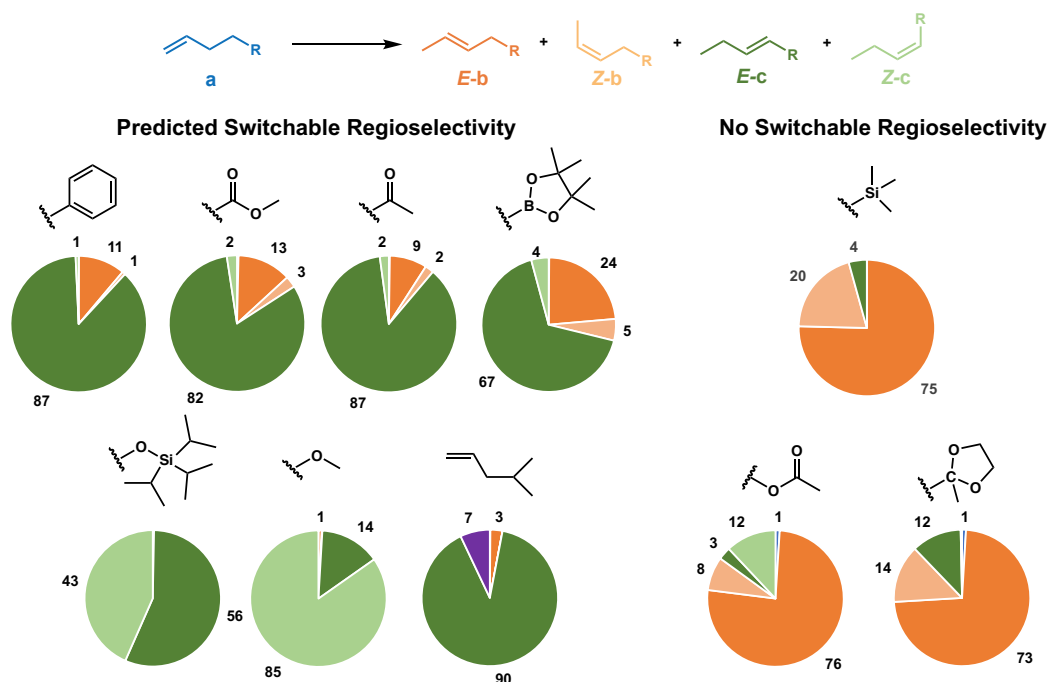
Figure 4.9. Calculated thermodynamic distributions of substrates for switchable regioselectivity Isomer distributions were calculated B3LYP/ 6-311G++(d,p) functional and basis set at 50 ºC, and 1,2-dichloroethane (DCE) was modeled as a continuous polarization. Calculations were run under tight convergence criterion.

The 1-butene derivatives can be organized into two categories based on their computed thermodynamic distributions of regioisomers. Seven substrates had a distribution where the **c** regioisomer was the lowest energy species, while three substrates showed a thermodynamic preference for the **b** regioisomer (Figure 9). Most substrates are strongly *E* selective in both the **b** and **c** regioisomers, with the exception of methoxy and silyl ether substituted alkenes.

III.   Discussion

The Influence of Crown Ether Size on Structure and Activity

These studies revealed several distinct advantages of using the newly developed **2-18c6b** complex for switchable regioselectivity studies. The observed massive (4,600-fold) difference in rate between the cation-free and Na⁺-promoted conditions make NaBArF4 an ideal chemical switch. This complex also benefits from using the commercially available NaBArF4, demonstrates

greater tolerance of added Lewis bases, and has a water-bound adduct that maintains switchable and relatively fast reactivity, making this system more attractive for exploring functionalized olefins.

2-18c6b shows a 2.8-fold decrease in the rate of olefin isomerization relative to 2-15cb. A more stable crown ether chelate afforded by more conformational freedom in larger crown structures may explain the decrease in isomerization activity. NMR and computational studies support multiple low-lying conformers present in solution, which may deplete the population of the olefin-Ir complex – a proposed key intermediate in catalysis – which may also explain the reduced activity with 2-18c6b.
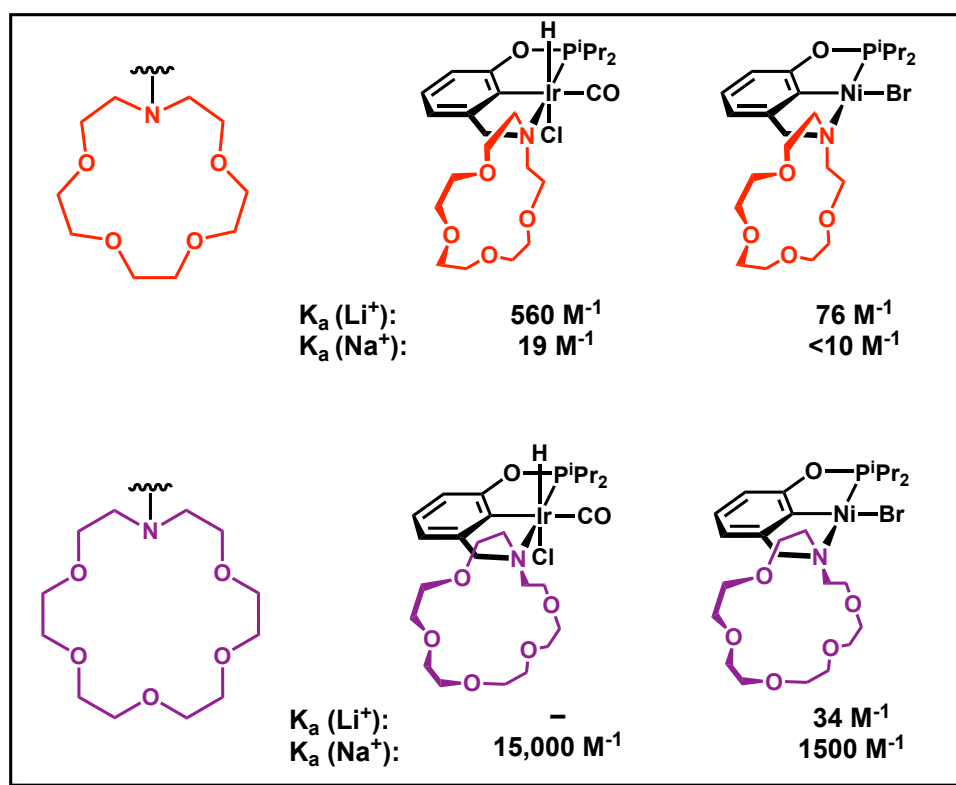
Figure 4.10. Comparing binding affinities of iridium pincer-crown ether complexes

While cation-crown interactions have been previously shown to promote substrate binding and increase the rate of olefin isomerization,[26] binding affinity studies of model

complexes prove key to understanding the large rate differential in the presence of salt.[25,53] The binding affinities for Li$^+$ are similar in nickel pincer complexes containing 1-aza-15-crown-5 (K$_a$ = 76 M^{-1}) or 1-aza-18-crown-6 (K$_a$ = 34 M^{-1}, Figure 4.10); the similar affinities for Li$^+$ are reflected in the similar rates of isomerization in **2-15c6b** (t$_{1/2}$ = 0.58) and **2-18c6b** (t$_{1/2}$ = 0.53).[53] Even more striking are the different binding affinities of iridium pincer complexes containing 1-aza-15-crown-5 (K$_a$ = 19 M^{-1}) or 1-aza-18-crown-6 (K$_a$ = 15,000 M^{-1}). We thus hypothesized that the new catalysts with 1-aza-18-crown-6 macrocycles would have similar activity to the original 15-crown-5-based catalysts in the presence of Li$^+$ salts and much higher activity in the presence of Na$^+$ salts.[25]

Catalytic studies comparing **2-15c5b** and **2-18c6b** adhere to expectations based on cation binding affinity studies. In the presence of NaBAr$^F_4$, the new catalyst **2-18c6b** isomerized an olefin with a half-life (t$_{1/2}$ = 0.041 hrs) that was 500 times shorter than that of **2-15c5b** under the same conditions (t$_{1/2}$ = 22 hrs), which agrees with a massive increase in binding affinity for Na$^+$ observed in 18-crown-6 analogues.. The ratio of the binding affinities of Na$^+$ vs Li$^+$ previously observed in nickel pincer-crown ether complexes (K$_a$(Na$^+$)/K$_a$(Li$^+$) = 40) roughly track with the observed rates of 4-phenyl-1-butene isomerization by **2-18c6b** in the presence of these salts (t$_{1/2}$(Na$^+$)/t$_{1/2}$(Li$^+$) = 14).[54]

The higher affinity for Na$^+$ has the added benefit of increasing the resistance of the system to reactivity dampening by added Lewis bases. At the 36 equivalents of Et$_2$O required to solubilize all added salts, isomerization by **2-18c6b** proceeds an order of magnitude faster with Na$^+$ than **2-15c5b** when Li$^+$ salts are added.

The aqua complexes **3-15c6b** and **3-18c6b** are substantially slower than the water-free variants in the absence of salts. The reduced activity may be due to strong hydrogen bonding interactions that additionally stabilize the aqua ligand. However, when Na$^+$ is added **3-18c6b**

demonstrates only a 3-fold decrease in the isomerization of **4a**, a much higher recover of activity than what is seen with **3-15c5b.** While the exact role of Na$^+$ is unclear, the cation likely disrupts the hydrogen bonding network between the crown and the aquo ligand, allowing substrate to bind and leading to a massive 18,000-fold enhancement in the rate of olefin isomerization. Given the aquo complexes are common impurities observed during long time courses and syntheses, the moderate activity and preservation of switchable behavior seen with **3-18c6b** is an exciting observation.

Rationalizing Observed Trends in Regioselectivity Control

Switchable regioselectivity is accessed across all studied arene functionalized butenes, as well as butenes with alkyl, boronic ester, and silyl ether substituents. In the absence of salts, the catalyst **2-18c6b** facilitates a single isomerization of the double bond to the first internal position, producing the **b** isomer in high yield and with high regioselectivity and high stereoselectivity (favoring the E isomer). The ratio of **b:c** regioisomers without salts often exceeded 40:1. In the presence of NaBAr$^F_4$, the doubly isomerized product is formed instead, also in high yield and good stereoselectivity (again favoring the E isomer in most cases). The regioselectivity is inverted, with the **b:c** ratio typically beyond 1:8.

The crux of understanding the observed reactivity lies in the thermodynamic landscape of olefin isomerization. Comparing the computed regioisomer distributions with the experimental outcomes under different conditions, it is clear that the catalytic reactions in the presence of NaBAr$^F_4$ generate the most thermodynamically favored isomer (the "thermodyamic product"). Conversely, the regio- and stereoselectivity of reactions catalyzed by **2-18c6b** in the absence of salts are consistent with a high degree of kinetic control: the thermodynamic product

is not obtained, and instead a specific and less stable isomer is produced. Thus, *switchable catalysis relies on a cation-induced change from kinetic control to thermodynamic control.*

The substrates for which switchable regioselectivity were observed all have the same reaction coordinate diagram, depicted in Figure 4.11. A "stair-step" pattern is apparent, with the starting terminal olefin **a** being the least stable, isomer **b** being intermediate, and isomer **c** being the thermodynamic product. In the absence of a salt, the kinetic barrier to convert **a** to *E*-**b** is surmountable, but further isomerization to *Z*-**b** or either **c** stereoisomer is not possible under the examined reaction conditions (even with prolonged reaction times). The kinetic product *E*-**b** is thus obtained, and **2-18c6b** alone produces high yields of this isomer with exquisite regioselectivity and stereoselectivity. If instead the reaction is performed with NaBAr$^F_4$, the barriers for both positional isomerizations are reduced dramatically, and the reaction proceeds under thermodynamic control to the most stable species **c** (Figure 4.11). Isomer **c** is the most stable species when the substituents engage in π-conjugation (arene, ketone, esters, and boronic esters),[8,20,50–52,55] or hyperconjugation[56] by alkyl substituents (Figure 4.11).
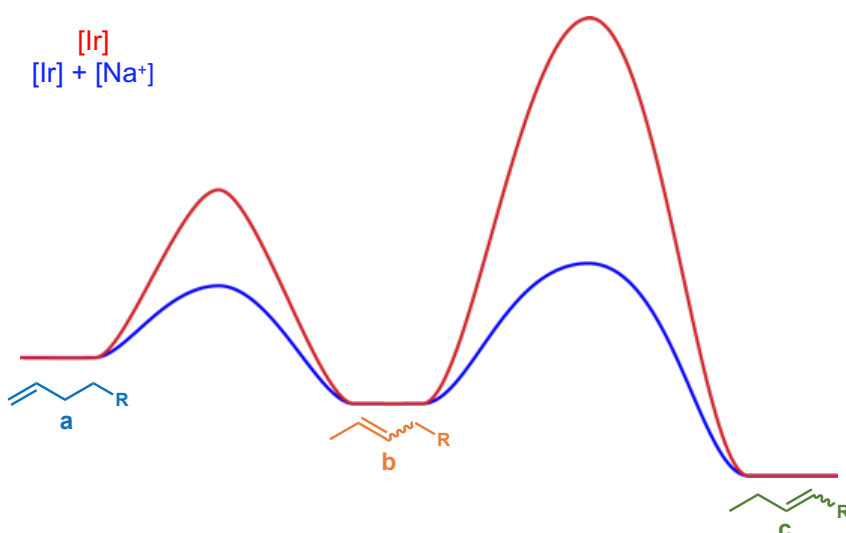
Figure 4.11. Simplified energetic scheme for the isomerization of switchable olefins

This model also explains why some substrates did not exhibit cation-switchable reactivity. For alkenes with silyl, acetyl, and ketal substituents, calculations reveal that **b** is the most stable isomer. Thus, the product is the same under kinetic or thermodynamic control (Figure 4.12). Substrates that are not stabilized by resonance or increased hyperconjugation and functionalized with electron withdrawing groups have a decreased preference for the **c** regioisomer. **17b** also shows a thermodynamic preference for the **b** isomer, which may be explained by decreased hyperconjugation and steric effects in the vinyl silane isomer, **c**.
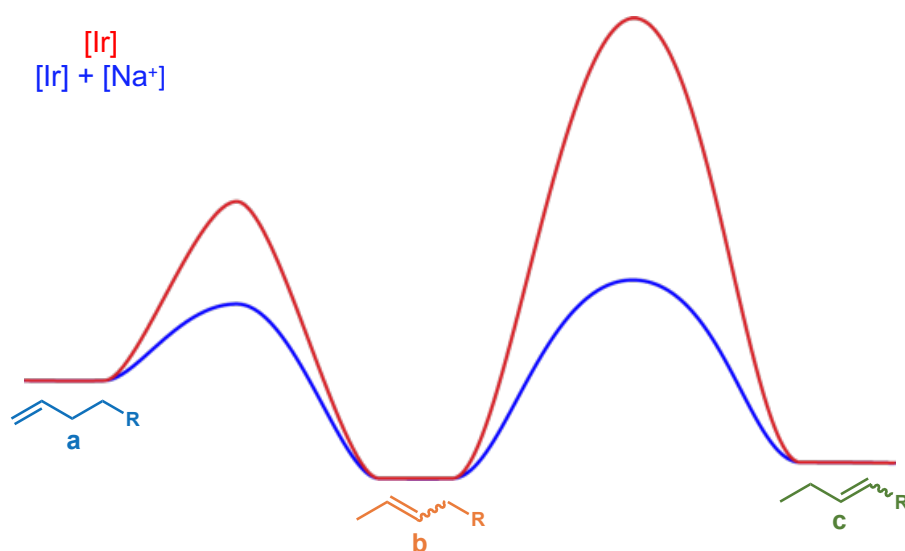
Figure 4.12. Simplifed thermodynamic landscape of isomerization of non-switchable substrates

The free energy landscape model does *not* explain the sluggish reactivity of alkenes with methoxy, ketone, or ester substituents. In these cases, DFT predicts the **c** isomer is the expected thermodynamic product (Figure 9). These substrates all feature Lewis basic functional groups, however, and the slow rates of catalysis are therefore attributed to substrate binding either to the catalyst or to the cation. The inhibitory effect of Lewis basic groups was apparent in the very slow isomerizations in presence of ethyl acetate. Overcoming inhibition of switchable regioselectivity by Lewis basic functional groups is a focus of ongoing work.

While switchable stereoselectivity has been demonstrated in other reactions,[57,58] a stimulus driven framework to switch regioselectivity has not been reported for olefin isomerization reactions. Instead, synthetic tuning of the ligand framework of catalytic systems[22,38,59] or substrate functionalization[59] have been typically used to modulate isomerization selectivity. The iridium pincer-crown ether platform offers the unique ability to control olefin isomerization, moving between kinetic and thermodynamic regioisomers with high selectivity.

Rationalizing Unique Stereoselectivity in Each Catalytic State

Previous studies of the influence of salt additives on rate and selectivity utilized **2-15c5** and allylbenzene; these studies found the isomerization to β-methylstyrene was highly *E* selective (>99%) both with and without Li$^+$ salts.[26] However, the thermodynamics of this system also highly favors the *E* isomer, making discrimination of selectivity of different catalyst states difficult (*E:Z* >8:1).[60] **4b** has smaller thermodynamic preference for the *E* isomer (Thermodynamic *E:Z* = 4:1),[23] allowing stereoselectivity for each catalytic state to be resolved more easily. Without salt, the isomerization of **4a** to **4b** by **2-18c6b** was found to be highly *E* selective (*E:Z* = 23:1) at room temperature, exceeding the expected thermodynamic ratio of 4:1. Even heating reactions at 50 °C still dramatically favors *E*-**4b** (13:1). Upon the addition of NaBAr$^F_4$, the selectivity of the system drastically changes, with *E*-**4b** still being favored (5:1), but rapidly decaying to thermodynamic distribution (*E:Z* = 4:1). This example illustrates that the *selectivity of each catalytic state (salt-free vs Na$^+$) is unique*. Even if the reactions with salt are optimized to maximize the yield of **b** isomers, the resulting product distribution is distinct from the salt-free condition.

The proposed mechanism for olefin isomerization using pincer-crown ethers is a hydride insertion, elimination pathway.[26] Without cation, the crown likely plays a role in the *E* selectivity observed in the system (Scheme 4.3). Computational studies have shown that the Ir-O bond

trans to phenyl are easiest to dissociate, which can open up a binding site for alkene to bind.[24]

Thus, crown-ether binding *trans* to the hydride is expected to remain, allowing the sterics of the

crown to influence the selectivity of the system. Grotjahn and coworkers have shown sterics of

the cyclopentadiene ring of Ru-imidazoyl plays a significant role in enforcing the high *E*

selectivity observed in their system,[23] and Jiao and Liu and coworkers have shown a strong

steric influence on selectivity seen in olefin insertion into cobalt hydrides.[21]

Scheme 4.3. Unique selectivity of each catalytic state
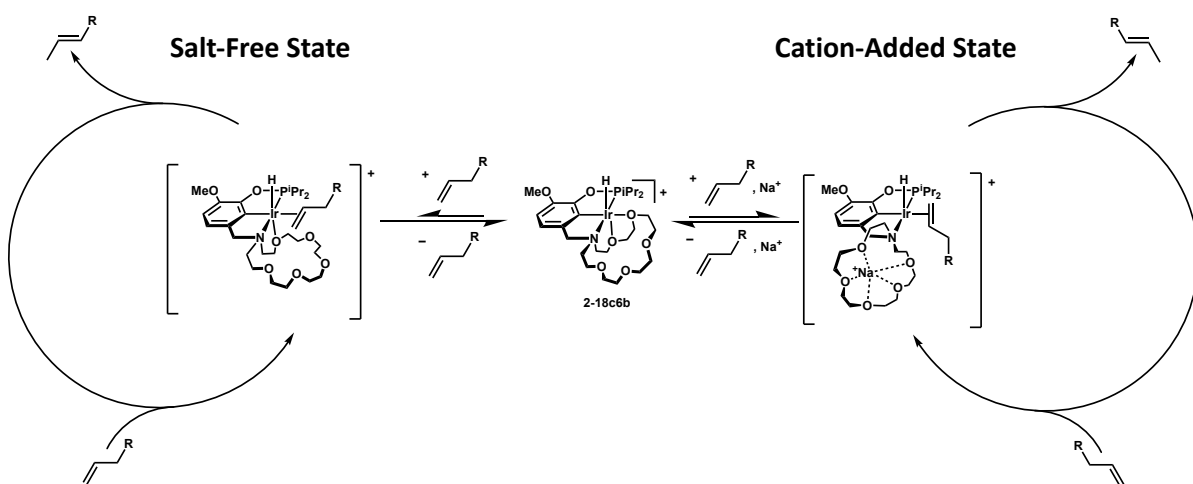
Upon the addition of cations, the crown ether is proposed to bind Na^+ while breaking

both Ir–O bonds present in the precatalyst. Model systems have shown that cation–crown

interactions can dramatically enhance ligand binding in pincer-crown ether complexes, and in the

catalytic reaction cation-crown interactions are proposed to similarly favor substrate binding,

thereby dramatically accelerating isomerization. With sufficient activity, and perhaps a different

steric environment imparted by crown ether dissociation from Ir, a thermodynamic distribution

of regio- and stereoisomers is observed.

IV.   Conclusions

In search of a system capable of olefin isomerization cation-switchable regioselectivity, a new iridium pincer-crown ether complex featuring a larger, 1-aza-18-crown-6 moiety was prepared. The strong binding affinity for Na^+ by complex **2-18c6** resulted in distinct reactivity with and without salts: the addition of Na^+ results in a 4,000-fold increase in the rate of isomerization of 4-phenyl-1-butene relative to the salt-free condition.

Switchable regioselectivity was demonstrated for the first time with a single catalyst. In the absence of salts, **2-18c6b** facilitates a single positional double bond isomerization of butenes containing phenyl, alkyl, siloxy, and boronic ester groups with high yields and exceptional regio- and stereoselectivity. Under otherwise identical conditions, but in the presence of $NaBAr^F_4$, the same catalyst produces the doubly isomerized product in high yields and high regio- and stereoselectivity.

Computational studies of relative isomer stability guided the development of a model that explains the selectivity outcomes observed for various functionalized olefins. The salt additives lead to two distinct catalytic states are accessed, one (salt-free) that exhibits high kinetic selectivity for a single E-selective double bond rearrangement, and another (salt-activated) that exhibits thermodynamic selectivity. When the relative stability of the olefins increases from **a** to **b** to **c** isomers, high yields of different regioisomeric *E* alkenes can be accessed from a single catalyst platform based on the inclusion of salt stimulus. Toggling the selectivity in the isomerization functionalized alkenes using a single scaffold presents a remarkable platform for regiodivergent alkene manipulation using simple additives, an important tool in manipulating alkene position in pharmaceuticals and fragrances.

V.   Experimental and Characterization of New Catalysts

General Considerations

All compounds were manipulated using standard vacuum line or Schlenk techniques or in a glovebox under a nitrogen atmosphere. NMR scale reaction mixtures were prepared under nitrogen in a glovebox and kept in Teflon-sealed tubes. ^{1}H, ^{31}P, and ^{13}C NMR spectra were recorded on 400, 500, and 600 MHz spectrometers. NMR characterization data are reported at 298 K, unless specified otherwise. All NMR solvents and isotopically labeled reagents were purchased from Cambridge Isotope Laboratories, Inc. 1,2-dichloroethane-d4 ($C_2D_4Cl_2$), chloroform-d ($CDCl_3$), and methylene chloride-d2 (CD_2Cl_2) were freeze−pump−thaw degassed three times before drying by passage through a small column of activated alumina. Chemical shifts for ^{1}H and heteronuclear spectra are reported in ppm and referenced relative to residual proteo solvent impurity.[61]

Computational Details

All calculations were performed using the Gaussian 16 software packages.[62] Calculations of iridium-containing molecules utilized the B3LYP[33,34] functional and a LANL2DZ [63] basis set. Initial geometries of iridium complexes were based on coordinates derived from experimental X-ray diffraction studies. Calculations of olefins utilized B3LYP and 6-311++G(d,p),[33,34] with tight convergence criteria. A polarizable continuum model (IEFPCM implementation in Gaussian, DCE solvent) was used.

General Procedure for Room Temperature Catalytic Studies

Stock solutions of **4a**, LiBAr^F$_4$, NaBAr^F$_4$, iridium catalysts, and di-*tert*-butylpyridine (Bu$_2$pyr) were prepared in 9:1 DCE:DCE-d_4. The stock solutions were combined such that each tube contained

0.5 mL of 0.2 M **4a**, 1 mol% iridium catalyst, 0 or 2 equiv MBAr$^F_4$ (M = Li$^+$ and Na$^+$), and 36 equiv Et$_2$O (relative to Ir concentration); 1.5 mol% di-*tert*-butylpyridine (^{t}Bu$_2$pyr) was added to each tube to suppress any possible side reactions promoted by adventitious protons. The reaction was monitored by NMR spectroscopy, with the residual DCE signal suppressed using a presaturation pulse sequence. Activity and selectivity were determined by integration of the olefinic peaks relative to added Et$_2$O.

General Procedure for Heated Shaker Catalysis Studies

Solutions of 0.2 M substrate, 1 mol% catalyst, and 0 or 2 mol% salt were heated at 50 °C in gas chromatography vials in a 24-well shaker. Aliquots were taken at 24, 48, 120, and 216 hrs. Each aliquot was immediately quenched with excess PPNCl in CDCl$_3$ to convert **2-18c6b** to chloride complex **1-18c6b** and halt the reaction.[24] Independent tests of **1-18c6b** and substrate showed no observable olefin isomerization and monitoring of the quenched aliquots show insignificant change in the isomer distributions after quenching. The quenching solution also contained mesitylene as an internal standard for quantification by integration of NMR spectra.

Substrates and Previously Reported Compounds

All substrates were freeze−pump−thaw degassed three times and stored over sieves. Substrates **4a**, **5a**, **13a**, **17a**, **18a**, and **19** were commercially available and passed through an alumina plug before storage over sieves. Substrates **14a**[64] and **16a**[65] were synthesized according to previously reported methodologies. LiBAr$^F_4$,[24] **1-18c6a**,[24] and **1-18c6b**[28] were prepared as previously reported and NaBAr$^F_4$ was purchased commercially and purified by recrystallization according to previously reported methods.[66]

Synthesis and Characterization of [κ⁴-(¹⁸ᶜ⁶NCOPⁱᴾʳ)Ir(H)(Cl)@Na)][BArᶠ₄] **(1-18c6a@Na)**

1-18c6a (54.4mg, 76.3 mmol) and 1.3 equivalents of NaBArᶠ₄ (85mg, 96.9 mmol) were stirred in CH₂Cl₂ at room temperature for 4 hours. Within minutes, the color deepened to brick-red. Subsequent characterization revealed the new species **(1-18c6a@Na)** (104.9 mg, 86% yield). Brick red crystals were grown by layering a solution of **1-18c6a@Na** in toluene with pentanes.

¹H NMR (500 MHz, CD₂Cl₂): -32.96 (d, J = 27.7 Hz, 1H, Ir-*H*), 0.77 (dd, J =15.5, 6.9, 3H, (CH)(C*H₃*)₂, 1.12 (dd, *J* = 19.2, 6.9 Hz, 3H, (CH)(C*H₃*)₂), 1.40 (dd, *J* = 12.9, 6.8 Hz, 3H, (CH)(C*H₃*)₂), 1.52 (dd, *J* = 17.6, 7.5 Hz, 3H, (CH)(C*H₃*)₂), 2.60 – 2.40 (m, 2H, (C*H*)(CH₃)₂), 2.91 (d, *J* = 14.5 Hz, 1H, crown-C*H₂*), 3.33 (d, *J* = 14.2 Hz, 1H, crown-C*H₂*), 3.79 – 3.38 (m, 15H, crown-C*H₂*), 3.83 (ddd, *J* = 10.7, 7.1, 3.4 Hz, 1H, crown-C*H₂*), 3.90 (d, *J* = 12.2 Hz, 1H, crown-C*H₂*), 4.09 (ddd, *J* = 11.5, 7.8, 2.8 Hz, 1H, crown-C*H₂*), 4.19 (dd, *J* = 15.5, 2.4 Hz, 1H, benzylic-C*H₂*), 4.46 (d, *J* = 15.6 Hz, 1H, benzylic-C*H₂*), 6.58 (t, *J* = 7.6 Hz, 2H, aryl-C*H*), 6.77 (t, *J* = 7.7 Hz, 1H, aryl-C*H*), 7.56 (s, 4H, *p*-B-Ar-*H*), δ 7.77 – 7.65 (t, 8H, *o*-B-Ar-*H*). **³¹P NMR** (202 MHz, CD₂Cl₂): 132.0.
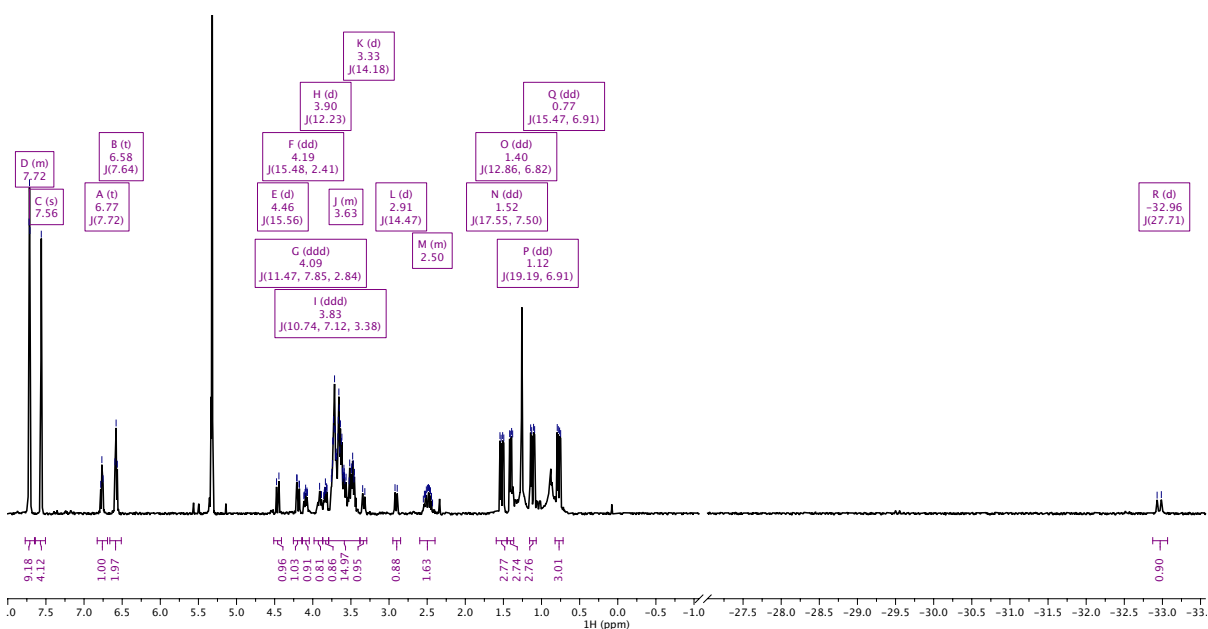
Figure 4.13. ¹H NMR of **1-18c6a@Na** in CD₂Cl₂
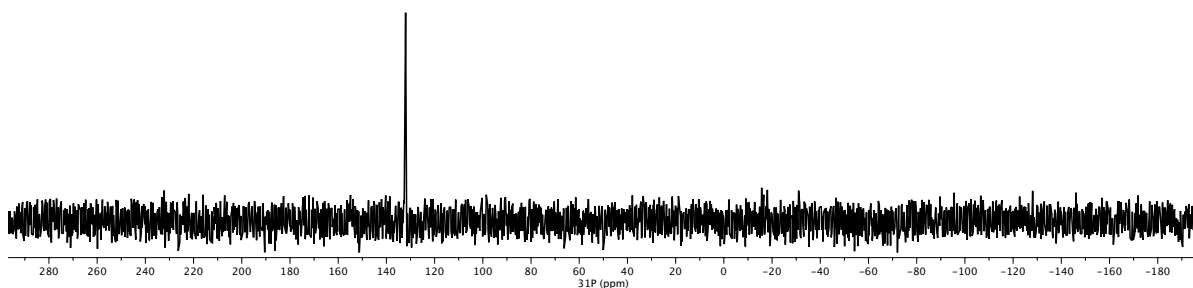
Figure 4.14. ^{31}P{^{1}H} NMR of **1-18c6a@Na** in CD$_2$Cl$_2$

Synthesis and Characterization of [κ^4-(^{18c6}NCOP^{iPr})Ir(H)(OH$_2$)][BAr$^F_4$] **(3-18c6a)**

1-18c6a (168.9 mg, 236.8 μmol) and NaBAr$^F_4$ (218 mg, 237 μmol) were dissolved in CH$_2$Cl$_2$ (4 mL). HPLC grade water was added (4 mL) and the reaction stirred vigorously for 1 hour. The water layer was abstracted, and replaced with 2 mL of fresh HPLC water, and the reaction allowed to stir for 15 minutes (2x). The yellow CH$_2$Cl$_2$ layer was abstracted and passed through an alumina plug, and concentrated on a rotary evaporated to yield a pale yellow solid (353 mg, 93.7 % yield). The solid was redissolved in ether (2 mL) and layered with pentanes (4 mL) to yield pale yellow crystals.

^{1}H NMR (600 MHz, CD$_2$Cl$_2$): δ −32.5 (d, *J* = 25.9 Hz, 1H, Ir-*H*), 0.84 (dd, *J* = 15.4, 7.0 Hz, 3H, CH(C*H$_3$*)$_2$), 1.12 (dd, *J* = 19.1, 7.0 Hz, 3H, CH(C*H$_3$*)$_2$), 1.4 (m, 6H, CH(C*H$_3$*)$_2$), 2.42 (dsep, *J* = 13.8, 6.7 Hz, 1H, C*H*(CH$_3$)$_2$), 2.68 (m, 2H, C*H*(CH$_3$)$_2$, crown-C*H$_2$*), 3.01 (dt, *J* = 13.9, 7.2 Hz, 1H, crown-C*H$_2$*), 3.22 (m, 2H, crown-C*H$_2$*) 3.32 (d, *J* = 13.2 Hz, 1H, crown-C*H$_2$*), 3.39-3.96 (m, 18H, crown-C*H$_2$*), 3.88 (m, 1H, benzylic-C*H$_2$*), 4.24 (m, 2H, crown-C*H$_2$*, benzylic-C*H$_2$*), 5.56 (s, O*H$_2$*), 6.58 (d, *J* = 7.7, 1H, aryl-C*H*), 6.61 (d, *J* = 7.6, 1H, aryl-C*H*), 6.74 (t, *J* = 7.8 Hz), 7.56 (s, 4H, *p*-B-Ar-*H*), 7.72 (t, 8H, *o*-B-Ar-*H*). **^{13}C{^{1}H} NMR** (151 MHZ, CD$_2$Cl$_2$): δ 16.4 (s, CH(*C*H$_3$)), 16.6 (d, *J* = 4, CH(*C*H$_3$)), 17.1 (s, CH(*C*H$_3$)), 17.6 (d, *J* = 8 Hz, CH(*C*H$_3$)), 28.7 (d, *J* = 40 Hz, *C*H(CH$_3$)), 30.0 (d, *J* = 34 Hz, *C*H(CH$_3$)), 59.3 (s, crown-*C*H$_2$), 62.6 (s, crown-*C*H$_2$), 66.5 (s,

crown-CH_2), 68.8 (s, crown-CH_2), 69.0 (s, crown-CH_2), 69.4 (s, crown-CH_2), 69.4 (s, crown-CH_2), 69.7 (s, crown-CH_2), 70.1 (s, crown-CH_2), 70.5 (s, crown-CH_2), 70.6 (s, crown-CH_2), 71.0 (s, crown-CH_2), 76.5 (s, benzylic-CH_2), 107.9 (d, J = 11, aryl-CH), 115.6 (s, aryl-CH), 117.5 (p, J = 4.1 Hz, p-CH, BArF), 124.0 (s, aryl-CH), 124.3 (s, aryl-C), 125.0 (q, J = 272.4 Hz, CF3, BArF), 129.3 (qdd, J = 31.2, 5.8, 2.9 Hz, C−CF3, BArF), 134.7 (s, o-CH, BArF), 135.2 (d, J = 3 Hz, aryl-C), 143.4 (s, aryl-C), 162.1 (dd, J = 99.7, 49.9 Hz, B−C, BArF), 163.7 (s, aryl-C). **^{31}P{^{1}H} NMR** (203 MHz, CD_2Cl_2): δ 138.6. **HRMS**: calculated m/z for $C_{26}H_{46}IrNO_7P$ (M[+] − H_2O) 678.25355, found: 678.25350.
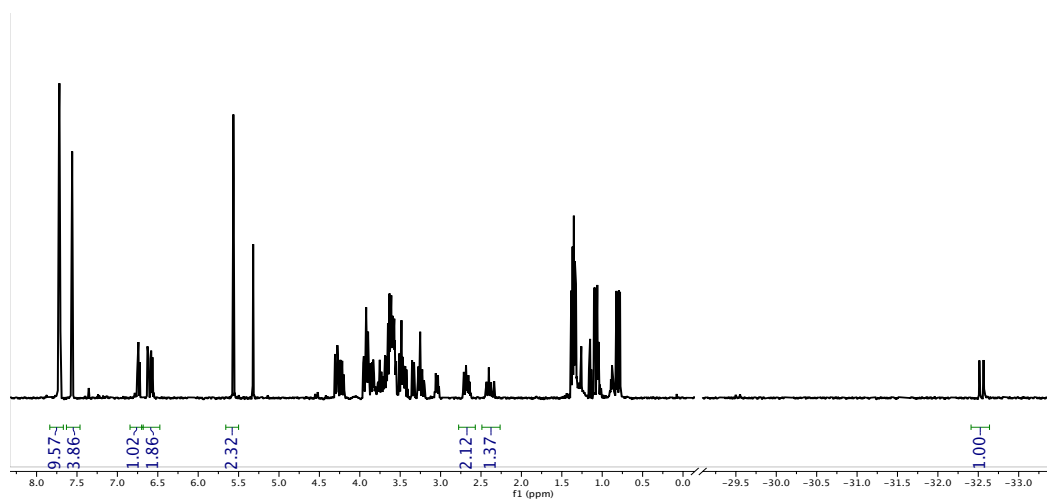
Figure 4.15. ^{1}H NMR of **3-18c6a** in CD_2Cl_2
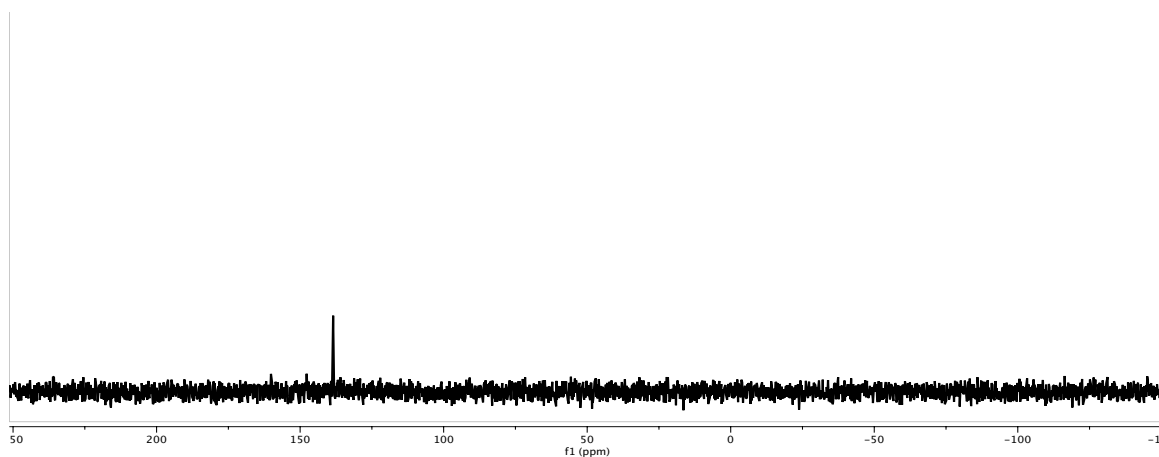
Figure 4.16. ^{31}P{^{1}H} NMR of **3-18c6a** in CD_2Cl_2
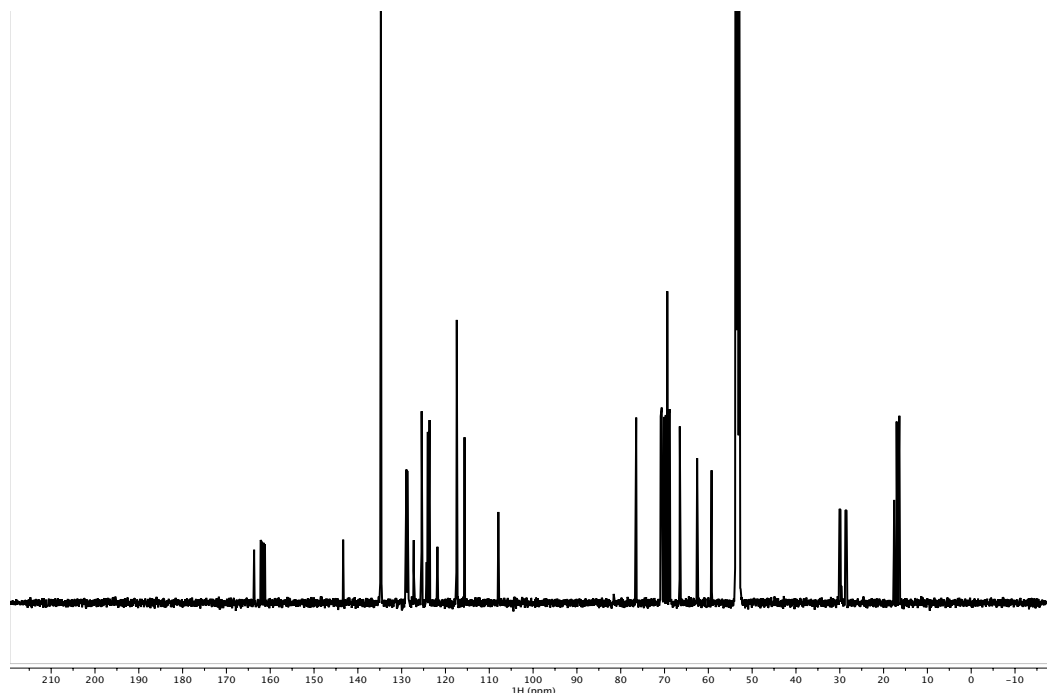
Figure 4.17. $^{13}C\{^1H\}$ NMR of **3-18c6a** in CD_2Cl_2

Synthesis and Characterization of $[\kappa^4\text{-}(^{Meo\text{-}18c6}NCOP^{iPr})Ir(H)(OH_2)][BAr^F_4]$ **(3-18c6b)**

1-18c6b (153 mg, 206 µmol) and $NaBAr^F_4$ (191 mg, 208 µmol) were dissolved in CH_2Cl_2 (4 mL). HPLC grade water was added (4 mL) and the reaction stirred vigorously for 1 hour. The water layer was removed, and replaced with 2 mL of fresh HPLC water, and the reaction allowed to stir for 15 minutes (2x). The yellow CH_2Cl_2 layer was passed through an alumina plug and concentrated on a rotary evaporated to yield a pale yellow solid. The solid was redissolved in ether (2 mL) and layered with pentanes (4 mL) to yield pale yellow crystals of **3-18c6b** (209 mg, 62.6% yield).

^1H NMR (400 MHz, CD_2Cl_2): δ −32.5 (d, J = 26.0, 1H, Ir-*H*), 0.79 (dd, J = 15.6, 6.8, 3H, CH(C*H*$_3$)$_2$), 1.07 (dd, J = 19.9, 6.9, 3H, CH(C*H*$_3$)$_2$), 1.37 (m, 6H, CH(C*H*$_3$)$_2$), 2.42 (dsep, J = 13.9, 7.0, 1H, C*H*(CH$_3$)$_2$), 2.68 (m, 2H, C*H*(CH$_3$)$_2$, crown-C*H*$_2$), 3.01 (dd, J = 13.9, 5.9, 1H, crown-C*H*$_2$), 3.22 (m, 2H, crown-C*H*$_2$) 3.32 (d, J = 12.0, 1H, crown-C*H*$_2$), 3.39-3.96 (m, 18H, crown-

138

CH_2), 3.77 (s, 3H, OCH_3), 3.88 (m, 1H, benzylic-CH_2), 4.42 (m, 2H, crown-CH_2, benzylic-CH_2), 5.56 (s, OH_2), 6.42 (d, J = 8.1, 1H, aryl-CH), 6.61 (d, J = 8.1, 1H, aryl-CH), 7.56 (s, 4H, p-B-Ar-H), 7.72 (t, 8H, o-B-Ar-H). ^{13}C{^{1}H} NMR (101 MHZ, CD$_2$Cl$_2$): δ 16.5 (d, J = 1.6, CH(CH_3), 16.6 (d, J = 4.6, CH(CH_3), 17.1 (d, J = 1.3, CH(CH_3), 17.6 (d, J = 8.9 Hz, CH(CH_3), 28.7 (d, J = 39.7, CH(CH$_3$), 30.0 (d, J = 34.0, CH(CH$_3$), 56.0 (s, OCH$_3$), 59.2 (s, crown-CH$_2$), 62.3 (s, crown-CH$_2$), 66.5 (s, crown-CH$_2$), 68.8 (s, crown-CH$_2$), 68.9 (s, crown-CH$_2$), 69.4 (s, crown-CH$_2$), 69.4 (s, crown-CH$_2$), 69.7 (s, crown-CH$_2$), 70.0 (s, crown-CH$_2$), 70.1 (s, crown-CH$_2$), 70.6 (s, crown-CH$_2$), 70.9 (s, crown-CH$_2$), 76.5 (s, benzylic-CH$_2$), 108.4 (s, aryl-CH), 116.0 (s, aryl-CH), 117.5 (p, J = 4.1 Hz, p-CH, BAr$^F_5$), 125.0 (q, J = 272.4 Hz, CF3, BAr$^F_4$), 125.6 (d, J = 5 Hz, aryl-C), 129.3 (qdd, J = 31.2, 5.8, 2.9 Hz, C−CF3, BAr$^F_4$), 134.7 (s, o-CH, BAr$^F_4$), 135.2 (d, J = 3 Hz, aryl-C), 143.0 (d, J = 10.0 Hz, aryl-C), 151.7 (d, J = 4 Hz, aryl-C), 162.1 (dd, J = 99.7, 49.9 Hz, B−C, BAr$^F_4$). ^{31}P{^{1}H} NMR (162 MHz, CD$_2$Cl$_2$): δ 140.4. **HRMS**: calculated m/z C$_{26}$H$_{46}$IrNO$_7$P (M$^+$ – H$_2$O): 708.26411; found 708.26456. **Anal. Calcd.** for C$_{58}$H$_{60}$BF$_{24}$IrNO$_8$P: C, 43.84; H, 3.81; N, 0.88. Found: C, 43.84; H, 3.52; N, 0.88.
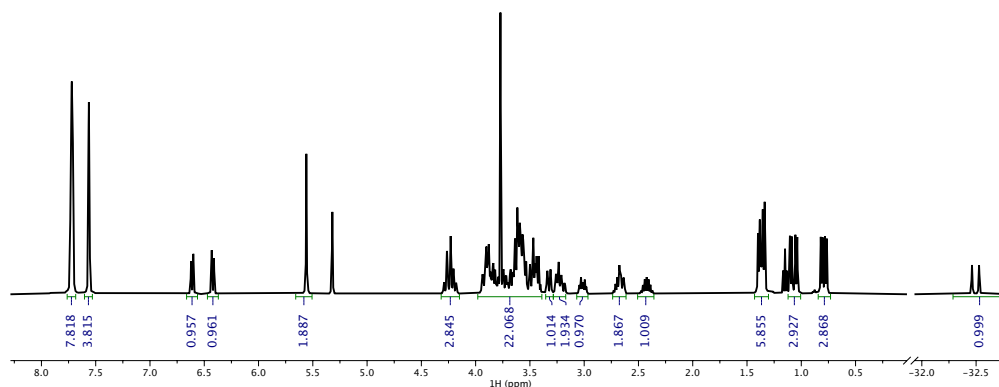
Figure 4.18. ^{1}H NMR of **3-18c6b** in CD$_2$Cl$_2$
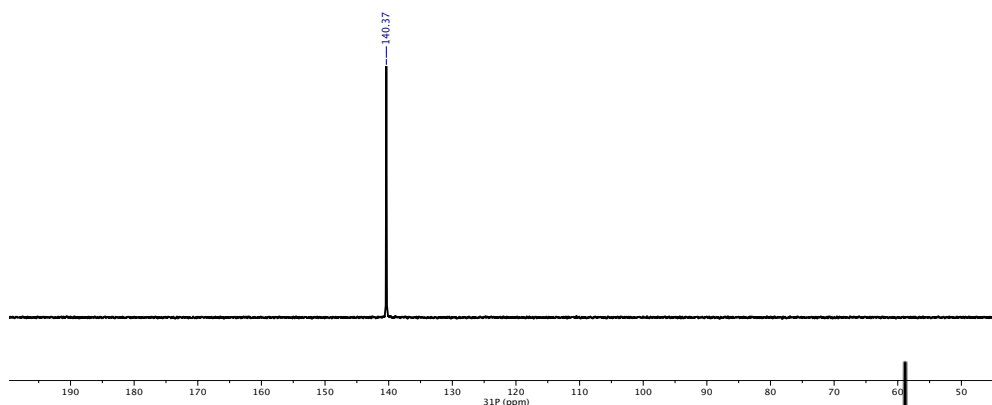
Figure 4.19. $^{31}P\{^1H\}$ NMR of **3-18c6b** in CD_2Cl_2
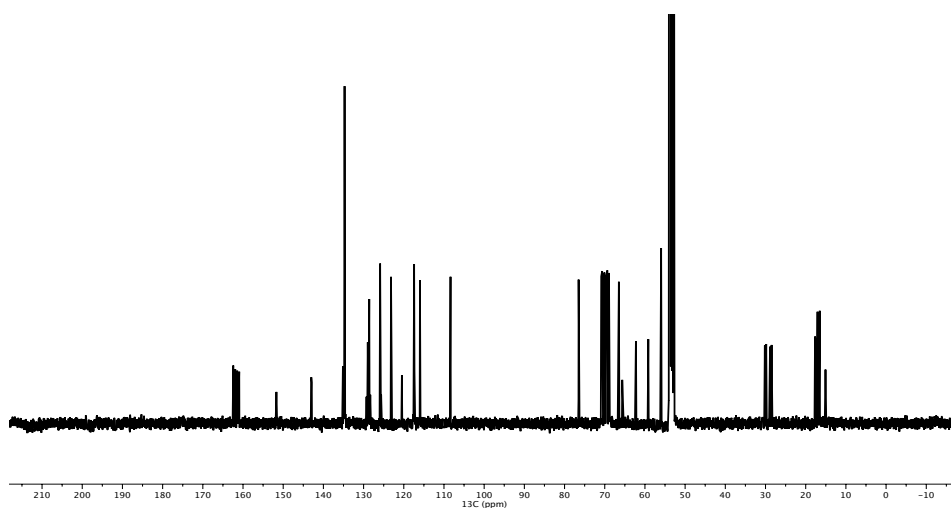
Figure 4.20. $^{13}C\{^1H\}$ NMR of **3-18c6b** in CD_2Cl_2

Synthesis and Characterization of [κ^4-($^{18c6}NCOP^{iPr}$)Ir(H)][BAr$^F_4$] **(2-18c6a)**

3-18c6a (100mg, 64 µmol) was dried at 140 °C under vacuum. P_2O_5 was placed on the same line to aid in water removal. An off-white powder was collected, yielding **2-18c6b** (97mg, 98% yield).

¹H NMR (600 MHz, CD_2Cl_2): δ -29.50 (d, J = 26.2 Hz, 1H, Ir-*H*), 0.89 (bdd, J = 15.2, 6.7 Hz, 3H, CH(C*H*$_3$)$_2$), 1.05 (dd, J = 20.0, 7.1 Hz, 3H, CH(C*H*$_3$)$_2$), 1.29 (bdd, J = 15.6, 7.2 Hz, 3H,

CH(CH_3)$_2$), 1.35 (bdd, J = 15.0, 6.9 Hz, 3H, CH(CH_3)$_2$), 2.34 (dsep, J = 6.9, 6.9, 1H, CH(CH$_3$)$_2$),

2.42 (sep, J = 6.9 Hz, 1H , CH(CH$_3$)$_2$), 3.11 (bd, J = 14. Hz, 1H, crown-CH_2), , 3.54-4.28 (bm,

23H, crown CH_2),), 4.40 (bd, J = 15.3, 1H, benzylic-CH_2), 4.54 (d, J = 15.3 Hz, 1H, benzylic-

CH_2), 6.56 (d, J = 8.0 Hz, 1H, aryl-H), 6.58 (d, J = 7.8 Hz, 1H, aryl-H), 6.79 (J = 7.8 Hz, 1H, aryl-

H), 7.56(s, 4H, p-B-Ar-H), 7.72 (t, 8H, o-B-Ar-H). **^{31}P{^{1}H} NMR (**243 MHz, CD$_2$Cl$_2$): δ 139.0.

HRMS: calculated m/z for C$_{26}$H$_{46}$IrNO$_7$P (M$^+$), 678.25355, found: 678.25360.

Alternate synthesis of **2-18c6a:**

Trityl tetrakis(pentafluorophenyl)borate (12.4mg, 13.5 μmol), triethylsilane (2.2 uL, 13.5 μmol),

and **1-18c6a** (9.6 mg, 13.5 μmol) were dissolved in separate stock solutions of chlorobenzene (2

mL). The triethylsilane was added dropwise to the trityl solution and the reaction stirred for 2

minutes. The resulting silylium solution was added dropwise to the **1-18c6a** solution and the

reaction stirred for 1 hr. The chlorobenzene was removed by vacuum, and the solid triturated

with pentanes. Product was extracted with cold benzene and lyophilized. The oily solid was

washed with pentanes and extracted with DCM (2 mL). An equal volume of pentanes was

added, crashing out an oily residue. The supernatant was removed, and dried to reveal the

product as a white solid (9.2 mg, 50% yield). Spectroscopic comparisons with **2-18c6a** derived

from tetrakis(3,5-trifluoromethyphenyl)borate show identical chemical shifts of the iridium

cation.

A solution of **2-18c6a** in CH$_2$Cl$_2$ was layered with pentanes (1:4), yielding colorless, X-Ray quality
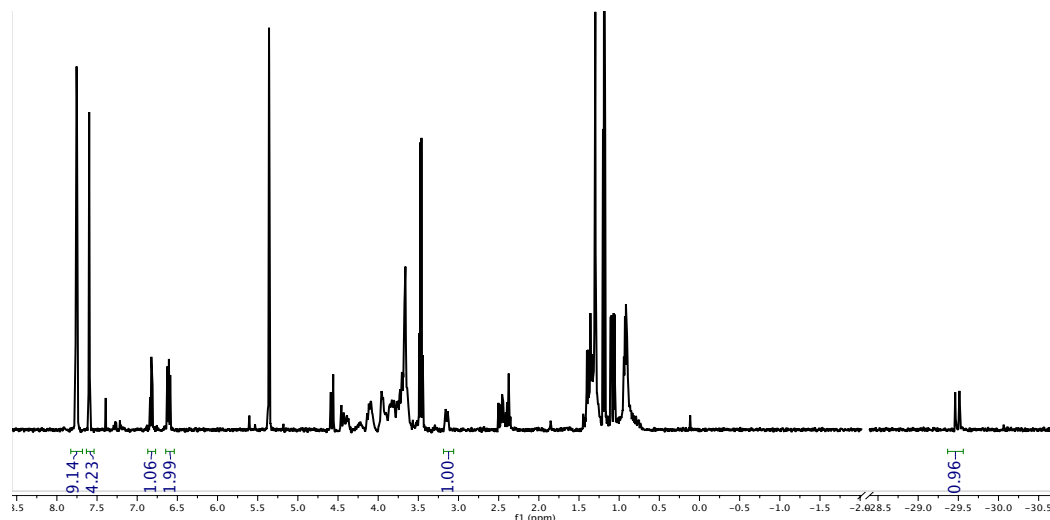
crystals.

Figure 4.21. ¹H NMR of **2-18c6a** in CD₂Cl₂
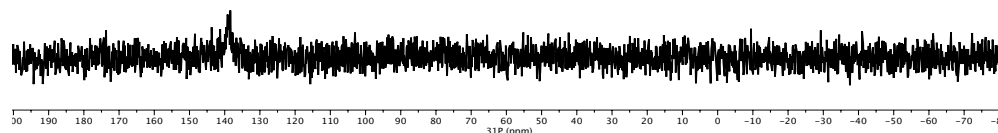
Figure 4.22. ³¹P{¹H} NMR of **2-18c6a** in CD₂Cl₂

Synthesis and Characterization of [κ⁵-(^{Meo-18c6}NCOP^{iPr})Ir(H)][BAr^F₄] **(2-18c6b)**

Crystals of **3-18c6b** (286 mg, 180 μmol) were crushed and heated under high vacuum at 145 °C on a schlenk line. P_2O_5 was placed on the same line to aid in water removal. After heating for 24 hours, the solid was cooled and transferred to a dry box, yielding the off-white product **2-18c6b** (281 mg, 99% yield). A solution of **2-18c6b** in CH₂Cl₂ was layered with pentanes (1:4), yielding colorless X-Ray quality crystals.

¹H NMR (400 MHz, CD₂Cl₂): δ -29.50 (d, *J* = 26.4 Hz, 1H, Ir-*H*), 0.86 (bdd, *J* = 16.2, 6.8 Hz, 3H, CH(C*H₃*)₂), 1.04 (dd, *J* = 19.7, 7.1 Hz, 3H, CH(C*H₃*)₂), 1.31(bdd, *J* = 15.8, 6.9 Hz, 3H,

142

CH(C*H*₃)₂), 1.36 (bdd, *J* = 14.9, 7.3 Hz, 3H, CH(C*H*₃)₂), 2.29-2.51 (m, 2H, C*H*(CH₃)₂), 3.09 (bd,

J = 14.1 Hz, 1H, crown-C*H*₂), 3.38 (bs, 1H, crown-C*H*₂), 3.50-4.30 (bm, 21H, crown C*H*₂), 3.76

(s, 3H, OC*H*₃), 4.35 (bm, 1H, crown-C*H*₂), 4.38 (d, *J* = 14.7 Hz, 1H, benzylic-C*H*₂), 4.47 (d, *J* =

14.7 Hz, 1H, benzylic-C*H*₂), 6.46 (d, *J* = 8.2 Hz, 1H, aryl-*H*), 6.57 (d, *J* = 8.2 Hz, 1H, aryl-*H*),

7.56 (s, 4H, *p*-B-Ar-*H*), 7.72 (t, 8H, *o*-B-Ar-*H*). **¹³C{¹H} NMR** (101 MHZ, CD₂Cl₂): δ 16.1 (s,

CH(*C*H₃), 16.6 (broad s, 2C, CH(*C*H₃)), 17.1 (s, CH(*C*H₃)), 30.0 (d, *J* = 39.4 Hz, *C*H(CH₃)),

30.7 (d, *J* = 33.3 Hz, *C*H(CH₃)), 56.0 (s, O*C*H₃), 59.2 (crown-*C*), δ 64.3 (crown-*C*), 68.6-72.6

(crown-*C*), 70.3 (benzylic-*C*H₂), 108.9 (aryl-*C*H, 115.5 (aryl-*C*H), 117.5 (p, *J* = 4.1 Hz, p-CH,

BAr^F₄), 125.0 (q, J = 272.4 Hz, CF3, BAr^F₄), 126.0 (d, *J* = 4.3, aryl-*C*) 128.9 (qdd, J = 31.2, 5.8,

2.9 Hz, C−CF3, BAr^F₄), 134.7 (s, o-CH, BAr^F₄), 135.4 (s, aryl-*C*), 143.0 (aryl-*C*), 151.7 (d, *J* = 3.7

Hz, aryl-*C*), 161.7 (dd, J = 99.7, 49.9 Hz, B−C, BAr^F₄).**³¹P{¹H} NMR** (162 MHz, CD₂Cl₂): δ

140.7. **HRMS:** calculated m/z for C₂₆H₄₆IrNO₇P (M⁺): 708.26411, found: 708.26379. **Anal.**

Calcd for C₅₈H₅₈BF₂₄IrNO₇P: C, 44.34; H, 3.72; N, 0.89. Found: C, 44.21; H, 3.61; N, 0.87.
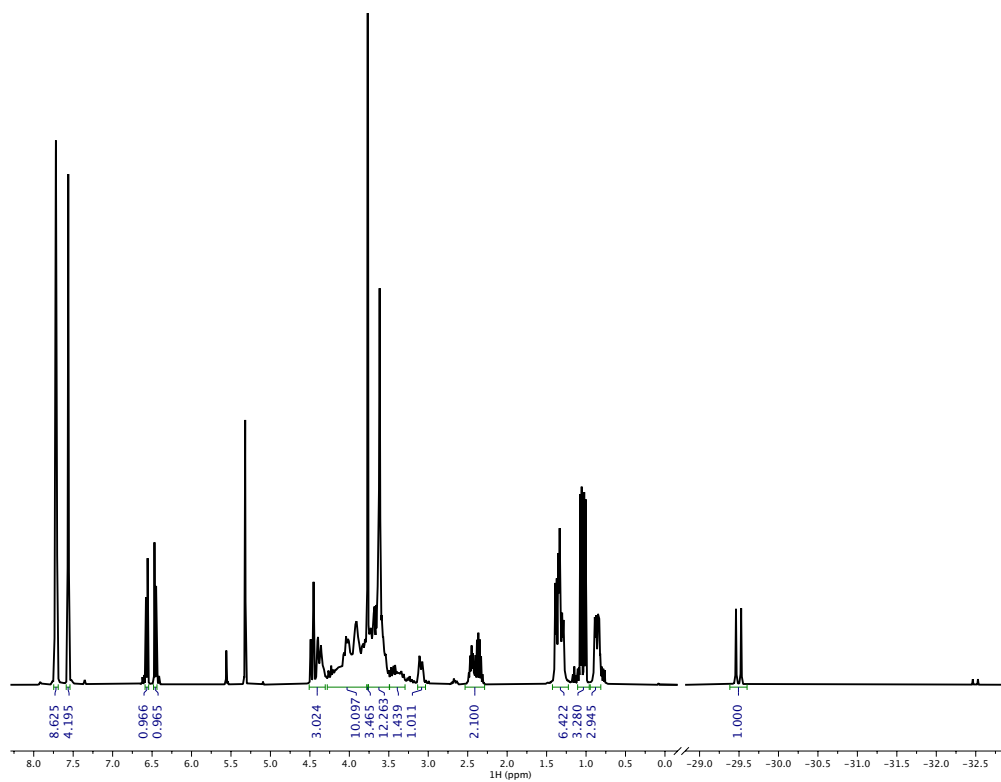
Figure 4.23. ^{1}H NMR of **2-18c6b** in CD$_2$Cl$_2$
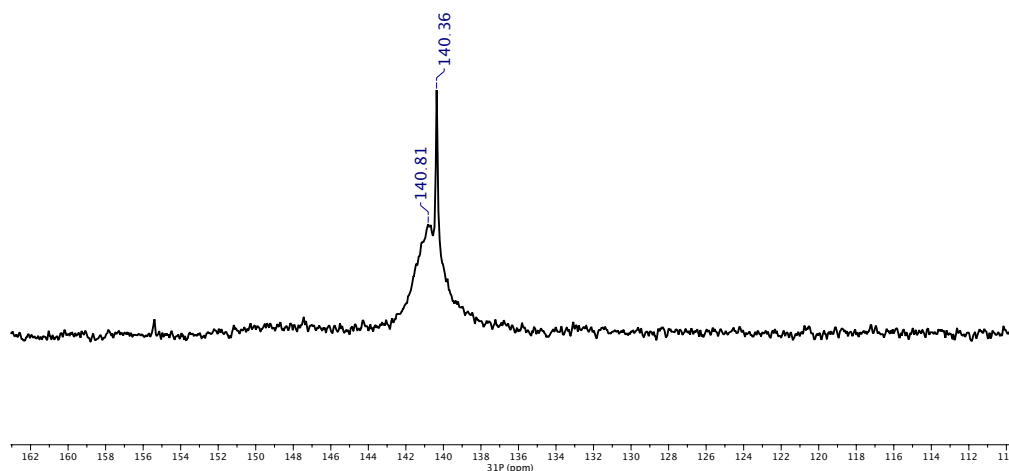
Figure 4.24. ^{31}P{^{1}H} NMR of **2-18c6b** in CD$_2$Cl$_2$

Approximately 3% of 3-18c6b is also present in this sample, corresponding to the sharp peak at 140.4 ppm.
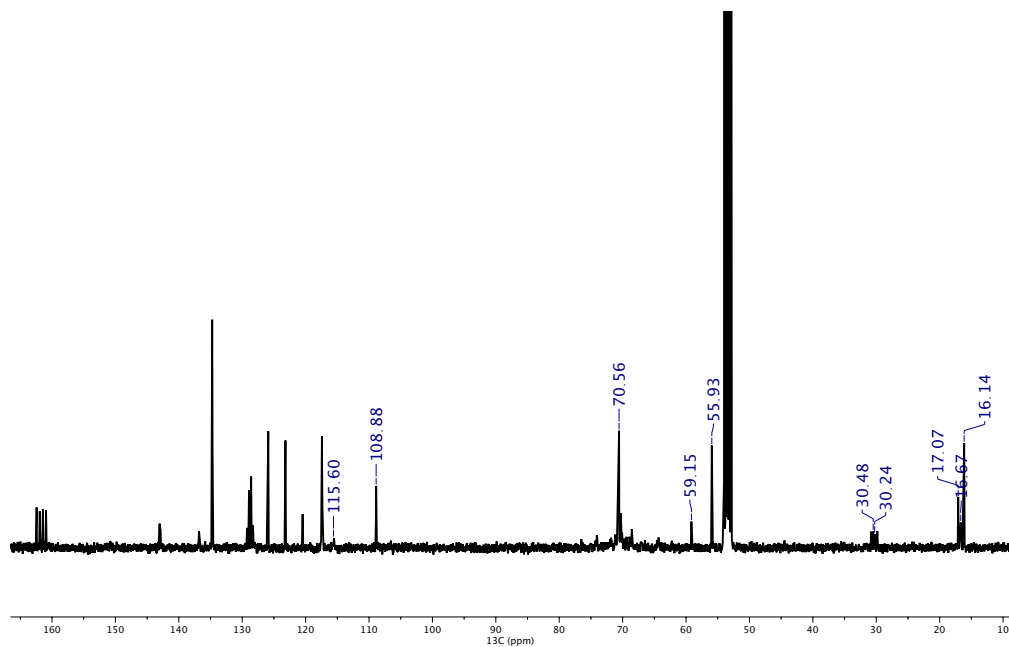
Figure 4.25. $^{13}C\{^1H\}$ NMR of **2-18c6b** in CD_2Cl_2
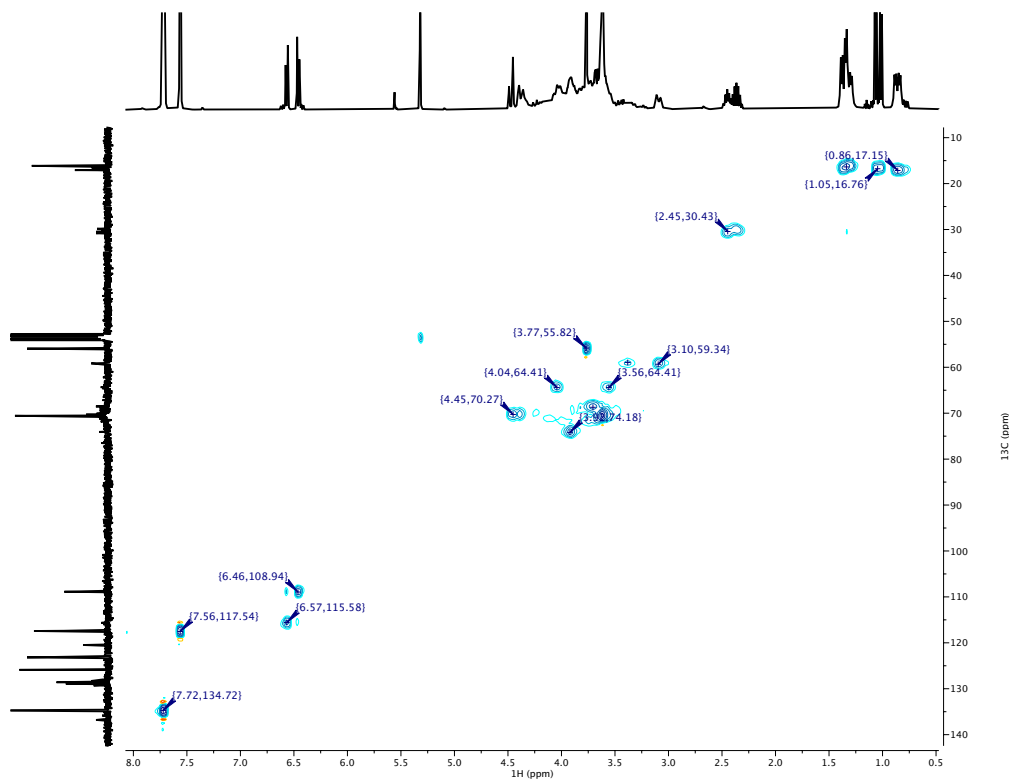
Figure 4.26. ^1H-^{13}C HSQC spectrum of **2-18c6b** in CD_2Cl_2

145

Synthesis and Characterization of [κ⁴-(^MeO-15c5^NCOP^iPr^)Ir(H)(OH₂)][BAr^F^₄] **(3-15c5b)**

2-15c5b was dissolved in wet CH_2Cl_2. Full conversion to the aqua adduct was observed by NMR. **2-15c5b** solid was dissolved in wet ether (2 mL) and layered with pentanes (4 mL) to yield pale yellow crystals.

¹H NMR (400 MHz, CD_2Cl_2): δ −32.5 (d, *J* = 26.1 Hz, 1H, Ir-*H*), 0.79 (dd, *J* = 16.4, 6.9 Hz, 3H, CH(C*H₃*)₂), 1.05 (dd, *J* = 20.1, 6.8 Hz, 3H, CH(C*H₃*)₂), 1.34 (dd, *J* = 17.0, 7.5 Hz, 3H, CH(C*H₃*)₂), 1.40 (dd, *J* = 13.8, 6.9 Hz, 3H, CH(C*H₃*)₂), 2.42 (dsep, *J* = 14.0, 6.6 Hz, 1H, C*H*(CH₃)₂), 2.56 (dsep, *J* = 8.4, 7.3 Hz, 1H, C*H*(CH₃)₂), 2.68 (m, 1H, crown-C*H₂*), 3.22 (m, , 2H, crown-C*H₂*), 3.36-3.97 (15H, crown-C*H₂*) 3.77 (s, 3H, OC*H₃*), 4.02 (dd, *J* = 13.1, 2.6 Hz, 1H, benzylic-C*H₂*), 4.17 (ddd, *J* = 12.7, 12.7, 3.4 Hz, 1H, crown-C*H₂*), 4.25 (d, *J* = 13.1, 1H, benzylic-CH₂), 4.33 (dd, *J* = 14.8, 5.8 Hz, 1H, crown-C*H₂*), 6.17 (s, 2H, O*H₂*), 6.42 (d, *J* = 8.1, 1H, aryl-C*H*), 6.62 (d, *J* = 8.1, 1H, aryl-C*H*), 7.56 (s, 4H, *p*-B-Ar-*H*), 7.72 (t, 8H, *o*-B-Ar-*H*).

¹³C{¹H} NMR (101 MHZ, CD_2Cl_2): δ 16.1 (m, 2C, CH(CH₃)₂), 16.8 (m, 2C, CH(CH₃)₂), 28.9 (d, *J* = 39.7 *C*H(CH₃)), 30.1 (d, *J* = 34.8, *C*H(CH₃), 56.0 (s, OCH₃), 61.1 (s, crown-CH₂), 62.4 (s, crown-CH₂), 65.2 (s, crown-CH₂), 67.2 (s, crown-CH₂), 68.5 (s, crown-CH₂), 68.9 (s, crown-CH₂), 69.9 (s, crown-CH₂), 70.6 (s, crown-CH₂), 71.2 (s, crown-CH₂), 71.7 (s, crown-CH₂), 74.3(s, benzylic-CH₂), 108.4 (s, aryl-*C*H), 116.0 (s, aryl-*C*H), 117.5 (p, *J* = 4.1 Hz, p-CH, BAr^F^₄), 125.0 (q, J = 272.4 Hz, CF3, BAr^F^₄), 125.6 (aryl-*C*), 129.3 (qdd, J = 31.2, 5.8, 2.9 Hz, C−CF3, BAr^F^₄), 135.2 (s, o-CH, BAr^F^₄), 135.4 (aryl-*C*), 143.0 (aryl-*C*), 153.2 (aryl-*C*), 162.1 (dd, J = 99.7, 49.9 Hz, B−C, BAr^F^₄). **³¹P{¹H} NMR** (162 MHz, CD_2Cl_2): 140.4. **HRMS:** calculated m/z for $C_{24}H_{42}IrNO_6P$ (M⁺− H₂O) 664.23779, found: 664.23790.
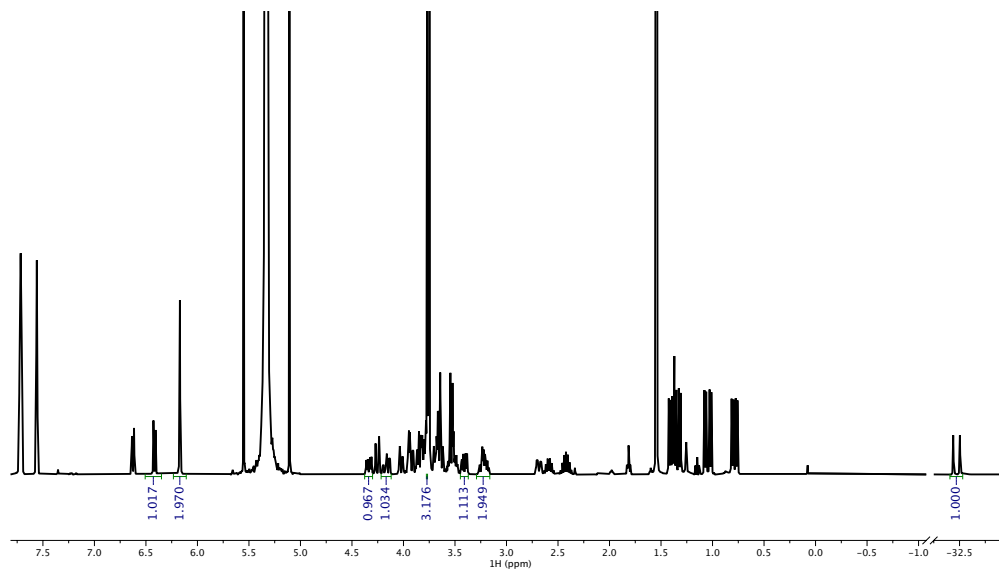
Figure 4.27. ^{1}H NMR of **3-15c5b** in CD$_2$Cl$_2$
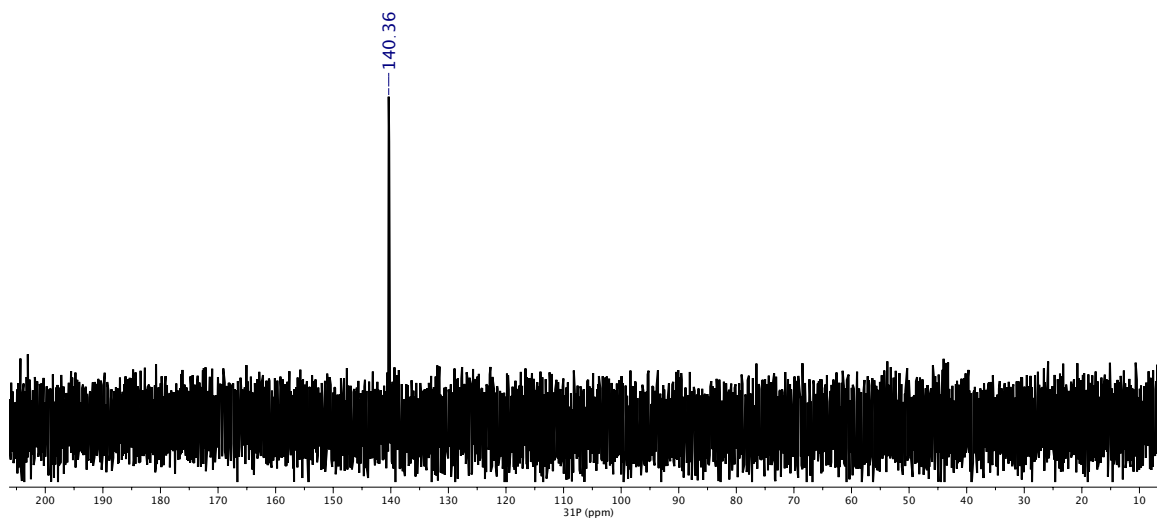
Figure 4.28. ^{31}P{^{1}H} NMR of **3-15c5b** in CD$_2$Cl$_2$
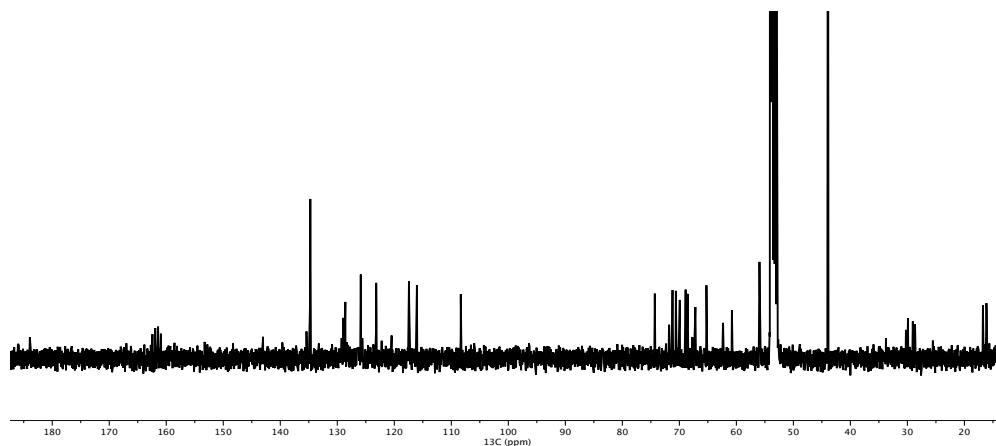
Figure 4.29. $^{13}C\{^1H\}$ NMR of **3-15c5b** in CD_2Cl_2

Synthesis of 2-(but-3-en-1-yl)-4,4,5,5-tetramethyl-1,3,2-dioxaborolane **(15b)**

3-butenyl-1-boronic acid (470mg, 4.7 mmol) and pinacol (516 *mg, 4.37 mmol)* were weighed into a 20 mL scint vial. Solids were stirred vigorously over 1hr, and filtered through a silica plug yielding a volatile, clear oil (248.8 mg, 31.3%). Chemical shifts match previous reports.[14]

REFERENCES

(1)   Larsen, C. R.; Grotjahn, D. B. The Value and Application of Transition Metal Catalyzed Alkene Isomerization in Industry. In *Applied Homogeneous Catalysis with Organometallic Compounds*; Cornils, B., Herrmann, W. A., Beller, M., Paciello, R., Eds.; Wiley-VCH Verlag: Weinheim, Germany, 2018; pp 1365–1378.

(2)   Donohoe, T. J.; O'Riordan, T. J. C.; Rosa, C. P. Ruthenium-Catalyzed Isomerization of Terminal Olefins: Applications to Synthesis. *Angew. Chemie - Int. Ed.* **2009**, *48* (6), 1014–1017.

(3)   Hassam, M.; Taher, A.; Arnott, G. E.; Green, I. R.; van Otterlo, W. A. L. Isomerization of Allylbenzenes. *Chem. Rev.* **2015**, *115* (11), 5462–5569.

(4)   Mol, J. Industrial Applications of Olefin Metathesis. *J. Mol. Catal. A Chem.* **2004**, *213* (1), 39–45.

(5)   Bidange, J.; Fischmeister, C.; Bruneau, C. Ethenolysis: A Green Catalytic Tool to Cleave Carbon–Carbon Double Bonds. *Chem. - A Eur. J.* **2016**, *22* (35), 12226–12244.

(6)   Li, H.; Mazet, C. Iridium-Catalyzed Selective Isomerization of Primary Allylic Alcohols. *Acc. Chem. Res.* **2016**, *49* (6), 1232–1241.

(7)   Kocen, A. L.; Klimovica, K.; Brookhart, M.; Daugulis, O. Alkene Isomerization by "Sandwich" Diimine-Palladium Catalysts. *Organometallics* **2017**, *36* (4), 787–790.

(8)   Yamasaki, Y.; Kumagai, T.; Kanno, S.; Kakiuchi, F.; Kochi, T. Selective Long-Distance Isomerization of Terminal Alkenes via Nondissociative Chain Walking. *J. Org. Chem.* **2018**, *83* (16), 9322–9333.

(9)   Grotjahn, D. B.; Larsen, C. R.; Gustafson, J. L.; Nair, R.; Sharma, A. Extensive Isomerization of Alkenes Using a Bifunctional Catalyst: An Alkene Zipper. *J. Am. Chem. Soc.* **2007**, *129* (31), 9592–9593.

(10)   Dunning, H. N. Review of Olefin Isomerization. *Ind. Eng. Chem.* **1953**, *45* (3), 551–564.

(11)   Sparke, M. B.; Turner, L.; Wenham, A. J. M. The Isomerization of Olefins by Palladium Complexes. *J. Catal.* **1965**, *4*, 332–3340.

(12)   Chen, C.; Dugan, T. R.; Brennessel, W. W.; Weix, D. J.; Holland, P. L. Z -Selective Alkene Isomerization by High-Spin Cobalt(II) Complexes. *J. Am. Chem. Soc.* **2014**, *136* (3), 945–955.

(13)   Hwan, J. L.; Smith, C. R.; RajanBabu, T. V. Facile Pd(II)- and Ni(II)-Catalyzed Isomerization of Terminal Alkenes into 2-Alkenes. *J. Org. Chem.* **2009**, *74* (12), 4565–4572.

(14)   Becica, J.; Glaze, O. D.; Wozniak, D. I.; Dobereiner, G. E. Selective Isomerization of Terminal Alkenes to (Z)-2-Alkenes Catalyzed by an Air-Stable Molybdenum(0) Complex. *Organometallics* **2018**, *37* (3), 482–490.

(15)   Larsen, C. R.; Grotjahn, D. B. Stereoselective Alkene Isomerization over One Position. *J. Am. Chem. Soc.* **2012**, *134* (25), 10357–10360.

(16)   Crossley, S. W. M.; Barabé, F.; Shenvi, R. A. Simple, Chemoselective, Catalytic Olefin Isomerization. *J. Am. Chem. Soc.* **2014**, *136* (48), 16788–16791.

(17)   Scarso, A.; Colladon, M.; Sgarbossa, P.; Santo, C.; Michelin, R. A.; Strukul, G. Highly Active and Selective Platinum(II)-Catalyzed Isomerization of Allylbenzenes: Efficient Access to (E)-Anethole and Other Fragrances via Unusual Agostic Intermediates. *Organometallics* **2010**, *29* (6), 1487–1497.

(18)   Kapat, A.; Sperger, T.; Guven, S.; Schoenebeck, F. E-Olefins through Intramolecular Radical Relocation. *Science (80-.).* **2019**, *396* (January), 391–396.

(19)   Schmidt, A.; Nödling, A. R.; Hilt, G. An Alternative Mechanism for the Cobalt-Catalyzed Isomerization of Terminal Alkenes to (Z)-2-Alkenes. *Angew. Chemie - Int. Ed.* **2015**, *54* (3), 801–804.

(20)   Molloy, J. J.; Morack, T.; Gilmour, R. Positional and Geometrical Isomerisation of Alkenes: The Pinnacle of Atom Economy. *Angew. Chemie Int. Ed.* **2019**, *58* (39), 13654–13664.

(21)   Liu, X.; Zhang, W.; Wang, Y.; Zhang, Z. X.; Jiao, L.; Liu, Q. Cobalt-Catalyzed Regioselective Olefin Isomerization under Kinetic Control. *J. Am. Chem. Soc.* **2018**, *140* (22), 6873–6882.

(22)   Meng, Q.; Schirmer, T. E.; Katou, K.; König, B. Controllable Isomerization of Alkenes by Dual Visible-Light-Cobalt Catalysis. *Angew. Chemie* **2019**, *131* (17), 5779–5784.

(23)   Paulson, E. R.; Moore, C. E.; Rheingold, A. L.; Pullman, D. P.; Sindewald, R. W.; Cooksy, A. L.; Grotjahn, D. B. Dynamic Pi-Bonding of Imidazolyl Substituent in a Formally 16-Electron Cp Ru(2-P, N)+ Catalyst Allows Dramatic Rate Increases in (E)-Selective Monoisomerization of Alkenes. *ACS Catal.* **2019**, *9* (8), 7217–7231.

(24)   Kita, M. R.; Miller, A. J. M. Cation-Modulated Reactivity of Iridium Hydride Pincer-Crown Ether Complexes. *J. Am. Chem. Soc.* **2014**, *136* (41), 14519–14529.

(25)   Smith, J. B.; Camp, A. M.; Farquhar, A. H.; Kerr, S. H.; Chen, C.-H.; Miller, A. J. M. Organometallic Elaboration as a Strategy for Tuning the Supramolecular Characteristics of Aza-Crown Ethers. *Organometallics* **2019**, *38* (22), 4392–4398.

(26)   Kita, M. R.; Miller, A. J. M. An Ion-Responsive Pincer-Crown Ether Catalyst System for Rapid and Switchable Olefin Isomerization. *Angew. Chemie Int. Ed.* **2017**, *56* (20), 5498–5502.

(27)   Smith, J. B.; Miller, A. J. M. Connecting Neutral and Cationic Pathways in Nickel-Catalyzed Insertion of Benzaldehyde into a C–H Bond of Acetonitrile. *Organometallics* **2015**, *34* (19), 4669–4677.

(28)   Yoo, C.; Dodge, H. M.; Farquhar, A. H.; Gardner, K. E.; Miller, A. J. M. Poly(Ether) Dissection by Pincer Iridium-Mediated Ether Decarbonylation.

(29)   Smith, J. B.; Kerr, S. H.; Miller, A. J. M. Cation Binding with Nickel Pincer-Crown Ether Complexes Cation – Crown Ether Interactions. *Manuscr. Prep.*

(30)   Dodge, H. M.; Kita, M. R.; Chen, C.-H.; Miller, A. J. M. Controlling Pincer Ligand Hemilability to Avoid Off-Cycle Intermediates in Cation-Tunable Olefin Isomerization.

(31)   Gregor, L. C.; Grajeda, J.; White, P. S.; Vetter, A. J.; Miller, A. J. M. Salt-Promoted Catalytic Methanol Carbonylation Using Iridium Pincer-Crown Ether Complexes. *Catal. Sci. Technol.* **2018**, *8* (12), 3133–3143.

(32)   Miller, A. J. M. Cation-Modulated Hemilability in Pincer-Crown Ether Ligands: A Strategy for Tunable and Switchable Catalysis. *Dalt. Trans.* **2017**, *46* (36*)*, 11987-12000.

(33)   Mclean, A.D; Chandler, G. S. J. No Title. *J. Chem. Phys.* **1985**, *72*, 5639.

(34)   Krishnan, R.; Binkley, J. S.; Seeger, R.; Pople, J. A. No Title. *J. Chem. Phys.* **1980**, *72*, 650.

(35)   Bols, M.; Pedersen, C. M. Silyl-Protective Groups Influencing the Reactivity and Selectivity in Glycosylations. *Beilstein J. Org. Chem.* **2017**, *13*, 93–105.

(36)   Ohmura, T.; Yamamoto, Y.; Miyaura, N. Stereoselective Synthesis of Silyl Enol Ethers via the Iridium-Catalyzed Isomerization of Allyl Silyl Ethers. *Organometallics* **1999**, *18* (3), 413–416.

(37)   Kovalenko, M.; Yarmoliuk, D. V.; Serhiichuk, D.; Chernenko, D.; Smyrnov, V.; Breslavskyi, A.; Hryshchuk, O. V.; Kleban, I.; Rassukana, Y.; Tymtsunik, A. V.; Tolmachev, A. A.; Kuchkovska, Y. O.; Grygorenko, O. O. The Boron-Wittig Olefination of Aldehydes and Ketones with Bis[(Pinacolato)Boryl]Methane: An Extended Reaction Scope. *European J. Org. Chem.* **2019**, *2019* (33), 5624–5635.

(38)   Larsen, C. R.; Erdogan, G.; Grotjahn, D. B. General Catalyst Control of the Monoisomerization of 1-Alkenes to Trans -2-Alkenes. *J. Am. Chem. Soc.* **2014**, *136* (4), 1226–1229.

(39) Kobayashi, T.; Yorimitsu, H.; Oshima, K. Cobalt-Catalyzed Isomerization of 1-Alkenes to (E)-2-Alkenes with Dimethylphenylsilylmethylmagnesium Chloride and Its Application to the Stereoselective Synthesis of (E)-Alkenylsilane. *Chem. - An Asian J.* **2009**, *4* (7), 1078–1083.

(40) Fidyt, K.; Fiedorowicz, A.; Strządała, L.; Szumny, A. B-Caryophyllene and B-Caryophyllene Oxide—Natural Compounds of Anticancer and Analgesic Properties. *Cancer Med.* **2016**, *5* (10), 3007–3017.

(41) Khomenko, T. M.; Korchagina, D. V.; Gatilov, Y. V.; Bagryanskaya, Y. I.; Tkachev, A. V.; Vyalkov, A. I.; Kun, O. B.; Salenko, V. L.; Dubovenko, Z. V.; Barkash, V. A. Synthesis and Transformations of Some Dienes with a Caryophyllane Skeleton in Acidic Media. *J. Org. Chem. USSR.* **1990**, *26*, 1839–1852.

(42) Fitjer, L.; Malich, A.; Paschke, C.; Kluge, S.; Gerke, R.; Rissom, B.; Weiser, J.; Noltemeyer, M. Rearrangement of (—)-β-Caryophyllene. A Product Analysis and Force Field Study. *J. Am. Chem. Soc.* **1995**, *117* (36), 9180–9189.

(43) Romanenko, E. P.; Tkachev, A. V. Acid-Catalyzed Isomerization of Caryophyllene in the Presence of SiO2 and Al2O3 Impregnated with Sulfuric Acid. *Russ. Chem. Bull.* **2018**, *67* (6), 1051–1058.

(44) Frisch, M. J.; Head-Gordon, M.; Pople, J. A. A Direct MP2 Gradient Method. *Chem. Phys. Lett.* **1990**, *166* (3), 275–280.

(45) Frisch, M. J.; Head-Gordon, M.; Pople, J. A. Semi-Direct Algorithms for the MP2 Energy and Gradient. *Chem. Phys. Lett.* **1990**, *166* (3), 281–289.

(46) Head-Gordon, M.; Pople, J. A.; Frisch, M. J. MP2 Energy Evaluation by Direct Methods. *Chem. Phys. Lett.* **1988**, *153* (6), 503–506.

(47) Head-Gordon, M.; Head-Gordon, T. Analytic MP2 Frequencies without Fifth-Order Storage. Theory and Application to Bifurcated Hydrogen Bonds in the Water Hexamer. *Chem. Phys. Lett.* **1994**, *220* (1–2), 122–128.

(48) Woon, D. E.; Dunning, T. H. Gaussian Basis Sets for Use in Correlated Molecular Calculations. V. Core-Valence Basis Sets for Boron through Neon. *J. Chem. Phys.* **1995**, *103* (11), 4572–4585.

(49) Kohls, E.; Stein, M. The Thermochemistry of Long Chain Olefin Isomers during Hydroformylation. *New J. Chem.* **2017**, *41* (15), 7347–7355.

(50) Nobbs, J. D.; Low, C. H.; Stubbs, L. P.; Wang, C.; Drent, E.; van Meurs, M. Isomerizing Methoxycarbonylation of Alkenes to Esters Using a Bis(Phosphorinone)Xylene Palladium Catalyst. *Organometallics* **2017**, *36* (2), 391–398.

(51) Shimizu, H.; Igarashi, T.; Miura, T.; Murakami, M. Rhodium-Catalyzed Reaction of 1-Alkenylboronates with Aldehydes Leading to Allylation Products. *Angew. Chemie - Int. Ed.* **2011**, *50* (48), 11465–11469.

(52) Camarena-Diáz, J. P.; Iglesias, A. L.; Chávez, D.; Aguirre, G.; Grotjahn, D. B.; Rheingold, A. L.; Parra-Hake, M.; Miranda-Soto, V. Rh (III) Cp∗ and Ir (III) Cp∗ Complexes of 1-[(4-Methyl)Phenyl]-3-[(2-Methyl-4'-R)Imidazol-1-Yl]Triazenide (R = t-Bu or H): Synthesis, Structure, and Catalytic Activity. *Organometallics* **2019**, *38* (4), 844–851.

(53) Smith, J. B.; Kerr, S. H.; White, P. S.; Miller, A. J. M. Thermodynamic Studies of Cation–Macrocycle Interactions in Nickel Pincer–Crown Ether Complexes Enable Switchable Ligation. *Organometallics* **2017**, *36* (16), 3094–3103.

(54) Smith, J. B.; Kerr, S. H.; White, P. S.; Miller, A. J. M. Thermodynamic Studies of Cation–Macrocycle Interactions in Nickel Pincer–Crown Ether Complexes Enable Switchable Ligation. *Organometallics* **2017**, *36* (16), 3094–3103.

(55) Nummelin, K.; Taskinen, E. Relative Thermodynamic Stabilities of PropenylBenzene. *J. Phys. Org. Chem.* **1994**, *7*, 256–258.

(56) Mulliken, R. S.; Rieke, C. A.; Brown, W. G. Hyperconjugation. *J. Am. Chem. Soc.* **1941**, *63* (1), 41–56.

(57) Sud, D.; Norsten, T. B.; Branda, N. R. Photoswitching of Stereoselectivity in Catalysis Using a Copper Dithienylethene Complex. *Angew. Chemie Int. Ed.* **2005**, *44* (13), 2019–2021.

(58) Wang, J.; Feringa, B. L. Dynamic Control of Chiral Space. *Science (80-.).* **2011**, *331* (March), 1429.

(59) Liu, X.; Zhang, W.; Wang, Y.; Zhang, Z.-X.; Jiao, L.; Liu, Q. Cobalt-Catalyzed Regioselective Olefin Isomerization Under Kinetic Control. *J. Am. Chem. Soc.* **2018**, *140* (22), 6873–6882.

(60) Hassam, M.; Taher, A.; Arnott, G. E.; Green, I. R.; Van Otterlo, W. A. L. Isomerization of Allylbenzenes. *Chem. Rev.* **2015**, *115* (11), 5462–5569.

(61) Harris, R. K.; Becker, E. D.; De Cabral Menezes, S. M.; Granger, P.; Hoffman, R. E.; Zilm, K. W. Further Conventions for NMR Shielding and Chemical Shifts (IUPAC Recommendations 2008). *Magn. Reson. Chem.* **2008**, *46* (6), 582–598.

(62) Frisch, M. J.; Trucks, G. W.; Schlegel, H. B.; Scuseria, G. E.; Robb, M. A.; Cheeseman, J. R.; Scalmani, G.; Barone, V.; Mennucci, B.; Petersson, G. A.; Nakatsuji, H.; Caricato, M.; Li, X.; Hratchian, H. P.; Izmaylov, A. F.; Bloino, J.; Zheng, G.; Sonnenb, D. J. . Gaussian09, Revision D.01. 2009, p Gaussian, Inc, Wallington, CT.

(63) Hay, P. J.; Wadt, W. R. No Title. *J. Chem. Phys.* **1985**, *82*, 270.

(64)   Cheung, L. L.; Marumoto, S.; Anderson, C. D.; Rychnovsky, S. D. Assignment of Absolute Configuration to SCH 351448 via Total Synthesis. *Org. Lett.* **2008**, *10* (14), 3101–3104.

(65)   Collins, P. W.; Gasiecki, A. F.; Perkins, W. E.; Gullikson, G. W.; Jones, P. H.; Bauer, R. F. 18-Cycloalkyl Analogues of Enisoprost. *J. Med. Chem.* **1989**, *32* (5), 1001–1006.

(66)   Martínez-Martínez, A. J.; Weller, A. S. Solvent-Free Anhydrous Li+, Na+ and K+ Salts of [B(3,5-(CF3)2C6H3)4]-, [BArF4]-. Improved Synthesis and Solid-State Structures. *Dalt. Trans.* **2019**, *48* (11), 3551–3554.

CHAPTER 5. OLEFIN ISOMERIZATION WITH CATION-SWITCHABLE REGIOSELECTIVITY: UNDERSTANDING INHIBITION BY LEWIS BASIC MOIETIES

I.   Introduction

Accessing Switchable Catalysis in Lewis Basic Olefins

Lewis basic moieties, such as alcohols, ketones, esters, and ethers are ubiquitous in highly functionalized olefinic species. While many successful isomerizations of functionalized allylic olefins have been reported,[1–4] maintaining high stereo- and regioselectivity in longer chain functionalized olefins poses unique challenges.[5–8] The strong driving force for conjugated olefinic products can favor overisomerization to thermodynamic regioisomers when a selective one-bond transformation is desired.[9] Lewis basic functional groups can also interact with the Lewis acidic metal center;[10] while in some cases this can enforce selectivity,[10,11] interaction with the metal center can also dampen catalytic activity with these groups.[12,13] Given the ubiquity of these moieties, poor selectivity for these systems holds back applications in the fragrance, commodity chemicals, and pharmaceutical industries.[14–18]

In the previous chapter, an iridium pincer crown-ether complex was shown to be capable of toggling the regioselectivity in functionalized olefins using cationic additives. Weak ether donors from the crown ether can bind the metal center, competing with substrate binding and enforcing kinetic selectivity; upon the addition of salt, the crown ether disassociation becomes more favorable, allowing thermodynamic olefinic products to be accessed (Figure 5.1A). An interesting facet of this system is the inability to toggle the regioselectivity of sterically unencumbered Lewis basic moieties, even in the presence of salt (Figure 5.1B, top).
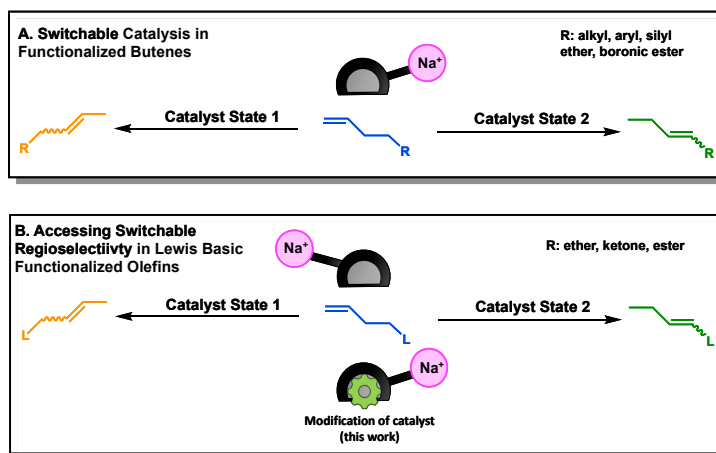
Figure 5.1. Accessing switchable isomerization in Lewis basic functionalized olefins.

While providing remarkable catalytic control, incorporating weak ethereal donors into the substrate leaves the metal center vulnerable to facile substitution by Lewis basic donors.[19] Furthermore, the addition of weak Lewis bases has been shown to inhibit the Lewis acidity of the cationic additives, dampening rate enhancement by salt additives.[20] The interaction between salt, catalyst, and Lewis basic substrates is explored through analysis of the catalytic state in the presence of substrate. While switchable rates of isomerization have been observed in the isomerization of allyl alcohols,[21] switchable regioselectivity has not been observed in Lewis basic functionalized olefins. Using new insight into the structural changes of the catalyst, switchable regioselectivity by iridium pincer crown-ether complexes of Lewis basic functionalized olefins was sought through modification of the primary and secondary coordination sphere (Figure 5.1B, bottom).

II.   Initial Isomerization Attempts of Lewis Basic Substrates

Influence of Catalytic Conditions

Cationic iridium pincer complexes, [κ⁵-(¹⁸ᶜ⁶NCOP^{iPr})Ir(H)][BAr^F_4] (**1-iPr18c6a**) and a

methoxy-blocked variant, [κ⁵-(^{MeO-18c6}NCOP^{iPr})Ir(H)][BAr^F_4] (**1-iPr18c6b**) ([BAr^F_4 = Tetrakis(3,5-

bis(trifluoromethyl)phenyl)borate)) were synthesized as reported in the previous chapter. Both

systems show very similar structure and reactivity, differing by substitution of a methoxy group

ortho to the phosphinite. Incorporation of a methoxy "blocking" group increases the stability of

the catalyst.[22] Early structural studies feature **1-iPr18c6a** and most isomerization studies use **1-

iPr18c6b**.

5-hexene-2-one (**2a**), ethyl pentanoate (**3a**), and 5-hexen-1-ol (**4a**) were chosen as model

substrates to explore isomerization with Lewis basic functional groups. Regioisomers are labeled

relative to the terminal olefinic starting material (**a**), with the first isomerization product labeled

b and each subsequent isomer labeled with the next letter. Beside featuring sterically

unencumbered Lewis basic moieties, these substrates have thermodynamically favorable **c**

isomerization products, through conjugation with electron withdrawing groups or

tautomerization to an aldehyde. In arenes, substituted alkenes, silyl ethers, and boronic esters,

this type of thermodynamic driving force allows cation-gated switchable regioselectivity (Chapter

4.2). Without cation, the kinetic **b** isomer is favored. In the presence of NaBAr^F_4, the

thermodynamic distribution of isomers is favored.

In comparison, isomerization of **2a** with **1-iPr18c6b** yields primarily the kinetic product, **2b** in

poor yield at room temperature (Table 5.1). Upon the addition an equivalent of NaBAr^F_4, a

modest 3-fold enhancement of the rate of isomerization **2b** is seen. However, even upon

reacting at room temperature for an additional 72 hours, **2c** is not observed in solution.

Table 5.1. Isomerization of 5-hexen-2-one at room temperature.

Salt	Time (hr)	Isomer Distribution % (E:Z)		
		a	b	c
–	24	73%	27% (3.5:1)	–
Na⁺	24	21%	79% (2.8:1)	–

Increasing the reaction temperature to 50 °C does not push the isomerization to thermodynamic products; only a decay in the E selectivity is observed (3.5 : 1 at rt, 1.8 : 1 at 50 °C, Figure 5.1), indicating inhibition of cation-crown interaction or substrate inhibition of the catalyst itself. To test for dampening of the Lewis acidity of added salts by substrate, the influence of salt concentration on observed reactivity was studied (Figure 5.2). 0.5 – 20 equivalents of NaBAr$^F_4$ and LiBAr$^F_4$ were added to solutions of **1-iPr18c6b** and **2a**. Examining the rate of isomerization under each salt condition reveals two regimes. At early time points, 0.5 equiv of Na⁺ shows less substrate conversion than 1 equiv of salt (Figure 5.2, top, left). This result agrees with previous observations that increasing salt concentration increases the rate of isomerization by iridium complexes.[20] Li⁺ concentration studies shows similar substrate conversion at low Li⁺ loadings; given previous observations that Li⁺ activity can be significantly dampened by ethereal donors, the similarity in rates at low Li⁺ loadings in the presence of 0.2 M **2a** is reasonable (Figure 5.2, top, right).

Surprisingly, moving to >1 equiv of salt *inhibits* the rate of isomerization, a trend opposite of what would be expected if only Lewis acidic dampening explained the slow rate of isomerization. Even heating for 216 hrs under large excess of Na⁺ yields almost no conversion

to the expected thermodynamic regioisomer, though complete conversion of **4a** is observed (Figure 5.2, bottom, left). Similar inhibition of substrate conversion is seen at early timepoints in the presence of Li$^+$, though at long timepoints, modest amounts of the expected thermodynamic product are observed (Figure 5.2, bottom, right).
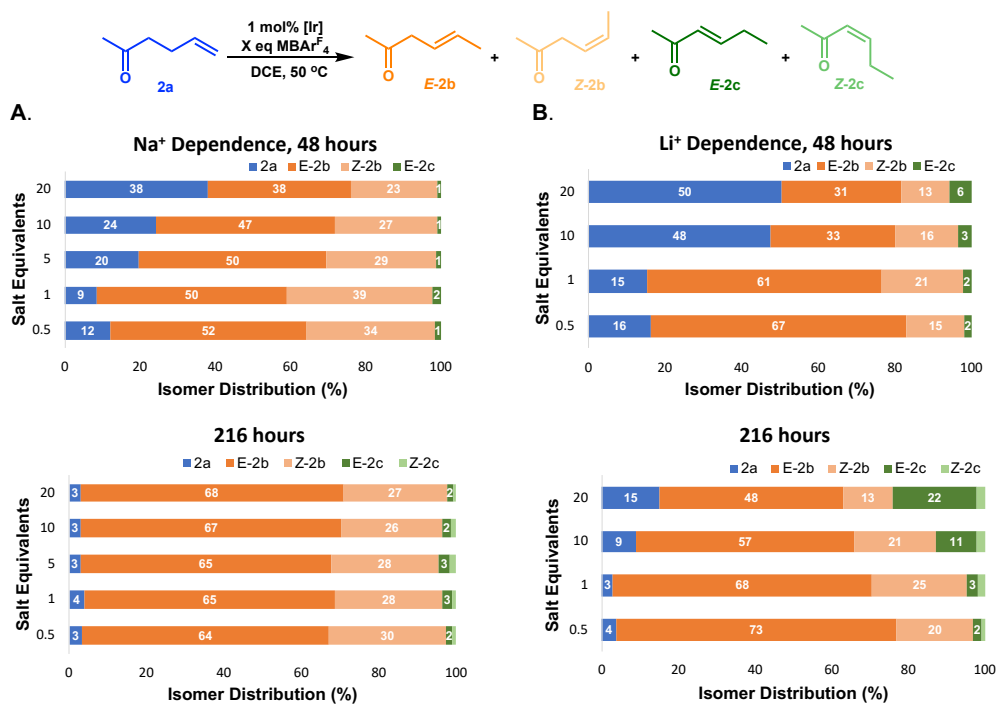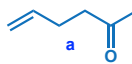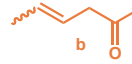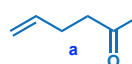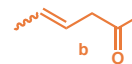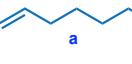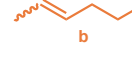
Figure 5.2. Salt dependence in 5-hexen-2-one isomerization.

These results support substrate inhibition of the catalyst was playing a large role in slow rates of isomerization, rather than dampening of the Lewis acidity of added salt by substrate. Selectivity for kinetic regioisomers **3b** and **4b** are also seen in isomerization attempts with substrates **3a** and **4a**, respectively, indicating a general trend of catalyst inhibition across the studied Lewis basic substrates (Table 5.2).

Table 5.2. Heated isomerization of olefins substituted with Lewis bases.

$$a \xrightarrow[\text{50 °C, DCE}]{\substack{\text{1 mol\% [1-iPr18c6b]} \\ \text{2 mol\% NaBAr}^F_4}} b + c$$

	Salt	Time (hr)	a	b	c	b:c
2	–	216	5%	93% (10:1)	3%	30 : 1
	Na⁺	216	3%	93% (2.5:1)	4%	20 : 1
3	–	216	7%	91% (9:1)	2%	50 : 1
	Na⁺	216	4%	93% (2.9:1)	3%	30 : 1
4	–	216	2%	95%*	3%*	32 : 1
	Na⁺	216	2%	87%*	11%*	7.9 : 1

*E:Z ratio unable to be determined by NMR

NMR Studies of Catalytic Resting States

To explore this phenomenon further, NMR studies of catalytic resting state during isomer isomerization was undertaken. When substrate **2a** is added to solution, the catalyst speciates into multiple products. Attempts to characterize the new products in stoichiometric studies were foiled by speciation of **1-ipr18c6a** and extensive broadening of spectral features.

Proposing that moving to a more Lewis basic substrate should interact more strongly with the metal center and reduce dynamic behavior, a stoichiometric reaction with **1** and **4a** was also studied. Upon the addition of **4a**, the hydride and aryl regions overlay with **1**, but broadening is observed in the crown. Little isomerization of **4a** is observed. Adding an equivalent of NaBAr$^F_4$ yields a new hydride at -27.6 ppm, with **1-18c6** being completely consumed over 2 days (Figure 5.3). The new species was characterized by ^{1}H-^{13}C HSQC and ^{1}H-^{1}H COSY experiments, which was assigned as a chelated **4c** bound to **1-iPr18c6a, 5-iPr18c6a**

(Figure 5.4).
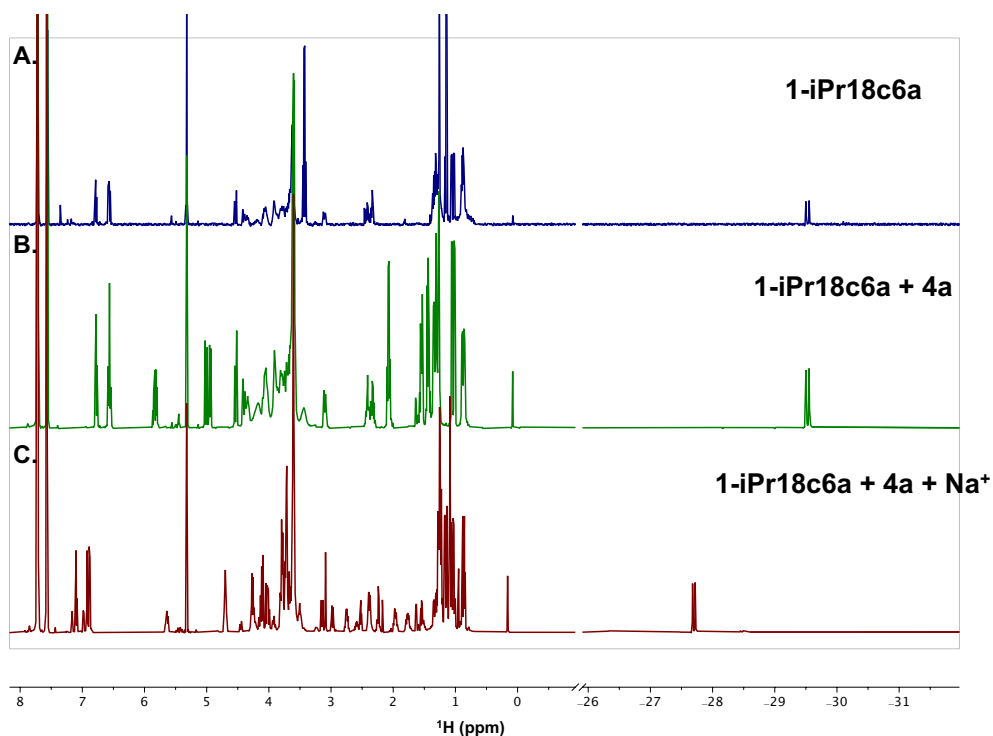
Figure 5.3. Speciation of **1-iPr18c6a** in CD$_2$Cl$_2$.
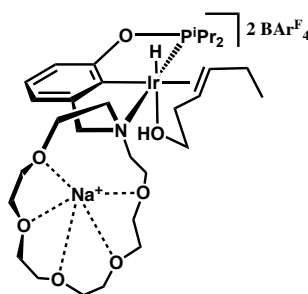
Figure 5.4. Proposed structure of **5-iPr18c6a.**

Given the slow isomerization seen when **4c** builds up in previous isomerization attempts and the full conversion of **1-iPr18c6a** to a substrate bound species, the formation of this species is proposed to explain the sluggish reactivity in Lewis basic functionalized systems. The stabilization of substrate binding through cation-crown interaction has been previously demonstrated to gate the binding of fluorinated benzonitrile towards Ni pincer-crown ethers;[23] a

similar phenomenon is believed to be operating here. Chelation of a Lewis basic functional group and the olefin leads to a new, more stable resting state that significantly inhibits the rate of isomerization.

The role of Na^+ in stabilizing the adduct explains the inhibition of catalysis under high salt loadings (Figure 5.2); increasing the salt concentration favors the formation of **5-iPr18c6a** and inhibits catalysis. Li^+ has a lower binding affinity for 1-aza-18-crown-6 based pincer-crown ethers than Na^+; this could serve to destabilize the chelated olefinic species and allow some conversion to the thermodynamic regioisomer. The increased % of **2c** at 216 hrs under high Li^+ loadings supports this hypothesis (Figure 5.2) and demonstrates the role the cation can plays in switchable selectivity.
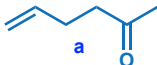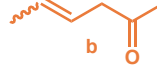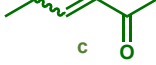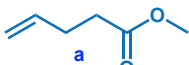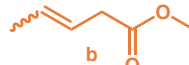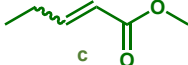
A similar study was done with the previously reported $[\kappa^4$-($^{18c6}NCOP^{iPr}$)Ir(H)(OH$_2$)][BAr$^F_4$] (**6-iPr18c6a,** Chapter 4.2). Without Na^+, the resting state is observed to remain at **6-iPr18c6a**. Upon the addition of Na^+, a broad species at -27.6 corresponding to **5-iPr18c6a** is observed alongside a broadened peak corresponding to **6-iPr18c6a**. This led to the proposal that **6-iPr18c6a** and the methoxy blocked variant $[\kappa^4$-($^{18c6}NCOP^{iPr}$)Ir(H)(OH$_2$)][BAr$^F_4$] (**6-iPr18c6b**) may afford faster catalysis given the increased resistance to substrate substitution. To test this hypothesis, isomerizations of **2a** and **4a** by **6-iPr18c6a** were explored. After reacting substrate and catalyst for 24 hours with 10 equiv. of Na^+ at rt, 10% of isomer **2c** was observed. Reactions with **4**a showed similar behavior, with **4c** growing in at early timepoints, but requiring long reaction times to push the distribution towards greater concentrations of **4c**. No aldehyde – the expected thermodynamic product – is observed in solution.

Repeating isomerization at 50 °C with **6-iPr18c6b** with **2a** and **3a** both with and without Na^+ shows increased conversion to the **c** regioisomer. While the regioselectivity towards the **b**

regiosiomer is able to be dramatically reduced (in contrast of what is seen with **1-iPr18c6b)**, full conversion to the expected thermodynamic regioisomer is not observed on a reasonable timescale.

Table 5.3. Isomerization of substituted olefins with **6-iPr18c6b.**

Salt	Time (hr)		Isomer Distribution % (E:Z)		b:c
2		**a**	**b**	**c**	
–	120	4%	92% (6:1)	3%	30 : 1
Na⁺	216	2%	65% (2.4:1)	33%	1.9 : 1
3		**a**	**b**	**c**	
–	120	7%	88% (4.9:1)	5%	20 : 1
Na⁺	216	3%	56% (2.5:1)	40%	1.4 : 1

Isomerization in Long Chain Olefins

Long chain olefins represent interesting substrates for screening substrate chelation. If chelation is responsible for deactivation of the catalyst, moving to longer chain olefins should allow isomerization to occur until a chelatable species is reached, inhibiting catalysis (Scheme 5.1). Long chain olefins themselves are substrates of interest for transforming fatty acids into higher value chemical feedstocks and biofuels.[24,25]

Scheme 5.1. Isomerization and chelation of substrate.
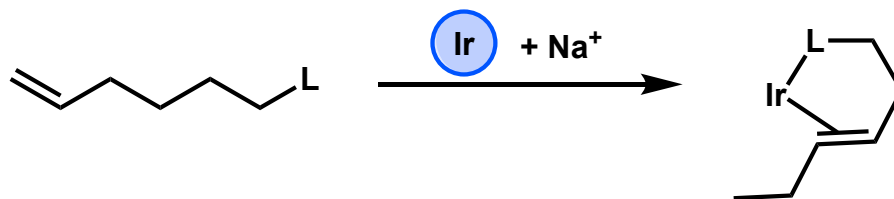
Model substrates ethyl heptenoate (**7a**) and 9-decen-2-one (**8a**), and undecylenic aldehyde (**9a**) were chosen as long chain model complexes. **7a** has a chain length with 5 regioisomers available, including the starting material. Isomerization of **7a** with **1-ipr18c6b** and Na$^+$ yields 5% **7c** after 120 hours at 50 °C. While greater than the yield of the shorter chain ester substrate, **3c**, **7b** is still the dominant product. Isomerization of a longer chain substrate, **8a** (7 regioisomers, including the starting material), **1-iPr18c6b**, and Na$^+$, shows conversion to internal regioisomer **8c** and **8d** in modest yields at 50 °C after 120 h. In the absence of cation, the major product is still the one bond isomerization product, **8b** (95% yield). Isomerizing an even longer chain olefin, **9a** (9 regioisomers available, including the terminal olefin), increasingly favors isomerization to internal olefins (**9c + 9d**), with the reaction proceeding with good conversion at room temperature.

Table 5.4. Isomerization of long-chain functionalized olefins.
*Sum of **9d** and other internal olefins.

7 R: $(CH_2)_2COOEt$
8 R: $(CH_2)_4COMe$
9. R: $(CH_2)_6COH$

1 mol% 2-18c6b
0 or 2 mol% NaBAr$^F_4$
1.5 mol% $^tBu_2pyr$
50°C, DCE

	Time (hr)	a	b	c	d
7	120	1%	83%	5%	–
8	120	0%	68%	13%	19%
9	120	1%	59%	25%	14%*

This study shows that proximity of the functional group is the chief inhibition of catalytic activity in Lewis basic olefins; increasing distance between the olefinic group increase catalytic activity and allows access to internal olefinic products. This result raises the intriguing possibility of switchable regioselective olefin isomerization *selective for internal olefins*. Catalysis of long chain functionalized olefins from terminal positions has been demonstrated with alkene "zippers", impressive feats of isomerization over 30+ bonds to a thermodynamic sink,[26,27] or demonstrate selectivity for the one bond isomerization products; access a framework that is both switchable and has selectivity towards internal olefins of long chain substrates makes this system a unique example.

III.   Synthetic Attempts to Disfavor Chelation

Changing Phosphinite Substitution

 Having proposed that chelated Lewis basic substrates result in the sluggish cation-induced isomerization observed, attempts were made to disfavor chelation through synthetic modification. New ligand scaffolds were generated by phosphinite substitution with a sterically

less bulky and electronically distinct diphenyl group and increasing the sterics around the metal

center through the incorporation of bulky t-butyl groups (Scheme 5.2).

Scheme 5.2. Synthesis of new phenyl phosphinite ligands.
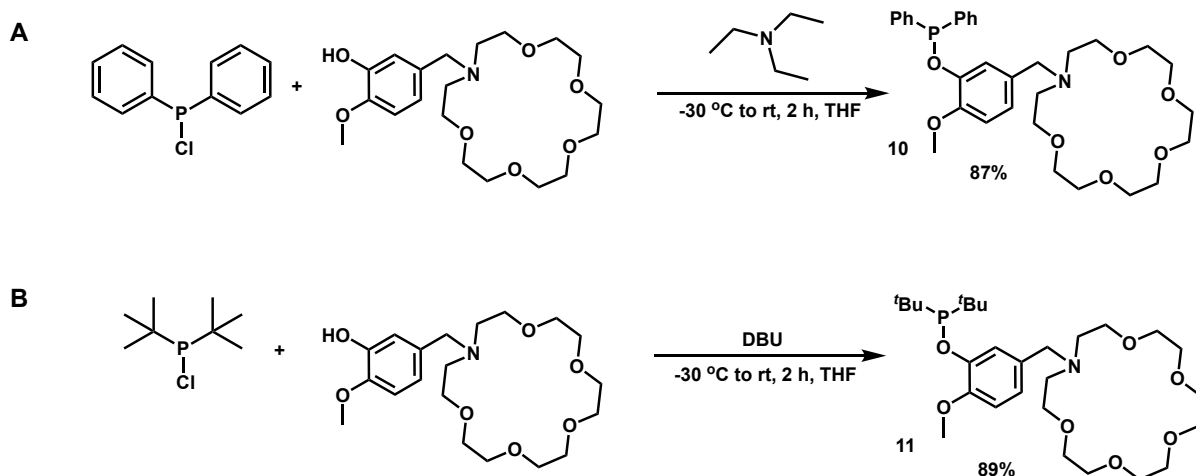
Reaction of the phenolic preligand with diphenylchlorophosphine yields the desired phenyl

substituted phosphinite, ($^{MeO-18c6}$NCOP^{Ph})H (**10**, Scheme 5.2). Phosphination of the t-butyl

substituted base requires a stronger base, 1,8-Diazabicyclo[5.4. 0]undec-7-ene (DBU) to

synthesize ($^{MeO-18c6}$NCOP^{tBu})H (**11**) in 89% yield (Scheme 5.2).

Metalation of **10** with [Ir(COD)Cl]$_2$ at 90 °C yields the expected tetradentate iridium complex, κ^4-

($^{MeO-18c6}$NCOP^{Ph})Ir(H)(Cl) (**12-Ph18c6b)** in a 55% yield post recrystallization (Scheme 5.3). XRD

suitable crystals were grown by layering pentanes over a solution of **12-Ph18c6b** dissolved in

toluene (8:1 pentane:toluene, Figure 5.5).

Scheme 5.3. Metalation and ligand modification of new catalysts.
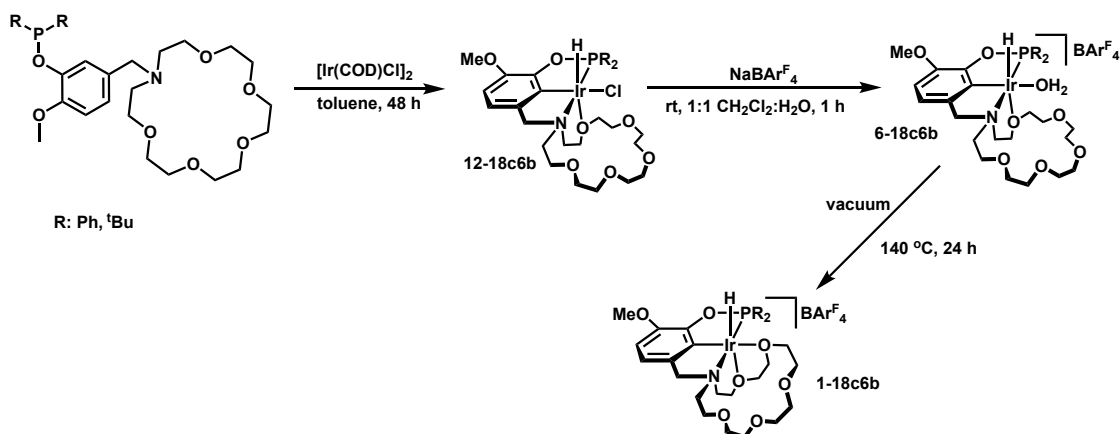
Following methodologies of halide abstraction outlined in Chapter 4.2 for 1-aza-18-crown-6

containing pincer complexes, the aquated cation pincer complex [κ^4-($^{MeO-}$

^{18c6}NCOP^{Ph})Ir(H)(OH$_2$)][BAr$^F_4$] in a 94% yield (**6-Ph18c6b**, Scheme 5.3). XRD suitable crystals

were grown from by layering a solution of **6-Ph18c6b** in Et$_2$O with pentanes (Figure 5.5).

Heating the complex at 140 °C for 24 h under vacuum yields the desired water-free, cationic

complex, [κ^5-($^{MeO-18c6}$NCOP^{Ph})Ir(H)][BAr$^F_4$] (**1-Ph18c6b**) in a 99% yield.

Metalation of **8** with [Ir(COD)Cl]$_2$ at 120 °C yields the expected tetradentate iridium complex,

κ^4-($^{MeO-18c6}$NCOP^{tBu})Ir(H)(Cl) (**12-tBu18c6b**) in a 68% yield, post recrystallization (Scheme 5.3).

Incorporation of the methoxy blocking group on the ligand framework is key for successful

metalation; initial attempts to synthesize the bulky t-butyl analogues without the blocking group

were unsuccessful. **12-tBu18c6b** was dissolved in CH$_2$Cl$_2$ and the halide abstracted with

NaBAr$^F_4$ according to previously outlined methods, yielding the aquated complex, [κ^4-($^{MeO-}$

^{18c6}NCOP^{tBu})Ir(H)(OH$_2$)][BAr$^F_4$] (**6-tBu18c6b**). XRD suitable crystals were grown from a

solution of **6-tBu18c6b** dissolved in Et$_2$O and layered with pentanes (2:1 pentanes:Et$_2$O, Figure

5.5).

Heating the **6-tBu18c6b** at 140 °C for 24 h under vacuum yields the desired water-free,

cationic complex, $[\kappa^5\text{-}(^{\text{MeO-18c6}}\text{NCOP}^{\text{tBu}})\text{Ir}(\text{H})][\text{BAr}^{\text{F}}_4]$ (**1-tBu18c6b**) in a 96% yield.
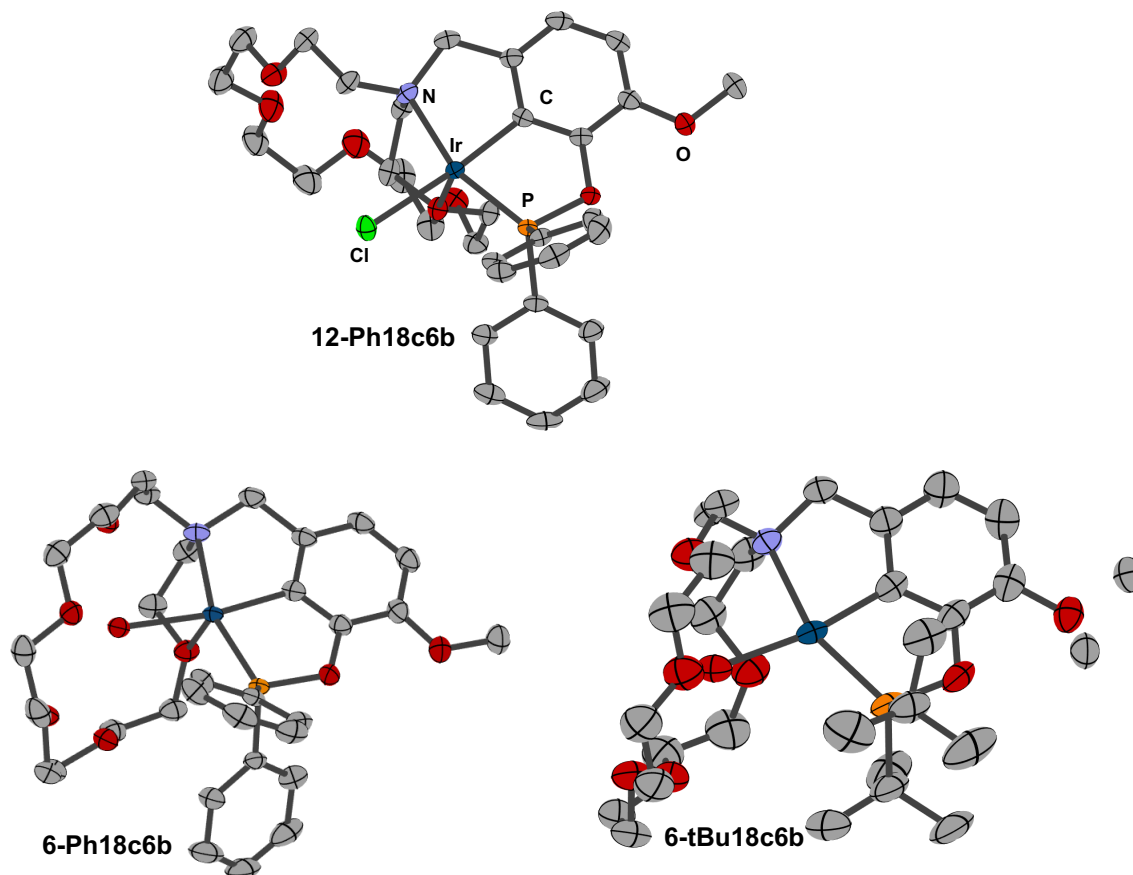
Figure 5.5. Structural representation of new complexes.
Ellipsoids shown at the 50% probability level; counteranions and hydrogens are hidden for clarity. Top: **12-Ph18c6b**; Bottom, left: **6-Ph18c6b**; Bottom, right: **6-tBu18c6b**. Disorder in the methoxy group was successfully treated as a two-site disorder, with both thermal ellipsoids shown in the figure.

Structural Studies of New Complexes

With new complexes in hand, the spectroscopic and structural characteristics of the newly synthesized substituted phosphinite complexes were explored. Comparing the spectrum of the previously reported $(^{18\text{c}6}\text{NCOP}^{\text{ipr}})\text{Ir}(\text{H})(\text{Cl})$ (**12-iPr18c6b**)[28] with the newly synthesized chloride complexes, **12-Ph18c6b** and **12-tBu18c6b**, shows that, aside from the shifts corresponding to the new functional groups, the crown and arene regions are very similar. The largest influence on chemical shift is observed in the hydride; a 3.5 ppm difference in chemical shift is observed

between **12-Ph18c6b** and **12-tBu18c6b** (Figure 5.6).
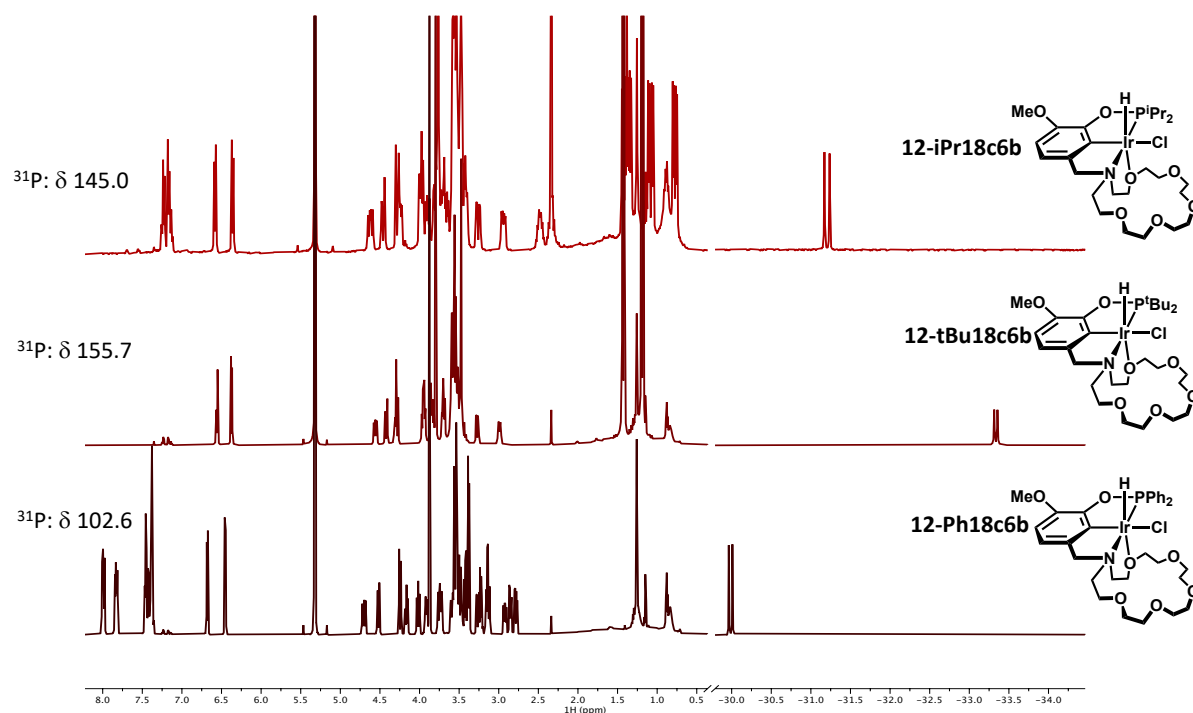
Figure 5.6. NMR comparison of new tetradentate chloride iridium complexes in CD$_2$Cl$_2$.

To explore the steric influence of phosphinite substitution on iridium pincer-crown ether complexes in more detail, the aqua complexes structural and spectroscopic features were compared. A diagnostic peak is the ^{2}H peak corresponding to bound water that shows up around 5.34 ppm (blue box, Figure 5.7). The aqua peak is shifted upfield slightly of **6-iPr18c6b** upon substitution with the more electron rich tert-butyl group[29] in **6-tBu18c6b**, while in the more electron deficient phenyl substituted complex, **6-Ph18c6b** the aqua protons are shifted downfield of **6-iPr18c6b**. This observation suggests the aqua chemical shift may be a useful marker of electron density on the iridium center – in the absence of other competing donors or cations – though given the steric differences in the studied phosphines, synthesis of additional systems would be required to confirm this trend.

Halide abstraction to the cationic aqua complexes causes an upfield shift the hydride

peak in the studied complexes. Once again the tert-butyl substituted aqua complex, **6-tBu18c6b** demonstrates the most downfield hydride shift at -36.9 ppm. Hydride chemical shifts show a strong dependence on the identity of the *trans* ligand,[30,31] indicating a difference in the Ir-O bond in solution.
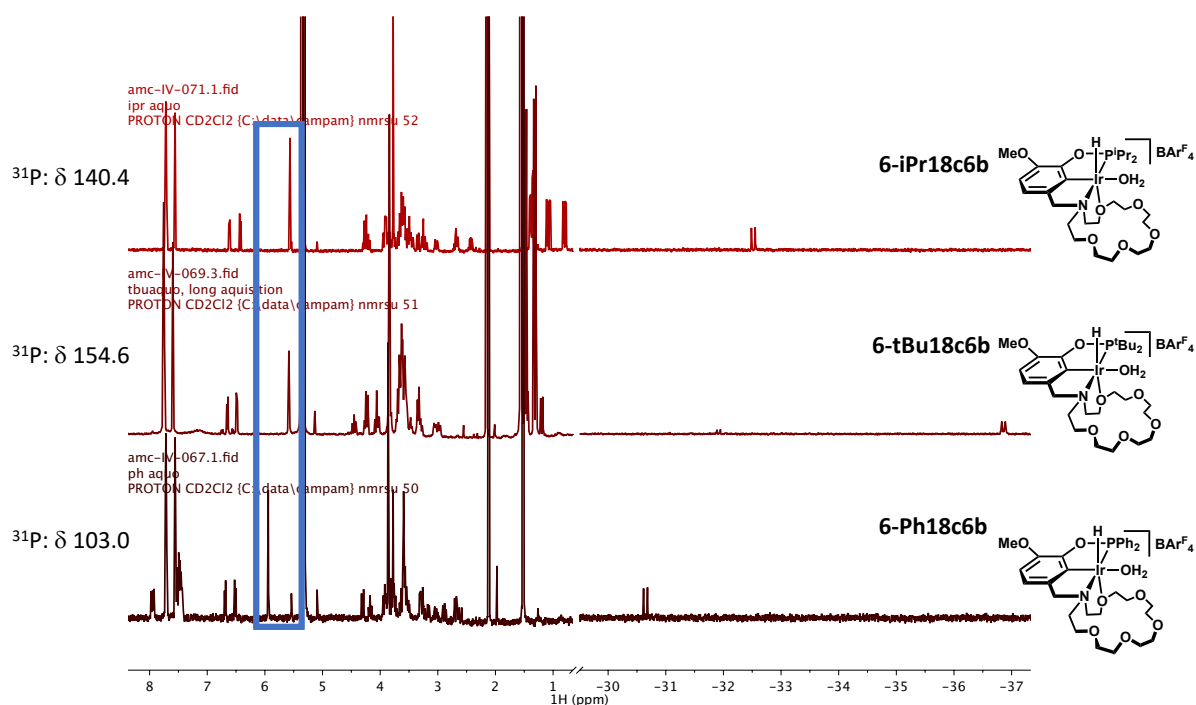
Figure 5.7. NMR comparison of new tetradentate chloride iridium complexes in CD$_2$Cl$_2$.

Structural studies of the aqua complexes **6-Ph18c6b** and **6-tBu18c6b** show similar structural features of the parent aqua complex, **6-iPr18c6b.** The crown completely encompasses the bound aqua ligand; bond distances between oxygen atoms in the crown and hydrogens on the water ligand suggest hydrogen bonding interactions are occurring (Figure 5.8). The aqua ligand of **6-Ph18c6b** shows the same hydrogen bonding partners as the parent isopropyl complex (O2 and O5). In contrast, **6-tBu18c6b** shows closest contact with a O2 and O4. Significant distortion of the crown-ether binding is observed in **6-tBu18c6b,** resulting in a 0.28 Å lengthening of the Ir-crown bond (Figure 5.9), which may explain this observation. Given the sensitivity of hydride chemical shifts to *trans* ligands, the lengthening of the crown ether bond

likely explains the significant upfield shifting of the hydride in the presence of tert-butyl containing complex. Stronger donors move the hydride downfield,[19] while weaker donors, such as an elongated Ir-crown bond move upfield. Overlaying the aquated crystal structures demonstrate steric effects of the substituents on phosphorus; the crown ether of **6-tBu18c6b** is visibly pushed away from the tert-butyl group, while minimal differences are seen in the phenyl phosphonite backbone (Figure 5.9).
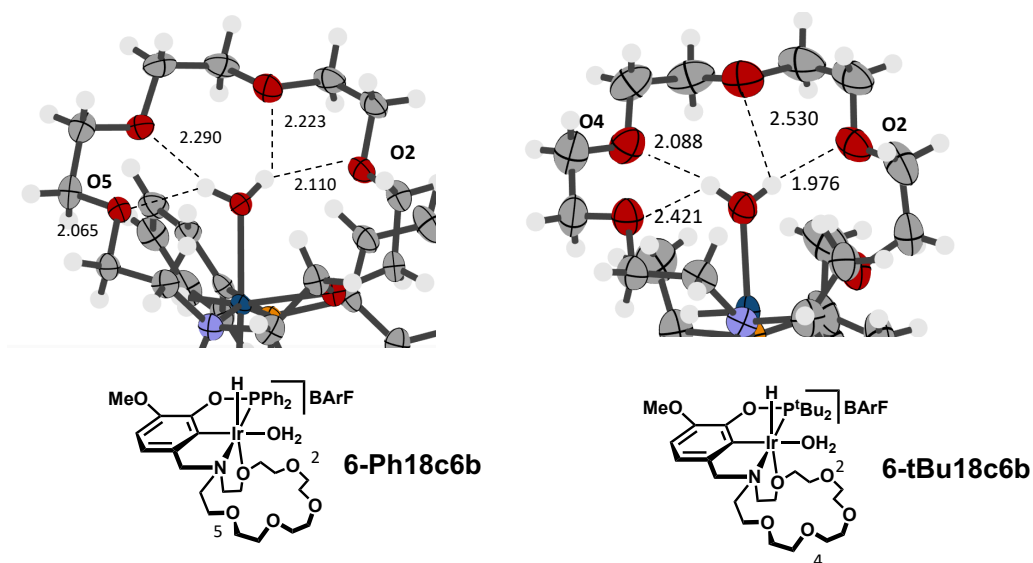
Figure 5.8. Comparison of hydrogen bonding in iridium-aqua complexes.

R₂:	C1-Ir-O (°)	P-Ir-O (°)	Ir-O (crown, Å)	Ir-OH₂ (Å)	P-Ir-OH₂ (°)
6-iPr18c6b iPr	96.44	106.36	2.298	2.187	109.89
6-Ph18c6b Ph	99.92	104.06	2.307	2.192	109.06
6-tBu18c6b tBu	105.5	111.66	2.576	2.192	109.65
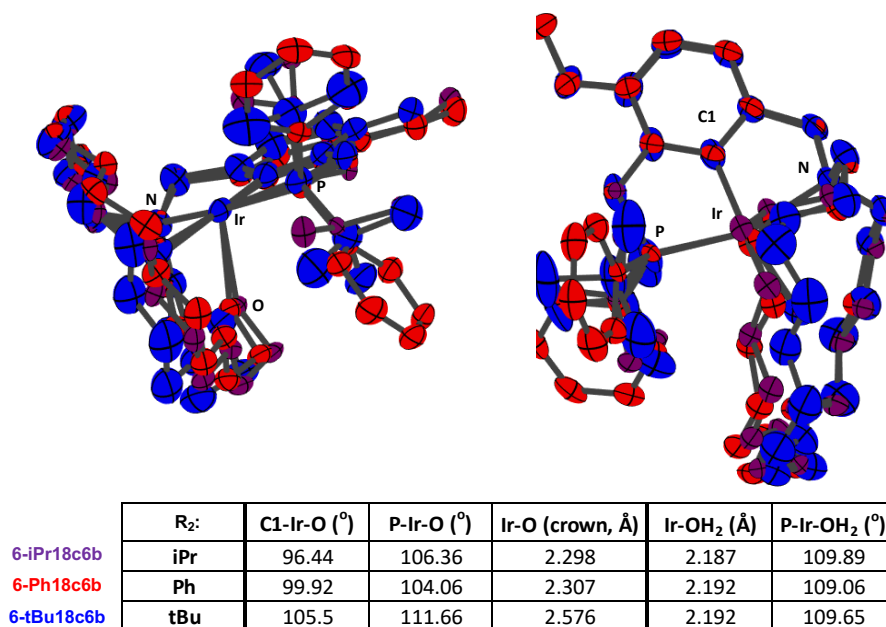
Figure 5.9. Structural overlay and key crystallographic feature of iridium-aqua complexes.

Heating the aquated complexes at high temperatures under vacuum removes the water ligand yielding the proposed high-coordinate, κ^5 complexes. While **1-Ph18c6b** and **1-tBu18c6b** were not characterized in the solid state, the complexes exhibit dynamic behavior, downfield shift of the hydride, and loss of the water ligand characteristic of this transformation (see Experimental Details).

Reactivity Studies of New Complexes

      To compare the reactivity of new iridium pincer complexes with previously studied complexes, an isomerization with 4-phenyl-1-butene (**13a**) was undertaken (Figure 5.10). At room temperature, the less sterically bulky **1-iPr18c6b** and **1-Ph18c6b** showed similar levels of activity. Incorporation of a tert-butyl group, however, greatly decreased the rate of isomerization; an over 100-fold decrease in the rate of isomerization of **13a** was observed with **1-tBu18c6b**. Increasing steric bulk of the phosphine group may disfavor coordination of the olefin

to the active site of the metal, even in the presence of Na$^+$ and significantly slowing the rate of isomerization. Isomerization of **13a** with and **1-iPr18c6b** and **1-Ph18c6b** demonstrates **13b** with a thermodynamic *E:Z* ratio of 4:1, and **1-tBu18c6b** shows an E:Z ratio of 5:1.While controlling sterics has been a powerful method to enforce regio- and stereoselectivity,[5,32] previous reports have shown increasing steric bulk can hamper reactivity towards substrates.[33]
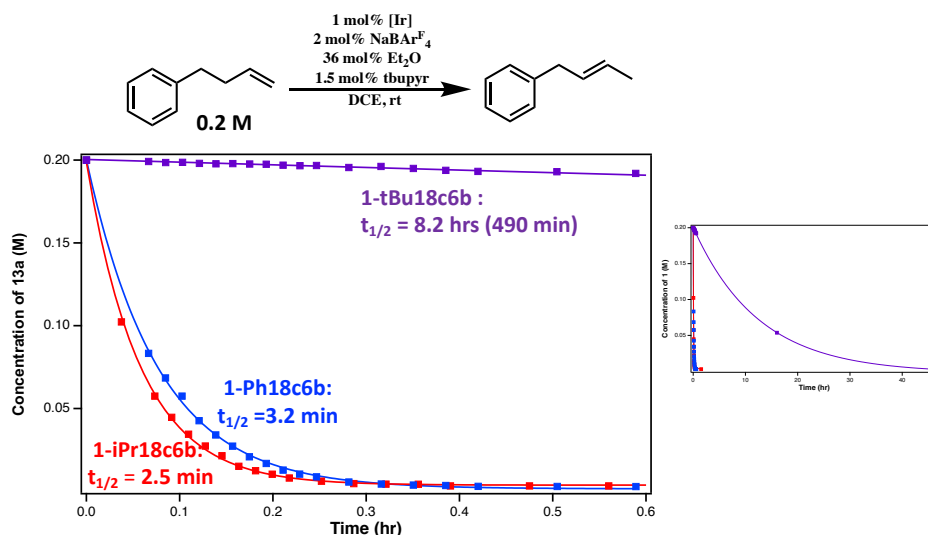
Figure 5.10. Consumption of 4-phenyl-1-butene over time by new iridium complexes.

Despite the poor reactivity towards of **1-tBu18c6b** for **13a,** isomerization of **2a** was studied as a representative reaction with a Lewis basic functionalized olefin to probe for favorable reactivity towards a thermodynamic product. New catalysts showed limited selectivity for **2c**; while the phenyl substituted, **1-Ph18c6b** showed similar activity as **1-iPr18c6b,** the aquated **6-Ph18c6b** did not produce **2c** in significant yield. The tert-butyl substituted **1-tBu18c6b** showed poor conversion of **13a,** indicating inhibition of substrate binding due to the increased steric bulk of the catalytic framework. The aquated analogue, **6-tBu18c6b** showed additional inhibition of the rate. While not demonstrating cation-induced isomerization initially targeted in the synthetic project, interesting changes to stereoselectivity were observed.

Calculated thermodynamic values suggest a thermodynamic distribution of 4:1 *E:Z* (Chapter

4.2), whereas a slightly lower *E:Z* ratio of 2:1 is observed in a previous thermodynamic

distribution with Pd based catalysts.[32] The ratios observed in the isomerization **2a** with **1-**

iPr18c6b and Na$^+$, which has previously accessed thermodynamic distributions of olefins at long

timepoints (See Chapter 4.2) also show an *E:Z* ratio of about 2:1 at long time points, indicating a

thermodynamic distribution under this condition.

The aquated isopropyl substituted complex, **6-iPr18c6b,** shows higher *E* selectivity than

the **1-iPr18c6b** in the isomerization of **2a** to **2b**, whereas the phenyl substituted complexes **1-**

Ph18c6b and **6-Ph18c6b** show increased selectivity for the *Z* isomer, even at long timepoints.

While the modulation of stereoselectivity is interesting, the highest conversion to the

thermodynamic **2c** regioisomer was observed in the parent isopropyl substituted aquo, **6-**

iPr18c6b. Other donors were sought to modify the primary coordination sphere to increase

isomerization to thermodynamic products.

Table 5.5. Comparison of 5-hexen-2-one regioselectivity with iridium complexes.

Time (hr)	Catalyst	Isomer Distribution % (E:Z)		
		a	b	c
120	1-iPr18c6b	3%	94% (2.2:1)	2%
	6-iPr18c6b	3%	69% (3.6:1)	28%
120	1-Ph18c6b	21%	75% (1.2:1)	4%
	6-Ph18c6b	8%	87% (1.3:1)	4%
120	1-tBu18c6b	74%	23% (1.9:1)	3%
	6-tBu18c6b	62%	34% (1.8:1)	4%

IV.   Using Additives to Change Catalytic Reactivity

Addition of Competing Donors to Solution

Given that the highest selectivity for the **c** regioisomer upon the addition of salt **6-iPr18c6b**, stronger donors were sought that might compete with substrate chelation of the metal center and allow isomerization to proceed towards thermodynamic distributions. Towards this goal, an ammonia coordinated analogue to **6-iPr18c6** was synthesized by stirring a solution of **12-iPr18c6b** with NaBAr$^F_4$ in CH$_2$Cl$_2$ with an excess of 30% aqueous NH$_3$ solution (Figure 5.11), yielding the cationic ammonia complex, [κ^4-($^{MeO-18c6}$NCOP^{Ph})Ir(H)(NH$_3$)][BAr$^F_4$] (**14-iPr18c6b)** in a 65% yield. Crystals suitable for X-ray characterization were grown by layering pentanes over a solution of **14**-**iPr18c6b** in Et$_2$O (Figure 5.11). Like the previous synthesized aqua complex, the crown ether is observed to encompass the bound ammine, indicating hydrogen bonding interactions were present in this complex. Other donors were also screened as additives to reactions to catalysis of **2a** with **1-iPr18c6b** to turn on cation gated switchable regioselectivity; in each case 1 mol % (1 equiv relative to catalyst) was added to the reaction solution (Table 5.6).
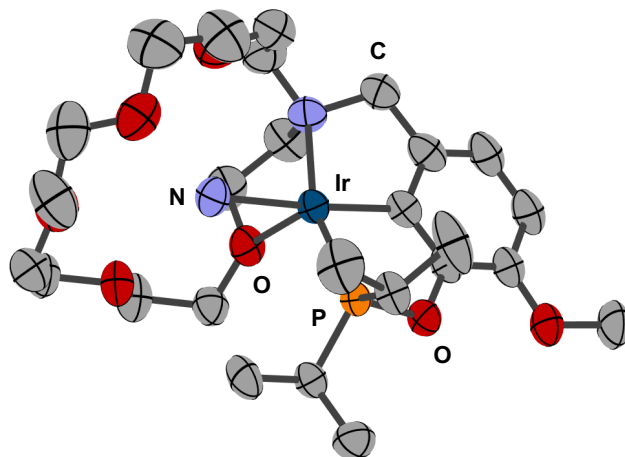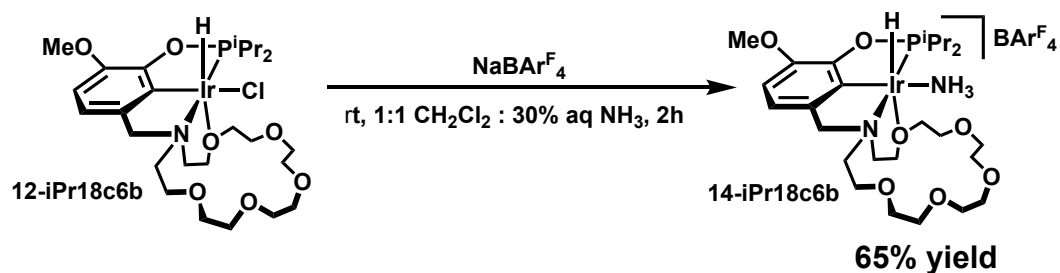
Figure 5.11. Synthesis and structural representation of **14-iPr18c6b**.
Ellipsoids are shown at the 50% probability level.

14-iPr18c6b showed 62% conversion of **2a** after 120 hrs, indicating significant inhibition by the ammine donor. The strong nitrogen donor coupled with an additional hydrogen bonding interaction with the crown likely competes with substrate coordination, preventing fast catalysis even in the presence of Na$^+$. Worse conversion is seen when pyridine is added to the reaction solution, with only 2% of **2b** observed after 216 hrs. Increasing substitution of pyridine additives improves conversion from **2a**. Greatest yield of **2c** among the studied additives is seen in the presence of lutidine. Increasing the bulk of added donors further with 2,6-di-tert-butylpyridine does not enhance the formation of **2c**; the distribution with this additive is very similar to **1-iPr18c6b** and Na$^+$ alone, indicating 2,6-di-tert-butylpyridine is not significantly interacting with the catalyst (Table 5.6).

Table 5.6. Isomerization of 5-hexen-2-one with added donors.

Time (hr)	Catalyst	Additive	Isomer Distribution % (E:Z)		
			a	b	c
120	14-iPr18c6b	–	62%	29% (1.4:1)	9%
216	1-iPr18c6b	THF	3%	98% (2.3:1)	4%
		NaI	33%	62% (1.9:1)	5%
		MeCN	9%	86% (1.5:1)	6%
216	1-iPr18c6b	pyridine	98%	2%	<1%
		2-picoline	11%	84% (1.9:1)	5%
		lutidine	<1%	92% (1.7:1)	8%
		2,6-di-tertbutylpyridine	3%	93% (2.4:1)	3%

The poor activity seen in the presence of strong Lewis basic additives indicates that the preferred binding site for the additives is *cis* to the hydride, inhibiting substrate binding to the metal insertion and disfavoring subsequent insertion into the metal hydride. The best conversion to **2c** is seen with the initially studied **6-iPr18c6b**.

Changing Stereoselectivity with Donors

While showing poor conversion to the thermodynamic regioisomer, the **1-iPr18c6b** showed moderately tunable stereoselectivity using external additives. The following *E:Z* ratios correspond to observed yields of *E*-**2b** and *Z*-**2b**. The **1-iPr18c6** features a strong *E* preference in the absence of cation at 24 hrs (*E:Z* = 14:1) which decays to 12:1 over 216 hours; in the presence of cation, an *E:Z* ratio of 1.3:1 is observed at 24 hrs, which increases to 2.6:1 over 216 hrs. **6-iPr18c6** demonstrates an *E:Z* ratio of 6:1 in the absence of Na$^+$; in the presence of Na$^+$, the *E:Z* ratio is 1.2:1 at 24 hrs, which inreases to 2.6:1 over 216 hours. The increased *Z* selectivity in the Na$^+$ conditions likely stems from substrate chelation; comparison with other substrates previously studied typically shows near thermodynamic values in the presence of cation (See Chapter 4.2).

Adding external donors can decrease the Z selectivity in the system. Upon the addition of 1 equiv of MeCN, an $E{:}Z$ ratio of 1.5:1 is observed across all timepoints. This trend is observed in presence of strong donors – NaI and 2-picoline also show a stable $E{:}Z$ ratio (1.9:1) over 216 hours. Weaker donors show the same decay observed with **1-iPr18c6b** and Na^+; lutidine shows an $E{:}Z$ ratio of 1.3:1 at 48 hrs, which decays to 1.7:1 at 216 hours. THF and 2,6-di-tert-butylpyridine show the same ratios as **1-iPr18c6b** alone, likely indicating that these donors are not strongly interacting with the metal center.

V.   Conclusions and Outlook

Switchable isomerization of sterically unencumbered Lewis basic olefins was targeted by synthetic modification of the ligand scaffold and additives to modify the primary coordination sphere of the iridium pincer complex. Modest switchable selectivity was achieved using the aquated iridium complex, **6-iPr18c6b**, allowing regioselectivity to be switched from >88% **2b,3b** in the absence of Na^+, to >30% **2c,3c** in the presence of Na^+. While modest, this is a significant increase from the 3% conversion observed in the parent **1-iPr18c6b** used in previous studies. The sluggish reactivity is explained with an olefin-Lewis base chelate that is capable of binding the metal center in the presence of cation; this new resting state of catalysis is significantly less active towards olefin isomerization and is driven by Na^+ coordination with the crown. Exploration of this chelate with longer chain olefins yields an interesting example of switchable catalysis: moving from selectivity to the **b** isomer in the absence of cation to internal isomers in long chain olefin in the presence of cation. This is a particularly interesting reaction given the small number of catalysts capable of this isomerization.

While high yielding switchable catalysis to thermodynamic products and internal olefins is elusive, this work lays the foundation for continuing efforts to increase the scope of switchable

olefin isomerization to functionalized olefins.

VI.   Experimental

General Considerations

      All compounds were manipulated using standard vacuum line or Schlenk techniques or in a glovebox under a nitrogen atmosphere. NMR scale reaction mixtures were prepared under nitrogen in a glovebox and kept in Teflon-sealed tubes. ^{1}H, ^{31}P, and ^{13}C NMR spectra were recorded on 400, 500, and 600 MHz spectrometers. NMR characterization data are reported at 298 K, unless specified otherwise. All NMR solvents and isotopically labeled reagents were purchased from Cambridge Isotope Laboratories, Inc. 1,2-dichloroethane-d4 ($C_2D_4Cl_2$) and methylene chloride-d2 (CD_2Cl_2) were freeze−pump−thaw degassed three times before drying by passage through a small column of activated alumina. Chemical shifts for ^{1}H and heteronuclear spectra are reported in ppm and referenced relative to residual proteo solvent impurity.[35] Single-crystal X-ray diffraction data were collected on a Bruker APEX-II CCD diffractometer at 150 K with Cu Kα radiation (λ = 1.54175 Å). The structure was solved using Superflip[36] and refined (full-matrix-least squares) using the Oxford University Crystals for Windows system.[37] The charge-flipping solution provided most non-hydrogen atoms from the E-map. Full-matrix least squares / difference Fourier cycles were performed, which located the remaining non-hydrogen atoms.

General Procedure for Heated Shaker Catalysis Studies

      Solutions of 0.2 M **2a, 3a, 4a**, 1 mol% catalyst, and various equivalents of salt were heated at 50 °C in gas chromatography vials in a 24-well shaker. Aliquots were taken at 24, 48, 120, and 216 hrs. Each aliquot was immediately quenched with excess PPNCl in CDCl$_3$ to

convert **2-18c6b** to chloride complex **1**-**18c6b** and halt the reaction.[38] Independent tests of **1-18c6b** and substrate showed no observable olefin isomerization, and monitoring of the quenched aliquots show insignificant change in the isomer distributions after quenching. The quenching solution also contained mesitylene as an internal standard for quantification by integration of NMR spectra.

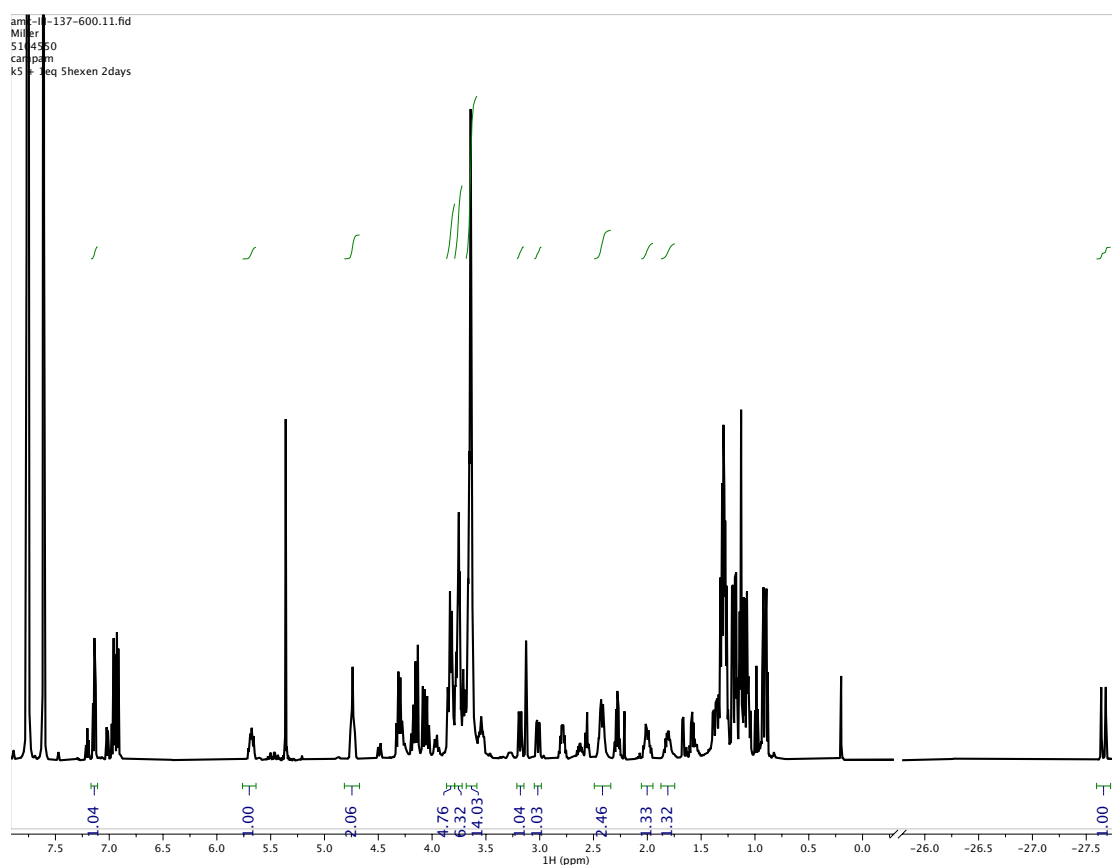*Characterization of [κ³-(¹⁸ᶜ⁶NCOP^{ipr})Ir(H)(3-hexen-1-ol)@Na][BAr^F_4]_2* **(5-iPr18c6b)**

Figure 5.12. ¹H NMR of **5-iPr18c6b** in CD$_2$Cl$_2$.
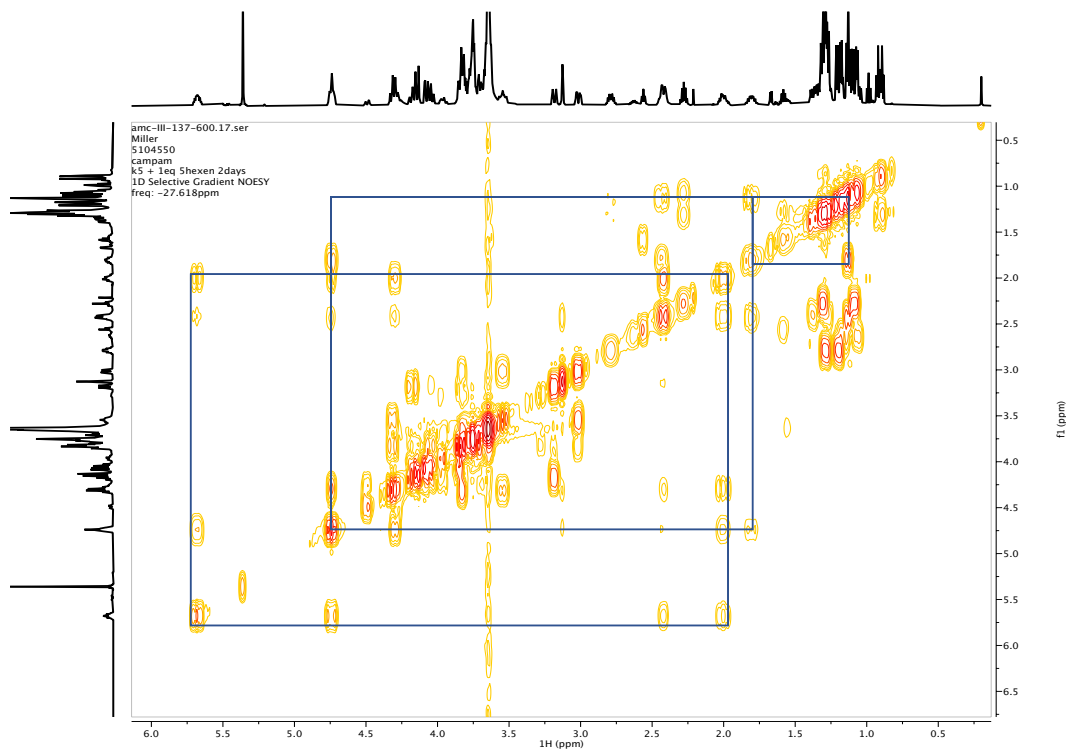
Figure 5.13. ^{1}H–^{1}H COSY NMR of **5-iPr18c6b** in CD$_2$Cl$_2$.
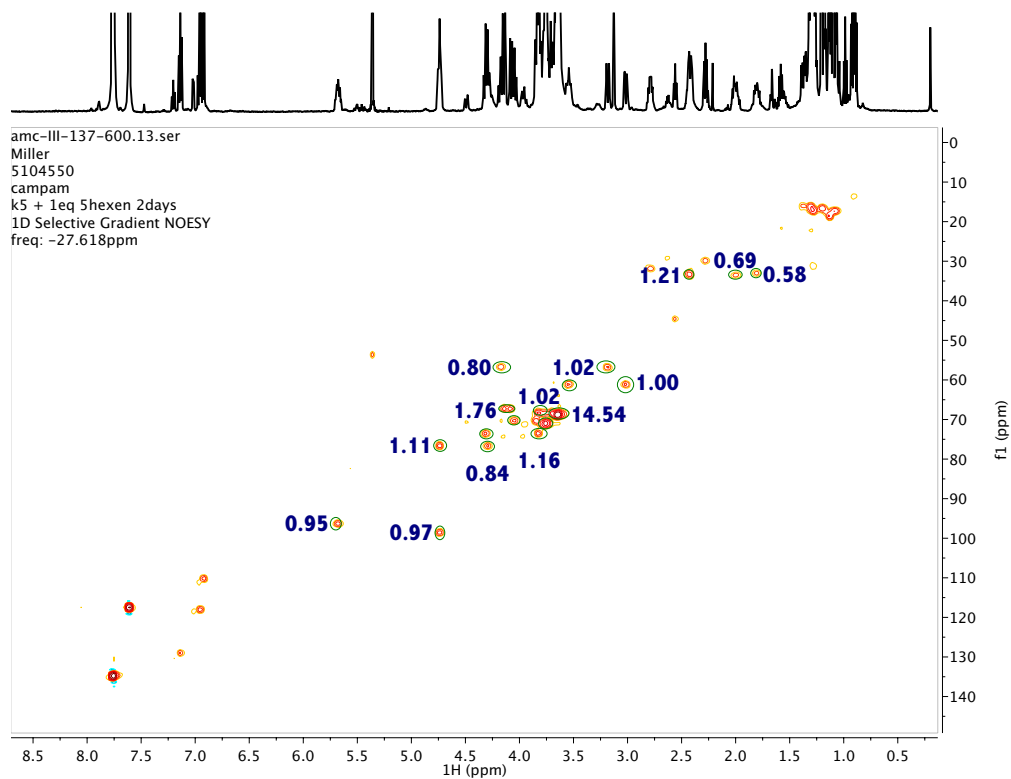

Figure 5.14. ^{1}H-^{13}C HSQC spectrum of **5-iPr18c6b** in CD$_2$Cl$_2$.

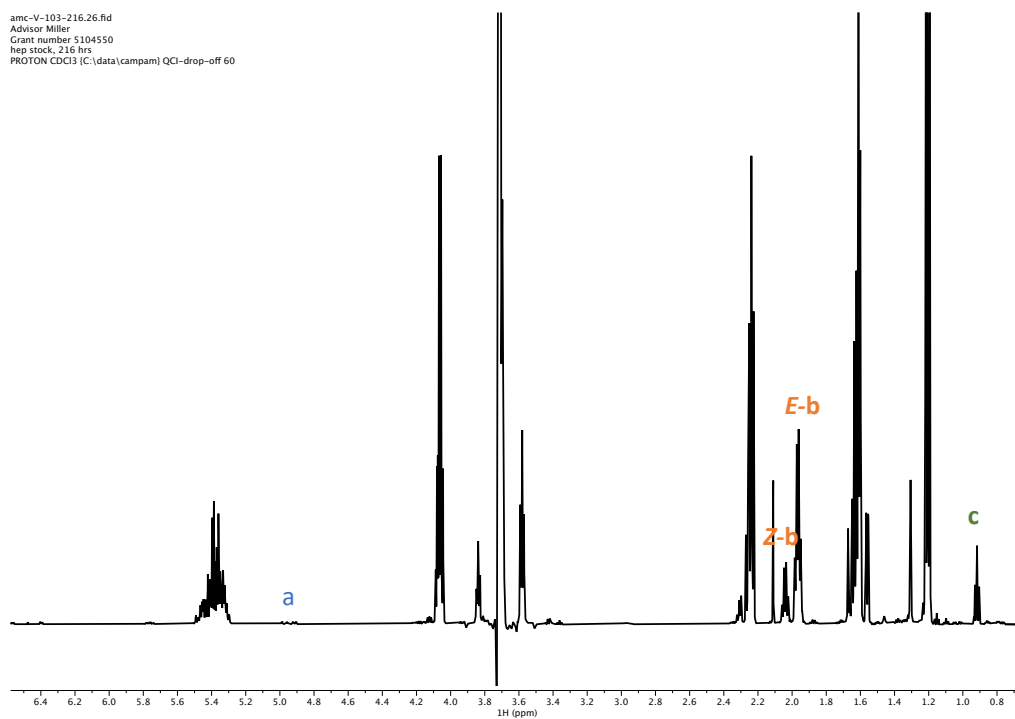*Spectra of Long Chain Olefin Isomerizations*

Figure 5.15. ^{1}H NMR of **7** isomers after heating for 216 hours in DCE-d^4.
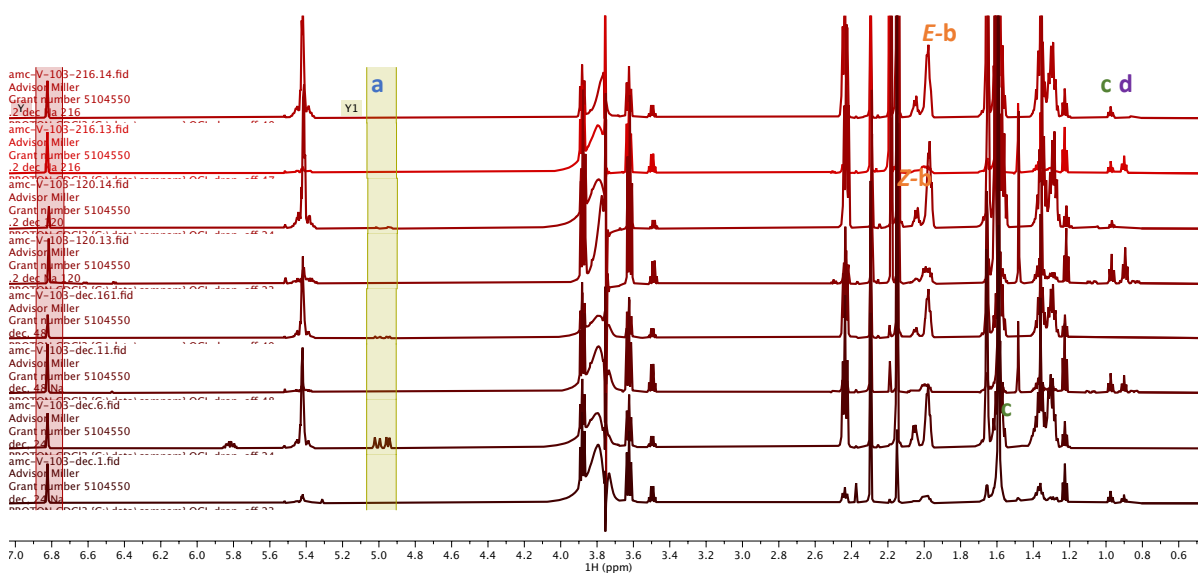

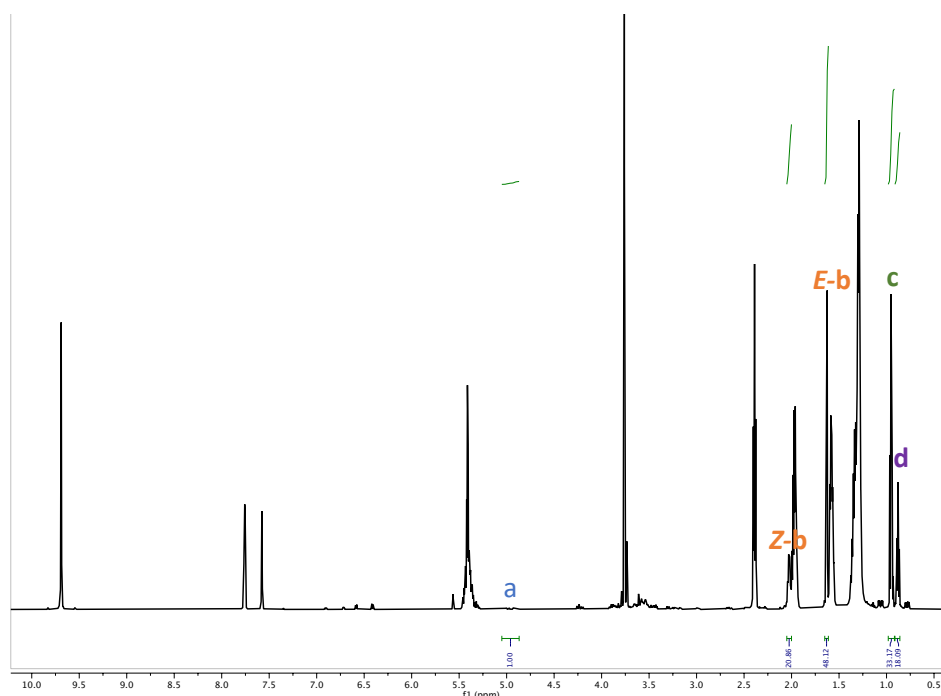Figure 5.16. ^{1}H NMR time course of **8** isomers after heating for 216 hours in DCE-d^4.

Figure 5.17. ^{1}H NMR of **9** isomers after heating for 120 hours in DCE-d^4.

*Synthesis and Characterization of ($^{MeO-18c6}NCOP^{Ph}$)H (**10**)*

($^{MeO-18c6}$NCOH)H (100.7 mg, 252 mmol) and triethylamine (45.8 mg, 454 mmol) were dissolved in 4mL of THF. Diphenylchlorophosphine (56.2 mg, 255 mmol) was dissolved in a separate vial of 4 mL of THF. Both solutions were cooled to -30 °C, then the chlorophosphine solution was added dropwise to ligand and base solution while stirring vigorously. The reaction stirred for 2 hours; the THF was removed and the product extract with diethyl ether (1 mL x 3) and passed through a short alumina plug. The product was concentrated to a clear oil (130.7 mg, 88.9% yield).

^{1}H NMR (400 MHz, CD$_2$Cl$_2$): d 2.67 (t, J = 5.9, N(CH_2)$_2$), 3.40-3.63 (m, 22H, crown-CH_2, benzylic-CH_2), 3.78 (s, 3H, OCH_3), 6.76 (d, J = , 1H, aryl-CH), 6.96 (d, J = 8.4 , 1H, aryl-CH), 7.03 (t, J = 1.9, 1H, arylCH), 7.40 (m, 6H, P-arylCH), 7.63 (m, 4H, P-arylCH). **^{31}P{^{1}H} NMR** (162 MHz, CD$_2$Cl$_2$): d 115.4.

amc–IV–023.1.fid
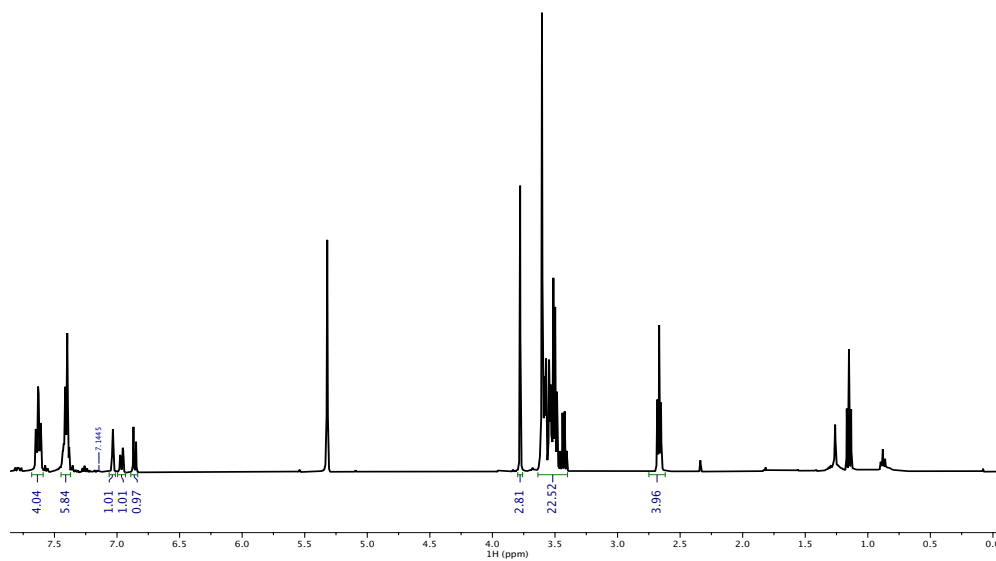diph phosphination
PROTON CD2Cl2 {C:\data\campam} nmrsu 16

Figure 5.18. ^{1}H NMR of ($^{\text{MeO-18c6}}$NCOP$^{\text{Ph}}$)H (**10).**

amc–IV–023–2.2.fid
diph phosphination
P31CPD CD2Cl2 {C:\data\campam} nmrsu 16
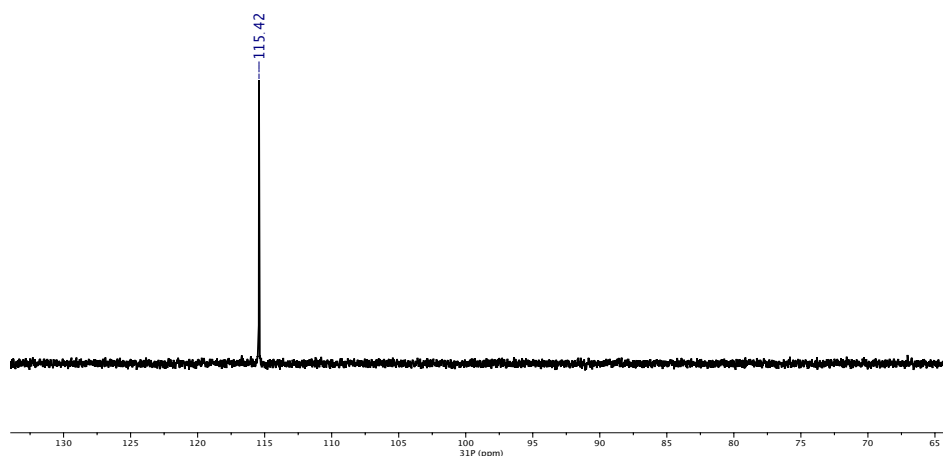
Figure 5.19. ^{31}P{^{1}H} NMR of ($^{\text{MeO-18c6}}$NCOP$^{\text{Ph}}$)H (**10).**

*Synthesis and Characterization of (*MeO-18c6*NCOP*tBu*)H (**11**)*

($^{MeO-18c6}$NCOH)H (101.2mg, 253 mmol) and DBU (45.4 mg, 279 mmol) were dissolved

in 4mL of THF. Ditertbutylchlorophosphine (46 mg, 253 mmol) was dissolved in a separate vial

of 4 mL of THF. Both solutions were cooled to -30 °C, then the chlorophosphine solution was

added dropwise to ligand and base solution. The reaction stirred for 72 hours; the THF was

removed and the product extract with diethyl ether (1 mL x 3) and passed through a short

alumina plug. The product was concentrated to a clear oil (120mg, 87% yield).

^{1}H NMR (400 MHz, CD$_2$Cl$_2$): d 1.20 (d, J = 11.7, 18H, C(CH_3)$_3$), 2.75 (t, J = 5.7, 4H,

N(CH$_2$)$_2$), 3.56-3.68 (m, 22H, crown-CH_2, benzylic-CH_2), 3.85 (s, 3H, OCH_3), 6.86 (m, 2H, aryl-

CH), 7.27 (s, 1H, arylCH). **^{31}P{^{1}H} NMR** (162 MHz, CD$_2$Cl$_2$): d 159.5.
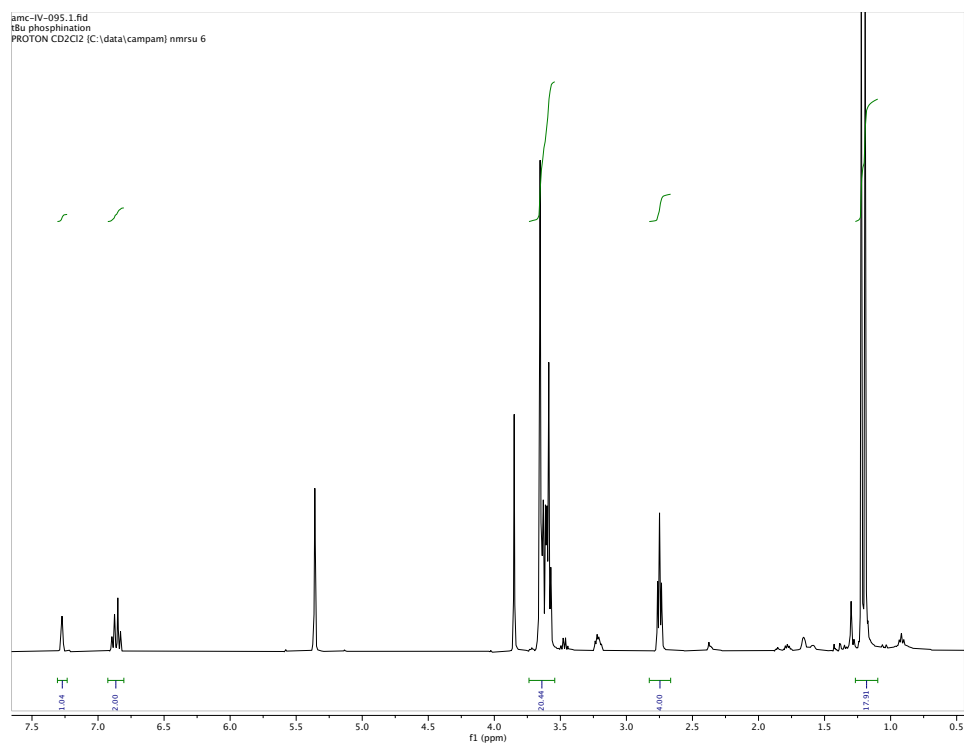
Figure 5.20. ^{1}H NMR of (*MeO-18c6*NCOP^{tBu})H in CD$_2$Cl$_2$.
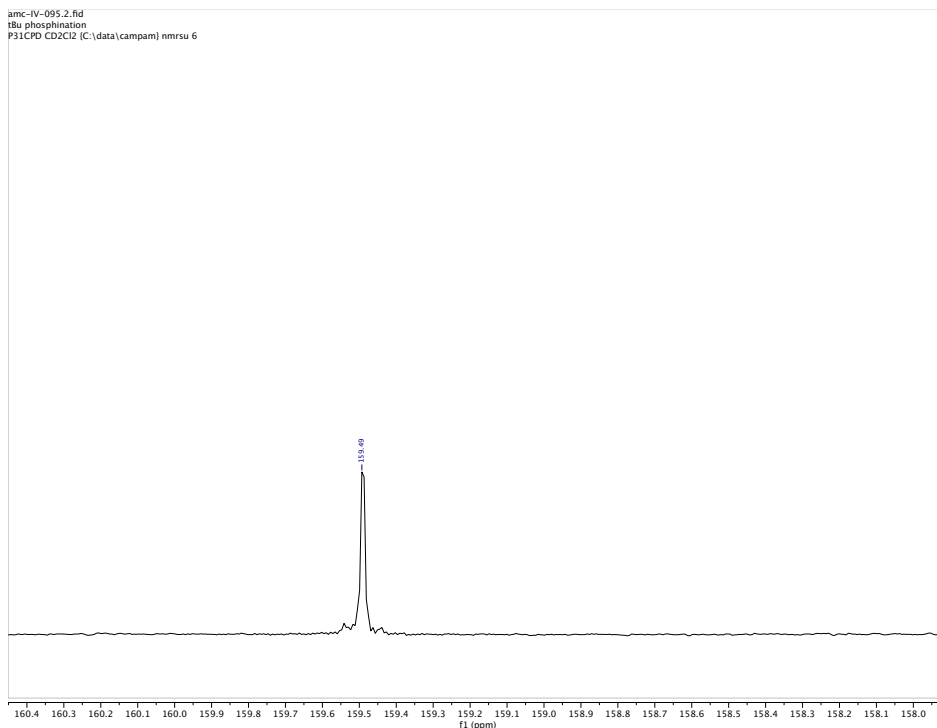
Figure 5.21. $^{31}P\{^{1}H\}$ NMR of $(^{MeO-18c6}NCOP^{tBu})H$ in CD_2Cl_2.

*Synthesis and Characterization of κ^4-$(^{18c6}NCOP^{Ph})Ir(H)(Cl)$ (**12-Ph18c6b**)*

10 (130.7mg, 224 mmol) and [Ir(COD)Cl]$_2$ (68.4 mg, 102 mmol) were dissolved in toluene (10 mL). The reaction was heated in a teflon-sealed pressure vessel for 48 hours at 90 °C, during which the reaction solution turned bright yellow). Toluene was removed under vacuum, and the product extracted with DCM (3 mL) and layered with pentane (8 mL), yielding yellow crystals (90.6 mg, 54.9 % yield). Crystals were of sufficient quality to be submitted for X-Ray analysis.

^{1}H NMR (600 MHz, CD$_2$Cl$_2$) δ -29.99 (d, J = 27.5 Hz, 1H, Ir-*H*) 2.78 (dd, J = 13.7, 6.3 Hz, 1H, crown-C*H*$_2$), 2.85 (dd, J = 12.1, 6.2 Hz, 1H, crown-C*H*$_2$), 2.92 (dd, J = 14.1, 8.6 Hz, 1H, crown-C*H*$_2$), 3.14 (td, J = 13.7, 13.0, 6.3 Hz, 2H, crown-C*H*$_2$), 3.20 – 3.29 (m, 2H, crown-C*H*$_2$), 3.33 – 3.63 (m, 11H, crown-C*H*$_2$), 3.80 – 3.69 (m, 2H, crown-C*H*$_2$), 3.87 (s, 3H, OC*H*$_3$), 3.91 (m, 1H, crown-C*H*$_2$), 4.02 (dd, J = 12.2, 9.4 Hz, 1H, crown-C*H*$_2$), 4.16 (ddd, J = 11.3, 8.6, 2.2 Hz, 1H, crown-C*H*$_2$), 4.25 (d, J = 14.1 Hz, 1H, benzylic-C*H*$_2$), 4.52 (dd, J = 14.2, 3.9 Hz, 1H, benylic-

CH_2), 4.70 (dd, J = 15.6, 9.4 Hz, 1H, crown-CH_2), 6.45 (d, J = 8.0 Hz, 1H, aryl-CH), 6.68 (d, J = 8.1 Hz, 1H, aryl-CH), 7.50 – 7.32 (m, 6H, P-aryl$H$), 7.83 (ddd, J = 12.8, 7.5, 2.1 Hz, 2H, P-aryl$H$), 7.94 – 8.05 (m, 2H, P-aryl$H$). **^{31}P{^{1}H} NMR (**243 MHz, CD$_2$Cl$_2$): δ 102.6.
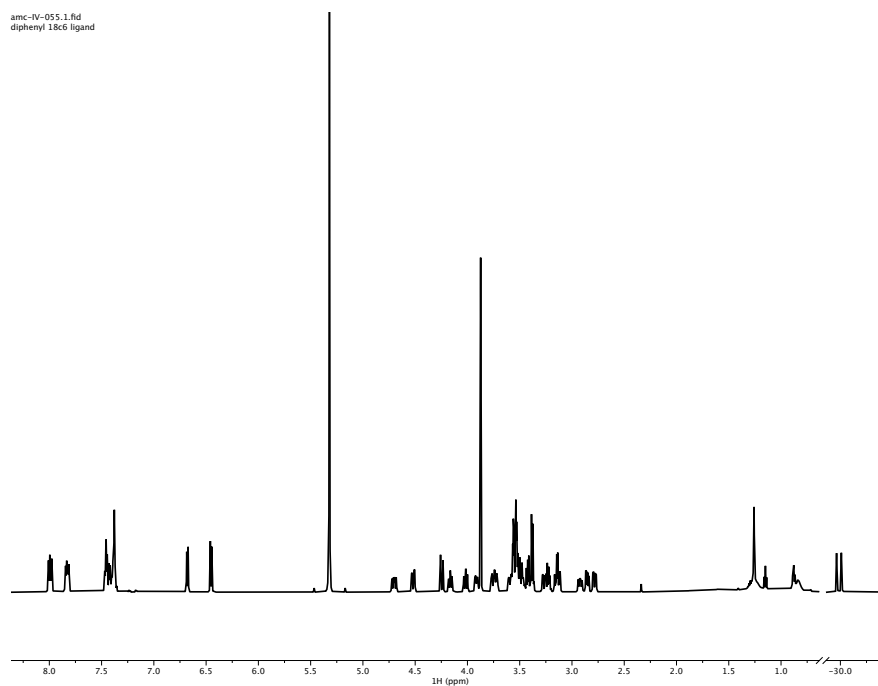

Figure 5.22. ^{1}H NMR of κ^4-(^{18c6}NCOP^{Ph})Ir(H)(Cl) (**12-Ph18c6b**) in CD$_2$Cl$_2$.
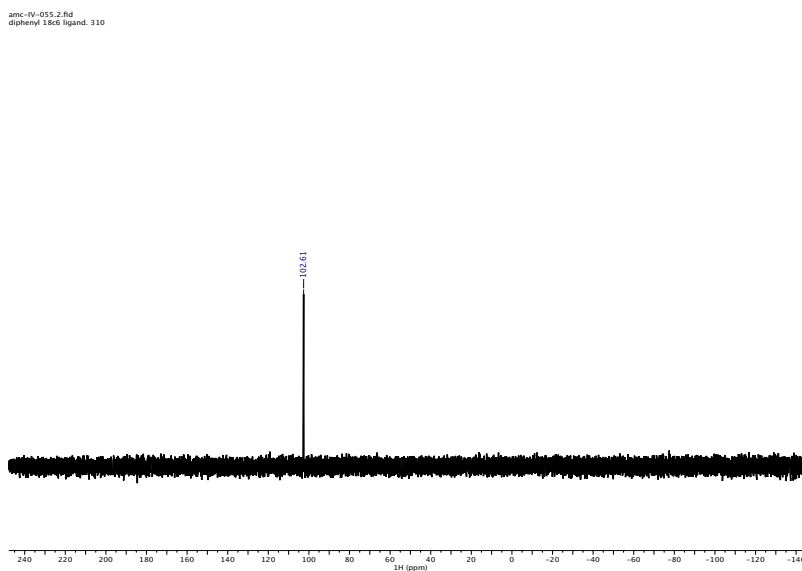

Figure 5.23. ^{31}P{^{1}H} NMR of κ^4-(^{18c6}NCOP^{Ph})Ir(H)(Cl) (**12-Ph18c6b**) in CD$_2$Cl$_2$.

Table 5.7. Crystallographic Information for κ^4-$(^{18c6}NCOP^{Ph})Ir(H)(Cl)$ (**12-Ph18c6b**).

Empirical formula	C32 H42 Cl1 Ir1 N1 O7 P1
Formula weight	811.33
Crystal color, shape, size	yellow block, 0.200 x 0.200 x 0.100 mm^3
Temperature	150 K
Wavelength	1.54178 Å
Crystal system, space group	Triclinic, P-1
Unit cell dimensions	a = 9.6600(3) Å α= 78.1486
	b = 11.8568(3) Å β= 89.4800
	c = 14.2939(4) Å γ = 88.8261
Volume	1601.92(8) Å^3
Z	2
Density (calculated)	1.682 Mg/m^3
Absorption coefficient	9.704 mm^{-1}
F(000)	812
Data collection	
Diffractometer	Bruker Apex Kappa Duo, Bruker
Theta range for data collection	3.159 to 72.413°.
Index ranges	-11<=h<=11, -14<=k<=14, -17<=l<=17
Reflections collected	31912
Independent reflections	6153 [R(int) = 0.023]
Observed Reflections	6080
Completeness to theta = 25.344°	99.5 %
Solution and Refinement	
Absorption correction	Semi-empirical from equivalents
Max. and min. transmission	0.38 and 0.14
Solution	Charge-Flipping methods
Refinement method	Full-matrix least-squares on F^2
Weighting scheme	w = [σ^2Fo^2+ AP^2+ BP]$^{-1}$, with
	P = (Fo^2+ 2 Fc^2)/3, A = 0.034, B = 2.690
Data / restraints / parameters	6128 / 1 / 388
Goodness-of-fit on F^2	1.1243
Final R indices [I>2sigma(I)]	R1 = 0.0235, wR2 = 0.0609
R indices (all data)	R1 = 0.0239, wR2 = 0.0611
Largest diff. peak and hole	1.55 and -0.57 e.Å^{-3}

*Synthesis and Characterization of κ^4-$(^{18c6}NCOP^{tBu})Ir(H)(Cl)$ (**12-tBu18c6b**)*

11 (122.3mg, 225 mmol) and [Ir(COD)Cl]$_2$ (69 mg, 103 mmol) were dissolved in toluene (10

mL). The reaction was heated in a teflon-sealed pressure vessel for 48 hours at 90 °C, then 120

°C for an additional 8 hrs. Slight darkening of solution was observed. Toluene was removed under vacuum, and the product extracted with toluene (3 mL) and layered with pentane (10 mL), yielding red/orange crystals (106.7 mg, 67.6 % yield).

^{1}H NMR (600 MHz, CD$_2$Cl$_2$) δ -33.34 (d, J = 24.9 Hz, 1H, Ir-H), 1.19 (d, J = 14.0 Hz, 9H, C(CH_3)$_3$), 1.43 (d, J = 14.1 Hz, 9H, C(CH_3)$_3$), 2.96 – 3.03 (m, 1H, crown-CH_2), 3.27 (dd, J = 15.1, 5.2 Hz, 1H, crown-CH_2), 3.40 – 3.64 (m, 14H, crown-CH_2), 3.66 – 3.74 (m, 2H, crown-CH_2), 3.80 (s, 3H, OCH_3), 3.84 (ddd, J = 14.5, 7.8, 5.0 Hz, 2H, crown-CH_2), 3.91 – 3.99 (m, 2H, crown-CH_2), 4.25 – 4.34 (m, 2H, benzylic-CH_2, crown-CH_2), 4.42 (dd, J = 14.8, 3.1 Hz, 1H, benzylic-CH_2), 4.56 (dd, J = 15.4, 8.8 Hz, 1H, crown-CH_2), 6.37 (d, J = 8.1 Hz, 1H, aryl-CH), 6.56 (d, J = 8.1 Hz, 1H, aryl-CH).
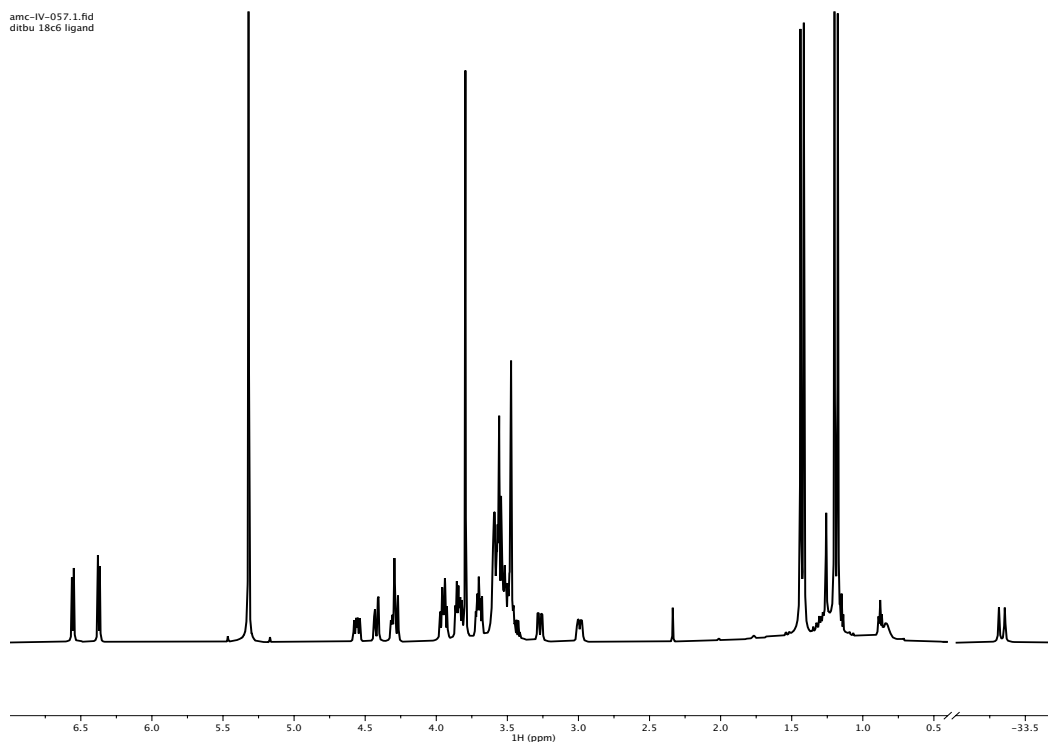

Figure 5.24. ^{1}H NMR of κ^4-(^{18c6}NCOP^{tBu})Ir(H)(Cl) (**12-tBu18c6b**) in CD$_2$Cl$_2$.
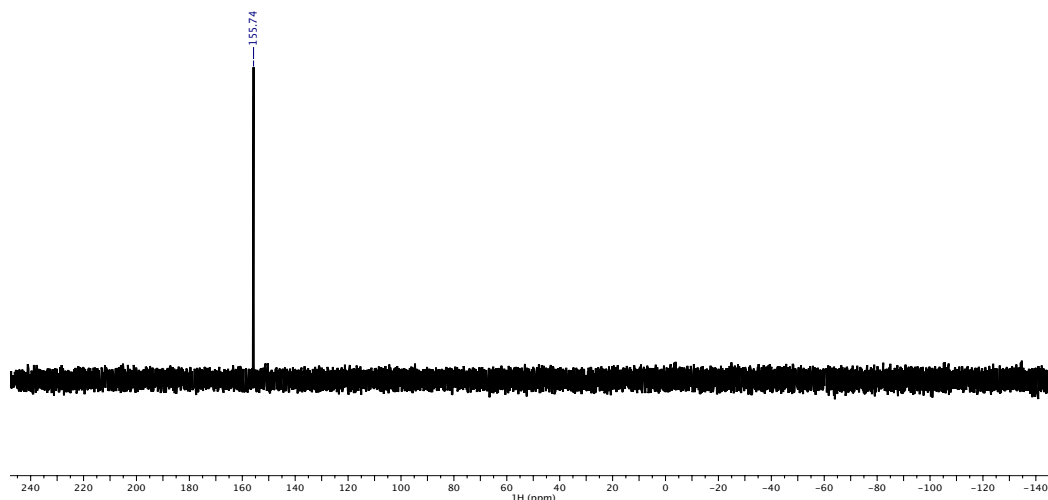
Figure 5.25. $^{31}P\{^1H\}$ NMR of κ^4-(^{18c6}NCOP^{tBu})Ir(H)(Cl) (**12-tBu18c6b**) in CD$_2$Cl$_2$.

Synthesis and Characterization of [κ^4-($^{MeO\text{-}18c6}$NCOP^{Ph})Ir(H)(OH$_2$)][BAr$^F_4$] **(6-Ph18c6b)**

12-Ph18c6b (52 mg, 59 μmol) and 1.01 equiv of NaBAr$^F_4$ (59 mg, 62 μmol) were dissolved in DCM (5 mL). The orange solution was layered with an equal volume of water (5 mL), and the biphasic reaction stirred vigorously over night. The organic layer was washed 3x with 2.5 mL of HPLC water, then the organic layer was passed through an alumina plug and concentrated by rotary evaporator to yield a very pale yellow solid (108.3 mg, 93.5 % yield).

X-ray quality crystals were grown by dissolution of solid in diethyl ether (1 mL) and layering with pentanes (2 mL) , yielding colorless crystals.

^1H NMR (400 MHz, CD$_2$Cl$_2$) δ -30.65 (d, *J* = 27.3 Hz, 1H, Ir-*H*), 2.49 – 2.75 (m, 2H, crown-C*H*$_2$), 2.81 – 2.93 (m, 1H, crown-C*H*$_2$), 3.03 (d, *J* = 13.8 Hz, 1H, crown-C*H*$_2$), 3.13 – 3.34 (m, 3H, crown-C*H*$_2$), 3.47 – 3.69 (m, 8H, crown-C*H*$_2$), 3.71 – 3.97 (m, 12H, crown-C*H*$_2$, OC*H*$_3$, benzylic-CH$_2$), 4.18 (t, *J* = 11.4 Hz, 1H, crown-C*H*$_2$), 4.31 (d, *J* = 14.4 Hz, 1H, benzylic-C*H*$_2$),

190

5.94 (s, 2H, O*H*₂), 6.52 (d, *J* = 8.1 Hz, 1H, aryl-C*H*), 6.69 (d, *J* = 8.1 Hz, 1H, aryl-C*H*), 7.30 –

7.59 (m, 12H, *p*-B-Ar-*H,* P-arylC*H*), 7.71 (s, 8H, *o*-B-Ar-*H*), 7.95 (dd, *J* = 12.9, 7.4 Hz, 2H, P-

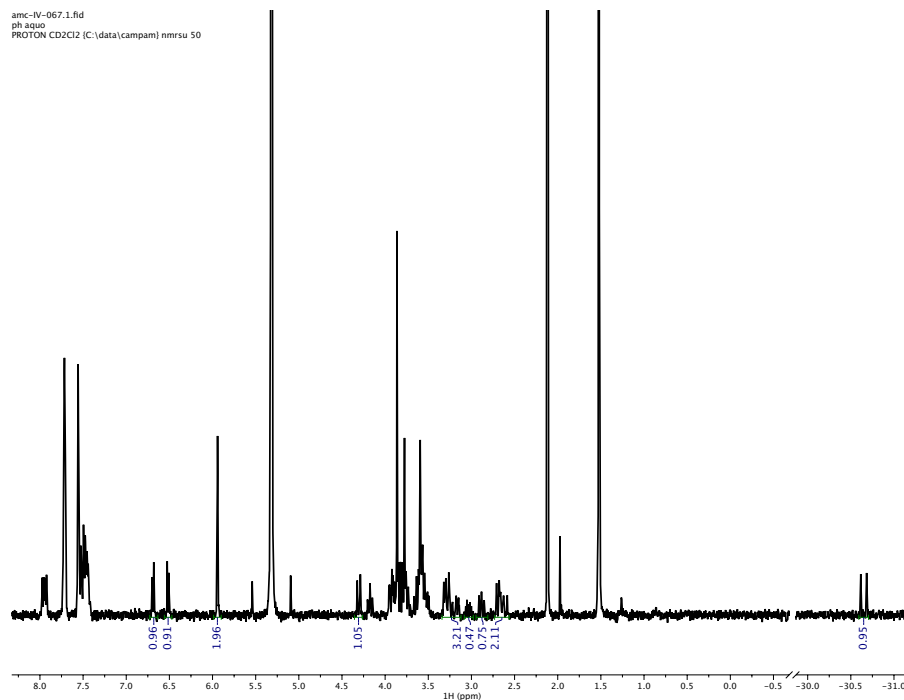arylC*H*). **³¹P{¹H} NMR** (162 MHz, CD₂Cl₂): δ 103.0.

Figure 5.26. ¹H NMR of [κ⁴-(^(MeO-18c6)NCOP^Ph)Ir(H)(OH₂)][BAr^F₄] **(6-Ph18c6b)** in CD₂Cl₂.

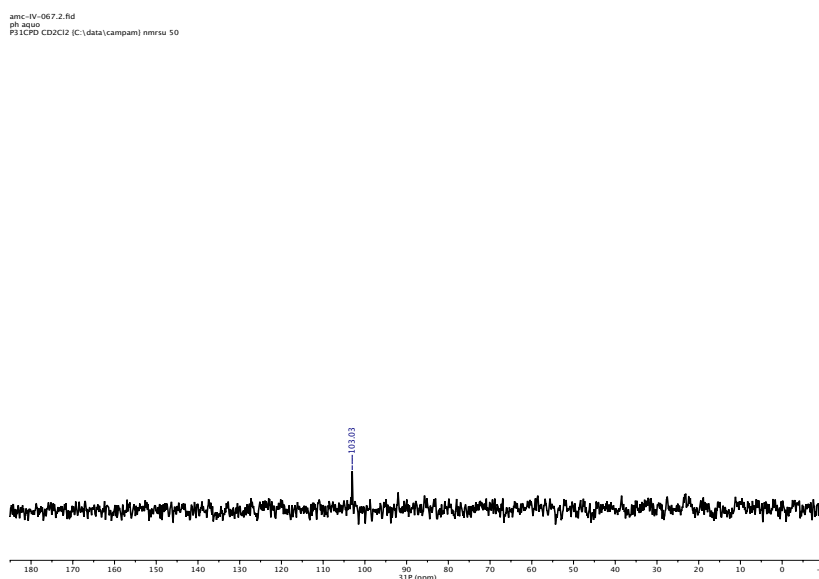

Figure 5.27. ³¹P{¹H} NMR [κ⁴-(^(MeO-18c6)NCOP^Ph)Ir(H)(OH₂)][BAr^F₄] **(6-Ph18c6b)** in CD₂Cl₂.

Table 5.8. Crystallographic Information for [κ^4-($^{\text{MeO-18c6}}$NCOP$^{\text{Ph}}$)Ir(H)(OH$_2$)][BAr$^{\text{F}}_4$] (**6-Ph18c6b**).

Empirical formula	C64 H56 B1 F24 Ir1 N1 O8 P1
Formula weight	1657.11
Crystal color, shape, size	yellow plate fragment, 0.150 x 0.150 x 0.050 mm^3
Temperature	150 K
Wavelength	1.54180 Å
Crystal system, space group	Triclinic, P-1
Unit cell dimensions	a = 14.4788(2) Å $\quad\quad$ α= 97.5152(12)°.
	b = 14.8467(3) Å $\quad\quad$ β= 106.6746(14)°.
	c = 15.9951(3) Å $\quad\quad$ γ = 90.9051(11)°.
Volume	3260.32(10) Å^3
Z	2
Density (calculated)	1.688 Mg/m^3
Absorption coefficient	5.317 mm^{-1}
F(000)	1648

Data collection

Diffractometer	Bruker Apex Kappa Duo, Bruker
Theta range for data collection	2.913 to 70.243°.
Index ranges	-17<=h<=17, -18<=k<=18, -19<=l<=19
Reflections collected	66689
Independent reflections	12068 [R(int) = 0.066]
Observed Reflections	10821
Completeness to theta = 25.288°	99.4 %

Solution and Refinement

Absorption correction	Semi-empirical from equivalents
Max. and min. transmission	0.77 and 0.45
Solution	Charge-Flipping methods
Refinement method	Full-matrix least-squares on F^2
Weighting scheme	w = [σ^{2}Fo^2+ AP^2+ BP]$^{-1}$, with
	P = (Fo^2+ 2 Fc^2)/3, A = 0.056, B = 6.320
Data / restraints / parameters	12015 / 99 / 940
Goodness-of-fit on F^2	1.0076
Final R indices [I>2sigma(I)]	R1 = 0.0378, wR2 = 0.0945
R indices (all data)	R1 = 0.0433, wR2 = 0.0983
Largest diff. peak and hole	2.35 and -1.16 e.Å^{-3}

Synthesis and Characterization of [κ⁴-(^{MeO-18c6}NCOP^{tBu})Ir(H)(OH₂)][BAr^F₄] **(6-tBu18c6b)**

12-tBu18c6b (49 mg, 63.5 mmol) and 1.01 equiv of NaBAr$^F_4$ (59 mg, 64 mmol) were weighted out and dissolved in DCM (2.5 mL). The orange solution was layered with an equal volume of water (2.5 mL), and the biphasic reaction stirred vigorously for 2 hrs. Washed 3x with 2.5 mL of HPLC water, then the organic layer was passed through an alumina plug and concentrated by rotary evaporator to yield a yellow powder (67.4 mg, 64.3 % yield).

X-ray quality crystals were grown by dissolution in diethyl ether (1 mL) and layering with pentanes (2 mL), yielding yellow crystals.

^{1}H NMR (400 MHz, CD₂Cl₂) δ -36.89 (d, J = 24.2 Hz, 1H, Ir-H), 1.28 (d, J = 13.7 Hz, 9H, C(CH_3)), 1.44 (d, J = 14.3 Hz, 9H, C(CH_3)), 2.97 (dd, J = 28.9, 13.3 Hz, 2H, crown-CH_2), 3.29 (d, J = 10.8 Hz, 2H, crown-CH_2), 3.43 (q, J = 7.1 Hz, 1H, crown-CH_2), 3.48 – 3.71 (m, 14H, crown-CH_2), 3.80 (s, 3H, OCH_3), 3.80 (m, 2H, crown-CH_2), 3.96 – 4.07 (m, 2H, crown-CH_2, benzylic-CH_2), 4.20 (t, J = 11.4 Hz, 2H, crown-CH_2, benzylic-CH_2), 4.41 (t, J = 12.7 Hz, 1H, crown-CH_2), 5.54 (s, 2H, OH_2), 6.45 (d, J = 8.2 Hz, 1H, aryl-CH), 6.61 (d, J = 8.2 Hz, 1H, aryl-CH), 7.56 (s, 4H, o-B-Ar-H), 7.69 – 7.75 (t, 8H, p-B-Ar-H). ^{31}P{^{1}H} NMR (162 MHz, CD₂Cl₂): δ 154.6.
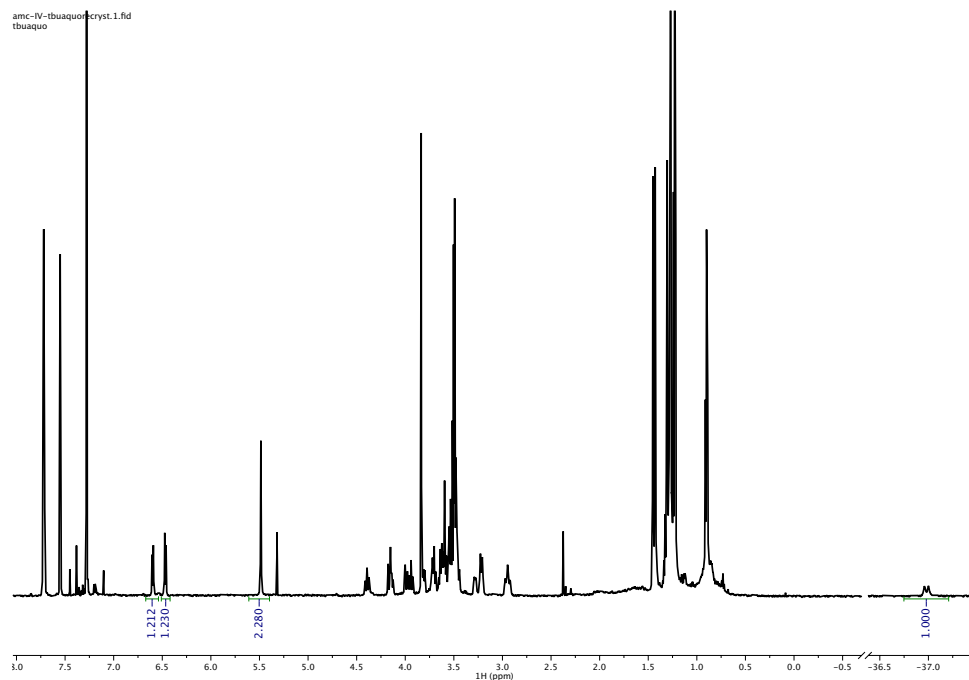
Figure 5.28. ^{1}H NMR for $[\kappa^4\text{-}(^{MeO\text{-}18c6}NCOP^{tBu})Ir(H)(OH_2)][BAr^F_4]$ **(6-tBu18c6b)** in CD_2Cl_2.
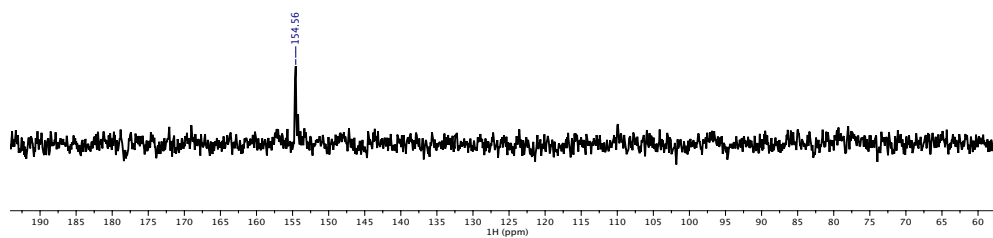
Figure 5.29. $^{31}P\{^1H\}$ NMR for $[\kappa^4\text{-}(^{MeO\text{-}18c6}NCOP^{tBu})Ir(H)(OH_2)][BAr^F_4]$ **(6-tBu18c6b)** in CD_2Cl_2.

Table 5.9. Crystallographic information for [κ⁴-($^{MeO-18c6}$NCOP^{tBu})Ir(H)(OH₂)][BAr$^F_4$] **(6-tBu18c6b).**

Empirical formula	C64 H74 B1 F24 Ir1 N1 O9 P1
Formula weight	1691.25
Crystal color, shape, size	yellow block, 0.050 x 0.050 x 0.050 mm³
Temperature	150 K
Wavelength	1.54180 Å
Crystal system, space group	Triclinic, P-1

Unit cell dimensions	a = 13.0170(2) Å	α= 101.0114(7)°.
	b = 14.0927(2) Å	β= 97.9651(8)°.
	c = 20.4466(3) Å	γ = 98.1983(10)°.

Volume	3590.68(9) Å³
Z	2
Density (calculated)	1.564 Mg/m³
Absorption coefficient	4.845 mm⁻¹
F(000)	1700.000

Data collection	
Diffractometer	Bruker Apex Kappa Duo, Bruker
Theta range for data collection	2.234 to 72.231°.
Index ranges	-16<=h<=16, -17<=k<=17, -25<=l<=25
Reflections collected	84221
Independent reflections	13748 [R(int) = 0.031]
Observed Reflections	13058
Completeness to theta = 25.281°	99.5 %

Solution and Refinement	
Absorption correction	Semi-empirical from equivalents
Max. and min. transmission	0.62 and 0.62
Solution	Charge-Flipping methods
Refinement method	Full-matrix least-squares on F²
Weighting scheme	w = [σ²Fo²+ AP²+ BP]⁻¹, with
	P = (Fo²+ 2 Fc²)/3, A = 0.045, B = 10.870
Data / restraints / parameters	13688 / 383 / 1096
Goodness-of-fit on F²	1.0217
Final R indices [I>2sigma(I)]	R1 = 0.0405, wR2 = 0.1006
R indices (all data)	R1 = 0.0423, wR2 = 0.1019
Largest diff. peak and hole	1.38 and -1.64 e.Å⁻³

Synthesis and Characterization of [κ⁵-(ᴹᵉᴼ⁻¹⁸ᶜ⁶NCOPᴾʰ)Ir(H)][BArᶠ₄] **(1-Ph18c6b)**

6-Ph18c6b (300 mg, 184 mmol) was heated under high vacuum at 140 °C on a schlenk line. P_2O_5 was placed on the same line to aid in water removal. After heating for 24 hours, the solid was cooled and transferred to a Nitrogen atmosphere box, yielding the off-white product phk5 (295 mg, 99% yield).

¹H NMR (500 MHz, CD_2Cl_2) δ -28.23 (d, J = 26.3 Hz, 1H, Ir-*H*), 2.89 (m, 1H, crown-C*H₂*), 3.11 (m, 2H, crown-C*H₂*), 3.29 (m, 2H, crown-C*H₂*), 3.52 – 3.77 (m, 8H, crown-C*H₂*), 3.80 (s, 3H, OC*H₃*), 3.85 – 4.14 (m, 10H, crown-C*H₂*), 4.39 – 4.58 (m, 3H, benzylic-C*H₂*, crown-C*H₂*), 6.52 (d, J = 8.2 Hz, 1H, aryl-C*H*), 6.66 (d, J = 8.3 Hz, 1H, aryl-C*H*), 7.51 – 7.63 (m, 12H, *o*-B-Ar-*H,* P-arylC*H*), 7.69 – 7.80 (m, 10H, t, 8H, *p*-B-Ar-*H,* P-arylC*H*). **³¹P{¹H}** NMR (500 MHz, CD_2Cl_2): δ 106.9. **Anal. Calcd** for $C_{64}H_{54}BF_{24}IrNO_7P$: C, 46.9; H, 3.32; N, 0.85. Found: C, 46.4; H, 2.24; N, 0.79. H measurement is low, perhaps due to NaBArᶠ₄ contamination in sample, excess BArᶠ₄ is not observed by NMR.

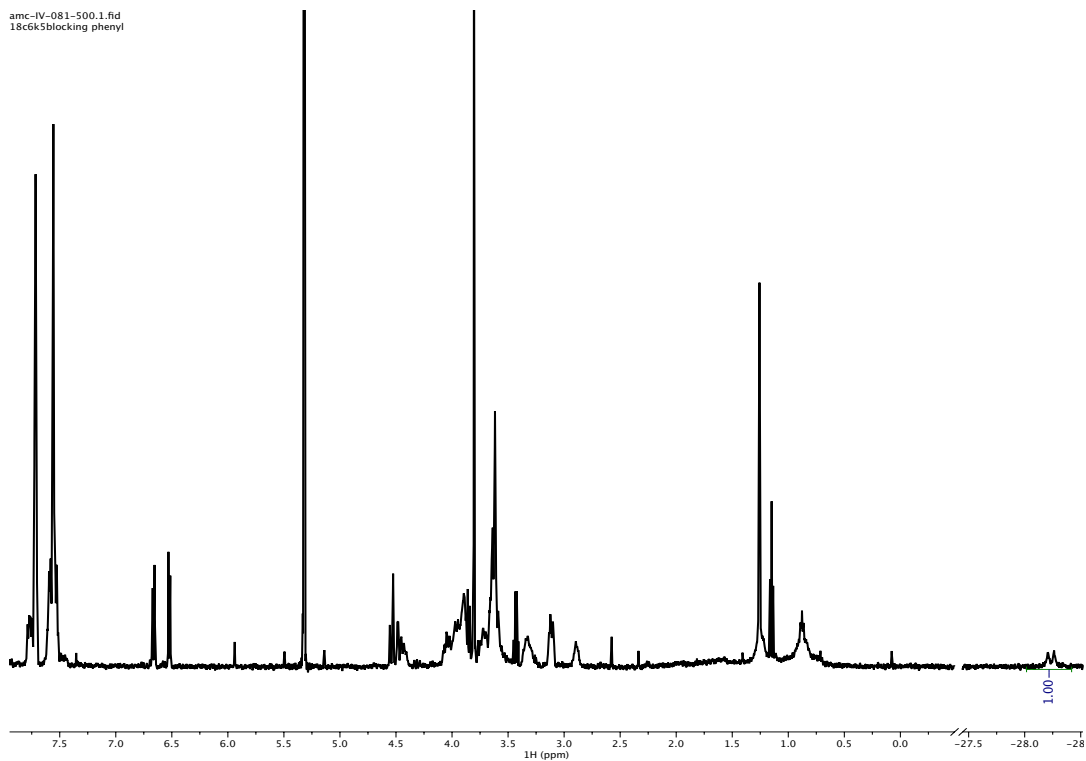Figure 5.30. ^{1}H NMR of [κ^5-($^{MeO-18c6}$NCOP^{Ph})Ir(H)][BAr$^F_4$] **(1-Ph18c6b)** in CD$_2$Cl$_2$.
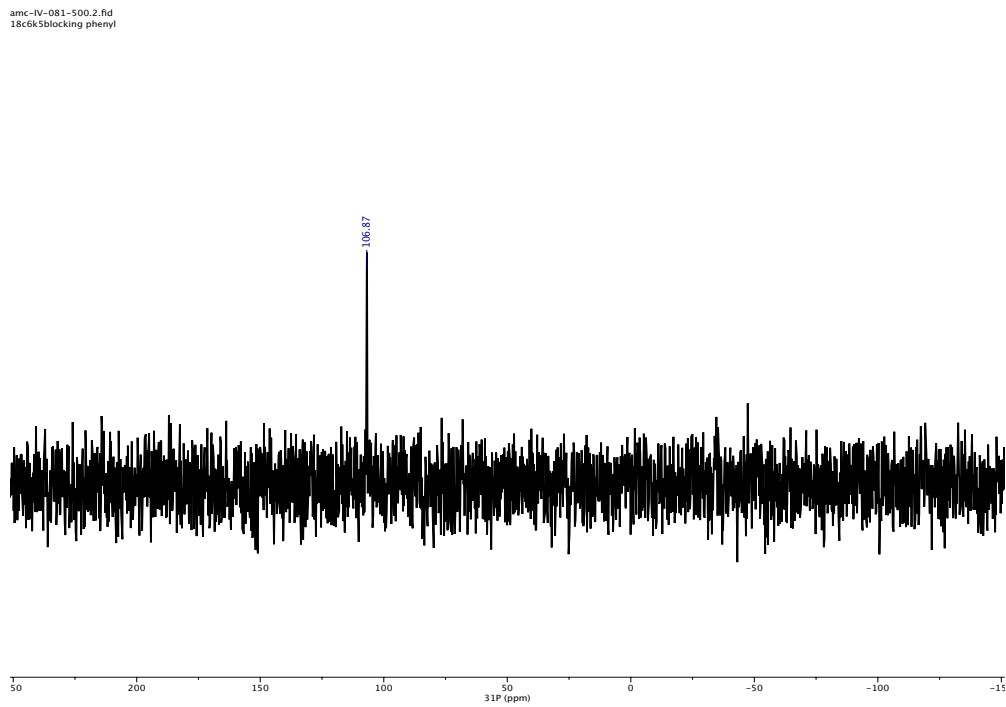
Figure 5.31. ^{31}P{^{1}H} NMR of [κ^5-($^{MeO-18c6}$NCOP^{Ph})Ir(H)][BAr$^F_4$] **(1-Ph18c6b)** in CD$_2$Cl$_2$.

Synthesis and Characterization of [κ⁵-(ᴹᵉᴼ⁻¹⁸ᶜ⁶NCOPᵗᴮᵘ)Ir(H)][BArᶠ₄] **(1-tBu18c6b)**

6-tBu18c6b (45 mg, 28 mmol) was heated under high vacuum at 140 °C on a schlenk line. P_2O_5 was placed on the same line to aid in water removal. After heating for 24 hours, the solid was cooled and transferred to a dry box, yielding the off-white product tbuk5 (41 mg, 92% yield).

¹H NMR (600 MHz, CDCl₃) δ -31.27 (bs, 1H, Ir-*H*), 1.07 – 1.30 (d, *J* = 14.4 9H,), 1.43 (d, *J* = 14.4 Hz, 9H), 3.09 (bd, *J* = 13.9 Hz, 1H, crown-C*H*₂), 3.35 – 4.23 (m, 25H, crown-C*H*₂, OC*H*₃), 4.31 – 4.45 (m, 3H, benzylic-CH₂, crown-C*H*₂), 6.49 (d, *J* = 8.3 Hz, 1H, aryl-C*H*), 6.55 (d, *J* = 8.2 Hz, 1H, aryl-C*H*), 7.56 (s, 4H, *o*-B-Ar-*H*), 7.72 (bt, 9H, *p*-B-Ar-*H*). **³¹P{¹H}** NMR (243 MHz, CDCl₃): δ 149.9. **Anal. Calcd** for $C_{60}H_{62}BF_{24}IrNO_7P$: C, 45.1; H, 3.91; N, 0.89. Found: C, 44.9; H, 3.71; N, 0.90.
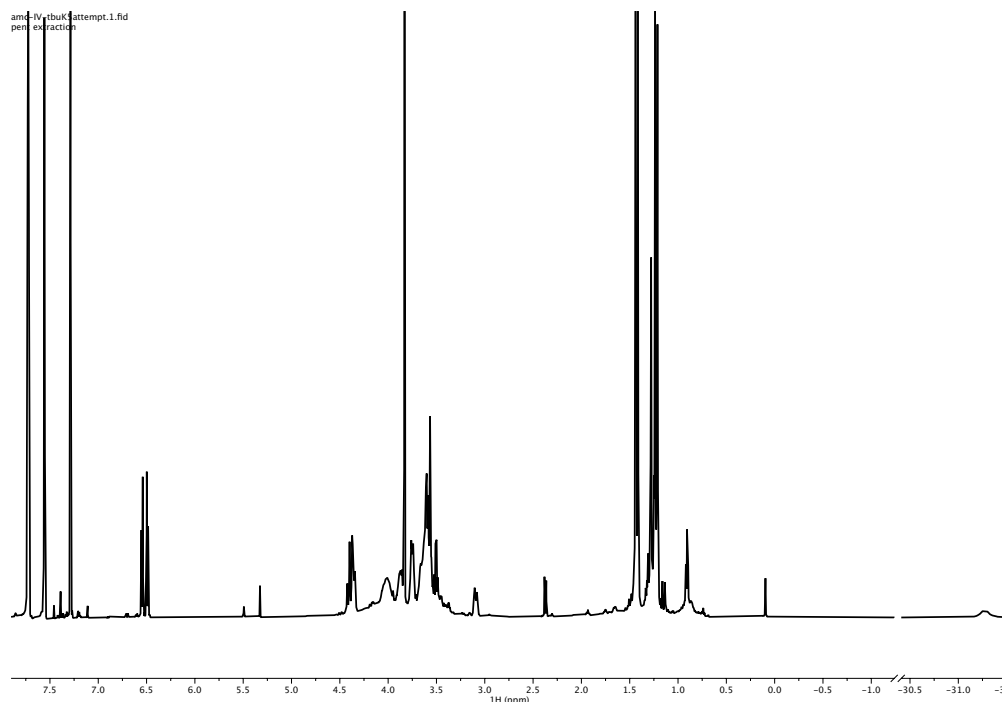

Figure 5.32. ¹H NMR of [κ⁵-(ᴹᵉᴼ⁻¹⁸ᶜ⁶NCOPᵗᴮᵘ)Ir(H)][BArᶠ₄] (**1-tBu18c6b**) in CD₂Cl₂.

amc-IV-tbuK5attempt.2.fid
pent extraction

149.90

270 260 250 240 230 220 210 200 190 180 170 160 150 140 130 120 110 100 90 80 70 60 50 40 30 20 10 0 -10 -20 -30 -40 -50 -60 -70 -80 -90 -100 -110
31P (ppm)
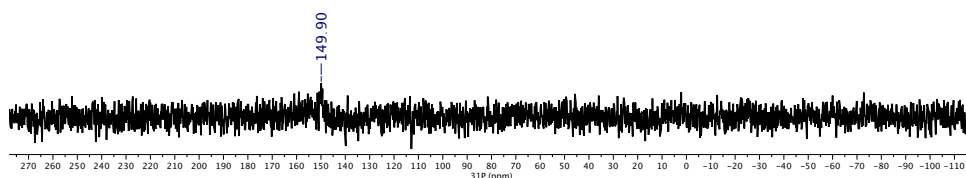
Figure 5.33. ^{31}P{^{1}H} NMR of [κ^5-($^{MeO\text{-}18c6}$NCOP^{tBu})Ir(H)][BAr$^F_4$] (**1-tBu18c6b**) in CD$_2$Cl$_2$. Even after 200 scans on a 600 MHz instrument, the fluxional behavior of the complex broadened the ^{31}P peak into the baseline.

Synthesis and Characterization of [κ^4-($^{MeO\text{-}18c6}$NCOP^{iPr})Ir(H)(NH₃)][BAr$^F_4$] **(14-iPr18c6b)**

12-iPr18c6b (57.2 mg, 77.0 mmol) was dissolved in DCM (2 mL). 2 mL of 30% aqueous ammonia solution was added, and the biphasic mixture n stirred vigorously for 2 hr. The aqueous layer was removed and the organic layer washed with HPLC water (3 x 3mL). The DCM layer was passed through an alumina plug, and concentrated to a pale yellow oil. Subsequent trituration with pentanes yielded the product as an off-white solid (80.4 mg, 64.5% yield). X-ray quality crystals were grown by dissolution in diethyl ether (1 mL) and layering with pentanes (2 mL).

^{1}H NMR (600 MHz, CD$_2$Cl$_2$): δ -32.58 (d, J = 27.1 Hz, 1H, Ir-*H*), 0.78 (dd, J = 15.2, 6.9 Hz, 3H, CH(C*H*₃)₂), 1.01 (dd, J = 19.5, 6.9 Hz, 3H, CH(C*H*₃)₂), 1.32 (dd, J = 17.9, 7.5 Hz, 3H, CH(C*H*₃)₂), 1.42 (dd, J = 13.2, 6.9 Hz, 3H, CH(C*H*₃)₂), 2.48 (m, 1H, C*H*(CH₃)₂), 2.61 (m, 1H,

C*H*(CH₃)₂), 2.88 (ddd, *J* = 11.4, 5.9, 2.9 Hz, 1H, crown-C*H₂*), 3.02 – 3.14 (m, 1H, crown-C*H₂*),

3.15 – 3.23 (m, 1H, crown-C*H₂*), 3.23 – 3.30 (m, 2H, crown-C*H₂*), 3.39 – 3.46 (m, 1H, crown-

C*H₂*), 3.47 (bs, 3H, N*H₃*), 3.51 – 3.66 (m, 11H), 3.72 (ddd, *J* = 11.0, 7.5, 3.7 Hz, 1H, crown-

C*H₂*), 3.77 – 3.87 (m, 7H, crown-C*H₂,* OC*H₃*), 3.99 – 4.07 (m, 2H, crown-C*H₂*m, benzylic-C*H₂*),

4.11 (ddd, *J* = 13.5, 11.7, 2.6 Hz, 1H, crown-C*H₂*), 4.24 (d, *J* = 14.2 Hz, 1H, benzylic-C*H₂*), 6.44

(d, *J* = 8.1 Hz, 1H), 6.67 (d, *J* = 8.1 Hz, 1H), 7.56 (s, 4H), 7.72 (dt, *J* = 5.0, 2.3 Hz, 9H). **³¹P{¹H}**

NMR (243 MHz, CD₂Cl₂) δ 140.5.
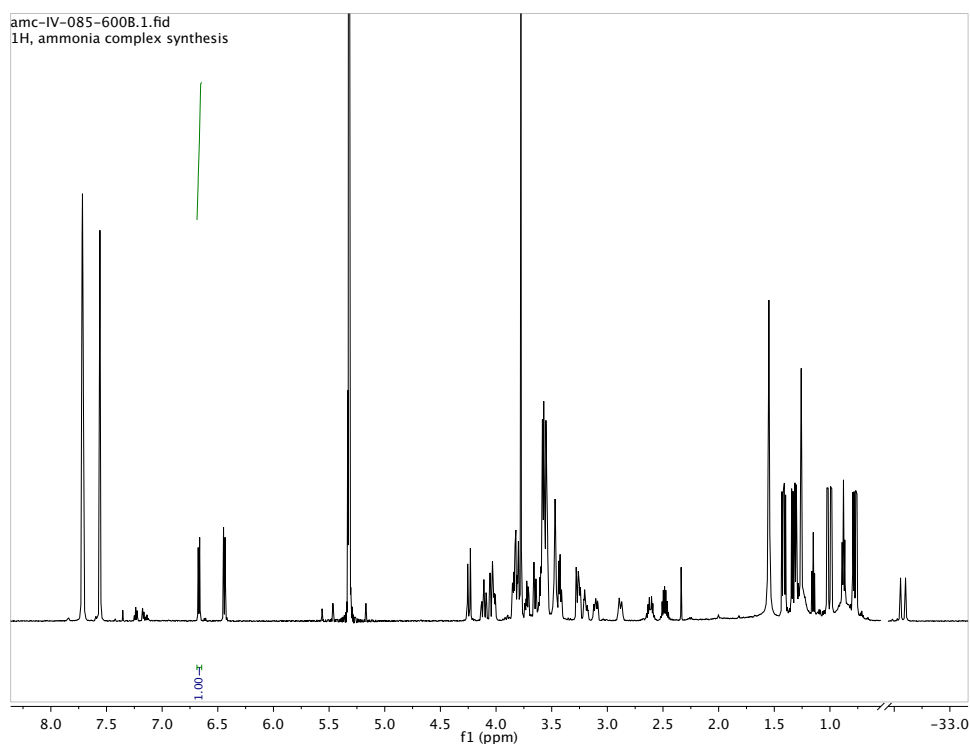
Figure 5.34. ¹H NMR of [κ⁴-(^MeO-18c6NCOP^iPr)Ir(H)(NH₃)][BArᶠ₄] **(14-iPr18c6b)** in CD₂Cl₂.
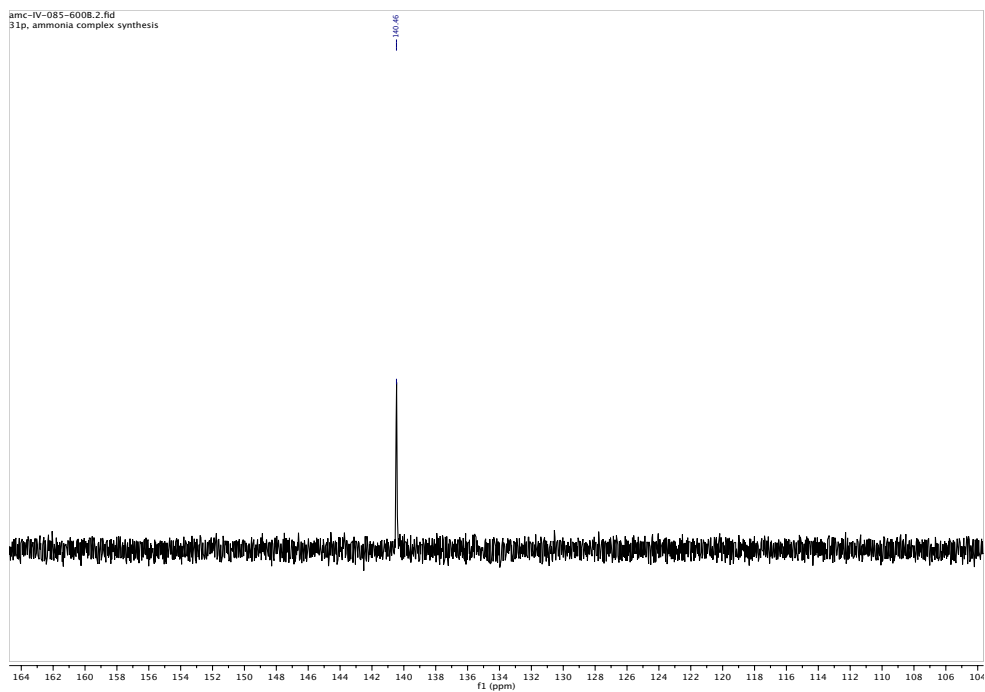
Figure 5.35. ^{31}P{^{1}H} NMR of [κ^4-($^{MeO-18c6}$NCOP^{iPr})Ir(H)(NH$_3$)][BAr$^F_4$] **(14-iPr18c6b)** in CD$_2$Cl$_2$.
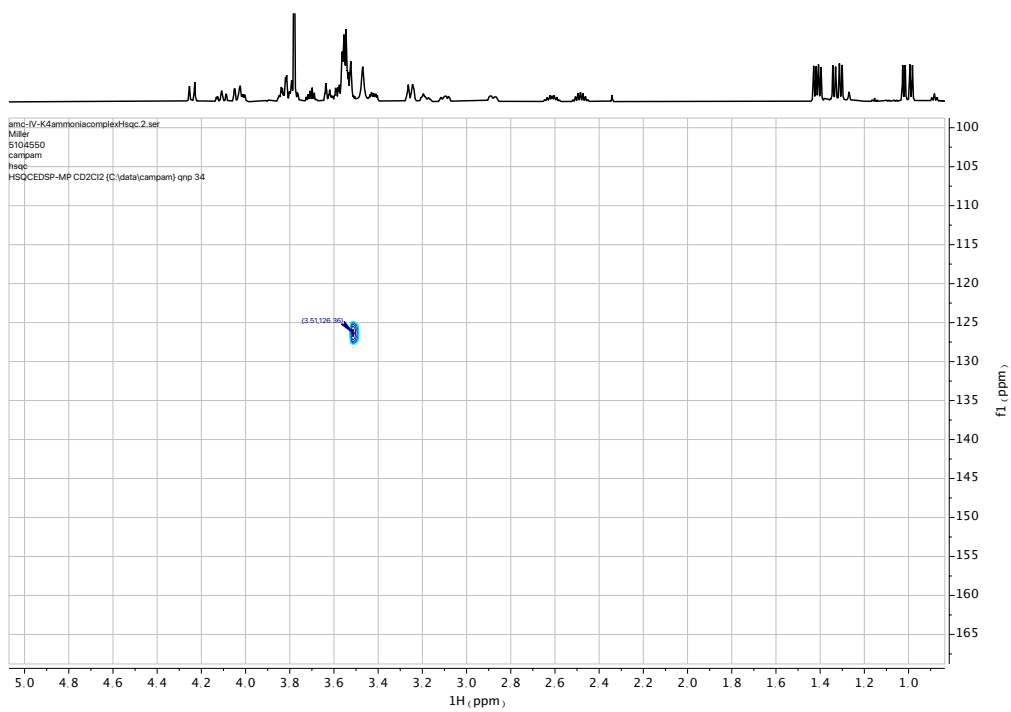
Figure 5.36. ^{1}H-^{15}N HSQC of [κ^4-($^{MeO-18c6}$NCOP^{iPr})Ir(H)(NH$_3$)][BAr$^F_4$] (**14-iPr18c6b**) in CD$_2$Cl$_2$. Referenced to nitromethane.

REFERENCES

(1)   Liu, X.; Li, B.; Liu, Q. Base-Metal-Catalyzed Olefin Isomerization Reactions. *Synthesis (Stuttg).* **2019**, *51* (06), 1293–1310.

(2)   Hassam, M.; Taher, A.; Arnott, G. E.; Green, I. R.; van Otterlo, W. A. L. Isomerization of Allylbenzenes. *Chem. Rev.* **2015**, *115* (11), 5462–5569.

(3)   Krompiec, S.; Krompiec, M.; Penczek, R.; Ignasiak, H. Double Bond Migration in N-Allylic Systems Catalyzed by Transition Metal Complexes. *Coord. Chem. Rev.* **2008**, *252* (15–17), 1819–1841.

(4)   Li, H.; Mazet, C. Iridium-Catalyzed Selective Isomerization of Primary Allylic Alcohols. *Acc. Chem. Res.* **2016**, *49* (6), 1232–1241.

(5)   Larsen, C. R.; Erdogan, G.; Grotjahn, D. B. General Catalyst Control of the Monoisomerization of 1-Alkenes to Trans -2-Alkenes. *J. Am. Chem. Soc.* **2014**, *136* (4), 1226–1229.

(6)   Larsen, C. R.; Grotjahn, D. B. Stereoselective Alkene Isomerization over One Position. *J. Am. Chem. Soc.* **2012**, *134* (25), 10357–10360.

(7)   Wang, Y.; Qin, C.; Jia, X.; Leng, X.; Huang, Z. An Agostic Iridium Pincer Complex as a Highly Efficient and Selective Catalyst for Monoisomerization of 1-Alkenes to Trans-2-Alkenes. *Angew. Chemie - Int. Ed.* **2017**, *56* (6), 1614–1618.

(8)   Chen, C.; Dugan, T. R.; Brennessel, W. W.; Weix, D. J.; Holland, P. L. Z -Selective Alkene Isomerization by High-Spin Cobalt(II) Complexes. *J. Am. Chem. Soc.* **2014**, *136* (3), 945–955.

(9)   Paulson, E. R.; Moore, C. E.; Rheingold, A. L.; Pullman, D. P.; Sindewald, R. W.; Cooksy, A. L.; Grotjahn, D. B. Dynamic Pi-Bonding of Imidazolyl Substituent in a Formally 16-Electron Cp Ru(2-P, N)+ Catalyst Allows Dramatic Rate Increases in (E)-Selective Monoisomerization of Alkenes. *ACS Catal.* **2019**, *9* (8), 7217–7231.

(10)   Paulson, E. R.; Delgado, E.; Cooksy, A. L.; Grotjahn, D. B. Catalyst versus Substrate Control of Forming (E)-2-Alkenes from 1-Alkenes Using Bifunctional Ruthenium Catalysts. *Org. Process Res. Dev.* **2018**, *22* (12), 1672–1682.

(11)   Bader, A.; Lindner, E. Coordination Chemistry and Catalysis with Hemilabile Oxygen-Phosphorus Ligands. *Coord. Chem. Rev.* **1991**, *108* (1), 27–110.

(12)   Vasseur, A.; Bruffaerts, J.; Marek, I. Remote Functionalization through Alkene Isomerization. *Nat. Chem.* **2016**, *8* (3), 209–219.

(13)   Kadyrov, R. Olefin Metathesis: Catalyst Inhibition as a Result of Isomerization. *ChemCatChem* **2016**, *8* (1), 113–116.

(14)   Larsen, C. R.; Grotjahn, D. B. The Value and Application of Transition Metal Catalyzed Alkene Isomerization in Industry. In *Applied Homogeneous Catalysis with Organometallic Compounds*; Cornils, B., Herrmann, W. A., Beller, M., Paciello, R., Eds.; Wiley-VCH Verlag: Weinheim, Germany, 2018; pp 1365–1378.

(15)   Wu, W.; Verkade, J. G. EtN=P(NMe2)N=P(NMe2)3: An Efficient Non-Ionic Base Catalyst for the Isomerization of Allylic Compounds and Methylene-Interrupted Dienes. *Arkivoc* **2004**, *2004* (9), 88.

(16)   Scarso, A.; Colladon, M.; Sgarbossa, P.; Santo, C.; Michelin, R. A.; Strukul, G. Highly Active and Selective Platinum(II)-Catalyzed Isomerization of Allylbenzenes: Efficient Access to (E)-Anethole and Other Fragrances via Unusual Agostic Intermediates. *Organometallics* **2010**, *29* (6), 1487–1497.

(17)   Kapat, A.; Sperger, T.; Guven, S.; Schoenebeck, F. E-Olefins through Intramolecular Radical Relocation. *Science (80-.).* **2019**, *396* (January), 391–396.

(18)   Sharma, S. K.; Srivastava, V. K.; Jasra, R. V. Selective Double Bond Isomerization of Allyl Phenyl Ethers Catalyzed by Ruthenium Metal Complexes. *J. Mol. Catal. A Chem.* **2006**, *245* (1–2), 200–209.

(19)   Camp, A. M.; Kita, M. R.; Grajeda, J.; White, P. S.; Dickie, D. A.; Miller, A. J. M. Mapping the Binding Modes of Hemilabile Pincer-Crown Ether Ligands in Solution Using Diamagnetic Anisotropic Effects on NMR Chemical Shift. *Inorg. Chem.* **2017**, *56* (18), 11141–11150.

(20)   Kita, M. R.; Miller, A. J. M. An Ion-Responsive Pincer-Crown Ether Catalyst System for Rapid and Switchable Olefin Isomerization. *Angew. Chemie - Int. Ed.* **2017**, *56* (20), 5498–5502.

(21)   Neumann, P.; Dib, H.; Caminade, A. M.; Hey-Hawkins, E. Redox Control of a Dendritic Ferrocenyl-Based Homogeneous Catalyst. *Angew. Chemie - Int. Ed.* **2015**, *54* (1), 311–314.

(22)   Dodge, H. M.; Kita, M. R.; Chen, C.-H.; Miller, A. J. M. Controlling Pincer Ligand Hemilability to Avoid Off-Cycle Intermediates in Cation-Tunable Olefin Isomerization. *Manuscript in Progress.*

(23)   Smith, J. B.; Kerr, S. H.; White, P. S.; Miller, A. J. M. Thermodynamic Studies of Cation–Macrocycle Interactions in Nickel Pincer–Crown Ether Complexes Enable Switchable Ligation. *Organometallics* **2017**, *36* (16), 3094–3103.

(24)   Goldbach, V.; Roesle, P.; Mecking, S. Catalytic Isomerizing ω-Functionalization of Fatty Acids. *ACS Catal.* **2015**, *5* (10), 5951–5972.

(25)   Ohlmann, D. M.; Tschauder, N.; Stockis, J. P.; Gooben, K.; Dierker, M.; Gooben, L. J. Isomerizing Olefin Metathesis as a Strategy to Access Defined Distributions of Unsaturated Compounds from Fatty Acids. *J. Am. Chem. Soc.* **2012**, *134* (33), 13716–13729.

(26) Grotjahn, D. B.; Larsen, C. R.; Gustafson, J. L.; Nair, R.; Sharma, A. Extensive Isomerization of Alkenes Using a Bifunctional Catalyst: An Alkene Zipper. *J. Am. Chem. Soc.* **2007**, *129* (31), 9592–9593.

(27) Yamasaki, Y.; Kumagai, T.; Kanno, S.; Kakiuchi, F.; Kochi, T. Selective Long-Distance Isomerization of Terminal Alkenes via Nondissociative Chain Walking. *J. Org. Chem.* **2018**, *83* (16), 9322–9333.

(28) Yoo, C.; Dodge, H. M.; Farquhar, A. H.; Gardner, K. E.; Miller, A. J. M. Poly(Ether) Dissection by Pincer Iridium-Mediated Ether Decarbonylation.

(29) Tolman, C. A. Steric Effects of Phosphorus Ligands in Organometallic Chemistry and Homogeneous Catalysis. *Chem. Rev.* **1977**, *77* (3), 313–348.

(30) Babbini, D. C.; Iluc, V. M. Iridium PCsp3P-Type Complexes with a Hemilabile Anisole Tether. *Organometallics* **2015**, *34* (13), 3141–3151.

(31) Appleton, T. G.; Clark, H. C.; Manzer, L. E. The Trans-Influence: Its Measurement and Significance. *Coord. Chem. Rev.* **1973**, *10* (3–4), 335–422.

(32) Kocen, A. L.; Klimovica, K.; Brookhart, M.; Daugulis, O. Alkene Isomerization by "Sandwich" Diimine-Palladium Catalysts. *Organometallics* **2017**, *36* (4), 787–790.

(33) Liu, X.; Zhang, W.; Wang, Y.; Zhang, Z. X.; Jiao, L.; Liu, Q. Cobalt-Catalyzed Regioselective Olefin Isomerization under Kinetic Control. *J. Am. Chem. Soc.* **2018**, *140* (22), 6873–6882.

(34) Schmidt, A.; Nödling, A. R.; Hilt, G. An Alternative Mechanism for the Cobalt-Catalyzed Isomerization of Terminal Alkenes to (Z)-2-Alkenes. *Angew. Chemie - Int. Ed.* **2015**, *54* (3), 801–804.

(35) Harris, R. K.; Becker, E. D.; De Cabral Menezes, S. M.; Granger, P.; Hoffman, R. E.; Zilm, K. W. Further Conventions for NMR Shielding and Chemical Shifts (IUPAC Recommendations 2008). *Magn. Reson. Chem.* **2008**, *46* (6), 582–598.

(36) Palatinus, L.; Chapuis, G. SUPERFLIP – a Computer Program for the Solution of Crystal Structures by Charge Flipping in Arbitrary Dimensions. *J. Appl. Crystallogr.* **2007**, *40* (4), 786–790.

(37) Betteridge, P. W.; Carruthers, J. R.; Cooper, R. I.; Prout, K.; Watkin, D. J. CRYSTALS Version 12: Software for Guided Crystal Structure Analysis. *J. Appl. Crystallogr.* **2003**, *36* (6), 1487–1487.

(38) Kita, M. R.; Miller, A. J. M. Cation-Modulated Reactivity of Iridium Hydride Pincer-Crown Ether Complexes. *J. Am. Chem. Soc.* **2014**, *136* (41), 14519–14529.